Investigating tonsillar diseases using advanced optical microscopy

Megan Clapperton

Submitted in fulfilment of the requirements for the degree of Doctor of Philosophy

Department of Physics

University of Strathclyde, Glasgow

April 22, 2024

For Mum and Dad

Declaration of Authorship

This thesis is the result of the author's original research. It has been composed by the author and has not been previously submitted for examination which has led to the award of a degree.

The figures presented in this work are a result of my own work, except those that have been adapted or reproduced from other published work. In these cases, citation is provided in the figure caption in accordance with copyright laws.

Collaborations with other researchers have been integral to the work of this thesis and any contributions from others have been clearly indicated in the text and are clearly listed below for each Chapter. Tissue was provided from via the Bioreprository Management Committee of NHS Greater Glasgow and Clyde. Hitesh Taylor and Holly Coleman (NHS GGC) took part in the clinical assessment study in Chapter 2. The bacterial strains used for controls were provided by Robin Braes (University of Strathclyde). The yeast strains used for controls were provided by Dr Katherine Baxter (formally University of Strathclyde). Resources and expertise for performing tonsillar homogenisation and western blotting were provided by Dr Margaret Rose Cunningham (University of Strathclyde).

Signed: Megan Clapperton

Date: January 2024

Abstract

The paired palatine tonsils at the opening to the oropharynx are an important immune organ during adolescence. Due to their location inherently opening them to exogenous agents, they play a large role in immune defence. Their role also opens them to a variety of disease; acute recurrent tonsillitis is an infection of the palatine tonsil typically thought to be cause by *Group A Streptococcal* species. Tonsil hypertrophy due to obstructive sleep apnoea is characterised by enlarged tonsils. For both diseases, the only absolute cure is the complete removal of the tonsil via a routine tonsillectomy. This operation is not without risk and up to 20% of patients are readmitted to hospital within two weeks following surgery due to complications associated with bleeding. In many cases, antibiotic treatment does not suffice in the treatment of tonsillitis, leading to recurring infections. Biofilms are known to have increased antibiotic resistance, and have been shown to be involved in tonsillitis.

This thesis aims to apply advanced optical microscopy and image analysis to quantify the biofilm presence on tonsil tissues, as well as to aid in discovery of biomarkers of tonsillitis infection.

Imaging based studies of the palatine tonsil are often limited by the trade off between field of view and resolution which is present in optical microscopy. It is usually possible to image a large field of view with poor spatial resolution, or to image a small field of view with good spatial resolution. Within Chapter

2, the Mesolens, a novel optical microscope capable of imaging up to 6 mm x 6 mm (x 3 mm) with subcellular resolution, is used to investigate biofilm abundance and spatial distribution on both infected and hypertrophied tonsils. Studies are typically performed on fixed tissues; Chapter 2 aimed to investigate biofilm presence on fresh *ex vivo* whole mounts of tonsillar tissue, with as little alteration to its *in vivo* state as possible. Using these methods, it was shown that biofilms are equally distributed throughout the tonsil mass regardless of disease type. Within this Chapter, biofilms were detected in 100% of examined tonsil tissue mounts, which is in stark comparison to the approximately 70% of cases previously reported in literature. This is due to the combination of minimal sample preparation, no fixation step, and the large tissue volumes which could be imaged using the Mesolens.

In Chapter 3, the Mesolens was used to image the distribution of bacteria and two interleukins within sections of tonsillar tissue. IL-17C is a cytokine which is selectively released in epithelial cells in response to bacterial stimulation, and had not previously been quantified in tonsil tissue. IL-1β is a pro-inflammatory cytokine which has previously been documented in tonsillitis, but with little information on its spatial distribution. It was hypothesized that, due to its production methods, IL-17C expression may be higher in tonsillitis patient tissue and therefore be a potential biomarker of disease. By using widefield mesoscopy and image analysis alongside standard molecular biology techniques, the ability to use IL-17C as a biomarker of infection was verified. IL-1β, however, could not be reliably identified as a biomarker for infection.

The aforementioned methods involved the detection of structures or proteins within the tonsil tissue which had been stained with a fluorophore. However,

it is possible to detect and differentiate between different cell types and disease types using the fluorescence lifetimes of endogenous fluorophores. Therefore, Chapter 4 aimed to use this property to determine if it was possible to use fluorescence lifetimes as an indicator of disease. Within this chapter, it was found that the τ_1 lifetime component was significantly longer in ART than in OSA tissues, with no such significance witnessed in the other lifetime components.

"You can do without the day if theres a lamp quiet-lighted and kind in your heart."

- Lewis Grassic Gibbon (*Sunset Song*)

Acknowledgements

Pursuing a PhD has been the greatest achievement of my life; though it has not been an easy feat. They say that it takes a village to raise a child: well, it took that and more to get me through this PhD. I am indebted to so many people for the support and expertise that I was surrounded by throughout this process. As such, this is absolutely not going to be short, but will definitely be sweet.

Gail, I could not have possibly asked for a better advisor and mentor throughout this process. You have guided me from (pre-Hong Kong – *that's me just letting you know I studied in Hong Kong*) baby physicist Meg, all the way to the somewhat fledged scientist I am today. Regardless of how busy you were, you were there to always lend a hand, bounce ideas between or get me back on track. Not only that, you have supported me through a myriad of personal troubles throughout the years and always have been there for me to rant / greet at. Thank you for encouraging me, for putting up with me, for teaching me the noise that a carrot makes and for being my own personal ambulance service. Most of all, you have always made me feel welcome, that nothing was ever too much to ask, that being myself wasn't a bad thing, and you have always made me feel like a valued scientist and member of the group. I could not have possibly asked for a better supervisor. It has been an absolute pleasure learning from and working alongside you. I'll miss our weird group. You can now continue life without the constant fear of having to fill out injury forms.

Cat, Catalina and Tash: thank you for encouraging me to explore the clinical nature of the PhD, for getting me excited about tonsils and for helping to upkeep my role as tonsil fairy!

Margaret, thank you for providing much needed support with the work in Chapter 3. Before this, I didn't know what a cytokine was, how to blot and certainly didn't know how to make 'tonsil smoothies'. Beyond the experimental and teaching, you were an excellent agony aunt and friendly face to talk to throughout my PhD, and I thank you greatly for this.

Thank you to Prof. Paul Hoskisson, Dr Becca McHugh and the whole group for providing microbiology guidance and support to this poor little physicist. Thank you to Dr Katherine Baxter, your insight into biofilms and fungi was invaluable during my PhD. I enjoyed our time in Palma together at Eurobiofilms and am happy to call you my pal.

Dr Liam Mark Rooney FRMS, SMOTY. Where to start? The heroic post-doc who rescued me with my broken foot, carrying me for miles over broken glass and fire, I'd be dead without you. You have been a source of wisdom, humour, degradation and encouragement all at once. I am, and will always be, in awe of what you are able to achieve academically, and your ability to always make the first talk at a conference despite the escapades of the prior evenings. I can only hope that some of your drive has actually worn off on me! I can confidently say that I will never have another workmate quite like you, so am glad to be keeping you as a pal. Give my love to Wendy and the kids.

Bea, my travel companion. It was a pleasure attending so many conferences with you in such cool places. From Birmingham to Busan (*where are my busandals?*), I enjoyed our similarities in wanting to explore supermarkets, beat jetlag

with 4am beach trips and sharing our disdain for the world. You have been so supportive during my PhD and put up with my mood swings (of which they were plentiful and extreme). I hope to continuously offend you throughout life with my insults to Italian cuisine. I am so thankful to have met you in this journey and to comfortably say that I have a friend for life.

Shannan, my Clydebank companion, Toast's maw: I genuinely don't think I could have done this without you. You have always kept me grounded and rational and talked me off many an anxious cliff. Thank you for putting up with my many daft questions, and for always being there to provide a nose boop when required. I am thankful to have had such a shining example of an interdisciplinary scientist to look up to throughout this process and I am thankful to call you my friend.

Thank you to the members of the McConnell group, specifically my low-key therapist Lisa, the MATLAB wizs Jan and Peter, big and wee Mollies, Tonsil Fairy 2.0 Kay and the others, past and present. I sincerely hope that you all think of me any time you see someone in a cast.

Isa, Phyllis, Senga and the rest of the auld yins on level 5, thank you for being such a great group of friends. I will miss you all but will be sure to keep in touch with the 'Baby Breakdown Club'. And to the rest of the crazy lot on HW514, you made my time here amazing.

A special thanks is needed for the office coffee machine which has kept me functioning for the last few months.

Rebecca and Jay, what can I say? We have now been pals for almost 10 years (grim), from little baby physicists up to (somewhat) capable scientists: check us oot. I am thankful for you both for your encouragement, roasting, coffee

chats and reality checks. I am so excited to see what the future has in store for you.

To my closest of pals: Joanne and Meg (yes, another Meg), you both have been such amazing supports over this PhD. Joanne, you have been my closest friend since I was 11 years old, you have always supported me in my weird and wonderful life choices and I am thankful to have such a good human by my side. Meg, it's been literal years since we were cool students studying abroad, and I never thought I would come back with a friend for life, but how could I have possibly left the alliance at UST?

Mr Wood, Mrs Waddell, Mrs Burns, Mrs McInally and Miss Irvine from Clydebank High School. I could not have gotten here without the support of you all. You constantly encouraged me to pursue whichever subject I wanted (even if it wasn't the one you taught), cheered me on and provided pastoral care during my darkest times. Thank you, this is for you all.

Miles, moving in together while approaching the end of our PhDs could have been make or break, but here we are. You always provided me with comfort in my times of need, with humour when I was down, and with keeping the hoose up to scratch when I was too sad to do so myself. All that and you never once complained when I showed up with yet another elderly rodent to take care of. Pudge and I are quite lucky to have you.

Dad, you have been my number one supporter from day 1 (or before, I suppose). You have never made me feel like I was weird or different, you have always encouraged me to pursue all of my hobbies and interest, and most importantly have been the best dad a gal could have asked for. Sorry for not pursuing a PhD in the history of heavy military vehicles. Rhona, Joanna and

the rest of the Fulton / Smith gang. Thank you for making me feel like I have always been a member of your family. You have always treated me and supported me like one of your own and for that I am grateful.

Finally, to those who never got to see me get here. Gran and Granda, you were always supportive of my endeavours into science, I am sad that Granda will not get to introduce me as the 'medical doctor' as no amount of explaining led him away from the belief that there would finally be a doctor in the family. Mum, you shaped me in my formative years and fostered an environment where learning was always encouraged. I have always been interested in reading, numbers and nature and attribute it to both you and dad. I thank Dad on your behalf, for continuing on with your morals and standards, and being both Mum and Dad when needed. I sincerely hope that I've made you proud.

Research Output

Published and submitted works

- Megan Clapperton, Tash Kunanandam, Catalina D. Florea, Catriona M. Douglas, Gail McConnell., (2024) **Multimodal optical mesoscopy reveals the quantity and spatial distribution of gram-positive biofilms in ex vivo tonsils**, *Journal of Microscopy*, https://doi.org/10.1111/jmi.13266.

- Megan Clapperton, Tash Kunanandam, Catalina D. Florea, Catriona M. Douglas, Margaret R. Cunningham, Gail McConnell., (2024) **IL-17C plays a role in the pathophysiology of acute recurrent tonsillitis**, *BioRxiv*, https://doi.org/10.1101/2024.02.08.578879. *Submitted to Discovery Immunology*

- Megan Clapperton, Tash Kunanandam, Catalina D. Florea, Catriona M. Douglas, Gail McConnell., (2024) **Label-free detection of acute recurrent tonsillitis using fluorescence lifetime imaging microscopy**, *Manuscript in preparation*

Oral Presentations

- **International Bioimaging Network Meeting, Birmingham, UK (2021)**
  "Mesoscopic investigation of tonsillitis"

- **Microscience Microscopy Congress, virtual (2021)**
  "Mesoscopic imaging of excised pediatric palatine tonsils confirms the presence of bacterial infection beyond the surface"

- **Focus on Microscopy, virtual (2022)**
  "Mesoscopic investigation of tonsillitis unveils widespread infection"
- **Frontiers in Bioimaging, Manchester, UK (2022)**
  "An optical imaging method for identifying biofilms in ultra-thick, live palatine tonsil for the detection and analysis of ENT diseases"
- **Early Career Microbiology Symposium, Bristol, UK (2023**
  "Multimodal optical mesoscopy for the study of biofilm infection in tonsils"
- **International Microscopy Congress, Busan, South Korea (2023)**
  "Optical mesoscopy for the study of biofilm infection in palatine tonsil"
- **Scottish Microscopy Society Symposium, Dundee, Scotland (2023)**
  "Searching for biomarkers of tonsillar disease"
- **Seminar, MRC Lab for Molecular Biology, Cambridge, UK (2024)**
  "Investigating tonsillar disease using advanced optical microscopy"

Poster Presentations

- **IOPP Twitter Conference, virtual (2021)**
  "Assessing bacterial infection in pediatric palatine tonsilis using mesoscopy"
  Best poster, optics and photonics division
- **Eurobiofilms, Palma, Spain (2022)**
  "Assessing the role of biofilms in tonsillar diseases using optical mesoscopy"

Covid Impact Statement

During my PhD funding from October 2020 to January 2024, the Covid-19 pandemic impacted my studies for several months. At the start of my PhD, social distancing rules and maximum occupation limits were still in place in my lab. This meant that my ability to be taught key techniques in the wet lab was disrupted and my access to the lab in general was limited. Until late 2021, only essential operations were performed in the Children's hospital where I collected samples. Tonsillectomy due to recurrent tonsillitis was not considered essential, therefore my access to samples at the start, and for the subsequent years was limited. Regular hospital testing of patients for Covid-19 prior to admission, which still occurs, meant that access to tonsil tissue was often disrupted due to patients having positive tests. In many cases, this information was not given until I had travelled to the hospital to collect the samples. As such, many hours were spent on travel for tissue that could not be taken. This meant that the data collection for Chapter 2 was significantly delayed for two reasons. Firstly, sample access at the start was severely limited, as previously discussed. Secondly, tonsillectomy for obstructive sleep apnoea was considered essential, meaning there was a skew in data towards OSA that had to be rectified by waiting for more tonsillitis patients.

Contents

List of Figures

List of Tables

List of Abbreviations

2D	**2**- **D**imensional
3D	**3**- **D**imensional
ADC	**A**nalogue to **D**igital **C**onverter
Ag	**A**nti**g**en
ANOVA	**AN**anylsis **O**f **VA**riance
ART	**A**cute **R**ecurrent **T**onsillitis
BLAST	**B**asic **L**ocal **A**lignment **S**earch **T**ool
BP	**B**ase **P**air(s)
BSA	**B**ovine **S**erum **A**lbumin
CCD	**C**harge **C**oupled **D**evice
CLAHE	**C**ontrast **L**imited **A**dapted **H**istogram **E**qualization
CLSM	**C**onfocal **L**aser **S**canning **M**ode
CMOS	**C**omplementary **M**etal - **O**xide **S**emiconductor
DAMP	**D**amage **A**ssociated **M**olecular **P**athways
DAPI	4',6-**DiA**midino-2-**P**henyl**I**ndole
DMEM	**D**ulbecco's **M**odified **E**agle **M**edium
DNA	**D**eoxyribonucleuc **N**ucleic **A**cid
ECL	**E**nhanced **C**hemi**L**uminescence
EPS	**E**xtracellular **P**olymeric **S**ubstances
FAD	**F**lavin **A**denine **D**inucleotide

FBS	**F**etal **B**ovine **S**erum
FD	**F**requency **D**omain
FIJI	**F**iji **I**s **J**ust **I**mageJ
FISH	**F**luorescent ***I**n **S**itu* **H**ybridisation
FL	**F**luorescence **L**ifetime
FLIM	**F**luorescence **L**ifetime **I**maging **M**icroscopy
FLIO	**F**luorescence **L**ifetime **I**maging **O**pthamology
FMN	**F**lavin **M**ono**N**ucleotide
FOV	**F**ield **O**f **V**iew
FWHM	**F**ull **W**idth at **H**alf **M**aximum
GAS	**G**roup **A** **S**treptococcus
GFP	**G**reen **F**luorescent **P**rotein
GP	**G**eneral **P**ractitioner
HBSS	**H**anks **B**alanced **S**alt **S**olution
HeLa	**He**nrietta **La**cks
HEV	**H**igh **E**ndothelial **V**enuoles
HI	**H**eat **I**nactivated
IF	**I**mmuno**F**luorescence
Ig	**I**mmuno**g**lobulin
IL	**I**nter**L**eukin
IRF	**I**nstrument **R**esponse **F**unction
LED	**L**ight **E**mitting **D**iode
L/G	**L**-**G**lutamine
MALT	**M**ucosa-**A**ssociated **L**ymphoid **T**issues
MCA	**M**ulti **C**hannel **A**nalyser
MCC	**M**anders **C**olocalisation **C**oefficient

MCP	**M**icro **C**hannel **P**lates
MIP	**M**aximum **I**ntensity **P**rojection
MOC	**M**anders **O**verlap **C**oefficient
NA	**N**umerical **A**perture
NADH	**N**icotinamide **A**denine **D**inucleotide **H**ydrogen
NBF	**N**eutral **B**uffered **F**ormalin
NHS	**N**ational **H**ealth **S**ervice
OCT	**O**ptimal **C**utting **T**emperature
OSA	**O**bstructive **S**leep **A**pnoea
PAMP	**P**athogen **A**ssociated **M**olecular **P**athway
PBS	**P**hosphate **B**uffered **S**aline
PCC	**P**earsons **C**orrelation **C**oefficient
PCR	**P**olymerase **C**hain **R**eaction
PFA	**P**olymeric **F**orm**A**ldehyde
PMT	**P**hoto **M**ultiplier **T**ube
PRR	**P**attern **R**ecognition **R**eceptors
P/S	**P**enicillin **S**treptomycin
PSF	**P**oint **S**pread **F**unction
RGB	**R**ed **G**reen **B**lue
RHC	**R**oyal **H**ospital for **C**hildren
RLD	**R**apid **L**ifetime **D**etermination
RNA	**R**ibo**N**ucleic **A**cid
ROI	**R**egion **O**f **I**nterest
ROUT	**R**egression and **OU**tlier **R**emoval
SNR	**S**ignal to **N**oise **R**atio
SPAD	**S**ingle **P**hoton **A**valanche **D**etector

TAC	**T**ime to **A**mplitude **C**onverter
TBS-T	**T**ris **B**uffered **S**aline with **T**ween-20
TCSPC	**T**ime **C**orrelated **S**ingle **P**hoton **C**ounting
TD	**T**ime **D**omain
TLR	**T**oll **L**ike **R**eceptor
TNF	**T**umour **N**ecrosis **F**actor
TTTR	**T**ime-**T**agged **T**ime-**R**esolved
WF	**W**ide **F**ield
WHO	**W**orld **H**ealth **O**rganisation
VRE	**V**ancomycin **R**esistant **E**nterococci

Chapter 1

Introduction

This chapter will provide an overview of the principles of optical microscopy used throughout this thesis, and it will provide biological context to the applications therein. I first outline the principles that underpin light microscopy by introducing resolution, contrast and fluorescence. I then give a brief history of optical microscopy followed by greater detail on the main optical microscopy and mesoscopy techniques used throughout the thesis. After the properties of microscopy are introduced, an overview of relevant biomedicine is presented. First, I introduce biofilms and their role in infection and antimicrobial resistance, followed by an introduction to the palatine tonsil and its morphological characteristics. I then introduce the two main diseases this thesis focuses on, namely acute recurrent tonsillitis and tonsillar hypertrophy due to obstructive sleep apnoea. Finally, I will outline the aims of this thesis.

1.1 Fundamentals of Optical Microscopy

Microscopes of many kinds are now found in most biological and medical-focussed research labs. To begin, I will start with an introduction to the essential physics that underpin the technique.

Microscopes are used in order to form magnified images of tiny objects, that is to make objects seem much larger than they actually are. In order to do this, various lenses are used, bending light from an object towards the observer in a process of refraction [1]. Additionally, objects of interest must appear different to their background or to other objects within the field of view, i.e they must have contrast [2].

Within this section, I will first introduce the principles behind image formation and ray optics. Then, I will introduce resolution and contrast as well as optical aberrations which may appear in an imaging system. Finally, I will introduce the concept of fluorescence and its applications in biological research.

1.1.1 Image formation

Light incident upon a refractive index boundary will have a portion reflected off the surface of the boundary, and a portion will travel through the boundary into the second media with a directional change, known as refraction. This phenomenon can be described using Snell's law [3]:

$$n_1 sin\theta_1 = n_2 sin\theta_2 \tag{1.1}$$

where n_1 and n_2 are the refractive indices of the different media, θ_1 is the angle of incidence upon the boundary and θ_2 is the angle of refraction.

Refraction is used within microscopy to aid in focusing light to the focal point of a lens at distance f from the lens [1]. This is performed with a series of lenses. In it's simplest set-up, rays from a source of light are focussed onto the object by a condenser lens. The light emitted from or transmitted through the specimen is focussed by the objective lens onto an intermediate image plane. To observe the image, the light is refracted again into an eyepiece focusing the light onto the retina of an observer. This process is demonstrated in Figure 1.1

1.1.2 Resolution and Numerical Aperture

The resolution of an optical microscope is defined as the shortest distance between to objects or points that can be distinguished as separate objects. The numerical aperture (NA) of an objective is its ability to collect light and resolve structure at fixed distances. Image forming light waves pass through or are emitted from the specimen and enter the objective in a cone; this cone determines the angular aperture which is determined by the focal length of the objective. NA is related to both refractive index (n) of a media in which light passes through alongside the angular aperture (α) of a given objective lens, this is described as [4, 5]:

$$NA = nsin\alpha \tag{1.2}$$

The resolution of an optical microscope does not solely depend on the NA of the objective lens, but on the NA of the whole system including the objective and condenser lenses. To get the best possible resolution out of a system,

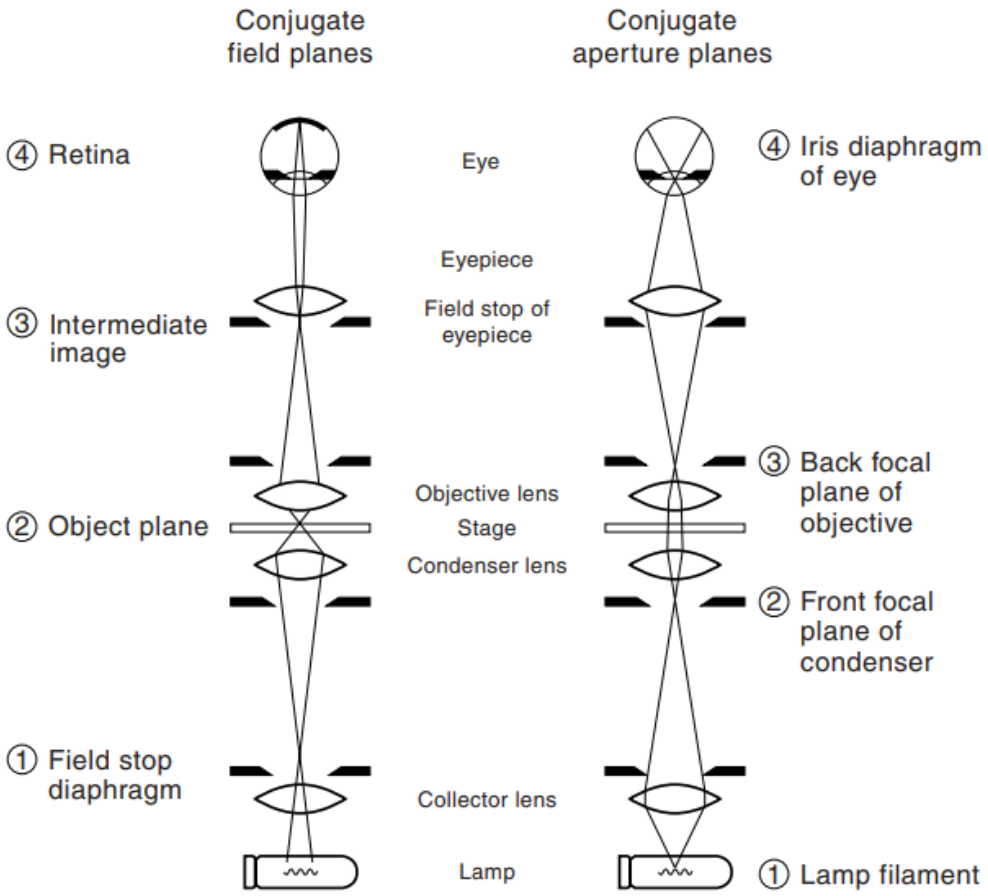

Figure 1.1: Schematic demonstrating image formation in a simple microscope. The left hand diagram represents the field (object) plane including the eyepiece and retina, and the right hand diagram represents the aperture plane incorporating the pupil of the eye. Reproduced from [1]

the system must be correctly aligned, have high NA lenses and make use of the optimal wavelength (shorter wavelengths are capable of resolving more structure than longer). In addition, as is apparent with equation 1.2, the NA is dependent on the refractive index, n. With air objectives, it is difficult to achieve an NA above 0.95. However, immersion lenses used with high refractive index mounting and imaging media can be used to increase NA, such as

water (n = 1.33), glycerin (n = 1.47) and oil (n = 1.51). These allow for achievable NAs of up to 1.4 with oil immersion lenses. Three general mathematical concepts must be understood when introducing resolution: Airy disks, Abbe's diffraction limit, and the Rayleigh criterion.

When light from points in a specimen pass through the objective lens, they are reconstituted as an image. These points of the specimen appear within the image as small patterns, not as points, which are known as Airy patterns. The central maximum of the Airy pattern is known as an Airy disk, and contains 84% of the luminous energy. This central maxima, or zeroth order maxima, is surrounded by concentric n^{th} order maxima of sequentially decreasing brightness. This pattern is a result of both diffraction and / or scattering of light as it passes through minute spaces in the specimen as well as the circular rear aperture of an objective lens. The diffraction pattern is determined by both the wavelength of light and the size of the aperture which the light passes through. Thus, more specifically, the resolution of a microscope is its ability to distinguish between two closely spaced Airy disks in the diffraction pattern. Figure 1.2 illustrates Airy disks which are at different spatial distances from each other. Objects are considered well resolved when the zeroth order maxima are far apart and their concentric maxima rings are able to be differentiated from one another. The corresponding intensity plot of an Airy disk is known as the point spread function (PSF) [6].

Ernst Karl Abbe was the first to define NA, and later produced his theory and formula explaining the resolution limits of optical microscopy [8]. He recognised that microscopy images of specimens are composed of overlapping Airy discs (or diffraction-limited points) of varying intensities [9]. According to Abbe's diffraction limit, the resolution d of a system can be explained as:

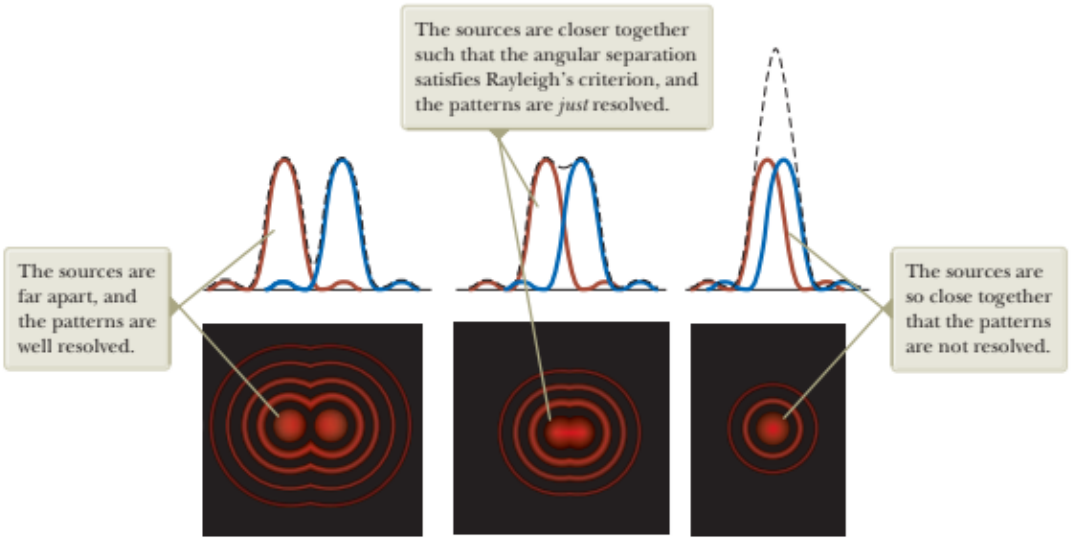

Figure 1.2: Left: objects are considered *well resolved* when objects are far apart. Centre: objects are resolved, or meeting the Rayleigh criterion. Right: objects are too close together and are not resolved. Reproduced from [7]

$$d = \frac{\lambda}{2NA} \tag{1.3}$$

where λ is the wavelength of light illuminating a sample and NA is the numerical aperture. Therefore, it is possible to increase the resolution of a microscope by using shorter wavelength (λ), by imaging through a medium of high refractive index, or by using a combination of high NA lenses [10]. This limit yields a theoretical lateral (x-y) resolution of approximately 250 nm and an axial (z) resolution of approximately 500 nm, if using 550 nm excitation and a NA of 1.4 [11]. In practice, however, these theoretical resolutions are not typically met: a standard $4\times$, 0.1 NA objective will yield a lateral resolution of approximately 2 μm in practice.

Rayleigh expanded upon the work of Abbe and defined the Rayleigh criterion, defining the limit of resolution of a diffraction-limited system [12]. This criterion is demonstrated in Figure 1.2 and states that if the diffraction pattern from two single Airy discs are not overlapping, then they are well resolved and meet the criterion. If the center of one Airy disc coincides with the first diffraction minimum of another, then the objects are 'just resolved' and still distinguishable. If they are closer, they cannot be distinguished and do not meet the criterion. The lateral resolution ($d_{x,y}$) for a brightfield transmission microscope as defined with this criterion is as follows:

$$d_{x,y} = \frac{1.22\lambda}{(NA_{obj} + NA_{cond})} \tag{1.4}$$

where λ is the wavelength of light used for imaging and NA_{obj} and NA_{cond} are the NAs of the objective and condenser lens respectively. According to this criterion, the resolution of an epifluorescence microscope (where incident and collected light propagate through the same objective lens) can be considered also in the following way:

$$d_{x,y} = \frac{0.61\lambda}{NA} \tag{1.5}$$

Lateral resolution is what is most commonly thought of when referring to the resolution of a microscope system. However, another important aspect is the axial resolution, measured parallel to the optical axis; this is most commonly referred to as the depth of field. Depth of field is determined by the distance from the nearest object plane in focus to the farthest object plane which simultaneously remains in focus [13]. In microscopy, this distance is typically very

small, measured in micrometers. Depth of focus refers to the corresponding region in image space, rather than object space; and refers to the distance over which the image plane can be shifted such that the object plane remains in focus [14]. In theory, the image plane would be expected to represent an infinitely small section of the specimen, however, this is not the case and each point is elongated (or spread) above and below the specimen plane. The axial resolution of a microscope, as described by Abbe, can be defined as:

$$d_z = \frac{2\lambda}{NA^2} \tag{1.6}$$

where d_z is the measurement of axial resolution. The depth of field of a microscope therefore shrinks inversely with the square of the NA, in comparison to lateral resolution which is inversely proportional to the first power of NA. Therefore, the axial resolution and resulting thickness of the attainable optical sections in a microscope are more affected by the NA of the system than the lateral resolution. The three dimensional intensity pattern of an Airy disk, generated by imaging serial planes in the z-axis of a microscope, is known as the 3D point spread function (PSF) [15]. The theoretical depth of field can be described as one quarter of the distance between the first axial minima above and below the central maxima in the 3D Airy pattern [13]. The PSF is typically measured by using immobilised fluorescent beads that approximate an infinitely small point object and is compared to the theoretical PSF to evaluate the performance of a system [15].

Another factor to consider when maximising resolution in a system, is ensure the ideal sampling density is chosen. This depends on the optics of the microscope, and ensures that under-sampling (where detail could be missed) is

prevented. The way in which this is considered in optical microscopy is to ensure that imaging is performed at a rate determined by the Shannon-Nyquist criterion [16]. This determines the minimum sampling density required to capture all information in an image. The ideal sampling rate is often defined in terms of spatial resolution and requires a sampling interval which is double the highest spatial frequency in order to preserve resolution in the resulting image. As an example, the diffraction limited resolution of an optical system is approximately 220 nm, therefore, an ideal detector would have to sample at a rate of 110 nm intervals to sample at Nyquist rate. In general, a sampling interval of 2.5 - 3 times the smallest resolvable structure is considered sufficient for optimal imaging.

1.1.3 Aberrations

The work of Abbe demonstrated that the diffraction-limited resolution of an optical microscope was not dependent on chromatic or spherical aberrations [17]. However, it is important to note that these aberrations can create artefacts in the image and therefore decrease image quality.

Aberrations can be broadly split into two categories: monochromatic, when only light of a single wavelength of light is present, and polychromatic, when white light is present. The most serious aberration that can occur is spherical aberration [18]. This causes the image to appear blurred and slightly out of focus, where the center of the image appears more focussed than the edges and the intensity at the edges is lower than that at the center. Although spherical aberration is well understood and corrected for within lens elements, it can also be induced when light passes through mismatched refractive index boundaries in samples where the indexes are not matched between immersion

and mounting media. It is often considered the most serious imaging artifact as the distance the image plane travels in the z-axis does not necessarily match the distance travelled by the object. This results in artificially elongated images (if objective immersed in higher NA medium than sample), or compressed imaged (if objective in lower NA medium than sample), altering the maximum sampling rate. Comatic aberrations (coma) can occur due to imperfections in lens or other microscope components [13]. This result in off axis points appearing distorted due to point points being focussed at sequentially differing heights, producing asymmetrical spots of increasing sizes that result in the Airy pattern having a comet-like shape. Chromatic aberration are wavelength-dependent artifacts that occur due to light of different wavelengths being refracted differently through lens components, resulting in a blurred image due to different wavelengths being focussed at different distances from the lens [13]. Astigmatism is found towards the outer regions of a field of view in uncorrected lenses, causing the Airy pattern to blur into a diffuse circle, ellipse, or line, and occurs due to off-axis illumination [13].

In order to overcome the effects of chromatic aberration, multiple lenses are generally used to bring all divergent wavelengths into focus at the image plane [17], though image processing algorithms now also exist for post-acquisition corrections [19, 20, 21]. A method to reduce the effects of monochromatic aberrations, and more particularly of spherical aberration, is to reduce the lens diameter [17]. However, this will reduce the NA of the system and hence lower the resolution. Another method is by minimising the optical path through different media, or by using refractive index matching immersion medium [18]. Correcting for aberrations within the optical system is a key component in ensuring maximum focus and resolution is achievable with a microscope.

Commercially available objective lenses have low degrees of aberrations, provided they are used for the correct application and according to manufacturers guidelines.

1.1.4 Contrast

Contrast is defined in the ability to distinguish an object from its background based on differences in signal of the object from its background [22]. Without image contrast it would be impossible to see the object in question; this is further compounded by the transparency of many thin biological samples. Therefore, it is common practice to involve contrast-enhancing methods or chemicals such as labelling with absorptive dyes, and by using optical processes such as reflection, birefringence, scattering, diffraction and phase differences.

Contrast itself is not an inherent property of a specimen, rather, it is dependent on the interaction of a specimen with light coupled with the efficiency of optical system with its ability to detect the image [23]. Homogeneous illumination of the sample within the optical system via Köhler illumination is key in ensuring optimal contrast can be achieved [24]. Köhler illumination ensures that light collected from the light source is imaged differently than light collected from the sample. Imaging both the sample and the light source would mean inhomogenous illumination of the sample as the structure of the light emitting elements would be imposed on the specimen. Köhler illumination requires several key components to function: collector lens (and / or field lens), field diaphragm, condenser diaphragm and a condenser lens. These components appear in this order between the light source and the specimen and control illumination of the specimen. The collector / field lens collect light from

the source and focus it at the plane of the condenser diaphragm. The condenser lens then projects this light through the sample without focusing the light source pattern. This scheme creates two conjugate image planes: one with the light source and its pattern image, and the other with the specimen and its images.

Staining thin samples with dye improves the contrast between structures within the sample and has been a common technique for a few hundred years [25]. Choice of dyes allows for selectivity of structural staining. For example, haematoxilin and eosin (H&E) stains are commonly used in histology to bind to different structures and provide the ability to diagnose structural abnormalities within, i.e, medical samples [26]. Absorbing dyes absorb light at different wavelengths and therefore provide the ability to differentiate between these different structures. However, these stains are usually only compatible with fixed cells and tissues for several reasons. Many absorption based stains can interfere with cellular processes and compromise cell viability. Cells with functional cell membranes work to restrict the entry of unwanted exogenous agents, therefore will have difficulty in entering the cell. Due to these factors, absorption stains would need to be used in high concentrations in order to increase the probability of penetrating a live cell, such quantities would prove to be toxic to the cell.

Similarly, fluorescent dyes which can be used to selectively increase contrast in usually fixed samples [27]; this will be discussed in greater detail in the following section.

1.1.5 Fluorescence

Luminescence is a family of processes where molecules may emit light from electronically excited states generated from physical, mechanical, or chemical processes; fluorescence is a member of this family [28]. Fluorescence is the property of molecules to absorb light at a particular wavelength and then emit light at a longer wavelength after a short time (the fluorescence lifetime) [29]. Fluorescence occurs in 3 stages, which are discussed below, and can be seen in Figure 1.3.

The first stage is excitation, where a photon of energy $h\nu_{ex}$, supplied by an external source, is absorbed by the fluorophore generating an excited electronic state (S_2). This process is extremely short, lasting femtoseconds. Next, the

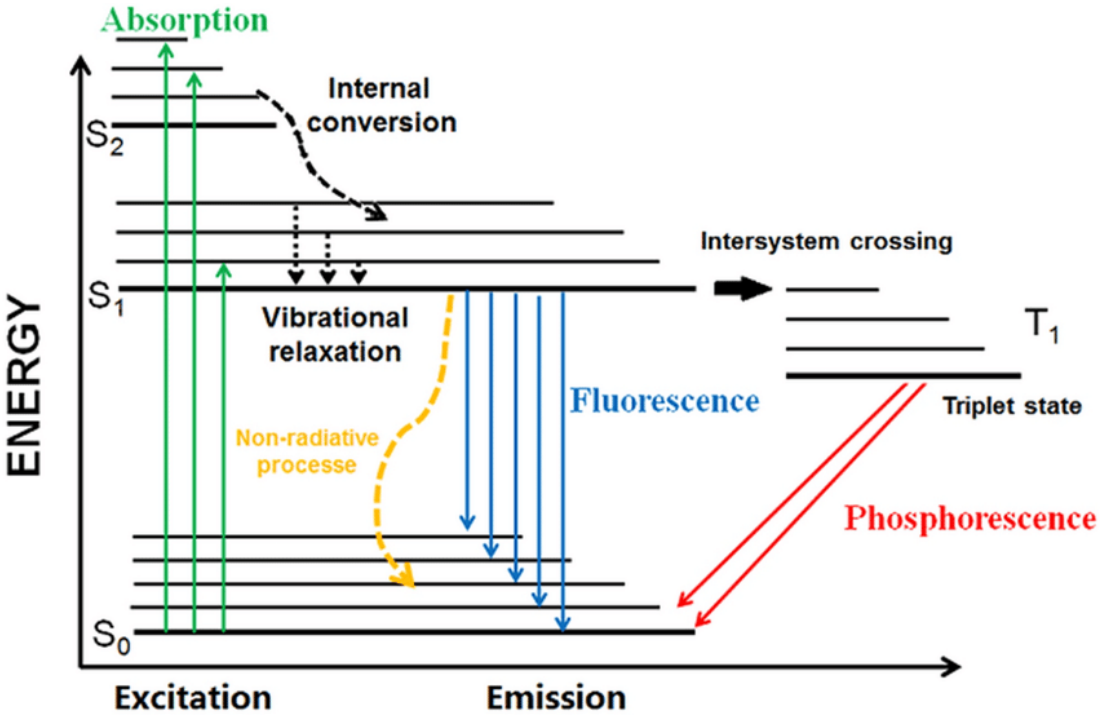

Figure 1.3: Jablonski diagram of fluorescence and phosphorescence (not discussed). Reproduced from [30]

fluorophore undergoes relaxation to a lower excited state S_1. The excited state lifetime lasts for approximately 1-10 nanoseconds. Finally, depopulation of the S_1 state is achieved by a photon of energy hv_em being emitted, returning the fluorophore to its ground state S_0. This emitted photon has lower energy (and therefore longer wavelength) than the input photon due to dissipation during the excited-state lifetime [31]. This energy difference is called the Stokes shift. This shift is essential to the sensitivity of fluorescence microscopy and other techniques since it allows for detection of emission photons to be differentiated from those of the excitation photons.

1.1.6 Fluorescence Lifetimes

A molecule which is excited transitions from ground level to excited state then rapidly undergoes non-radiative relaxation to the lowest vibrational level, before returning to the ground level via non-radiative or radiative (photon emission) decay.

The time that a fluorophore remains in its excited state is known as the fluorescence lifetime (FL), τ [32]. This time typically varies from as little as a few picoseconds to up to hundreds of nanoseconds [33], though microsecond lifetimes have been observed in select cases [34, 35]. Within this time, the intensity *I(t)* decreases to $\frac{1}{e}$ of its original intensity. In the ensemble description, the emitted fluorescence will decay according to:

$$I(t) = I_0 e^{\frac{-t}{\tau}} \tag{1.7}$$

where I_0 is the initial fluorescence at $t = 0$ and τ defined as:

$$\tau = \frac{1}{k_r + k_{nr}} \tag{1.8}$$

where k_r is the radiative rate constant and k_{nr} is the nonradiative rate constant. τ_0 is the natural or radiative lifetime, defined as:

$$\tau_0 = \frac{1}{k_r} \tag{1.9}$$

and is related to the fluorescence lifetime, τ, via the fluorescence quantum yield, ϕ:

$$\phi = \frac{\tau}{\tau_0} = \frac{k_r}{k_r + k_{nr}} \tag{1.10}$$

Equation 1.1.6 assumes no quenching within the biological system. If there is quenching via additional molecules, Q, then the above turns into:

$$\phi = \frac{\tau}{\tau_0} = \frac{k_r}{k_r + k_{nr} + k_Q[Q]} \tag{1.11}$$

where k_Q is the quenching rate constant and Q is the concentration of quenching [36].

The mean lifetime (τ_m) of a multi-exponential mixture of decays is defined as the sum of each lifetime (τ_i) weighted by the fraction of each contributing lifetime species (α_i):

$$\tau_m = \sum_i \tau_i \alpha_i \tag{1.12}$$

The number of excited molecules (n) at any given time, t, is defined as [37]:

$$n(t) = n(0)e^{\frac{-t}{\tau}} \tag{1.13}$$

The FL of a particular fluorophore is a measure of its ability to transfer energy to its surroundings, therefore, it is dependent on its surrounding environment [36, 33]. The FL is also independent of the concentration of the fluorophore. Since FL is a measure relating to local molecular environment, it may be used in tissue to differentiate between tissue and cell types, with each cell or cellular component exhibiting different characteristic lifetimes [33, 38, 39].

1.1.7 Fluorescence for biological imaging

The use of fluorescence for biological imaging is now routinely used in various lab-based assays, for example for localising proteins or determining the spatial organisation of structures within a specimen [13, 40, 41]. Fluorescence microscopy has been used for just over 100 years, with its first applications being in autofluorescence imaging of biological samples [42]. In 1937, synthetic molecular compounds known as fluorophores or fluorochromes were developed with molecular specificity for tagging to cellular structures [43, 44]. Around 20 years later, fluorescently tagged antibodies for the visualisation of specific proteins were developed [45].

Fluorescent dyes offer distinct advantages over absorption dyes which have been previously discussed. In general, fluorophores have high molecular specificity compared to absorption dyes which can often suffer from non-specific binding, they also offer higher sensitivity and improved bio-compatibility [46]. However, non-specific binding may also be a problem in antibody labelling when the concentration of antibody is too high. This can be overcome with the use of blocking agents [47].

The concentration of absorption-based dyes need to be much higher than fluorescence based dyes in order to achieve similar contrast levels [48, 49]. This increased concentration is often cytotoxic and is prohibitive for live-cell imaging. This is not to say that fluorescent dyes cannot be cytotoxic. Phototoxicity is an effect which occurs when reactive oxygen species are generated by a fluorescent protein, leading to a decrease in cell viability. This can also occur when cells are exposed to high laser power for prolonged periods of time, which can have cytotoxic effect. Several mechanisms that induce cytotoxicity as a result of laser irradiation are discussed next. High irradiation intensities can generate reactive oxygen species through excited state reactions in both endogenous and exogenous fluorophores which have the ability to damage cells [50]. Light induced cell death (phototoxicity) can cause cell membrane degradation, and cell death [51]. However, this latter effect is usually mitigated by controlling the exposure time and intensity of the excitation source at the specimen plane to ensure minimal photodamage to the specimen. Additionally, photobleaching can occur in fluorescence-based imaging applications. Photobleaching is a phenomenon wherein excessive excitation radiation degrades the fluorophore in the singlet or triplet states, which results in a loss in available ground state fluorophores [51]. This effect can reduce the amount of time available for

live-cell imaging techniques and can reduce the potential for imaging single molecules. Techniques such as fluorescence recovery after photobleaching use this phenomenon to their advantage as a method to analyse protein mobility and diffusion rates [52].

1.2 A brief history of light microscopy

The optical microscope is a relatively new invention in historical timescales, but we have had a general understanding of the properties of light and lenses for quite some time. The first recorded instances of lenses comes from ancient Egypt and Mesopotamia more than 5000 years ago [53, 54]. Several lenses from this time period have been found, the most famous example being the Nimrud lens, manufactured in ancient Assyria [55]. These lenses were manufactured by polishing crystals and were thought to be used as decorative ornaments, for focusing light to a point to create fires, or as magnifying glasses. It was quite some time before the next instance of optical history was found; at approximately 60 A.D Emperor Nero used emerald lenses to better view gladiator games, with Nero's tutor noting "*Letters, however small and indistinct, are seen enlarged and more clearly through a globe of glass filled with water*" in his book '*Naturalis Historiae*' [56]. It was not until the 13th century, however, that the first text on optical properties was written by Persian mathematician Ibn al-Haytham, entitled '*Book of Optics*'[57]. What soon followed was an acceleration of developments as the properties of lenses and light were better understood. The earliest eyeglasses were thought to be manufactured in Italy in the 1290s [58]. By the 1400s, accompanied by the invention of the printing press and the widespread popularity of books, reading glasses began to be worn by much of society.

Hans Lippershey, Hans Janssen and his son Zacharias Janssen, all from the Netherlands, were the most well known eyeglass manufacturers of the 16th century and have been accredited with independently inventing the first telescope and the microscope [59]. Their design was simple: it comprised two lenses with a sliding tube, allowing for approximately three to ten times magnification depending on positioning of the sliding tube [60]. Galileo Galilei later described his own version of the telescope, which was similar to Lippershey's, in 1610 [61]. He was able to view what he described as *"flies as large as hens"* with his telescope [62], as well as observing and supporting Copernicus's claims of Earth existing within a heliocentric solar system. In 1590, Lippershey and the Janssens reversed the telescope to develop the first compound microscope, again followed quickly but separately by Galileo in 1624 [63]. A colleague of Galileo, Giovanni Faber, was the first to refer to this invention as a microscope [64], derived from the Greek words for "*small*" and "*to look at*" or "*to see*".

Later, in 1660, Robert Hooke and Christopher Cock added an additional lens to the compound microscope to create a system with three lenses, allowing for up to 50× magnification on a static system that did not have to be held close to the eye as Hooke was concerned about damaging his eyesight while using standard microscopes of the time [65]. Soon after, in 1665, he published '*Micrographia*' where he recorded his observations with his microscope and introduced the term and concept of a cell [66]. Dutch tradesman Anton van Leeuwenhoek read '*Micrographia*' and became *"hooked"* on microscopes. He produced small, powerful lenses, with less aberrations and much increased magnification in comparison to others of the era [67]. He made the first easily transportable microscope and created 247 microscopes over his lifetime, with 9

surviving to this day [68]. Leeuwenhoek used his microscope to study and report protozoans [69] from pond water as well as bacteria from tooth scrapings [70].

Carl Zeiss, one of the most famous names in modern microscopy, opened his optical repair workshop in the mid 1800s in Germany, and he quickly moved into the manufacture of microscopes [71]. He realised that in order to improve the design, he would need to combine both manufacturing knowledge with scientific knowledge. To this end, he hired Professor of Physics Ernst Carl Abbe. Abbe showed that the optical properties and quality of a lens may be predicted and thus standardised by calculating the exact size, position and shape of each lens in a microscope system by use of his formula called 'Abbe's Sine Condition' [72]. This formula meant that for the first time in history, microscopes could be mass produced.

As the manufacturing of microscopes quickened, so did improvements and upgrades. The 18th century saw improvements to the tripod microscope from Edmund Culpeper, alongside improved focus mechanisms [73]. In the early 19th century, due to new formulas for glass manufacturing and the invention of the achromatic lens, improvements in the manufacturing of optics were made [74]. The achromatic lens (designed to bring different wavelengths into focus in the same plane) reduced the spherical aberration that had been plaguing microscopes until then.

Today, microscopy has applications across diverse fields including biology, physics, material science, and medicine.

1.3 Optical Microscopy

The optical microscopy techniques used within this thesis are introduced in the following sections.

1.3.1 Brightfield transmission microscopy

Brightfield transmission microscopy is one of the simplest optical microscopy techniques. A sample is illuminated by a white light source from below the sample, and the transmitted light is detected above the sample, with image contrast arising from attenuation of the transmitted light in dense sample regions [75].

A brightfield microscope has a simple set-up: a trans-illumination white light source is focused onto the sample by a condenser lens. Transmitted light from the sample is collected by an objective lens, and magnifies the image. This image is then detected via the human eye using oculars or digitally with a camera.

This method often has low contrast, so contrast enhancement methods such as absorption staining are often required to achieve the required detail within samples [76]. Multi-colour detection is possible with the use of absorption filters placed within the detection path of the microscope, which are typically made from dyed glass or pigmented gelatin resin [77].

1.3.2 Widefield epifluorescence microscopy

Widefield (WF) epifluorescence microscopy involves exciting a fluorophore within a sample which will ultimately release photons (emission) that can be

detected to view structure of the sample. A schematic demonstrating the optical path of a widefield fluorescence microscope can be seen in Figure 1.4 (b). In WF epifluorescence, excitation light from a source passes through an excitation filter which selects the desired wavelength range. This light is then reflected by a dichroic mirror and focused onto the specimen using an objective lens. The dichroic mirror within a microscope system is designed to selectively reflect and transmit light of particular values. This allows for the direction of the correct wavelength to the sample and to the image plane. When this focused light reaches the sample, fluorophores within the sample are excited as described in section 1.1.5 and light of a longer wavelength is emitted. Some of this emitted light is collected again by the objective lens, transmitted through the dichroic mirror and passed through an emission filter to select the correct detection wavelength range and reject the excitation light. The resulting fluorescence image will be detected using oculars with the eye, or using a camera.

The most commonly used excitation sources for WF epifluorescence are light emitting diodes (LEDs) [79], which allow for precise control over the wavelength and intensity of light to be used. In addition, they are relatively low cost, and compact, which makes them a preferred choice against their historic counterparts of arc-lamps and tungsten-halogen lamps. Arc-lamps have high intensities at precise wavelengths, but produce a lot of heat, may have inhomogeneity in illumination [80], and are difficult to dispose of due to their hazardous manufacturing components [79]. Tungsten-halogen lamps improve on most aspects of the arc-lamps: they are less expensive and provide a more even illumination, but they are of such low intensities that they struggle to excite weak fluorophores, and have relatively short lifespans compared to LEDs [79]. LEDs are therefore the preferred choice due to large range of available

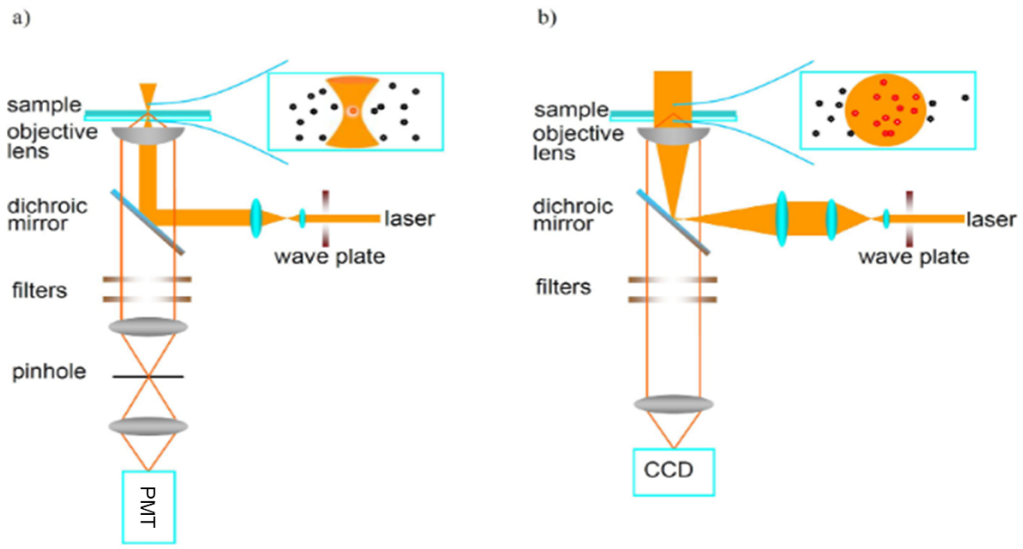

Figure 1.4: A) Confocal fluorescence microscopy set-up , where '*PMT*' is a photomultiplier tube and B) widefield fluorescence microscopy setup, where '*CCD*' is a charge-coupled device (one of several camera types that can be used as a detector in WF microscopy). Reproduced from [78]

wavelengths, low cost, and much longer lifetime than their predecessors.

Illumination of the specimen occurs over the entire achievable FOV, therefore regions above and below the focal plane will fluoresce and this fluorescence is captured by the detector. Due to the inability of a WF system to perform optical sectioning, they are not compatible with imaging of thick and / or highly scattering samples. However, WF systems are extremely useful when imaging fast dynamic processes, thin samples, photosensitive samples and is generally compatible with live-cell imaging when using specialised contrast-enhancing stains designed for live cells.

1.3.3 Detectors for Widefield imaging

While light from a WF can be seen via an eyepiece, a camera is required for recording images digitally. The most commonly used cameras are charge coupled detectors (CCDs) [81], complimentary metal oxide semiconductors (CMOS) [82], or scientific CMOS (sCMOS) [81, 83], with choice depending on required frame rates, sensitivity and noise. These cameras contain millions of photodiodes, each containing semi-conductor based sensors that convert photons to electrons [13, 84, 81]. Each photodiode in the camera sensor chip can correspond to one pixel in a digital image [85, 86]. When a photon hits a photodiode, an electron may be released due to the photoelectric effect [87]. Each individual photodiode on a chip acts as a reservoir for these electrons (or photoelectrons) and collects charge over the defined camera exposure time. These diodes can hold a number of photoelectrons, referred to as the full well capacity, if the charge gained in a photodiode during a single exposure time reaches this capacity, it simply will not collect more electrons and results in a saturated pixel in the final image, suggesting the camera exposure was too high [86]. After the exposure time is complete, the accumulated charge (charge packet) is read out via a read amplifier which amplifies to a range which is appropriate for digitisation and converted to a grey value by an analogue to digital converter. The method in which this transfer is achieved is different depending on the camera used [86]. CCD based sensors have a single read amplifier and analogue to digital converter where all charge is transferred for digitisation. CMOS sensor chips have individual amplifiers and converters for each photodiode.

To achieve the best possible resolution, the pixel number of a camera must be

considered alongside the pixel size. More pixels that are smaller does not necessarily mean higher resolution. Instead, the optimal resolution is achieved by selecting the correct pixel size / number in relation to the NA and magnification of the optical system alongside the spatial frequency of the sample. The sensitivity of a camera should also be considered; this is determined by the quantum efficiency (the number of photons which are converted to electrons) [13, 84] and pixel area. In addition, the frame rate of the camera is important for applications with dynamic imaging. Faster frame rates that can collect data at video rate (minimum of 30 frames per second) are essential when performing live cell imaging of fast processes [85]. Ensuring best image contrast is achieved during acquisition is controlled by the dynamic range of the camera used, with higher bit-depths (16-bit) being the gold-standard of high end cameras.

CCD sensors, with their high sensitivity, high dynamic range, and low noise, were historically the most commonly used digital camera sensor [84]. However, they have slow readout speeds, high power consumption, are expensive compared to sCMOS and CMOS and have limited resolution compared to other techniques. EMCCD (electron multiplying CCD) sensors are a specialised version of CCD for poorly emitting samples [88, 89, 86]. They use amplification processes that increase the sensitivity of the sensor, achieved by electron multiplication by application of high voltage to the sensor. These detectors offer high sensitivity, low noise, high frame rates and high dynamic range, but these benefits come at a much increased fiscal cost and limited lifetime of the sensor in comparison to others. CMOS sensors offer some distinct advantages of CCDs [81]. They have low power consumption, low cost, high frame rate (up to video rate), high resolution and often have a large sensor size.

However, they also have their disadvantages, namely lower sensitivity, lower dynamic range and increased noise when compared to CCD sensors. Scientific CMOS sensors are a hybrid between CCD and CMOS cameras, providing a balance between sensitivity, speed and resolution [81, 86]. They have high frame rates capable of video rate imaging, high sensitivity meaning poorly emitting samples can be imaged, high dynamic range meaning bright and dim regions can be captured without compromising detail and a large field of view due to large chip sizes. Again, these are not without disadvantages, namely they are expensive, have limited lifetime due to high readout speeds and temperature increases during operation and can have limited resolution compared to CCD. In sum, detectors all have their applications and use cases depend on trade offs between required resolution, FOV, dynamic range, sensitivity and frame rate, as well as the cost of the detector.

1.3.4 Confocal laser scanning microscopy

The confocal microscope offers a resolution increase from widefield microscopy, due to the rejection of out of focus light. The first confocal scanning microscope was built in 1957 [90, 91], followed soon after by the first confocal laser scanning microscope (CLSM) in 1969 by David Egger based upon scanning the objective lens over a sample [92]. In 1985, William Bradshaw Amos and John Graham White built the first CLSM involving scanning of the beam while keeping the sample stationary. Most commercial confocal laser scanning microscopes are based off their design [93, 94].

Illumination in a confocal system is provided by lasers of specific wavelengths [13]. Light emitted by the laser source passes through a pinhole aperture situated in a conjugate plane, and is brought into focus by the objective lens

onto the specimen. The laser is scanned across the sample in a defined focal plane using galvo-scanning mirrors, and fluorescence emission is emitted from points in the sample within this focal plane. The emission passes through a dichroic and focussed as a confocal point at the detector via a second pinhole aperture. Fluorescence emission will also occur at points above and below the focal plane however, most of this is rejected by the detection pinhole and therefore does not contribute to the resulting image. A schematic demonstrating the optical path of a confocal microscopy set-up is demonstrated in Figure 1.4 (a).

The scan head is one of the most important features of the CLSM, containing the galvo-scanning mirrors which scan the beam. The scanning methods and out-of-focus light rejection of confocal microscopy allow for imaging of thin (as small as 500 nm [95]) focal planes, otherwise known as optical sectioning. This is in contrast to physical object sectioning using a microtome, where samples are manually sliced to be thin enough to image. With CLSM, specimens can be imaged at different focal planes throughout the sample, creating many optical sections which may be reconstituted into a 3D image using image processing.

CLSM systems use PMTs for detection of light emitted from samples. PMTs contain a photosensitive surface which captures incident photons and produces a series of photoelectrons, generating amplified electric charge [96]. They contain photocathodes which emit electrons through the photoelectric effect upon photon exposure [3]. PMTs consist of a vacuum tube in which a glass or quartz window encapsulates the photodiode, where a series of dynodes (electron multipliers) and anodes complete this electrical circuit. PMTs offer great sensitivity to low intensity emissions, and great gain characteristics, however they do have some disadvantages. They are extremely sensitive to high intensity illumination and therefore can be irreparably damaged and they are

expensive to purchase and to run due to requiring a high voltage power supply. In addition, they have a relatively low quantum efficiency of around 45%, meaning that only 45 out of every 100 excited photons will be converted to electrons and therefore detected as signal. The speed of acquisition in a CLSM slow due to the point scanning of the sample, therefore it is typically not possible to perform fast dynamic process imaging with a confocal system.

1.3.5 Fluorescence Lifetime Imaging Microscopy

Fluorescence lifetime imaging microscopy (FLIM) is an imaging technique which is based upon intrinsic differences in the exponential decay rate of fluorescence emission from a sample [97]. Unlike standard microscopy techniques where the intensity of fluorophores is used to generate the image, FLIM uses the lifetime of fluorophores to generate contrast in images.

A fluorophore, whether endogenous or exogenous, will have a characteristic emission spectrum as well as a distinct fluorescent lifetime which is indicative of how long it remains in its excited state. Fluorophores excited by photons will drop to the ground state with a given probability based upon their decay rates through different radiative and / or nonradiative decay pathways, as shown in Figure 1.3. In order to detect fluorescence, one of the decay paths the fluorophore must follow is the emission path which emits a photon. This fluorescence decay will happen with a given lifetime, τ, which is different for different molecules [97]. Therefore, images generated using FLIM are able to give a spatial map of the distribution of different lifetimes of molecules. An example of this is shown in Figure 1.5 where examples of lifetime heatmaps and lifetime distributions are observed in biological samples [98].

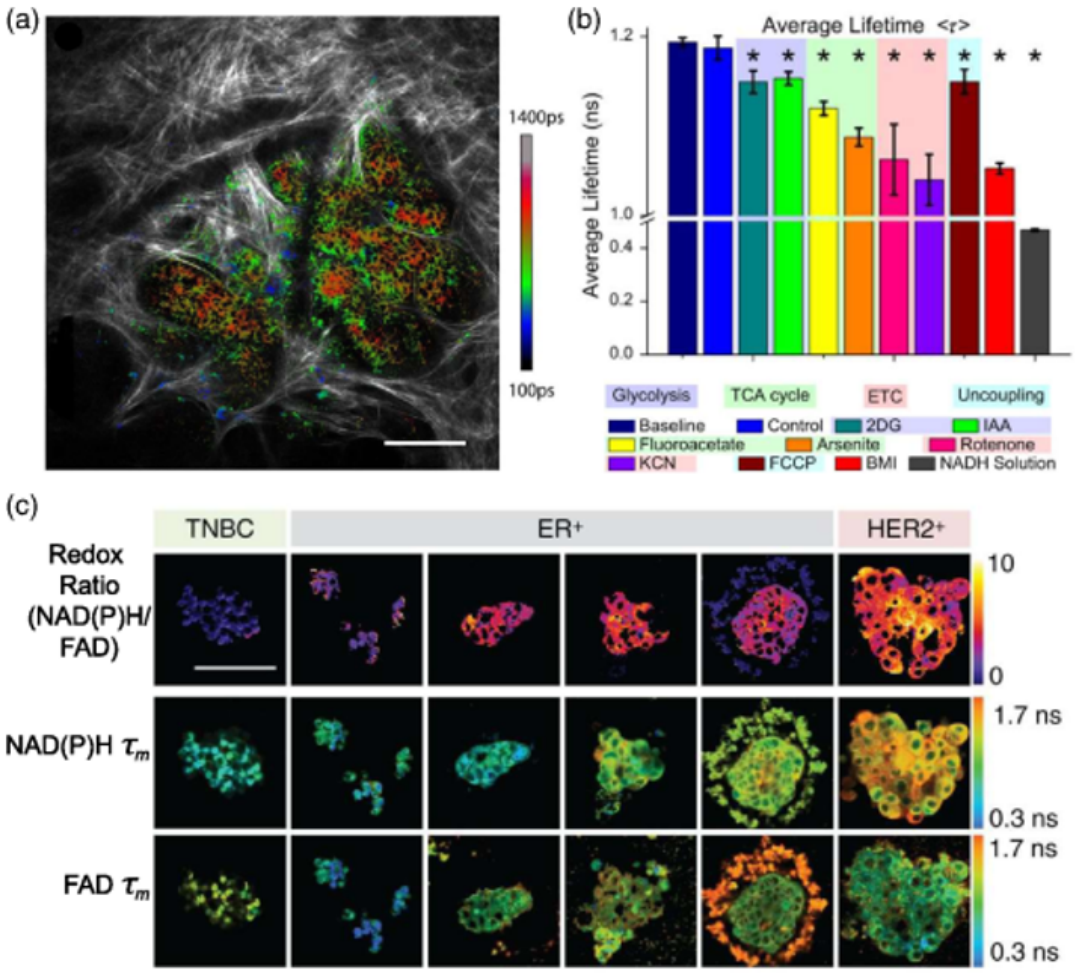

Figure 1.5: A representation of results generated by FLIM analysis of endogenous fluorophores within a sample. (a) Endogenous fluorophore heatmap overlayed on collagen image (greyscale) of mouse mammary tumour, (b) shows relative lifetimes in solution and in rat brain *in vivo* of various molecules under different conditions and (c) shows the a measurement of metabolic activity and endogeous fluorophore lifetimes on tissue organoids. Reproduced from [98]

These lifetime measurements are independent of the concentration of fluorophores present in a sample. Therefore, FLIM provides a sensitive method for imaging of molecular function, interactions and local chemical environments.

FLIM requires expensive and highly specialised pulsed laser sources to excite fluorophores and subsequently detect them after time, τ, by use of specialised single-photon-counting detectors. The precise instrumentation used for FLIM will be discussed at greater length in Chapter 4.

1.3.6 Limitations in imaging with microscopy

Imaging in life sciences is tending towards increasingly large samples, such as 3D cell and tissue culture, whole organs and even entire animals. To image these most effectively, a large field of view (FOV) with sub-cellular resolution is required. However, most standard optical microscopes are limited by a trade off between the achievable size of the FOV and the diffraction-limited attainable resolution. This is due to the relationship between NA and magnification in conventional optical lens design and results in either being able to image a large FOV but not be able to resolve sub-cellular small objects, or being able to resolve these small objects but over a very small FOV. The FOV of a microscope is limited by a number of factors including objective lens, eyepiece and camera sensor size. The maximum FOV of a commercial microscope is generally found by reading the field number which can be read from the eyepiece or from some objectives. This number corresponds to the maximum FOV of the objective (or eyepiece) in the absence of magnification. For example, a field number of 20 would represent a maximum FOV of 20 mm. However, to calculate the whole FOV including the magnification, the field number needs to

be divided by the objective magnification. Therefore, the aforementioned hypothetical objective, would have a reduced FOV to e.g 1 mm if it was a 20× objective.

Many researchers overcome this problem by sequentially imaging small regions at high resolution and stitching and tiling these together to create a pseudo-larger FOV. However, stitching and tiling can introduce artefacts in the final image due to inhomogeneities in the illumination and stage drift over acquisition time, resulting in a checkerboard pattern across the sample [99, 100]. Additionally, stitching and tiling offers poor temporal resolution due to having to image and subsequently accurately stitch many images together. Therefore, it would be desirable to have a large FOV (low magnification) with subcellular resolution in order to capture sub - micron level detail over a large imaging area, or large volume of capture.

1.4 Optical Mesoscopy

A method of overcoming the resolution / FOV trade off discussed previously is to have a microscope with specialised optics which allow for large FOV imaging with sub-cellular resolution [101]. This space where imaging objects between the micro and macro scale with subcellular resolution is desired, is referred to optical mesoscopy. Optical mesoscopy generally uses low magnification, high NA lenses capable of imaging objects from mm to cm size while being able to resolve nm or μm. Techniques to achieve such a system are discussed in this section.

1.4.1 The Mesolens

The Mesolens is a novel optical microscope objective developed at the University of Strathclyde with the intention of imaging whole 12.5 day old whole mouse embryos with sub-cellular resolution. It has a unique combination of a low magnification ($4\times$) and high NA (0.47) multi-immersion objective lens [102]. The NA offered by the Mesolens is almost a 5 times improvement upon its conventional $4\times$ counterparts on the market [103, 104, 105]. The low magnification results in a lateral field of view of up to $6\ \text{mm}\ \times\ 6\ \text{mm}$, meanwhile the lens prescription allows a working distance of $3\ \text{mm}$. Because of its unusually high NA for the magnification, the Mesolens has an unprecedented lateral resolution of $0.7\ \mu m$ and an axial resolution of $7\ \mu m$ throughout the whole $108\ mm^3$ volume of capture. The fixed magnification of the Mesolens results in a large FOV image with its sub-cellular details being apparent when digitally zooming post-acquisition in software such as ImageJ [106], as is demonstrated in Figure 1.6. The Mesolens is chromatically corrected over the whole visible

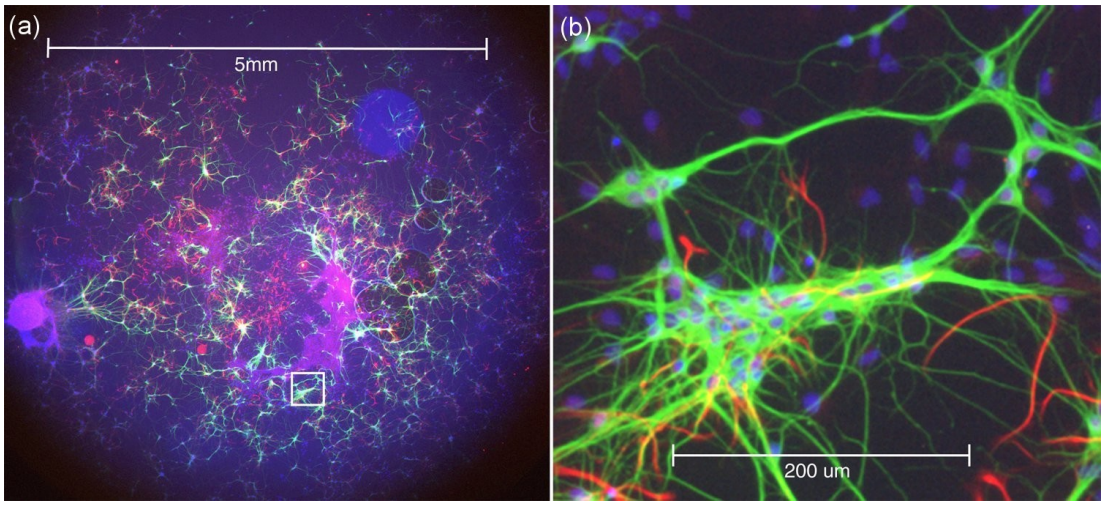

Figure 1.6: A widefield epifluorescence image of rat embryonic brain cells, nuclei stained with DAPI appear blue, neurons tagged with an Alexa-488 conjugated antibody show green, astrocytes tagged with an Alexa-546 conjugated anti-GFAP antibody appear red. a) full FOV image of the widefield Mesolens modality with b) a zoomed in region demonstrating the sub-cellular resolution capabilities by resolving nuclei (blue). Reproduced from [102]

spectrum covering a range of fluorophores from 400 nm to 700 nm.

The Mesolens currently operates in several modalities including widefield (epifluorescence, brightfield transmission)[102], confocal [107, 102, 108, 109, 110], multi-photon [111], standing wave [112], lightsheet[113] and total internal reflection fluorescence (TIRF) [114]. In this thesis, I focus on the use of WF epifluorecence and brightfield transmission mesoscopy as well as confocal fluorescence and reflection mesoscopy.

In widefield camera mode, the Mesolens uses a chip-shifting camera to obtain the full FOV pixel number required to perform Nyquist [16] sampling (approximately 20,000 pixels wide). This is possible with the equipped Vieworks camera which shifts the 29-megapixel camera chip by two piezoelectric transducer

mechanisms in a 3 $\times$ 3 array, occupying a total of 9 positions per acquisition, resulting in an effective 260-megapixel image. The process of image capture in camera mode takes approximately 5 seconds per frame, per channel, including the image reconstruction. Therefore, it is only possible to measure relatively slow dynamic processes with the Mesolens with its present camera.

In confocal mode, up to 3 photomultiplier tubes are used for multi-channel imaging. In confocal laser scanning mode, the Mesolens is similar in optical setup to a conventional confocal, albeit at a much larger scale. The Mesolens itself is composed of 15 separate optical elements measuring 55 cm in length and 6.3 cm in diameter [102]. Due to its unusually large size, the Mesolens is presently unable to be screwed into a conventional microscope, meaning that the microscope surrounding it must be custom built. The precise optical set-up of the Mesolens used in this thesis is introduced in Chapter 2.

With imaging such large images, comes equally large data sizes. A full volume 3-channel confocal stack sampled according to the Nyquist criterion would create a data size of almost 2 TB [102]. Therefore, powerful computational hardware and software is required in order to process the large data sizes. Large specimens with many pixels mean large acquisition times: a full single colour Nyquist-sampled confocal z-series with a pixel dwell time (the length of time the scanned beam remains in a unit of space equal to a single pixel in the image) of $1\mu s$ would take over a day to image. Adding in multiple channels and frame averaging means that it sometimes takes days to image full samples, which limits the technique predominantly to fixed samples.

1.4.2 Other techniques for optical mesoscopy

The Mesolens is not on its own in the field of optical mesoscopy. Several other specialised systems exist which compete with the high resolution and large FOV combination of the Mesolens [115, 116, 117, 118]. However, none have the same unique combination that makes the Mesolens suitable to this work - these points are discussed in more detail below.

Light sheet microscopy has often been thought of as a gentler approach to imaging than confocal laser scanning, while allowing for high resolution imaging of large specimens [119]. Light sheet microscopy illuminates a only a thin section (hundreds of nm to a few μm) of a sample using a laser beam which has been through a series of optics to produce a thin sheet of light [120]. It offers similar lateral resolution to confocal, however, its axial resolution is poorer due to the inherent properties of Gaussian optics causing divergence of the beam waist [121]. To its advantage, due to the nature of light sheet illuminating only a single optical section at a time, the effects of out of focus illumination are mitigated since only a single optical section is illuminated. The speed of acquisition of light sheet systems are much greater than CLSM where the beam must be scanned over the whole image plane. This gentler approach, with relatively lower phototoxicity and lower photobleaching means that specimens may be imaged over long time scales with high temporal resolution in a single plane; allowing for complex biological processes to be observed such as embryonic development [122, 123] and calcium signalling [124]. Meanwhile, large volume fixed and cleared specimens can be captured in 3D in order to

image structures such as whole organs [125, 126, 123] or embryos in development at specific moments in time [123]. Specialised light sheet systems capable of imaging mesoscale samples have been developed recently [127, 128], including the mesoSPIM (mesoscale Selective Plane Illumination Microscopy) [129]. The mesoSPIM is optimised for imaging optically cleared sections, using air objectives to allow for a wide range of clearing solutions to be used. This comes at the disadvantage of a relative resolution cost due to refractive index mis-matching and the use of lower NA objectives.

AMATERAS is a novel microscope system developed by Ichimura *et al*, first published in 2021 [115]. This system uses a low magnification 2× (0.12 NA) objective lens coupled with a 100 MP camera capable of imaging over 1 cm field of view, but with comparatively low theoretical lateral resolution of 2 μm. This system is able to image millions of cells during dynamic processes such as calcium signalling, but at a resolution which is almost 3 times poorer than the Mesolens. This system would be unable to resolve many bacteria which are often below 2 μm in diameter [130, 131], which makes it not favourable for study of infection at the bacterial level, but applicable to larger scale cell dynamics. Therefore, for our applications, particularly in Chapter 2, the Mesolens is the preferred option due to the ability to image over large spatial volumes while retaining the resolution capable of imaging single bacterial cells.

High-resolution ultrasound [132, 133], optical coherence tomography [134, 135] and magnetic resonance imaging (MRI) [136, 137, 138] have all been used to image whole organs, including whole tonsils. While these offer the ability to image intact whole 3D specimens, they all lack the spatial resolution to compete with the Mesolens which can resolve sub-cellular structures over a similarly large FOV.

1.5 Bacterial biofilms

Leeuwenhoek was the first to observe bacteria, which he initially referred to as "*animalcules*" [139]. He described microorganisms which attach and grow on surfaces which were later described as biofilms, however other microscopists at that time could not reproduce the resolution provided by his microscopes and so doubted his discoveries [69]. Later studies of surface-associated bacteria in the 20th century showed that the bacteria that grew attached on surfaces were phenotypically different from those that existed as planktonic single cells, verifying Leeuwenhoek's earlier observations [140, 141].

Decades later, researchers employed electron microscopy to examine communities of bacteria, showing a polysaccharide matrix encasing bacteria [142]. In 1978, the first paper defining biofilms was published, explaining a mechanism allowing microorganisms to adhere to both living and non-living surfaces alongside the benefits that living in such a way present [143].

Biofilms are described as a community of microorganisms embedded within a self-secreted extracellular matrix comprised of extracellular polymeric substances (EPS) [144]. The EPS is formed of polysaccharides, proteins, extracellular DNA and RNA and lipids, forming a sticky layer around the community of bacteria, holding the cells both to each other and to an abiotic (non-living) or biotic (living) surface. Biofilms were historically described as surface-adherent aggregates of bacteria, however, this definition has recently been reshaped by Sauer *et al* [145]. The previous model [146] did not take into account the biofilm-forming capabilities of bacterial suspensions in liquid [147, 148], such as those found for example in the mucus of the lungs of patients with cystic

fibrosis [149] or human serum [150]. The new model of biofilm formation encapsulates most of the possible ways of biofilm formation *in vitro, in situ* and *ex vivo*, including attached and suspended aggregates which do not follow the traditional definition from the original model.

By forming biofilms, bacteria have an array of benefits. Some of the most well characterised benefits include:

1. Biofilms, due to their EPS, adhere well to surfaces, increasing persistence of the bacterial population [151]. Additionally, bacteria encased within this EPS are more resistant to environmental stresses, such as mechanical or chemical stress, low nutrient concentrations and antimicrobials, than planktonic bacterial cells [152]. The cells within biofilms also often exhibit increased resistance to antibiotics [153, 154, 155].

2. Mature biofilms have complex 3D architecture, with spatial gradients of nutrient availability and oxygen, allowing for distinct micro-environments catered towards survival of the community [108].

3. By forming communities and micro-environments within, sub-populations within the community may form [156]. This effectively splits labour between different groups within the biofilm, increasing the ability of the biofilm to persist in unfavourable environments.

4. Biofilms are known for exchanging genetic material between different cells of the same and different species [157, 158, 159, 160]. This facilitates the survival of bacterial populations within the biofilm as the bacteria which posses a fitness advantage will transfer their genetic traits to allow the community to adapt to new or changing environments, including enhanced antibiotic resistance.

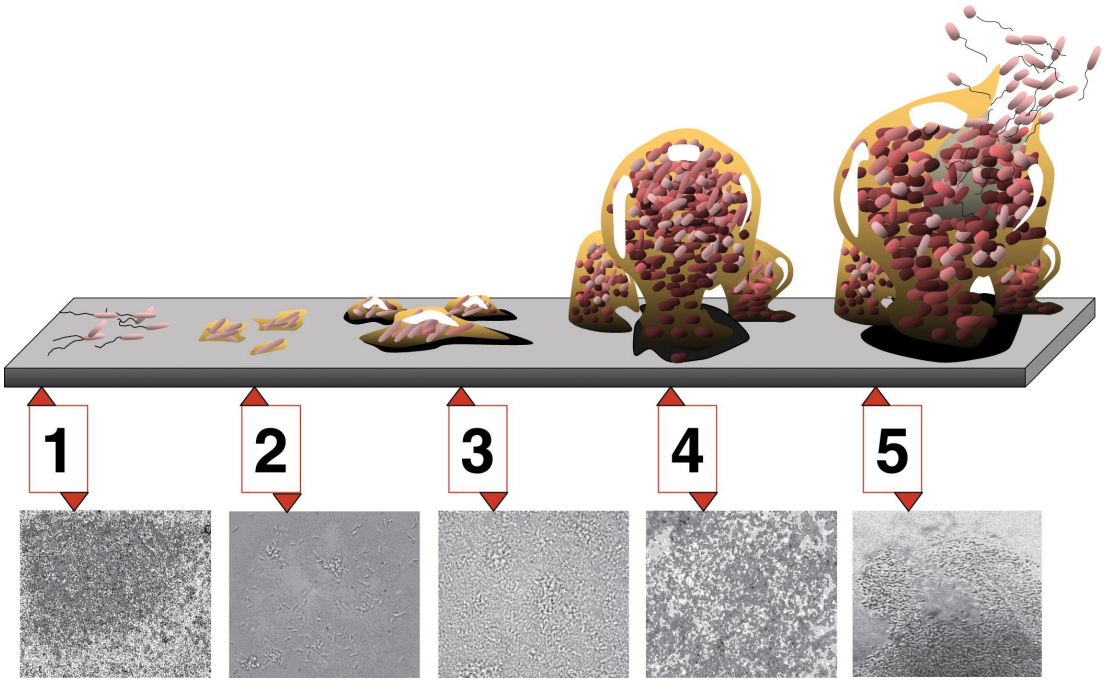

Figure 1.7: Overview of the growth and dispersal of bacterial biofilm according to the model of [146].Stage 1) Initial attachment where a single planktonic bacteria lands on surface, stage 2) Irreversible attachment where bacteria adhere to each other and to the surface, stage 3) Maturation 1 where bacterial colony grows and divides to form biofilm, stage 4) Maturation 2 where the biofilm is formed and stage 5) Dispersion, where bacteria shed from the biofilm to facilitate the formation of more biofilms elsewhere. Reproduced from [161]

1.5.1 Gram-positive and Gram-negative bacteria

Most bacterial cell walls are comprised of peptidoglycan, a large polymer composed of sugars and amino acids which is unique to bacteria [162].

Bacteria can be broadly split into two categories based on the structure of their cell walls: Gram-positive and Gram-negative [163]. Gram-positive bacteria have cell walls which are composed of a thick peptidoglycan later [164], whereas Gram-negative bacteria have a comparatively thin layer of peptidoglycan but also have a lipopolysaccharide outer membrane [165] which is absent in Gram-positives. This is demonstrated schematically in Figure 1.8.

This characterisation is based on a staining procedure developed by Christian Gram in 1884 which allowed him to classify almost all bacteria into two distinct groups [166]. In this protocol, crystal violet dye is retained within the thick cell walls of Gram-positive bacteria. Next, cells are treated with Gram's iodine solution, which acts as a mordant to retain the crystal violet solution within Gram-positive cells. Ethanol is then used as a decoloriser, dehydrating the cell wall causing it to shrink and tighten. This retains the crystal violet solution within the thick-walled Gram-positive bacteria, but the thin cell wall of Gram-negative bacteria is unable to retain the dye and it leaks out. The cells are further stained with safranin. As such, Gram-positive bacteria will appear purple and Gram-negative bacteria will appear reddish-pink.

1.5.2 Biofilm infections

The first medical study involving biofilms was published in 1982 by Marrie *et al* [170], who found biofilm infection on a pacemaker removed from a patient suffering from bacteremia (the presence of bacteria within the blood)

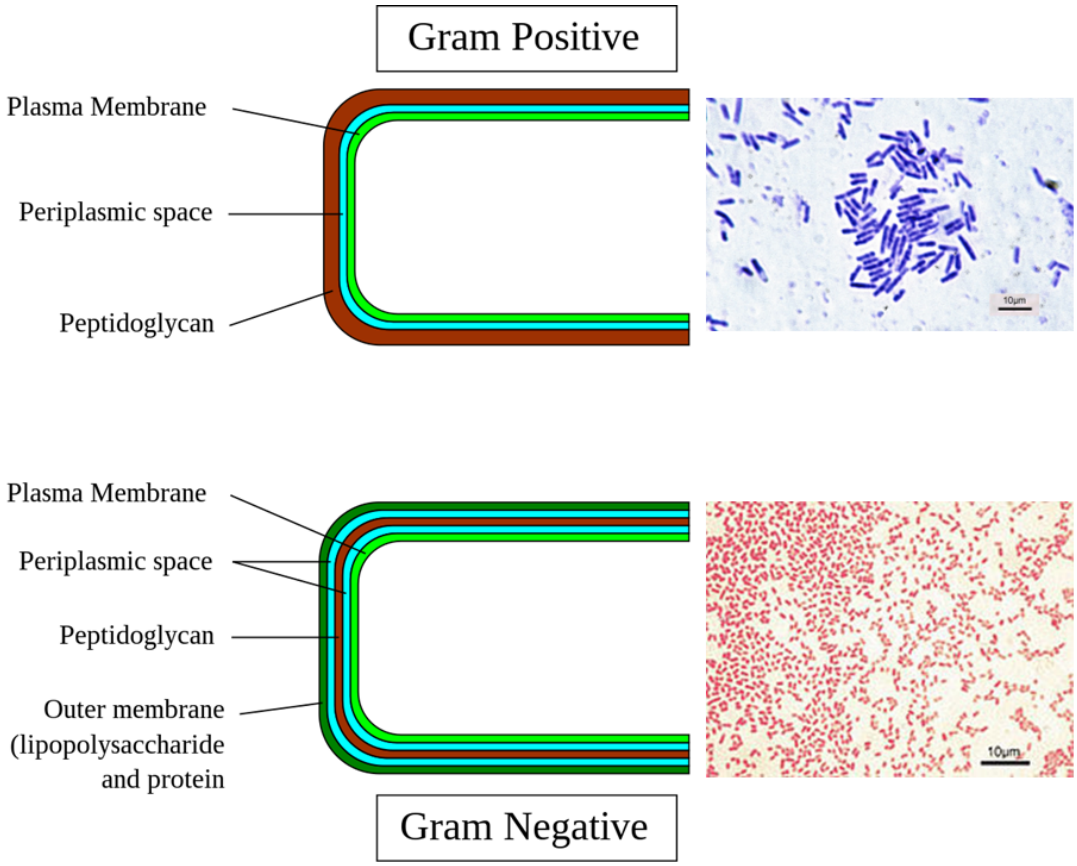

Figure 1.8: Gram-positive and Gram-negative cell walls with representative images of their Gram stain. Left: schematic depicting Gram-positive cell wall (top) and Gram-negative cell wall (bottom) (reproduced from [167]). Top right: Gram-positive *Bacillus. subtilis* with purple staining (reproduced from [168]). Bottom right: Gram-negative with reddish-pink staining (reproduced from [169]))

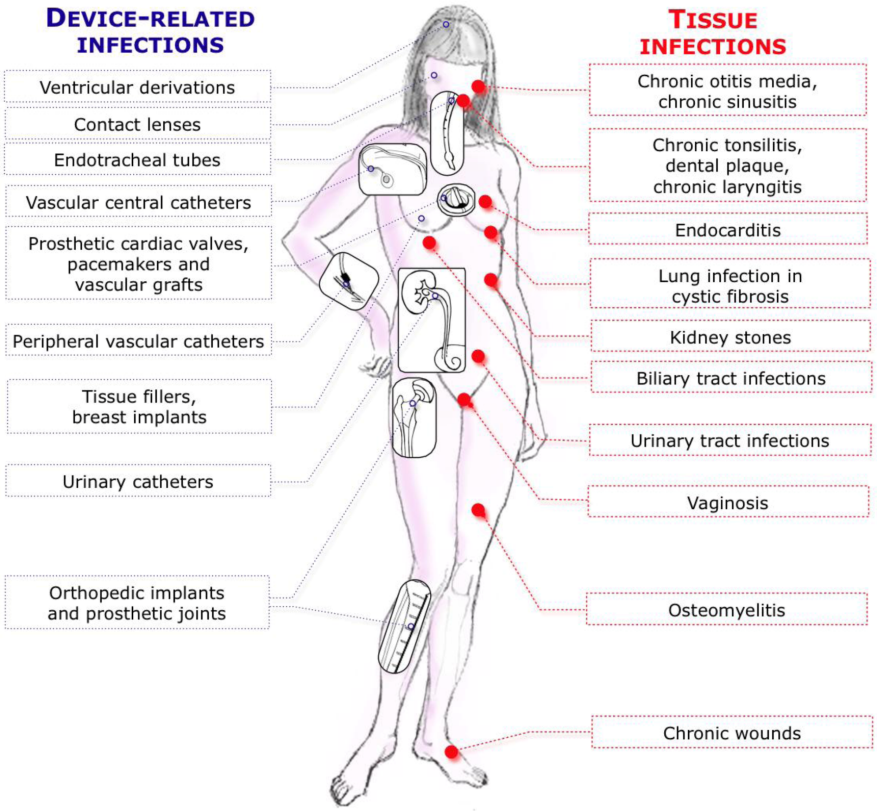

Figure 1.9: Overview of most commonly studied biofilm-associated infections in medicine. Reproduced from [175].

[171]. Since then, the biofilm-forming capacity of many bacterial species involved with infections have been extensively studied including *Pseudomonas aeruginosa* biofilms in cystic fibrosis [172], *Escherichia coli* in chronic urinary tract infections [173], and *Staphylococcus aureus* in chronic rhinosinusitis [174]. Biofilms are commonly found in chronic diseases and infections, where they resist antibiotic treatment, explaining their persistence and resistance to treatment in these cases. An overview of the diseases involved with biofilms can be seen in Figure 1.9.

As discussed in the previous section, bacterial sub-populations in biofilms can be functionally different depending on their location, and are able to perform

cell-cell communication within and outwith their different sub-populations within the community. This evolved as a mechanism to sense and adapt to environmental conditions such as nutrient deprivation, stress and drug resistance [176, 177, 178]. It is this ability to sense and adapt to different niches that affords biofilms their virulence and persistence in clinical settings [179, 180].

There is an important difference between infection and colonisation. Pathogenic bacteria such as *P. aeruginosa* [181], *S. aureus* [182, 183, 184] and *Haemophillus. influenzae* [185, 186] are commonly found in asymptomatic hosts, and the detection of colonies of these bacteria within asymptomatic hosts is referred to as colonisation rather than infection. The switch to infection typically occurs when additional evidence of infection such as inflammatory responses or physical symptoms accompany the colonisation. The difficulty with studying biofilm-related infections is particularly obvious when considering that many studies have found biofilms within healthy patients as well as the infected patients. Therefore, efforts have been made to create specific diagnostic criteria for biofilm-related infections [153]: the biofilm must be surface associated, and the microbial aggregates causing localised infections must be resistant to antibiotic treatment despite the susceptibility of the biofilm species to the antibiotic in planktonic culture. However, as we know from the work of Sauer *et al* [145], the definition of biofilm requiring surface aggregation is changing, and it is possible that the diagnostic criteria for biofilm-related infections will also need to change.

Clinically, biofilm infections are important to study due to their increased persistence and recalcitrance to antimicrobial agents. Biofilms have been estimated to be involved with anywhere between 65% to 80% of infections [175]. They also confer resistance to host defences: the first instance indicating this

was shown by Lam *et al* in 1980 by an electron micrograph showing that clinical biofilms could be surrounded by antibodies and inflammatory cells but not necessarily penetrated by them [187]. More recently, studies have shown that phagocytic cells do not penetrate chronic wounds infected with *P. aeruginosa* and *S. aureus* biofilms [188], and that Immunoglobulin G, an antibody which makes up approximately 75% of serum antibodies in humans, fails to penetrate the biofilm matrix [189].

1.5.3 Antimicrobial resistance

As biofilms grow and develop, they form gradients of anoxic and acidic zones at their centres, often inducing dormancy in these central regions [190, 191]. This dormancy may account for some of antibiotic resistance seen in biofilms rather than the diffusion capabilities of the particular antibiotic itself [192, 193]. While the matrix itself may not fully inhibit the penetration of antibiotics into the biofilm, it can slow their diffusion. Additionally, biofilms can confer resistance due to differential expression of genes which are associated with antibiotic resistance by different sub-populations within the biofilm [194].

Biofilms have high numbers of persister cells within, making up approximately 1% of the biofilm population [154]. Persister cells are metabolically inactive, phenotypic variants of bacteria within the biofilm which are known to be highly tolerant to antibiotics due to their metabolic inactivity. These cells form in response to environmental stressors such as nutrient and oxygen deprivation and chemical stress [195]. The cells remain viable after antibiotic treatment, and have been shown to be involved with growth the biofilm when the level of antibiotic drops [196]. While antibiotic-resistant cells will grow in the presence of antibiotics, persister cells simply remain dormant but viable. The presence

of these cells within biofilms may explain the high recurrence rates of biofilm-related infections [197, 198, 175].

1.5.4 The Mesolens as a tool for investigating biofilms

The Mesolens has been utilised as a powerful tool for investigating biofilms in recent years. Rooney *et al* have used the Mesolens to characterise the presence of nutrient uptake channels in mature colony *E. coli* biofilms [108] at the single cell level over whole colonies due to the unique prescription allowed with Mesolens imaging. Bottura *et al* further characterised and quantified these channels and their morphologies on a variety of growth substrate conditions [109] and demonstrated the fractal nature of biofilm channels [199]. Furthermore, Baxter *et al* have been exploring the formation and morphology of dual species *Candida albicans* and *Staphylococcus aureus* biofilms, revealing that the *C. albicans* hyphae have structural roles [200].

1.6 The palatine tonsil

The paired palatine tonsils are located at the boundary of the mouth to oropharynx, as shown in Figure 1.10 A [201]. The position of the tonsils is at the shared entrance to the gastrointestinal tract and respiratory tract. This location at the entrance to these key systems implies their role as secondary lymphoid organs, providing defence against antigens which may enter the body through the oral and nasal cavities [202].

Waldeyer's ring, a ringed collection of lymphatic tissue located within the pharynx, comprises of the palatine tonsils, nasopharyngeal tonsils (adenoids),

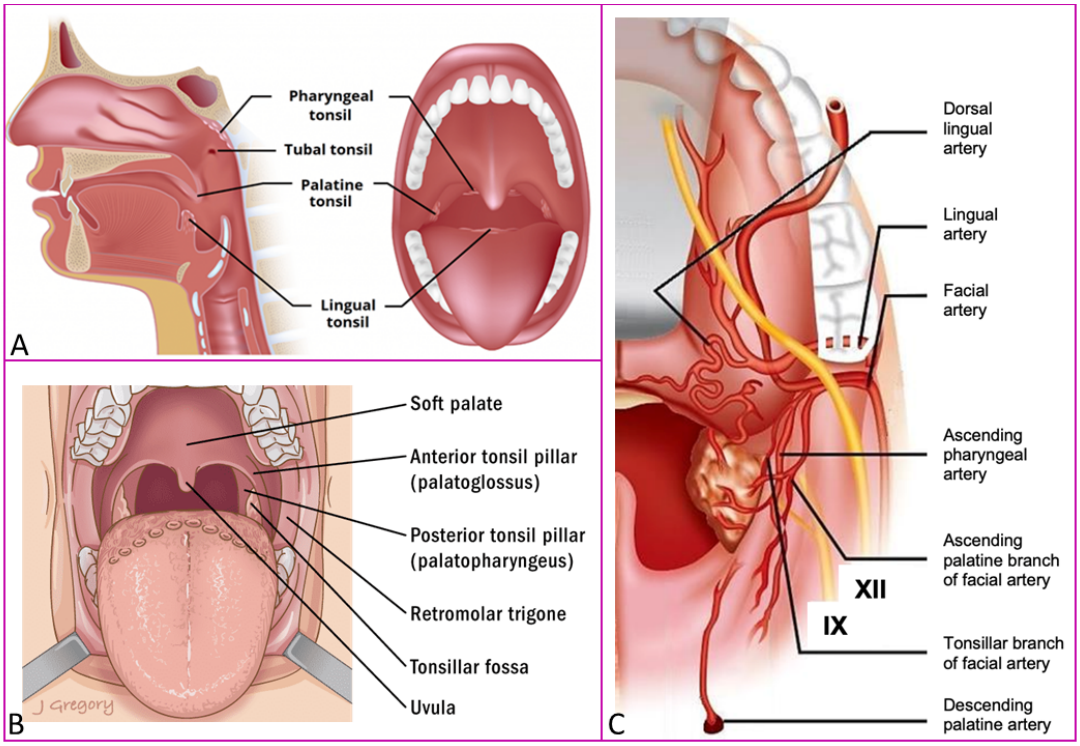

Figure 1.10: A) Location of the four tonsil sub-types in the Waldeyers ring, B) Location of the tonsils in relation to supporting musculature, C) Depiction of the vasculature delivery to the tonsil and surrounding fossa. Adapted from [201, 203].

paired tubal tonsils and lingual tonsil [204]. The palatine tonsils are situated between the palatopharyngeal arch and the palatoglossal arch of the oropharynx, as shown in Figure 1.10 B. The tonsillar fossa is supported by a muscular base consisting of the palatopharyngeal muscle, the palatoglossal muscle and the superior constrictor muscle to the pharynx, the latter forms their lateral wall. The blood supply to the palatine tonsil is provided by the tonsillar branches of either the palatine artery or the facial artery, alongside smaller arterial branches which have originated from the lingual and pharyngeal arteries, this is depicted in Figure 1.10 C. The palatine tonsils are covered by an outer epithelial layer, supported by a mass of connective tissues, lymphatic tissue and blood vessels, depicted in Figure 1.11 [205].

The palatine tonsil is most active in its role of immune defence in childhood, where they are physically their largest size. The size of the tonsils have been shown to be related to bacterial load and number of immune cells [207, 208]. There is also an age-related reduction in overall size of the tonsil [209]. The tonsil may be split into two categories: the external tonsillar tissues, which include the tonsil surface and crypts, and the internal tonsil tissues, which include the lymphoid follicles and extrafollicular regions.

The palatine tonsil is the most easily accessible lymphoid organ and as such is often used as a model for other lymphoid organs and for the study of immune response [206, 210, 211, 212]. As a consequence of its ease of access and removal, tonsillectomy remains one of the most common operations performed in paediatrics within the UK when treating afflictions of the tonsil [213]. A tonsillectomy is the complete removal of the paired palatine tonsils [214] and has been practiced for centuries [215]. However, the operation is not without risk with up to 20% of patients being readmitted to hospital within two weeks of

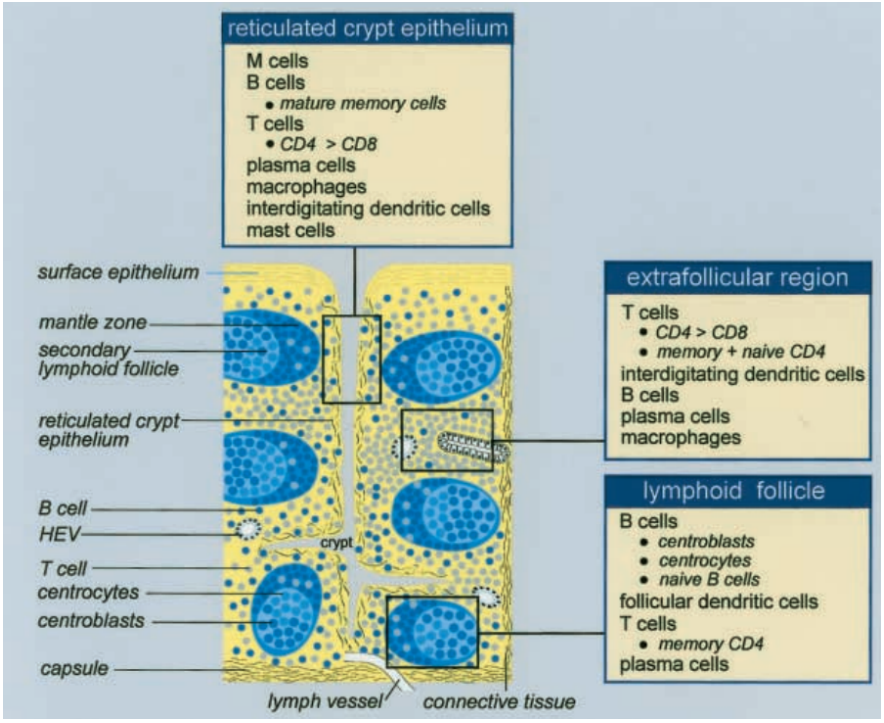

Figure 1.11: Schematic diagram of the human palatine tonsil and its cellular composition. Different cellular compartments are highlighted including the reticulated crypt epithelium, the lymphoid follicles and the extrafollicular region. Reproduced from [206] under license number 5678670545035.

the operation due to complications associated with bleeding [216]. Additionally, the benefit of tonsillectomy is contested among clinicians: it is argued that removal of a key component of immune defence in adolescence brings higher risk of infections further down the oropharyngeal tract [217, 218].

1.6.1 Tonsil Epithelium

Palatine tonsils are covered by a stratified squamous non-keratinising epithelium which makes up most of its external surface [206]. The squamous epithelium is supported by a 10 - 40 μm thick connective tissue layer comprised of

collagenous material [219]. This layer carries a network of blood vessels, separating the epithelium from the underlying lymphoid tissues. The collagenous materials in the palatine tonsil are thought to be primarily consisting of type III / IV collagen [204, 220], but are more generally referred to as simply *collagen* in most tonsillar studies.

The tonsil is covered in a network of 10-30 branched crypts which extend through the full tonsil thickness. The purpose of these crypts is to extend the surface area for immune defence in adolescence and enlarges the tonsil surface area [219]. Kawabata *et al.* showed that the tonsil crypts have both branches and anastomoses; connecting branches which connect one crypt to another [221]. The number, size and formations of crypts are highly varied between individuals.

The crypt epithelium is a modified form of the stratified squamous epithelium that lines the oropharynx and tonsil, with highly varying reticulation [206]. The reticulated crypt epithelium consists both of epithelial and non-epithelial cells such as lymphocytes, macrophages and dendritic cells. In contrast to the surface epithelium, there is a distinct lack of collagenous connective tissues underlying the crypt epithelium; limited to few fine fibers [219]. Crypts often contain degenerated cells, cellular debris, food, fungi and bacteria [222]. The structure of the crypt epithelium is largely affected by its proximity to the underlying lymphoid follicles; the reticulated regions of crypt epithelium are infiltrated with lymphocytes and are responsible for antigen sampling [223]. Within tonsillar crypts, the epithelium is interrupted with specialised tonsil membranous (M) cells, resembling those of the intestinal M cells. These cells are important in immune defence by endocytosing antigens and transporting

through their membranes to exocytose them to intra- and sub-epithelial regions, where they come to contact with lymphoid cells [224, 225, 226]. While the percentage of tonsil M cells makes up only a small number of total tonsil epithelial or crypt cells, their functionality is optimised. Their position and function play a key role in immune surveillance, however, it also can provide a mechanism for infection as some pathogens are known to use M cells as host invasion sites [227].

1.6.2 Internal tonsil tissues

The tonsil core can be differentiated into two main categories: lymphoid follicles and the extrafollicular region.

Lymphoid follicles in the palatine tonsil appear as approximately round capsules seen just below the tonsil or crypt surfaces, as can be seen in Figure 1.11 [205, 206]. These are sites of strong immune importance: containing specialised subsets of cells involved with immune cell development and proliferation [228].

The extrafollicular region is comprised of T cells, interdigitating dendritic cells (IDT), macrophages and high-endothelial venules (HEV) which are necessary for the transport of immune cells from the blood to the tonsil [206] as is depicted in Figure 1.11. The extrafollicular region contains a myriad of cytokine-producing cells and is involved in antibody production [229]. The immune response of palatine tonsils will be discussed in greater detail in Chapter 3.

1.6.3 The use of models in the study of human disease

Common studies of infection use model organisms and / or model systems such as liquid cultures, synthetic fluids or animal models. However, various studies have shown that model organisms, animals in particular, may not represent how pathogens acts within a human host. One of the earliest examples of this was from Louis Pasteur: after infecting their model chickens with anthrax, the chickens remained alive and recovered well [230]. This initially caused confusion, but it was later discovered by Pasteur that the reason for this was the raised basal temperature of poultry (41°C as opposed to our 37°C). Thus, an experiment was conducted where the basal temperature of the birds was lowered to mimic that of humans by placing the chickens in a cold water bath, and the chickens no longer survived.

Newer studies have involved evaluating the current infection models for cystic fibrosis (CF) patients. Lewin *et al* studied 5 common models for the study of infection in CF, concluding that a modified CF sputum model had 90% accuracy when analysing gene expression in comparison to human samples [231]. When combining this model with a mouse model, one can identify 95% of the genes expressed in human-derived samples. However, even with these highly specialised models, it is not possible to create an exact replica of the human environment for infection studies. Therefore, it is desirable to study infection *in vivo*.

The ideal model specimen for any lab study involving human infection is human tissue. However, this is difficult to acquire. Additionally, whole tissue imaging studies are difficult to perform on unfixed tissue due to the tissue degrading over time [232, 233, 234]. A common workaround to this issue is

examining excised whole tissues or biopsies, by fixing and staining the specimens and examining them with histological methods. Typically performed on thin tissue sections, this is both destructive to the samples and gives little spatial information other than on a single plane. To best investigate infection, it would be desirable to examine freshly excised infected tissues, then stain and image a larger 3D volume. This would give *close to in vivo* results in an *ex vivo* environment, offering extended spatial information over the 3D tissue architecture.

In addition, most animal species do not have a tonsil that mimics that of the human tonsil. The sheep has palatine tonsils comprising of only 1-3 crypts [235]. The goat has more crypts than sheep but less than human, and more tonsil lobes than human. Oxen palatine tonsils are larger (4-5 cm in diameter) and are bifollicular like the human tonsil, however they do not have as many crypt invaginations [235]. The horse has a significantly different structure than most for the palatine tonsil, which appears as an elongated flat surface which is morphologically non-comparable to human tonsils [235]. Rabbits have monocryptic palatine tonsils, while tonsils from cats and dogs are void of crypts. It should also be noted that several inconsistencies have been noticed in the literature when reporting the presence of palatine tonsils in pigs: a 2011 study reported that pigs do not have palatine tonsils present [235], whereas others have noted their presence [236, 237, 238]. In short, there is no directly comparable animal model to use in the study of human palatine tonsil disease, and current tonsil organoids [239, 240] and tissue rafts [241, 242, 243, 244] are not yet comparable to human samples. Therefore, it was of upmost of importance within the work documented in this thesis to use human tissue.

1.7 Tonsillitis

The term 'tonsillitis' refers to any inflammatory process involving the palatine tonsils, but it more commonly refers to an infection of the palatine tonsils. Acute recurrent tonsillitis occur predominantly in school age children under the age of 16. Approximately 70% of tonsillitis cases are thought to be caused by a viral infection, with 30% being attributed to bacterial infections [245]. The bacterial infections may be caused by a host of different bacteria and are often polymicrobial, however, the most commonly isolated bacterium is *Streptococcus pyogenes*, or Group A Strep (GAS) [246, 247, 248]. Clinically, tonsillitis can vary in its presentation significantly between patients, but most common presentations include fever, pain, discomfort when swallowing and redness of the tonsils.

Biofilms are known to be present within infected tonsils. Chole and Faddis were the first to demonstrate this in 2003 [249]. Further evidence of biofilms in tonsillar diseases has been shown in both imaging based studies [250, 251, 252] and evaluating the biofilm forming capabilities of tonsil cultures [253, 254]. Biofilms in tonsil disease and the limitations of current studies will be discussed in greater detail in Chapter 2.

Acute recurrent tonsillitis (ART) is defined as seven or more episodes in a single year, five or more episodes a year for two years, or three or more episodes a year for three years [214]. A proposed reason for the recurrence of these episodes of infection is due to antibiotic-resistant bacteria [255, 256]. Presently, the only true cure for ART is the removal of the tonsils via a tonsillectomy. At the point of tonsillectomy, it is suggested that all tonsils which are being removed due to ART will have positive cultures for GAS, even if they are not

actively involved in the infection [257]. This may be due to the aforementioned poor biofilm clearing capabilities of antibiotics: animal models have exhibited surface proteins on GAS that resist tonsillar clearance [258, 259]. Despite these, in the UK it is not common practice to perform throat or tonsillar cultures on suspected ART patients; instead, a physical examination is performed. If patients exhibit the clinical presentations mentioned previously they are prescribed with penicillin, clarithromycin or erythromycin [260]. While these antibiotics are still widely proficient in treating GAS infections, an increased incidence in β-lactamase (an enzyme which break the β-lactam ring involved with β-lactam antibiotics) producing bacteria may warrant a change in prescribing [261, 262]. β-lactamase secreted by bacteria other than GAS may confer community-mediated resistance and protect GAS, with one study showing that β-lactamase producing bacteria were found in 82% of tonsillitis patients [263]. β-lactam penicillins target bacteria penicillin-binding proteins to block peptidoglycan cross linking in metabolically active bacteria, which leads to bacterial death [264]. By producing alterations in this binding site, species of bacteria can confer resistance to penicillin [265, 266, 267]. However, this type of resistance has not been reported in GAS. *S. pyogenes* does not acquire exogenous DNA, thus is less likely to acquire resistance [265]. Additionally, GAS are known to persist intracellularly in tonsil tissues, but penicillin has poor penetration into mammalian cells and thus these intracellular bacteria are at a distinct advantage to persist [268].

The only remaining absolute treatment of tonsillitis remains a tonsillectomy, which is the commonest paediatric operation performed in the UK [269]. Treatment of tonsillitis without the need for surgery is imperative. Surgery not only has risks such as bleeding [245] and anaesthesia-related complications [270]; it

is costly to the economy and has a high emotional burden on children and their families [271]. Moreover, repeated infections without effective treatment have a severe impact on children's learning and development, with days missed off school and normal socialising being missed due to illness [272]. In addition, repeated infections can lead to further medical complications such as peritonsillar abscesses and deep neck space infections [273]. Therefore, understanding the role of bacteria and biofilms in tonsillar infections and how they may be better detected or treated is timely and important.

1.8 Tonsil hypertrophy due to obstructive sleep apnoea syndrome

Obstructive sleep apnoea syndrome (OSA) relates to a collection of symptoms that present including snoring, mouth breathing and partial repeated airway collapse during sleep [274]. The average prevalence of this syndrome in paediatric patients is not exactly known but is estimated to be between 1-6% [275]. OSA can be a result of hypertrophied, or enlarged, adenoids or tonsils as well as from craniofacial abnormalities and other diseases [275]. It has a negative impact on the health and development of millions of children worldwide and is a risk factor in several diseases such as heart failure and hypertension [276, 277]. Histologically, tonsil hypertrophy is defined by hyperplasia of the lymphoid tissues and significant enlargement of follicles, however disruption of the tonsil epithelia may also be observed [278].

The tonsil microbiome of OSA patients has been shown to be different from that of ART. This has been documented in a metagenomics study by Galli *et al* [279], where they examined tonsil swabs taken from children who were suffering from ART or tonsil hypertrophy due to OSA. They noted that *Melaninogenica spp* was the most commonly occurring species in healthy tonsils, whereas *S. aureus* and *S. nigrescens* were most common in ART and *H. influenzae* and *H. parainflurenzae* in OSA. Other studies using standard culture methods and genetic sequencing techniques generally isolated *Streptococcal spp, Haemophilus spp* and *S. aureus* [280].

1.9 Research Aims

The work contained within this thesis aims to gain a deeper understanding of the factors which may be used to delineate between ART and OSA using advanced optical microscopy techniques.

Firstly, since biofilms are known to play a role in recurrent tonsillitis, I aimed to understand if their presence was greater in ART than in OSA. I also aimed to investigate whether the spatial distribution of biofilms throughout the tonsil was different between disease types, by using the Mesolens to sample fresh tonsil tissue over greater spatial scales than before. The 3D data volumes were quantitatively assessed using image processing techniques to extract information on the relative biofilm volumes present throughout the tissue.

Secondly, I aimed to determine whether it was possible to identify a reliable biomarker for ART. IL-17C is a newly discovered cytokine which is expressed predominantly by epithelial cells upon bacterial stimulation, whose presence had not yet been quantified in tonsil tissue. IL-1β is a pro-inflammatory cytokine whose presence in diseased tonsils is known, but its role in different disease types is currently unclear. Using immunoblotting, a standard molecular biology technique used to probe the protein concentrations cell and tissue samples, I aimed to determine if the expression of these cytokines at the protein level could be used as an indicator of disease. In addition to this, immunofluorescence was used alongside the Mesolens in order to gain understanding of the spatial distribution of these probes alongside their expression. This was quantified using area-based intensity measurements. Alongside these, a customised fluorescence *in situ* hybridisation probe targeting all bacterial species was used to determine the spatial distribution of bacteria within these samples

to determine if the spatial expression of the cytokines was dependent upon the distribution of bacteria and biofilms within the samples.

Finally, I aimed to see if endogenous fluorophores within fresh tonsil tissue samples could be used as an indicator of disease type. Using fluorescence lifetime imaging microscopy, I first determined the differences of lifetimes between fresh, frozen and fixed tissue to determine the differences in lifetime which may be apparent after additive fixation. Following this, sections of frozen tonsil were imaged using a fluorescence lifetime imaging system and the lifetimes generated were assessed to determine if the average lifetime of the endogenous fluorophores could be used as an indicator of ART or OSA. Additionally, the spatial differences in lifetimes were looked at to determine the lifetime profiles along tonsillar epithelia and core tissues.

Chapter 2

Multimodal optical mesoscopy for the study of biofilms in live tonsil tissue

2.1 Introduction

Little is known about the spatial location and size distribution of biofilms throughout the tonsil. Studies of the location and distribution of biofilms in tonsil specimens have thus far been limited to either high-magnification methods such as electron microscopy, which enables high resolution imaging but only from a tiny tissue volume, or lower magnification techniques such as light microscopy, which allow imaging of larger specimens but with poor spatial resolution. To overcome these limitations, I report the use of multimodal optical mesoscopy to visualize and quantify the number and spatial distribution of biofilms containing Gram-positive bacteria in fresh, excised paediatric tonsils.

First, I aimed to confirm the presence of predominantly Gram-positive bacteria using a combination of 16S colony PCR as well as Gram-stain imaging.

The multimodal mesoscopy methodology developed in this chapter supports simultaneous imaging of both the tonsil host and biofilms in whole mounts of tissue up to 5 mm x 5 mm x 3 mm with subcellular resolution throughout. A quantitative assessment of thirty-six tonsil specimens revealed no statistically significant difference between biofilm presence on the tonsil surface and the interior of the tonsil. This new quantitative mesoscale imaging approach may prove useful in understanding the role of biofilms in tonsillar diseases and other infections.

Sections from this chapter have been reproduced from [110]

2.1.1 Tissue Fixation

Fixation is the process of preserving biological cells and tissues in a life-like state, with as little change to the structures as possible [281]. There is no perfect method of fixation, so care must be taken by the researcher to choose the correct technique for their purpose.

There are two broad categories of fixation: chemical or physical [281]. Chemical fixation is generally achieved by immersion of tissue or cells in a chemical fixative (or by perfusing through the circulatory system of small mammals) [281]. Physical fixation encompasses methods including cryo-preservation and heat fixation [282, 283].

Chemical fixation typically occurs by one of two main mechanisms: cross linking or coagulation [284]. Cross linking involves the formation of covalent bonds between and within proteins, resulting in stiffened tissue which is resistant to decomposition [285]. Coagulation uses alcohols to dehydrate the proteins within tissues by replacing the free water in tissue, changing the tertiary structure of proteins by destabilization of the hydrophobic bonds [285].

The most commonly used chemical fixative in the study of tissues is formaldehyde [286]. In histology it is commonly used as a 10% neutral buffered formalin (NBF) solution, approximately 4% formaldehyde in phosphate buffer, pH 7. Formaldehyde solution works primarily by cross linking the residues of lysine. Paraformaldehyde is another common fixative based on its usefulness in long-term storage of samples and excellent tissue penetration [287]. Another is glutaraldehyde, however, the glutaraldehyde molecules are larger than those of formaldehyde and results in much slower tissue penetration [288]. Its distinct benefit is it may offer a more comprehensive fixation than formaldehyde:

glutaraldehyde is large and has two aldehyde groups, meaning it is able to cross link more distant protein pairs than the former. It is considered the superior fixative for electron microscopy methods, however, it has shown problems for immuno-staining [289].

While tissue fixation is a widely used technique in many biological studies, it is not without flaws. There are a number of changes that may be induced on tissues by fixation, including tissue shrinking [290, 291, 292, 293, 294] or swelling [295, 296, 294], and the tissue may become brittle [294]. Additionally, formaldehyde based fixatives are known to disrupt the mucosal membrane of some tissues, resulting in loss of structure and potential to dislodge mucosal biofilms [297].

At the time of writing, only one study could be found that used fresh tonsil tissues to study biofilm infection [250]. However, it is not entirely clear if they used fresh tissue for their microscopy assay or how promptly after excision it was used.

2.1.2 Fluorescently tagged antibiotics

Using fresh tissue in biological studies imposes some limitations on the fluorescent probes that it is possible to use for the study of bacteria or biofilms within. For example, Wheat Germ Agglutanin (WGA) can provide fluorescent gram staining of Gram-positive bacteria [298], however, it binds to tissues [299, 300] and fungi [301, 302, 303] so does not work for biofilm or bacterial *in situ* studies in mammalian hosts. Another common probe, Concanavalin A (Con A) effectively stains bacteria [304, 305, 306] as well as tissue and mammalian cells [307, 308, 309]. Thus, in order to stain bacteria within tissue, while not staining the tissue, a more targeted approach is needed.

Antibiotic tagged fluorophores are becoming more popular in studies involving probing of bacterial biofilms [310, 311, 312]. Many of these stains exist, covering a broad range of antibiotics. Vancomycin is an antibiotic which may be used to treat a number of infections caused by Gram-positive bacteria [313]. In a hospital setting it is generally considered a last-resort antibiotic, administered intravenously for treatment of complex skin and blood infections, including meningitis caused by methicillin-resistant *Staphylococcus aureus* (MRSA) [314, 315, 316, 317]. The cell wall of Gram-positive bacteria contains a peptidoglycan layer containing cross-linked polymers of N-acetylmuramic acid (NAM) and N-acetylglucosamine (NAG), providing structural rigidity [318]. Vancomycin is a glycopeptide antibiotic that has bactericidal effects by binding to D-alanyl D-alanine, inhibiting cell wall synthesis by preventing the synthesis and polymerisation of NAM and NAG [319]. This weakens the bacterial cell walls, causing leakage of the interior bacterial components, resulting in death. Few bacteria confer resistance to vancomycin, especially so when in a biofilm. Thus, vancomycin was considered an appropriate choice for this work.

Vancomycin BODIPY FL (V34850, ThermoFisher Scientific, USA) is a green-fluorescent analog of vancomycin, with a single BODIPY dye per vancomycin molecule. Alongside an appropriate tissue contrast, this conjugate provides location information of bacteria and would indicate the presence of Gram-positives within the tissue.

2.1.3 Polymerase Chain Reaction (PCR)

Polymerase chain reaction (PCR) is a common lab technique which is used to make millions, or billions, of copies of a specific sample of DNA [320, 321]. This allows for rapid exponential amplification of a very small region of DNA

to a sufficient quantity to study. The large number of copies is required both to account for losses during PCR processes and to increase the probability of detecting the genetic region required.

Most PCR procedures rely on thermal cycling, exposing reactants to repeated cycles of heating and cooling. A general schematic overview of the PCR process is depicted in Figure 2.1 Specific primers must be designed to target the DNA of interest PCR reactions. The PCR process requires thermostable DNA Taq polymerase whose function is make new strands of DNA after the denaturation step in thermal cycling. This step uses a heating phase to split double stranded DNA into single strands, to complete DNA replication. Taq polymerase [323], like and DNA polymerase, requires primers to make more DNA. A primer is a short sequence of nucleotides (ATGCs) which provide a starting point for DNA synthesis. Two single stranded DNA primers (approximately 20 base nucleotides in length) are typically used in PCR: these two primers are known as forward and reverse primers and they bind to the flanking regions of

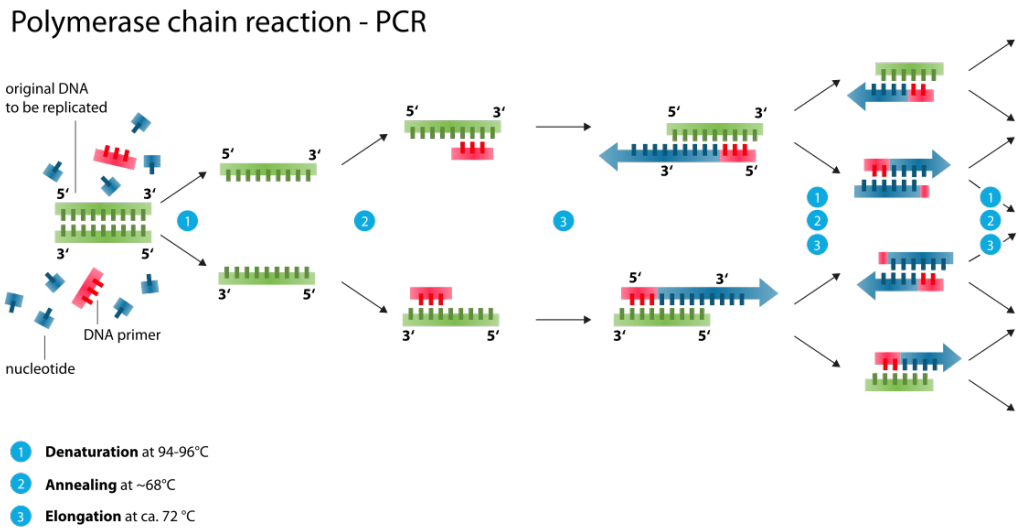

Figure 2.1: Overview of PCR thermal cycling process. Reproduced from [322]

opposite strands of the template DNA by complimentary base pairing (annealing), to ensure maximum amplification of the given target. Once primers have bound to template, they are extended by Taq polymerase, copying the region that lies between both primers. These steps are repeated, or cycled, between 25-35 times to exponentially produce copies of the target DNA for amplicon sequencing.

The 16S sequence of the bacterial genome is a conserved region within all bacterial species and has been exploited for its ability to distinguish between bacterial species and strains due to polymorphisms within the gene [324, 325, 326, 327, 328]. It is commonly used in medical microbiology settings due to its relative low cost compared to standard phenotypic identification methods [329, 330]. The high degree of conservation between species is thought to be due to its important role in cell function, playing a role which is involved in defining the positions of ribosomal proteins [331]. When probing a sample for the 16S region, primers are typically chosen which target the highly conserved regions at the beginning of the gene and then at the 540 bp region or the whole gene [332, 333]. The variability of the sequence between these points is what is used to delineate between species. The 16S rRNA gene sequence has already been determined for thousands of species, making its use as an identifier simple. The largest databank of genetic sequences, GenBank, contains close to 100,000 16S rRNA gene sequences alone [332, 334].

2.1.4 Evidence of biofilms in palatine tonsils

Antibiotics are routinely prescribed to patients presenting with tonsillar diseases such as acute recurrent tonsillitis with the aim of eradicating bacterial

infection [335]. However, tonsillar diseases are becoming more resistant to antibiotics due to the persistence of bacteria through the formation of biofilms. Biofilms are communities of bacteria encased in a protective matrix, and they are known to be more resistant to antibiotic treatment than planktonic bacteria [336].

Imaging studies have confirmed the presence of biofilms in tonsil tissue but data are limited because tonsils are too large to study with a conventional microscope. In children (0 – 16 years), mean tonsil volume is 1.5 ± 0.9 cm^3 [337]. At small spatial scales, Chole and Faddis [249] used a combination of light microscopy and transmission electron microscopy in combination with absorption contrast agents to study biofilms in fixed tonsil specimens. Their work showed strong anatomical evidence for the presence of biofilms in chronically diseased tonsils, but their method was limited, visualising only a single biofilm with light microscopy at high optical magnification. Also, the absorption contrast staining methods used in their work rely on chemical fixation of tissues prior to imaging, which causes tissue shrinkage and distortion of both host and bacterial structures that can complicate morphometric analysis [338, 339]. Diaz *et al* [250] evaluated the performance of both absorption staining and fluorescence staining using brightfield transmission microscopy and confocal laser scanning microscopy for the study of biofilms in pediatric tonsillar disease. Their findings suggest that biofilms are present in diseased tonsils. As with the work of Chole and Faddis [249], imaging was performed at high optical magnification ($100\times$) with additional digital magnification (resulting in images of up to $400\times$) and imaging was only performed within very tiny subregions of the whole tonsil. Quantitative studies of biofilms in tonsils have been performed with light microscopy and electron microscopy methods but

the small imaging volumes possible with these methods have thus far offered only very few insights into the size or location of biofilms in the tissue [249, 252, 251].

In sum, little is currently known about the spatial extent and location of biofilms in tonsil tissues because of limitations in imaging technology, yet this information could prove vital in helping to identify biofilm burden and disease pathogenesis.

2.1.5 Imaging tonsils across spatial scales

At larger spatial scales, optical coherence tomography has been used to image excised human tonsils and has proven successful for identifying different tonsil tissue components including epithelium, dense connective tissue, lymphoid nodules, and crypts [135]. This method relies on scattering for low-contrast imaging of structures, and features such as biofilms could not be discriminated from the tonsil host. Additionally, although imaging of tissues several millimetres in size was possible the spatial resolution of the images was considerably poorer than that possible in the light microscope studies previously discussed, with a reported resolution of tens of microns. Another technique offering a large imaging volume is magnetic resonance imaging (MRI) [340, 138]. However, the resolution of conventional clinical MRI is around 1-2 mm [341], which is too poor to resolve small biofilms. Specialized high-resolution MRI setups, such as that of Herrmann *et al* [342], have increased the resolution but only to around 100 μm. MRI solutions offer poorer resolution than optical coherence tomography, but both techniques lack the molecular specificity required to identify biofilms in tissue.

2.2 Methods

Throughout this chapter, I refer to tissue locations in two distinct ways:

1. Surface: containing the tonsillar epithelia and openings to tonsillar crypts. This is the region which is first exposed to pathogens arising from oral exposure. See section 1.6.1 for more information.
2. interior: contains interior tonsil tissues including tonsil crypt epithelium (referred to as crypts) and core regions (containing extrafollicular region and lymphoid follicles. See section 1.6.2 for more information.

2.2.1 Tonsil acquisition

This study was approved by Biorepository Management Committee of NHS Greater Glasgow and Clyde, UK (Biorep 548). The institutional review board approval (Biorep 548) was awarded to allow anonymous patient tissue use, waiving the need for individual level patient consent. No information of patient age, sex or socio-economic status was provided. Thirty-seven pediatric tonsils were collected after routine tonsillectomy at the Royal Hospital for Children, Glasgow, UK. Whole tonsils were rapidly transported in sterile saline solution (0.9% Sodium Chloride, Baxter Healthcare Ltd, UK) to the Strathclyde Institute of Pharmacy and Biomedical Sciences at the University of Strathclyde, Glasgow, UK, within 2 hours of excision from the patient. One patient was excluded due to having co-morbid ART and OSA, resulting in the data from 36 patient tonsils being shown.

2.2.2 Patient exclusions

All patients who participated in this study were under the age of sixteen, to adhere to the requirement of inclusion of only paediatric patients. Patients had either recurrent episodes of tonsillitis requiring tonsillectomy, or hypertrophied tonsils requiring tonsillectomy, according to the SIGN (Scottish Intercollegiate Guidelines Network) [343] and NICE (National Institute for Health and Care Excellence) [260] guidelines. Patients did not receive antibiotic interventions within two weeks prior to tonsillectomy occurring. Patients who presented with co-morbid tonsillitis and obstructive sleep apnoea were excluded from presented results.

At the time of collection and subsequent analyses, specimens were blinded to patient disease type. After completion of the analysis, the data was unblinded to disease type such that conclusions could be made.

2.2.3 Microbiological study

Methods to determine the bacterial species, confirming the presence of Gram-positive bacteria and biofilm producing capacity of bacteria isolated from tonsil tissue are outlined here. All media recipes are found in Appendix A.

2.2.3.1 Bacterial Culture

Swabs were taken from the tonsillar surfaces, crypts and cores of tonsils using a sterile inoculation loop. This was subsequently streaked onto agar plates containing Nutrient Agar or Blood Agar then cultured aerobically or anaerobically. Bacteria was cultured aerobically in a static 37°C incubator until individual colonies were grown. Bacteria were cultured anaerobically in a static

anaerobic incubator at 37°C until individual colonies were seen. The capacity of bacterial strains isolated from tonsil tissues to form biofilms was qualitatively assessed by their phenotype displayed on plates.

2.2.3.2 Gram Staining

Initial checks on tonsils were performed to determine if bacteria remained on samples after A) transportation on public roads in saline and B) after fixation. To do this, a routine gram staining procedure was employed. A schematic depicting the process of sample acquisition and gram staining procedure can be seen in 2.2. Swabs were taken from the tonsils surface, crypts, core (after tonsillar bisection) and transport saline using sterile inoculation loops. These samples were then streaked onto a coverslip, and promptly heat-fixed using a Bunsen burner. After fixation, staining was performed. Coverslips were flooded with crystal violet solution for 1 minute and then gently rinsed with running tap water for 5 seconds. Coverslips then flooded with Grams Iodine solution, remaining for 1 minute then rinsed under a gently running tap for 5 seconds. Holding the slide at a tilt with tweezers, ethanol was washed over the coverslips for 1-5 seconds, until the run-off was clear. The coverslips were then flooded with safranin for 30 seconds, before being gently washed a final time under gently running tap water. Coverslips were allowed to air dry before being affixed to a slide for subsequent imaging.

2.2.3.3 16S Colony PCR

Three tonsils were used to determine the most commonly isolated bacterial species from tonsils. From each tonsil, 3 swabs were taken from the surface, 3 from the crypt and 3 from the core and cultured as previously described. One

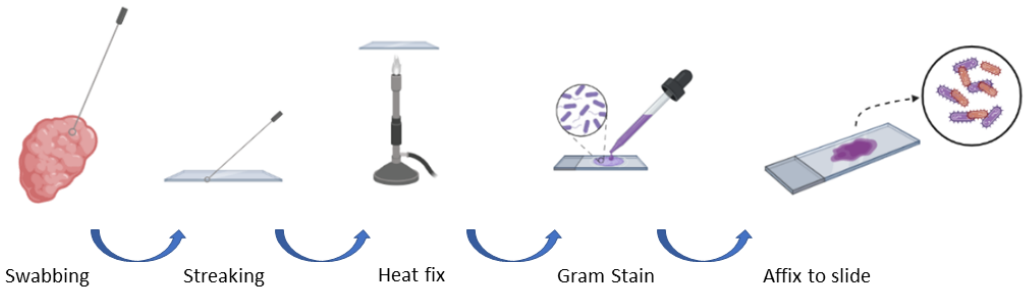

Figure 2.2: Figure depicting the process of sample acquisition and gram staining as described in section 2.2.1.3

colony each from the three most common biofilm morphologies were used for 16S colony PCR. 16S colony PCR involves amplification of the conserved 16S region in the bacterial genome and is a rapid method for verifying bacterial species. Bacterial DNA was extracted using a Wizard Genomic DNA purification kit following the manufacturers instructions (Promega, France).

A PCR reaction for sequencing was performed using universal 16S rRNA primers: forward (5' AGA GTT TGA TCC TGG CTC AG 3') and reverse (5' ACG GCT ACC TTG TTA CGA CTT 3') (UN-PR005-005 and UN-PR001-005, Eurogentec, Belgium). Amplification was performed in a 50 μL reaction volume consisting of 25 μL REDTaq® ReadyMix™PCR Reaction Mix (R2523, Sigma-Aldrich, USA), 2 μL forward and 2 μL reverse primers each at 10 mM concentration, 16 μL nuclease free water and 5 μL of sample DNA. Initial denaturation was performed at 94 °C for 5 minutes for one cycle. Then, 34 cycles of denaturation at 95 °C for 30 s, annealing at 60 °C for 30 s, extension at 72 °C 1 kb/min. A final single extension cycle is performed at 72 °C for 5 minutes. Reaction is held at 4 °C indefinitely at the end of cycling. DNA samples were examined by gel electrophoresis using a Bio-Rad gel dock system in a 1% (w/v) agarose gel with $100\mu g/mL$ ethydium bromide as the contrast agent in 1X TAE buffer.

10 μL of DNA was pipetted into wells in gel and gel electrophoresis was performed for 60 minutes at 100V. The gel was examined under UV excitation using a Syngene Bioimaging Ingenius trans-illuminator. A PCR cleanup was performed using a Wizard® SV Gel and PCR Clean-Up System (A9281, Promega, France) following the manufacturers instructions. PCR products were sent to Eurofins (Eurofins scientific, France) for sequencing. Sequencing results were assembled using SnapGene™ and were compared to a database of known sequences in nucleotide BLAST [344]

2.2.4 Investigating biofilms on whole mounts of *ex vivo* tonsillar tissue

2.2.4.1 Tissue preparation

Care was taken to minimise mechanical disruption to the sample by keeping it as still as possible during transport, and by using saline at an appropriate volume to only just fully submerge the tonsils. Tonsils were dissected using a fresh, sterile No. 27 surgical blade (12474070, Fisher Scientific, UK) to produce whole mounts of either the outer tonsillar surface or interior tonsillar tissue with volumes of approximately 5 mm x 5 mm x 3 mm

2.2.4.2 Staining biofilm on *ex vivo* tonsil tissue mounts

Gram-positive bacteria located within tonsil tissue were labelled using a Vancomycin-BODIPY FL conjugate (V34850, ThermoFisher Scientific, USA). The stain was diluted in dH_2O to yield a final concentration of 0.5 $\mu g ml^{-1}$. The dissected specimens were incubated in 5 ml of this working solution in 15 ml universal tubes for 60 minutes at room temperature. Specimens were covered with

aluminium foil to reduce bleaching by ambient light. After staining, the specimen was gently washed without agitation in Hanks Balanced Salt Solution (HBSS, Gibco, Fisher Scientific, UK), pH 7.7(3x, 1 min). Imaging of the tonsil specimens began within 3 hours of surgery.

2.2.4.3 Mounting of *ex vivo* tonsillar tissue

Individual whole mount specimens were secured in a custom-designed mount for long-term imaging with the Mesolens. A diagram of the disassembled specimen holder is shown in Figure 2.3. The specimen mounts were manufactured using Invar to minimise thermal expansion to the specimen holder and hence reduce any specimen movement during image acquisition. The top and bottom sections correspond to the immersion chamber. The bottom part of the chamber is comprised of an Invar plate that incorporates a glass window to form a well. The whole mount of tonsil tissue was placed into this well and was surrounded with HBSS as the imaging mountant. A 70 mm x 70 mm type 1.5 coverslip (0107999098, Marienfeld, Germany) was placed atop the specimen and bottom plate, avoiding bubbles in the HBSS mounting medium. The top plate of the specimen mount contained a 48 mm diameter hole in the top plate. The underside of this top plate incorporated a nitrile 'O' ring of 38 mm diameter to be held against the coverslip using screws at the exterior of the chamber. When in contact with the coverslip this arrangement created a well. After assembly, dH_2O was added into this well, creating a stable water bath within the ring with the coverslip as its base and the front of the Mesolens dipping into it. Surface tension proved sufficient to preserve the water column (up to 3 mm high) for extended periods (>18 hours).

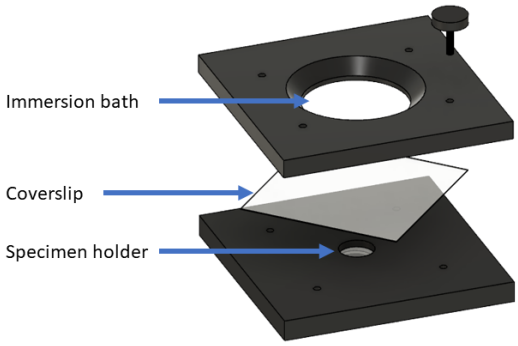

Figure 2.3: Computer-aided design drawing of the disassembled specimen holder and multipart chamber for long-term imaging of whole mounts of tonsil tissue using water immersion. The top and bottom sections correspond to the immersion chamber. The top plate includes a 38 mm diameter 'O' ring (not shown) that was brought into contact with the large coverslip. Screws (only one shown, though four were used in practice) brought the three sections together. Distilled water was added to the bath created by the contact of the top plate and coverslip of the specimen slide for long-term imaging.

2.2.4.4 Control for staining

Staphylococcus aureus (ATCC 43300) and *Pseudomonas aeruginosa* (ATCC 27853) were used as positive and negative controls for staining, respectively. Frozen stocks were streaked onto petri dishes with LB agar and incubated at 37°C for 48 hours. After incubation, a single colony was picked from each plate with a sterile inoculation loop, and diluted into 5 ml of LB broth in 15 ml universal tubes. These suspensions were left to incubate overnight at 37°C in a shaking incubator. The following morning, rebound cultures were created by making

a 1 in 100 dilution of overnight culture into fresh LB broth, then further incubating in 37°C shaking incubator for 3-4 hours. During incubation, custom mesolens imaging mounts [109] were UV and ethanol sterilised. Rebounds were diluted 1:1$\times 10^6$, seeded onto the LB plates and left to incubate at 37°C over 72 hours to ensure formation of lawns. Lawns were briefly stained for 10 minutes with 0.5 $\mu g ml^{-1}$ Vancomycin-BODIPY FL and briefly washed with water. *P. aeruginosa* is subject to detaching upon submersion, so time in liquid was optimised to be as brief as possible.

Biofilm lawns were imaged using the Mesolens in WF epifluorescence mode, with 490 nm excitation and 1000 ms exposure, in absence of immersion fluid in order to maintain *P. aeruginosa* lawns, at a slight resolution cost.

2.2.5 Microscopy

2.2.5.1 Conventional brightfield microscopy

Gram-stained bacterial slides were imaged on a conventional WF-epifluorescence inverted Eclipse Ti2 (Nikon instruments, USA) coupled to a PrimeBSI sCMOS camera (Teledyne Photometrics, USA) and images acquired using a 60×, 1.4NA PlanApo oil objective lens (Nikon instruments, USA). A built in white light LED was used for illumination. Red, green and blue gelatin filters were used to obtain full colour images using these methods.

2.2.5.2 Brightfield Mesoscopy

Brightfield mesoscopy was performed with the Mesolens correction collars set for water immersion (n = 1.33) to reduce spherical aberration, a schematic of the Mesolens in brightfield transmission mode is seen in Figure 2.4.

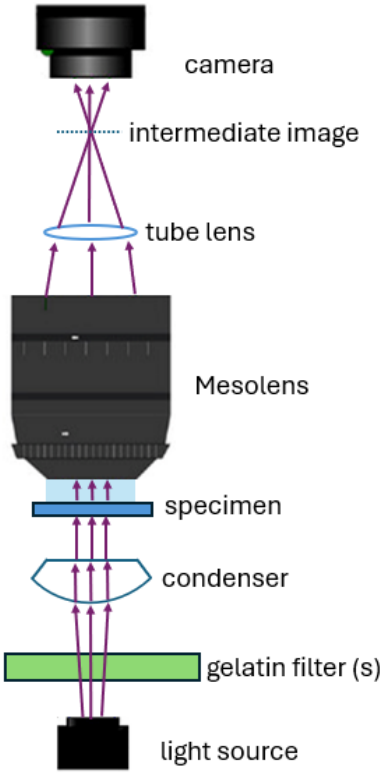

Figure 2.4: Schematic diagram of brightfield transmission with the Mesolens. A white light LED is used for illumination. A gelatin filter (red, green or blue) was used in the illumination path. A pixel shifting camera was used for detection. Images taken sequentially with red, green and blue gelatin filter to generate RGB images.

Brightfield transmission images were captured using a chip-shifting camera sensor (VNP-29MC, Vieworks, Republic of Korea). This system captures imaging by shifting the 29 megapixel CCD chip in a 3 x 3 array, resulting in an effective 260 megapixel image to capture full field of view of the Mesolens with high resolution. Three colour images were obtained with the use of gelatin filters in the illumination path.

2.2.5.3 Multimodal optical mesoscopy

A schematic of the multimodal setup using the Mesolens is shown in Figure 2.5. A 488 nm laser (Multiline Laserbank, Cairn Research) was used as an illumination source to produce reflection contrast images resulting from the refractive index boundary at the HBSS to tonsil interface, and the same laser was used to excite fluorescence from gram-positive bacteria labelled with Vancomycin-BODIPY FL. Reflection contrast was chosen over autofluorescence to map the tonsil tissue. Tonsil tissue is autofluorescent and has previously been used for the study of tonsil architecture [135] but the autofluorescence emission signal spectrally overlaps with the fluorescence emission of Vancomycin-BODIPY FL and therefore was not suitable for multimodal imaging of specimens in this work. The reflection signal at 488 nm was easily spectrally discriminated from the fluorescence from Vancomycin-BODIPY FL using optical filters, and this arrangement resulted in high contrast images in both reflection and fluorescence channels. A total laser power of 4 mW at the specimen plane was used for imaging of all specimens.

The Mesolens was used in point-scanning confocal laser scanning mode for imaging of all specimens. A 5 mm x 5 mm lateral field of view was scanned with a sampling rate of 2 pixels per micron to satisfy the Shannan-Nyquist criterion [16]. The pixel dwell time was set to 1 µs, and no frame averaging was performed. This led to an acquisition time of 100 s for a single optical section of the full 5 mm x 5 mm field.

The reflection and fluorescence signals were spectrally separated for detection using a 505 nm dichroic mirror (DMLP505R, Thorlabs, USA) that reflected only this wavelength, and transmitted longer wavelength fluorescence signals.

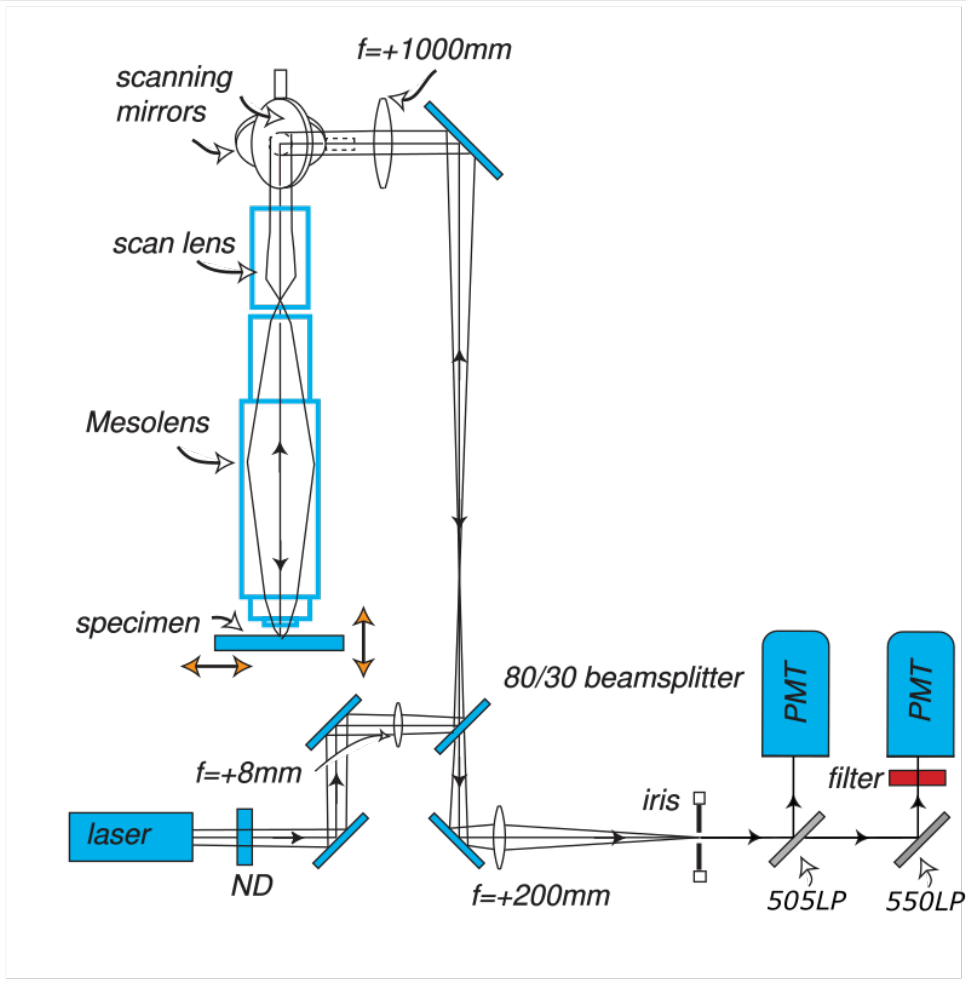

Figure 2.5: Schematic diagram of the multimodal point-scanning confocal Mesolens. A laser of 488 nm wavelength was used for simultaneous imaging with reflection contrast and fluorescence contrast. A single confocal iris was used in the detection path. Two photomultipliers (PMTs) were used for detection of the reflection (PMT 1) and fluorescence (PMT 2) contrast with 505 nm and 550 nm long pass filters, respectively. The filter in the detection path between the 505LP dichroic and PMT 2 was a 520 $\pm$ 35 nm band pass filter, and this served to block scattered laser light and transmit only fluorescence from Gram-positive bacteria labelled with Vancomycin-BODIPY FL to the photodetector.

The fluorescence signal between 505 nm and 550 nm was reflected by a second dichroic mirror (DMLP550R, Thorlabs, USA), and an additional band pass filter specified for transmission of 520 $\pm$ 35 nm (520/35 BrightLine HC, Semrock, USA) was used to reject any backscattered laser light and transmit only fluorescence. Two photomultiplier tubes (PMTs) (P30-01, Senstech, UK) were used for detection of reflection (PMT 1) and fluorescence (PMT 2).

Movement of the specimen along the optical axis for imaging at discrete z planes using the confocal method was performed using a computer-controlled z-positioning system (Optiscan II, Prior Scientific). To minimise data acquisition time the z-step size was set to between 3 μm and 7 μm, with smaller step sizes used for thinner specimens and larger step sizes used for thicker tissues. The system was controlled using an in-house, laser scanning software package, 'Mesoscan', designed to handle scanned images. Images were stored in the Open Microscopy Environment OME.TIFF format.

2.2.6 Image Processing

A single-colour optical section of the 5 mm x 5 mm field of view of the Mesolens with lateral sampling of 2 pixels per μm corresponds to a file size of just over 190 Mb. With multimodal imaging and millimetre thick specimens, the datasets generated from these specimens ranged in size from 30 Gb to 130 Gb depending on the complexity of the tonsil specimen surface and the overall depth of imaging. Datasets were processed and analysed using a 64-bit Windows server with two intel Xeon Silver 4114 CPU processors at 2.20 and 2.19 GHz and 1.0 TB installed RAM.

2.2.6.1 FIJI presentation and analysis

Images for presentation purposes were first contrast adjusted using the Contrast Limited Adaptive Histogram Equalization (CLAHE)[2] function in FIJI [106] with the default parameters (block size = 127, histogram bins = 256, maximum slope = 3.00). FIJI was also used to create dual-channel maximum intensity projections (MIP) of multimodal mesoscopy datasets that gave a two-dimensional overview of the size and location of biofilms relative to the whole mount of tonsil tissue.

Line intensity profiles were used to measure object sizes to determine both the size of bacteria and biofilms within images. The intensity along the profile was generated using the *plot profile* tool, and the full width at half maximum of the peaks taken as a measurement of object (bacteria / biofilm) width.

2.2.6.2 Imaris Image Analysis

To visualise and quantify data in three-dimensions, OME.TIFF files from the two channels were sequentially opened with Imaris and these data were subsequently converted to the proprietary Imaris file format (Imaris 9.8, Oxford Instruments). The 'Surfaces' tool was used to segment objects in each channel from the background to facilitate measurements [113]. Next, the 'Statistics' function was used to extract volumetric information from the image data. The volume of the tonsil imaged using reflection contrast was measured with this simple method, and no additional processing was required.

To evaluate the presence of planktonic bacteria in the tonsil specimens, I assumed a single spherical coccus of between 1 µm and 2 µm in diameter [345], and therefore calculated the volume of a single bacterial cell to be between

0.52 μm^3 and 4.19 μm^3. The number of discrete object volumes within this volumetric range in the fluorescence channel were counted using the 'Filter' tool in Imaris and these data correspond to the number of single bacterial cells in the tonsil specimens.

To assess the total biofilm volume, based on previous work which reported biofilms to be spherical bacterial aggregates with a minimum diameter of 20 μm [257] I calculated biofilms had a volume equal to or greater than 4180 μm^3. The number of discrete object volumes with this minimum volume in the fluorescence channel were counted using the 'Filter' tool in Imaris and these data corresponded to the number of biofilms in the tonsil specimens. These numerical data were extracted from Imaris and were exported to Microsoft Excel (Microsoft 365 Apps for Enterprise, Microsoft Corporation, USA) for further analysis.

To quantify the biofilm volume relative to the volume of the tonsil host, the ratio of the total biofilm volumes to the tonsil volume was calculated for each specimen from the tonsil surface (n=17) and tonsil interior (n=19) respectively. Plots of these data were generated using GraphPad Prism (GraphPad Prism v.8.0.2, GraphPad Software).

2.2.6.3 Statistical Analysis

Statistical analysis was performed using GraphPad Prism (GraphPad Prism v.8.0.2, GraphPad Software). All data were non-normally distributed and as such a Mann-Whitney U test was used to assess significance between two groups. Where data have been normalised for presentation purposes, it follows the convention of being normalised to appear between 0 and 1, with 0

corresponding to the minimum numerical value in the group and 1 being the maximum numerical value in the group.

2.3 Results

2.3.1 Fresh tissue over fixed tissue

Most studies assessing the presence of biofilm in tonsil tissues use fixed tissue. Therefore, I intended to do the same initially. I noted that PFA fixation caused extreme hardening of the tissue, and made it difficult to dissect for staining which is apparent from Figure 2.6.

Figure 2.6: Left: freshly excised tonsil after transportation in saline. Centre: Tonsil which has been fixed in 4% PFA has drastic colour change and severe tissue hardening. Right: tonsil fixed in Carnoys solution has been decolourised and hardened.

Then, sections of tissue which had already been dissected to the appropriate size for imaging were fixed, there was no biofilm after fixation, with very few individual bacteria present (Fig. 2.7 A). Literature suggests aldehyde fixation may disrupt and disaggregate mucous from tissue which would explain this. Therefore, Carnoys solution was attempted, however, as can be seen from figure 2.6, this fixative drained all colour from the tissues, and severely hardened it as well. Similarly to aldehyde fixation, no bacteria was left after fixing. This was confirmed by swabbing the tonsillar surface and performing a Gram-Stain as described in section 2.2.3.2 which revealed no stained bacteria, in fact, cells

did not even lift from the tissue when swabbing after Carnoy fixation (Fig. 2.7 B).

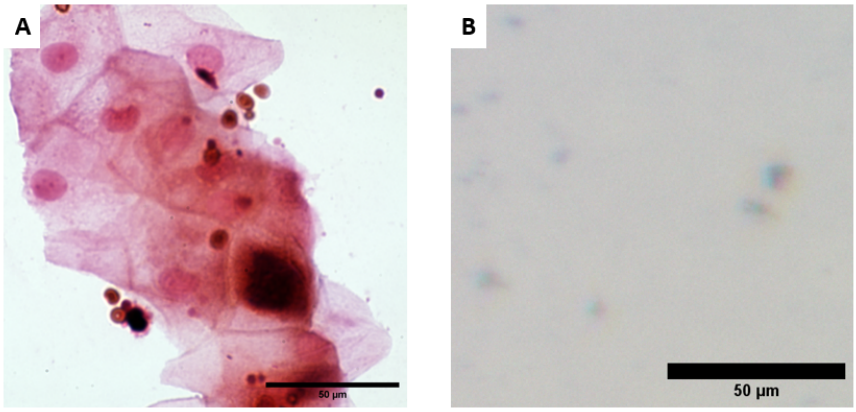

Figure 2.7: A) Swab from the surface of a PFA fixed tonsil sample. Tonsil epithelial cells can be seen alongside red blood cells, very few bacteria is present. B) Swab from the surface of a Carnoys fixed tonsil sample. Nothing is present within the sample, the tissue has hardened such that cells do not shed upon swabbing.

Since I found no method of fixation which retained the same level of bacteria which was present prior to fixation, it was decided to pursue the study on fresh, *ex vivo* tissue without the use of fixative.

2.3.2 Bacterial burden in paediatric palatine tonsils

2.3.2.1 Biofilm forming capacity of tonsil pathogens

Biofilm forming capabilities were assessed by visual inspection of plates grown from tonsillar swabs. An n = 3 patients were used for this study, with no knowledge of patient disease type. Every plate (n = 9 plates, from 3 patient tissues) had biofilms of varying morphologies growing after 48 hours, an example of growth is seen in figure 2.8. In the surface swab plates, a degree of alpha haemolysis (partial lysis of the red blood cells in substrate) can be seen

surrounding many of the colonies. This was also seen in the crypt swab plates but was mostly absent in the core swab plates with the exception of a few colonies.

The surface and crypt swab plates typically exhibit similar morphologies characteristic of bacterial biofilms. The core plates, however, have distinctly different morphologies which are typically larger and more varied. These results may indicate different bacterial species are present between surface / crypt and core, which is supported by literature. However, no conclusions about species were able to be drawn solely from visual assessment, so PCR was used for examination.

2.3.2.2 Gram-positive bacteria and biofilms predominate tonsillar tissues

Several (n = 3) colonies from each (n = 9) plate were taken for performing 16S PCR. The most common morphologies on the plate were estimated with visual inspection, with one of each of the top 3 most common morphologies

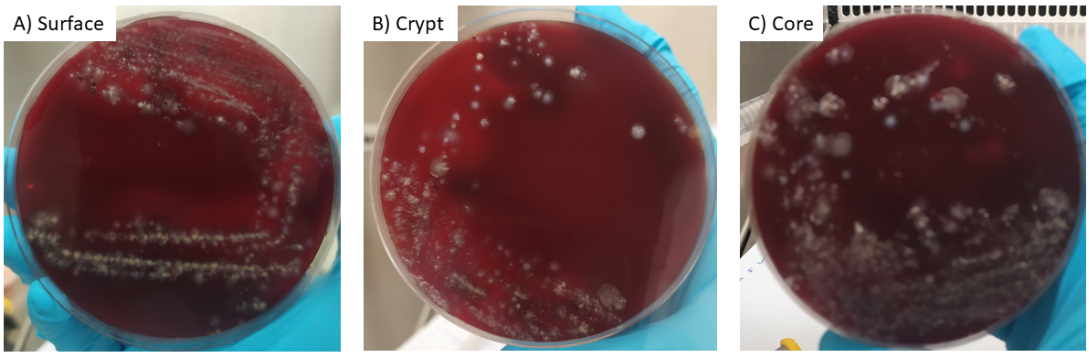

Figure 2.8: Blood Agar plates grown from swabs taken from freshly collected tonsil, to demonstrate the biofilm forming capacities of bacteria isolated from the tonsil. A) Biofilms grown from tonsil surface swab, B) biofilms grown from tonsil crypt swab, C) biofilms grown from tonsil core swab.

taken for 16S PCR. It was shown that almost all bacteria isolated and grown in the methods applied were gram-positive species (Table 2.1); *Streptococcal spp.* were the most common isolates. *Moraxella nonliquiefaciens* was the only Gram-negative bacterium isolated in this study.

Moreover, examination of Gram-stained tonsillar swabs qualitatively demonstrated distribution of Gram-positive and Gram-negative bacteria from tonsils. More than half of the detected bacteria within these images appeared blue / purple, indicative of gram-positive bacteria. Meanwhile, less than half were pink / red, indicating gram-negatives as is indicated in Figure 2.9. These images acquired using a standard brightfield microscope are limited by a small field of view while using a 100× objective lens due to the requirement for a high enough resolution to be maintained in order to resolve bacteria. Therefore, limited information can be obtained this way since only small populations of bacteria can be examined.

	Isolated from		
Species	Surface	Crypt	Core
Streptococcus pneumoniae		+	
Streptococcus pseudopneumoniae		+	
Streptococcus oralis	+		
Streptococcus mitis			+
Streptococcus anginosus			+
Moraxella nonliquiefaciens	+		
Staphylococcus aureus			+

Table 2.1: Results of 16S colony PCR performed from swabs obtained from human palatine tonsil (n = 27 colonies), and grown under nutrient conditions described in 2.2.1.4. A '+' indicates from which tonsil swab location a particular bacterium was cultured from.

2.3.3 The Mesolens as a tool for high-throughput screening of tonsillar swabs

To overcome the limits imposed by the high magnification lens used in the conventional system in section 2.3.2.2, swabs were examined with the Mesolens. Figure 2.10 demonstrates this well, showing a gram stained tonsil swab using the full field of view of the Mesolens.

By drawing line profiles across bacteria within the image using Fiji and measuring the FWHM of the peaks, it was determined that individual bacteria could be resolved within the Mesolens images, as demonstrated in Figure 2.10. With several purple and pink objects shown to be between 1 to 2 μm in diameter which is indicative of bacterial cells. By imaging over this much increased FOV with subcellular resolution, the throughput of imaging clinical swabs is

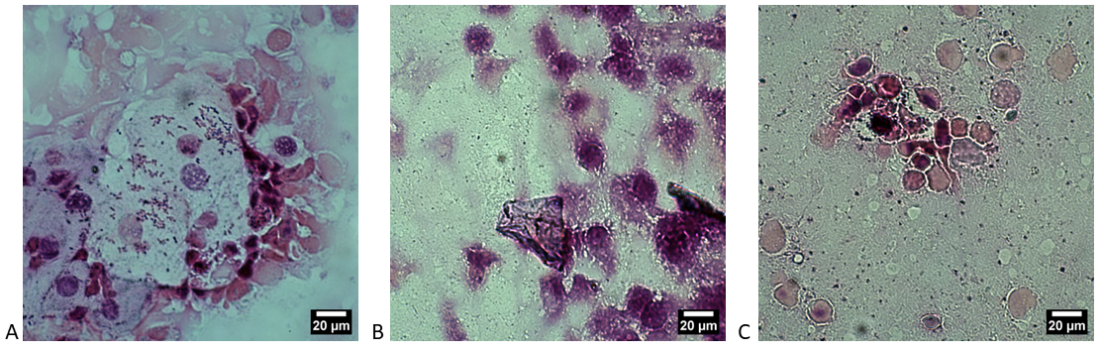

Figure 2.9: Brightfield transmission image obtained by use of RGB gelatin filters in the detection path of Gram-stained swabs obtained from tonsils where Gram-positive bacteria appear purple and Gram-negative bacteria appear pink. A) Gram-stained tonsil surface swab containing both Gram-negative and Gram-positive bacteria as well as tonsillar cells. B) Stained tonsil crypt with tonsillar cells as well as mostly Gram-positive bacteria. C) Tonsil core with some tonsil cells and bacteria appearing mostly Gram-positive.

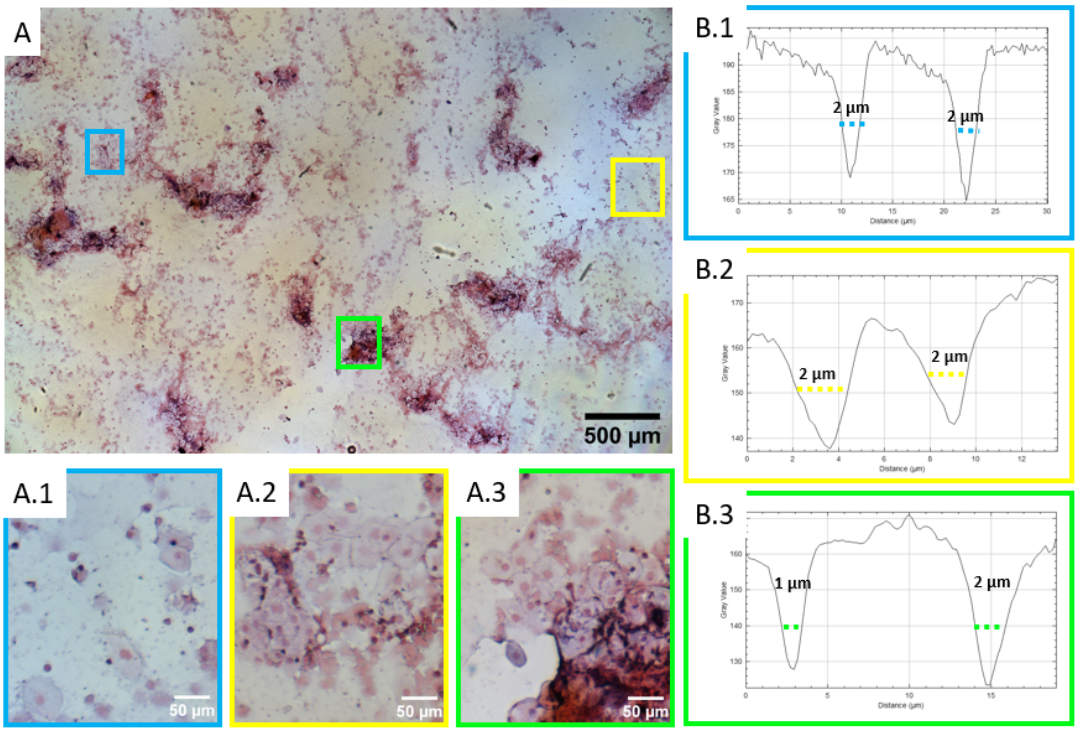

Figure 2.10: A) False RGB brightfield Mesolens image obtained using gelatin filters in the excitation path. Tonsil swab was streaked onto a cover slip, heat fixed and Gram-stained. A (1 - 3) digitally zoomed regions demonstrate the presence of both Gram-positive and Gram-negative bacteria within swabs. B (1 - 3) corresponding line profiles of images A (1 - 3) taken over 2 bacteria per image. The FWHM of the troughs represent the drop in intensity where bacteria are present, each FWHM corresponds to 1 - 2 μm in size, indicating that they correspond to a single bacterium

.

much greater than that of a standard brightfield microscope. That is to say that within a single Mesolens FOV, a much greater region of the tonsil can be seen in comparison to standard brightfield techniques which would achieve similar resolution. Additionally, the increased FOV means a higher probability of detecting bacteria (or other clinical specimens) within the sample due to this increase in sampling area.

2.3.4 Multimodal optical mesoscopy: Imaging across spatial scales

2.3.4.1 Control for staining

Specificity of Vancomycin-BODIPY (VB) was assessed by staining of *P. aeruginosa* and *S. aureus* biofilms. *S. aureus* biofilms showed uptake of the stain after 10 minute incubation, *P. aeruginosa* did not, confirming the specificity of VB to selectively stain Gram-positive pathogens. This is evidenced in Figure 2.11

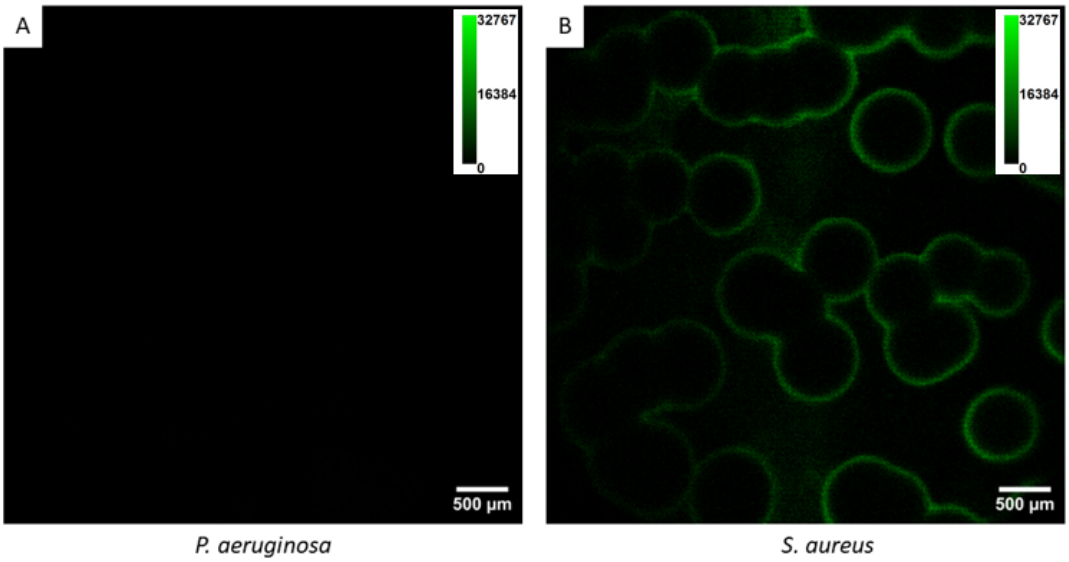

Figure 2.11: Biofilm lawns of A)*P. aeruginosa* and B)*S. aureus* stained with vancomycin-BODIPY FL to demonstrate specificity of the fluorescent antibiotic to gram-positive bacteria. Intensity scale shown. After only 10 minutes of exposure, the entire outer ring of gram-positive *S. aureus* biofilms have visible staining, whereas the gram-negative *P. aeruginosa* do not

.

2.3.4.2 Confirming presence of bacteria and biofilm on tonsillar tissue using multimodal optical mesoscopy

Using multimodal optical mesoscopy it proved possible to visualize the presence of individual bacteria and biofilms within an unusually large volume of fresh tonsil tissue.

Figure 2.12 shows a maximum intensity axial projection of a whole mount of tonsil tissue prepared for imaging. The tonsil was imaged as described in Section 2.2.4, using a 5 μm z-step size over a total axial range of 810 μm. These data took just over 4.5 hours to acquire. The tonsil tissue is shown in green and gram-positive bacteria are shown in magenta. The tonsil specimen extended beyond the imaged field, but even within this 5 mm x 5 mm lateral area it is evident that biofilm spread was highly heterogeneous in this specimen. A large biofilm extending over several square millimetres is shown close to the centre of the field. Several smaller discrete biofilms are also visible, and these are distributed unevenly within the tissue. A region of interest (ROI) is highlighted with a yellow box. A digital zoom of this ROI is shown in Figure 3(B). This ROI shows the level of spatial detail that is obtained at all positions in the maximum intensity projection dataset. A biofilm is visible adjacent to hundreds of individual bacterial cells. A white dotted line in 3(B) shows a further ROI that includes both the biofilm in the centre of the image and adjacent individual bacteria. The intensity of the magenta channel only is plotted in Figure 3(C). These data confirm that the diameter of this biofilm is approximately 25 μm and that individual bacteria between 1 μm to 2 μm in size are clearly resolved.

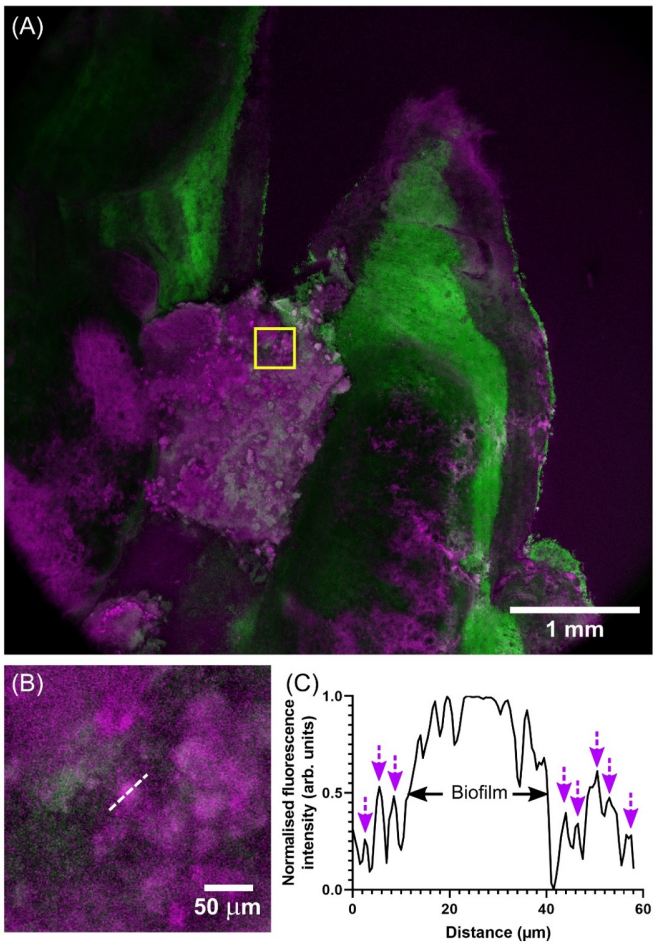

Figure 2.12: Multimodal optical mesoscopy provides an extended view of large biofilms in whole mounts of fresh tonsil with sub-cellular resolution. (A) Maximum intensity projection of a whole mount of fresh tonsil. The tonsil specimen was imaged over a 5 mm x 5 mm 810 μm volume using a z-step size of 5 μm. The tonsil tissue is shown in green, and biofilms are shown in magenta. Biofilms are unevenly distributed throughout the tissue volume. A yellow box shows a tiny region of interest. (B) Digital zoom of the region highlighted with the yellow box in 3(A). Several biofilms are surrounded by individual bacteria. A white dotted line highlights a sub-ROI through the centre of one biofilm. (C) Line intensity profile of the magenta channel only from the white dotted line ROI indicated in 3(B). The biofilm is measured to be around 25 μm in diameter and it is surrounded by individual bacteria of between 1 μm to 2 μm in size. The position of bacteria along this line ROI are indicated by magenta arrows.

.

2.3.5 Multimodal optical mesoscopy offers 3D visualisation of biofilm on tissues

Figure 2.13 shows a three-dimensional render of a different tonsil specimen to that presented in Figure 2.10. These data were obtained over a 5 mm x 5 mm x 1 mm imaging volume with a z-step size of 5 μm, which took just over 5.5 hours to acquire. In these data the complex three-dimensional topography of the tonsil surface (shown in green) is clearly visible with voids in the tissue corresponding to the opening of crypts. An example of a visible crypt is highlighted with a cyan arrow. The highly heterogeneous spatial distribution of gram-positive bacteria (shown in magenta) is clearly visible in three-dimensions. Without further digital zoom individual bacteria are not visible, but they are present and can be seen in the raw data (available for download). However, individual biofilms are present at this level of display zoom, both across the tissue surface and at the opening of tonsil crypts. An example of biofilms surrounding the mouth of a crypt is shown with a yellow arrow. Throughout the tissue biofilms appear as bright punctate magenta objects on the order of 20 μm to 200 μm in diameter. I note that these thick biofilms are frequently connected to thinner biofilms, which are more widely spread across the tissue surface. There are only a few regions where the green and magenta signals spatially coincide: this co-occurrence is visible as white areas. Areas of white would indicate that biofilm or bacteria are occurring intracellularly. Therefore, I observe that most bacteria or biofilms in these samples appear to be adherent to the tonsillar tissue, rather than embedded within.

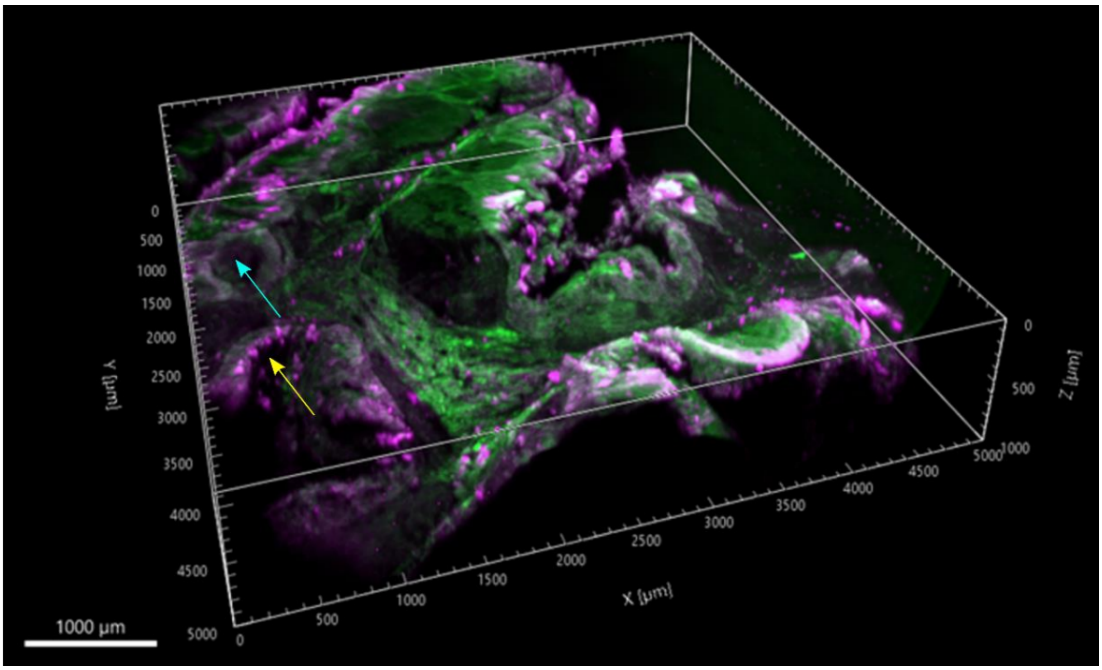

Figure 2.13: Three-dimensional render of a whole mount of fresh ex vivo tonsil. Tonsil tissue is shown in green, and biofilms are shown in magenta. The image volume is 5 mm x 5 mm x 1 mm, and this was obtained with a z-step size of 5 μm. The complex tonsil tissue architecture is clearly visible, with voids in the tissue corresponding to the opening of crypts, an example of which is highlighted with a cyan arrow. The spatial distribution of biofilms is heterogeneous, with biofilms of various shapes and sizes extending over the tonsil surface and lining the entrance to crypts: an example region showing biofilms surrounding the mouth of a crypt is shown with a yellow arrow.

.

2.3.6 Biofilm burden is almost equal between patient disease types and tissue location

Data from n = 36 specimens (n = 17 tonsil surface, n = 19 tonsil interior) was analysed as described using the methods in Section 2.2.5.1. Figure 2.14 (A) shows, biofilms were detected in all image datasets, with the minimum and maximum number of biofilms observed per sample being 58 and 1229, respectively. A larger number of gram-positive biofilms was measured in whole mounts of tissue from the tonsil surface with a mean of 481 biofilms compared to tissue from the tonsil interior with a mean of 339 biofilms. Data were not statistically significant. Figure 2.14 (B) shows the ratios of total biofilm volume to tonsil volume for image datasets obtained from the tonsil surface and tonsil interior. Specimens with both a high (close to 1.5 : 1) and low (0.001 : 1) biofilm volume were measured, with similar mean biofilm: tonsil ratios obtained for both specimens from the tonsil surface and tonsil interior and between disease states. These values were measured as 0.32 : 1 and 0.35: 1, respectively. I interpret these data to mean that irrespective of location in the tonsil the ratio of gram-positive biofilms to tonsil tissue is broadly consistent.

Figure 2.14.C shows the ratio of ART tonsil biofilms on interior (0.32 : 1) and surface (0.31 : 1) tissue. Once again, this demonstrates that there is very little difference in the mean ratio observed between spatial distributions. Similar results are seen in Figure 2.14.D where the interior (0.34 : 1) and surface (0.32 : 1) ratios are once again similar. I then compared the aforementioned ratios between disease state (i.e ART vs OSA 'surface' and ART vs OSA 'interior'), finding no statistical significance between the ratios. This indicates that regardless of patient condition or sample location, biofilms are spread equally

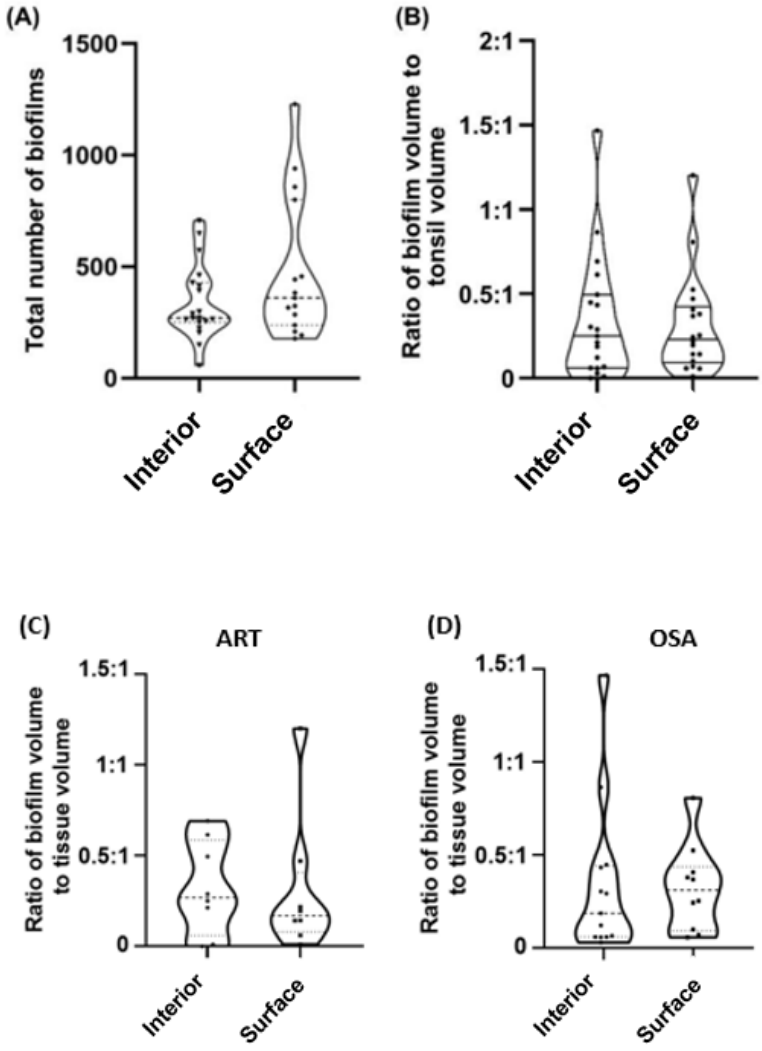

Figure 2.14: Quantitative analysis of biofilms in whole mounts of fresh tonsil. (A) Measured total number of biofilms. Biofilms observed in all (n = 36) specimens. Each point on the graph represents a single patient. Dotted lines correspond to median and 95% confidence intervals. A larger number of biofilms was measured in tissue from the tonsil surface (mean = 481 biofilms) compared to interior (mean = 339 biofilms). Data were not statistically significant. (B) Ratios of total biofilm volume to tonsil volume for image datasets obtained from the tonsil surface and tonsil interior. Similar ratios were obtained for both regions, with mean values of as 0.32 : 1 and 0.35 : 1 for the surface and interior, respectively. Looking at individual disease types: (C) Ratio of ART tonsil biofilms on interior (0.32 : 1) and surface (0.31 : 1) tissue. Data were not significant. (D) Ratio of OSA tonsil biofilms on interior (0.34 : 1) and surface (0.32 : 1) tissue. Data were not significant (Mann-Whitney, $\alpha = 0.05$).

throughout the diseased tonsils.

A representative set of tonsillar tissue maximum intensity projection images which demonstrate different biofilm and tonsillar morphologies can be seen in Figure 2.15. Figure 2.15.A shows surface specimen, a small collection of biofilms in the order of approximately 100 μm^2 can be seen lining a crypt, whereas the biofilms are more thinly distributed within the tissue in Figure 2.15.B. Figure 2.15.C biofilm can be seen spread over the tonsillar surface and lining the entrance to crypts. Whereas a singular biofilm which permeates deep into a tonsillar crypt takes up most of the biofilm volume in Figure 2.15.D, with additional smaller biofilms found towards the bottom of the image. In Figure 2.15.E, biofilm can be seen covering over half of the tonsillar surface, with biofilm infiltrating deeper into the tonsillar tissue which is not apparent in the maximum intensity z-projection. In Figure 2.15.F, a large, deeply penetrating biofilm is seen to be taking up most of the tissue on the bottom half of the image, with further biofilm lining bisected crypts towards the top.

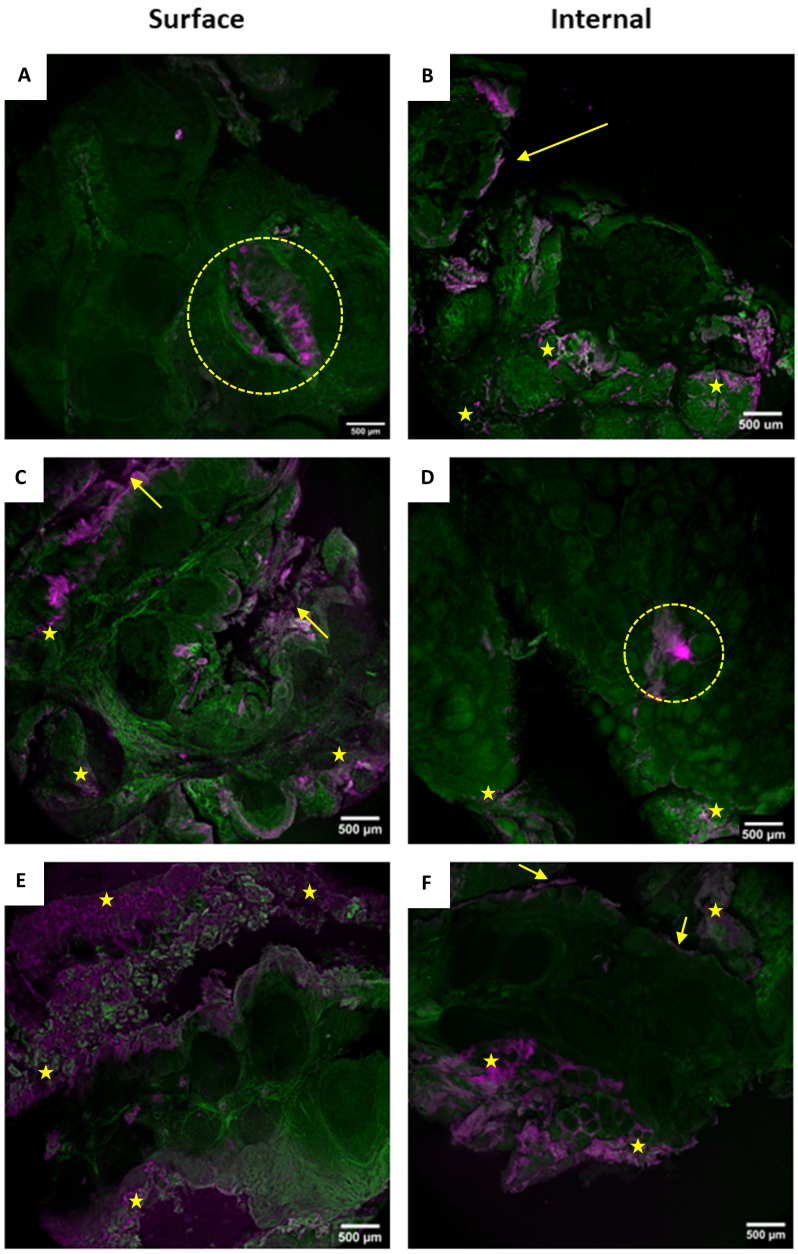

Figure 2.15: Representative images of varying morphologies, presented as MIPs. Tissue appears in green while bacteria and biofilms are magenta. A) Surface specimen with low biofilm presence: small, connected biofilms can be seen lining the opening to a crypt (dotted circle). B) interior specimen with biofilms distributed within the core tissues (stars) and lining a crypt (arrow). C) Surface specimen with biofilm lining entrances to crypts (arrows) and distributed across surface (stars). D) interior specimen with small volume of biofilm distributed throughout the tonsil (stars) and a large (order of 300 µm diameter) biofilm occupying a crypt branch (dotted circle). E) Surface specimen with large biofilm is spread over epithelium (stars). F) interior specimen with large biofilm distribution in interior tissue (stars) and lining a crypt (arrow).

2.4 Discussion

I have demonstrated multimodal optical mesoscopy for the visualization and analysis of biofilms in situ in multi-millimetre-sized whole mounts of fresh, *ex vivo* tonsil tissue with subcellular resolution. The results presented in this Chapter show that biofilms were present in all n=36 specimens imaged. This result is to the contrary of other studies including the work of Chole and Faddis [249] which have reported smaller positive outcomes. I attribute these findings to the greatly increased imaging volume with high spatial resolution that is possible with the Mesolens compared to other imaging methods. If I assume imaging of a whole mount of tonsil tissue using a conventional point-scanning confocal microscope equipped with a 20x objective this gives a calculated imaging volume of approximately 700 μm x 700 μm x 500 μm. By comparison, the Mesolens can image a specimen that is more than 300-times greater in volume. This increase in imaging volume considerably increases the probability of detecting biofilms – or even single bacteria – in these large specimens.

The analysis reveals little difference in the number of biofilms present in on the surface and interior of tonsil tissues, but the number of biofilms varies considerably between different specimens, with the maximum number of biofilms observed being 20$\times$ that of the specimen with the fewest biofilms present. Again, this measurement can only be made at present using multimodal optical mesoscopy. In addition, little difference in the number and volume of biofilms between ART and OSA has been shown, suggesting that biofilms may play a key role in both ART and OSA.

By using Vancomycin-BODIPY FL conjugate, I aimed to capture the presence

of all gram-positive bacteria within these samples. Vancomycin resistance is rare [346], so it has good activity against most commonly encountered gram-positives. While resistance to vancomycin is rare, especially in staphylococcal species, there are reports emerging stating that cases involving vancomycin resistant enterococci (VRE) are rising [347]. VRE strains are typically resistant to other antibiotics, and so would be unlikely to be captured by using an alternative fluorescently tagged antibiotic such as BOCILLIN. This being said, with the relatively low abundance of isolated VRE's in the UK [348, 349], this is not considered within this analysis.

By using the Mesolens, I aimed to image over a much larger volume than other studies involving tonsillar biofilms could achieve. Gram-staining allowed for the visualisation of Gram-positive and Gram-negative bacteria within tonsillar swabs which were streaked onto coverslips. Paired with sequencing results, it was confirmed that Gram-positive bacteria make up the majority of the microbiome of tonsillar tissues analysed in this thesis. Several studies have examined the tonsillar microbiota during ART and OSA episodes, noting differing bacterial abundances between studies and geographical location [350, 338, 280]. Hence, we aimed to examine the tonsils from the local Glaswegian patient cohort to inform staining. Using the Mesolens, it was possible image over $60\times$ the area of a lens with similar resolution [102]. This greatly increased the probability of detecting bacteria within a sample, especially if there was sparse distribution. Although detailed quantitative analyses was not performed on these slides as they were simply used as a screening aid for bacterial presence, using algorithms such as trainable weka [351] would be beneficial for determining the distribution of bacteria. Weka allows for the user to define classes of objects, and, in theory, it would be possible to define Gram-positive and

Gram-negative bacteria as two distinct classes and have additional classes for cell types which may be in the sample after swabbing. This way it would be possible to count the total number of bacteria within the slide and to determine the relative burden of each bacterial category. This could present itself as useful for both screening of bacterial swabs alongside other medical tests such as blood smears [352].

This work was performed with the aim to study gram-positive biofilms, but this methodology could be adapted to include the visualization and analysis of gram-negative biofilms in the tonsil host. For example, fluorescent BOCILLIN 650/665 (10246962, Fisher Scientific, USA) could be used to label both gram-negative and gram-positive bacteria, and the Vancomycin-BODIPY FL conjugate used could be used as a specific label for gram-positive bacteria only. The difference in peak fluorescence emission wavelength between these two labels is over 100 nm, and hence they would be compatible for simultaneous labelling and multimodal imaging. Another possibility is the use of fluorescence in situ hybridisation (FISH) for the direct visualisation of specific bacterial species. FISH has previously been applied for simultaneous imaging of five bacterial species in microscopic volumes of tissue [353]. However, while multimodal optical mesoscopy with FISH would enable species-level study of much larger specimens, FISH presently requires fixation and, as described previously, this may cause tissue distortion. It would also be possible to use an additional fluorescent label for the study of the tonsil architecture rather than using reflection contrast but given the large volume of the whole mount specimens this would soon become costly for imaging of more than a small number of specimens.

Although there are powerful open-source software tools such as BiofilmQ [354] and BASIN [355] for the analysis of biofilm image data, the large file sizes

of the Mesolens data are not immediately compatible with these resources. The utility of image analysis tools with general applications in biology and biomedicine such as DeProj [356] were also explored, but similar difficulties in working with large Mesolens file sizes were encountered. Imaris was used in this work for rendering and analysis of image datasets, but recognize the potential of napari [357] as an open-source alternative for future multimodal optical mesoscopy studies.

The standard treatment for ART is antibiotic medication but reports suggest that biofilms in tonsils may be eradicated by wiping the tonsil surface to mechanically disrupt biofilms [358]. While the complex architecture of tonsils includes crypts that serve as reservoirs for biofilms [249], this work confirms that biofilms can also be large and widely spread across the tonsil surface, covering areas extending many square millimetres in size. This new observation may prove useful in developing new cleaning protocols and antimicrobials that target biofilms on the tonsil surface.

The Mesolens has previously been used in point-scanning confocal fluorescence mode to study whole mature colony biofilms [108, 109], but this work reports the first application of the Mesolens to the study of fresh, ex vivo, human tissue. With proof-of-principle now established, this newly developed multimodal optical mesoscopy imaging method can be readily applied to biofilm research related to other areas of human health including diseases of the middle ear such as otitis media with effusion and wounds in skin [359].

2.5 Conclusion

In this chapter, several methods were used and developed to determine and quantify the presence of biofilms on ART and OSA tonsils.

First, the presence of predominantly Gram-positive bacteria was verified using 16S colony PCR on colonies grown from swabs of the tonsillar tissue after surgery. In parallel to this, swabs were streaked onto coverslips and stained with a Gram-stain to determine the distribution of Gram-positive to Gram-negative bacteria. These slides were imaged on a conventional brightfield microscope. To increase the throughput of imaging, this was scaled to brightfield using the Mesolens, to allow for a field of view of up to 5 mm x 4 mm to be seen per tonsillar slide. This was an increase of over 60$\times$ that of a conventional system with comparable magnification and allowed for rapid screening of bacterial Grams-status when compared to typical techniques.

A pipeline for the analysis of biofilms in fresh *ex vivo* tonsil tissue was established, using reflection confocal to visualised unstained tissue and a fluorescent antibiotic to visualise bacteria and biofilms. The specificity of staining was confirmed with lab-grown biofilm colonies demonstrating the specificity for Gram-positive bacteria. Biofilm abundance and spatial distribution was quantified using Imaris '*surfaces*' tool. Here it was shown that biofilm spatial distribution and relative abundance was independent of location within the tissue and independent of disease. This suggests that biofilms may play a larger role in OSA than previously thought. The high rate of biofilm presence (found in 100% of examined samples) may be explained by both the gentle sample preparation used within this study alongside the exceptionally large volume of imaging achievable with the Mesolens, meaning that the chance of

detecting biofilms in a single acquisition are high.

Chapter 3

IL-17C plays a role in the pathophysiology of Acute Recurrent Tonsillitis

3.1 Introduction

The previous chapter has established the presence of biofilms throughout the tonsil mass regardless of infection status. This post-surgical analysis is useful in the study of chronicity of infection, however, it does not aid in early diagnostics. The aim of this chapter was to determine if two interleukin's, IL-17C and IL-1β could be used as a biomarker for ART or OSA in patient tissues. This was carried out by using thinly sectioned tissue from both ART and OSA patients, and staining for both interleukin's alongside bacteria as well as by using conventional molecular biology techniques. Interleukin staining was performed using immunofluorescence to selectively target both interleukin's.

On the same tissue, fluorescence *in situ* hybridisation (FISH) was used with

a custom 16S eubacteria probe to stain for both Gram-positive and Gram-negative bacteria within the tissues. Brightfield transmission mesoscopy was used to image tissue, with widefield epifluorescence mesoscopy to image the interleukins and bacteria therein.

An open source image analysis pipeline was designed to determine the levels of expression of interleukin in the tissue relative for the surface and core tissues. Alongside this, an open source FIJI plugin was used to determine the colocalisation of interleukin's to bacteria to determine if the expression of either interleukin was spatially correlated with bacteria.

To compliment this work, Western Blotting was used on homogenised sections of patient tissue to determine the levels of expression of both interleukin's at the protein level.

There are currently no point of care detection methods for ART in GP practices in the UK, other than examination based diagnoses provided by the SIGN guidelines [360]. Within this work, the expression and spatial distribution of IL-17C has been characterised for the first time, demonstrating its significantly higher expression levels both in immunofluorescence imaging and western blotting in tissue from ART patients than the OSA patients tissue. It was also shown that IL-1β expression was significantly higher at the epithelium of ART tissues compared to OSA. To further evidence the use of IL-17C as a potential biomarker, Western Blot analysis confirmed its significantly increased expression throughout the ART patient tissue compared to OSA. Finally, it was shown that in OSA, IL-17C and IL-1β was spatially correlated with bacteria, but with no significance. This was not the case in ART, with no spatial correlation being shown in either case.

Sections from this chapter have been reproduced from [361].

3.1.1 Immunology of the palatine tonsil

Every time we breath we risk intake of antigenic material from our surroundings. Most of these antigens are harmless, however, there is a nonzero probability of some of these being pathogenic. The potential for pathogenic antigen material is why we have developed targeted immune responses to provide protection from these dangerous antigens. Mucous membranes which cover much of the internal surfaces of the body have developed a specialised immune system known as the mucosa-associated lymphoid tissue (MALT). The purpose of the MALT tissues (which line the respiratory, gastrointestinal and urogenital tracts), is to detect antigens, direct these to immune cells (or bring immune cells to antigen) to destroy the antigen, and to produce memory lymphocytes which have the ability to migrate to other mucosal sites and generate secondary immune responses. The process of the immune response in the palatine tonsil is discussed in detail below.

Healthy palatine tonsils are sites of constant stimulation of lymphoid cells [362, 206]. The first step in the immune response of the palatine tonsil occurs after a pathogen enters the oropharyngeal cavity. The reticulated crypt epithelium is the first immunologically challenged compartment [206]. Within these cells exist specialised tonsillar microfold (M) cells, which are cells that endocytose antigens at their apical membrane and transport to their basal membrane where they exocytose them to sub-epithelial lymphoid regions [363, 364]. M cells encounter the antigens and transport them over the epithelial boundary, creating an area where there is high concentration of both foreign antigens as well as lymphocytes and antigen-presenting cells such as macrophages and dendritic cells. The cells found in the reticulated epithelium of the crypt are

mostly composed of B and T cells, and the immune response requires the addition of cytokines [206]. Cytokines will be discussed in greater detail in section 3.1.2.

After passing through the crypt epithelium, foreign pathogens are presented to the extrafollicular region, where interdigitating dendritic cells and macrophages process the antigens and pass to lymphocytes [202, 206]. B lymphocytes are stimulated to proliferate and migrate, developing into B memory cells and antibody-producing plasma cells [206, 228]. The antigen contact of the B memory cells play an important role in generation of a secondary immune response, where the immune system eliminates the pathogen [206]. Pathogens which stimulate the immune response discussed above include viruses, fungi and bacteria.

Tonsillitis occurs when the presence and proliferation of pathogens in the tonsil exceed the defense instilled by the lymphoid and immunoglobulin producing cells [202]. For treatment-resistant cases of tonsillitis, tonsillectomy is still considered the only cure, however, as previously discussed this is still a controversial topic.

When pathogenic bacteria invades the epithelial surface of the tonsil they are immediately met with cells and molecules which begin an innate immune response. The methods in which the immune system eradicates bacteria are discussed below.

Immune proteins and antibodies may bind to the surface of bacteria (via opsonisation), coating cells in material that phagocytes recognise [365]. Phagocytic macrophages detect and bind to common constituents of bacterial membranes, or immune proteins that have attached to cell, which trigger the macrophages

to engulf the bacterium as well as secrete signalling molecules to inform of the bacterial presence [366].

Another method of bacterial killing is by the complement system of proteins which attack pathogens [365]. Activation of this system can occur spontaneously on some pathogens, or by antibody binding to a specific pathogen. These assist in killing bacteria either via phagocytosis or via the complement, alternative complement and lectin pathways. Briefly, the complement pathway activates a cascade of reactions on the bacterial cells, while leaving the host cells untouched. This pathway essentially coats the bacterial surfaces with proteins (opsonins) which are recognised by macrophages. The alternative complement pathway induces lysis of the bacterium via a protein cascade and the lectin pathway again leads to cell lysis. The complement system release molecules which contribute to inflammation.

Inflammation is typically thought of as heat, pain, redness and swelling [365]. These all reflect the effect that immune response has on local blood vessels. Dilation of the blood vessels during inflammation leads to increase blood flow and leakage of fluid to surrounding components. This accounts for heat, redness and swelling. The pain is accounted for by the translocation of leukocytes from blood vessels to infection sites.

The main cells found within early immune response are neutrophils [365]. These cells are similar to macrophages in that they have receptors for common bacterial constituents and they are the predominant cells which engulf and destroy invading pathogens. Shortly after the influx of neutrophils, monocytes appear which are rapidly differentiated into macrophages. Therefore, macrophages and neutrophils are referred to as inflammatory cells.

3.1.2 Cytokine expression in human palatine tonsils

Interleukin's (IL) are a group of proteins that are involved in communication between immune cells and the immune system in general via a cascade of signalling pathways [367]. They are a type of cytokine: proteins which are produced in response to pathogens and / or other antigens and are involved in regulating and mediating inflammatory and immune responses [368]. The cytokine family is made of a range of proteins, including chemokines, interferon's, and tumor necrosis factors, to name a few [369]. ILs act as messengers between cells to coordinate and modulate immune responses such as inflammation, differentiation and migration. They gain their name from the word 'leukocyte' since these cell types act on other leukocytes (inter-leukin) [368]. ILs can be involved with both pro- and anti-inflammatory reactions. They stimulate switching of antibody types in B cells, stimulate differentiation of T helper cells, activate antimicrobial mechanisms in phagocytes and have influence on production and stimulation of other ILs [367]. While they have relatively small molecular weights (a few 10s of kDa), they have high affinity, therefore, they are able to bring about effects at even picomolar concentrations [370, 371].

At the time of publication, there were 40 known ILs; with the majority belonging to the IL-1 family [367]. Each IL has its own function and effects on different immune cells. I.e IL-2 stimulates the proliferation and activation of T cells [372], where IL-10 represents a family of cytokines that inhibit inflammatory responses [373].

Abnormal expression of particular ILs can be involved with the development of bacterial and viral infection [374, 375] as well as disease such as cancer [376,

377], allergies [378, 379] and autoimmune diseases [380, 381]. This opens a route of examination for potential use of ILs as both biomarkers for disease [382, 383, 384] and as therapeutic targets [385, 386].

3.1.2.1 IL-1β

Interleukin-1-beta (IL-1β) is a pro-inflammatory cytokine belonging to the IL-1 family of cytokines [367] . IL-1β is produced primarily by macrophages and works alongside lymphocytes to fight infection [387, 388]. However, it can also be produced in keratinocytes, astrocytes and mesangial cells [367]. Unlike IL-1, it is a secretory cytokine and it is not membrane bound [367]. It also aids in the translocation of leukocytes from blood vessels to infection sites and is known to cause fever by having an effect on the regions of the brain involved in temperature regulation [389, 390, 391, 392]. The function of IL-1β is primarily to induce inflammation after pathogenic infection [367, 393, 394] and may be involved with the generation of an autoimmune response [395, 396, 397].

Increased production and levels of IL-1β has been reported to be associated with several autoimmune / auto-inflammatory diseases, such as multiple sclerosis [398] and Crohn's disease [396]. Unrestrained production of IL-1β can also be involved with carcinogenesis or tumorgenesis, with some studies showing increased levels of IL-1β in lung cancer cell lines [399].

IL-1β is known be involved in host response to bacterial [394, 400, 392], fungal [401] and viral infection models [402, 403]. Some studies have shown that inhibition of IL-1β production results in increased susceptibility to bacterial infection [394]. IL-1β is one of the most powerful cytokines in the human body and has involvement with almost every organ, as shown in figure 3.1, with its respective RNA tissue abundance characterised in figure 3.2.

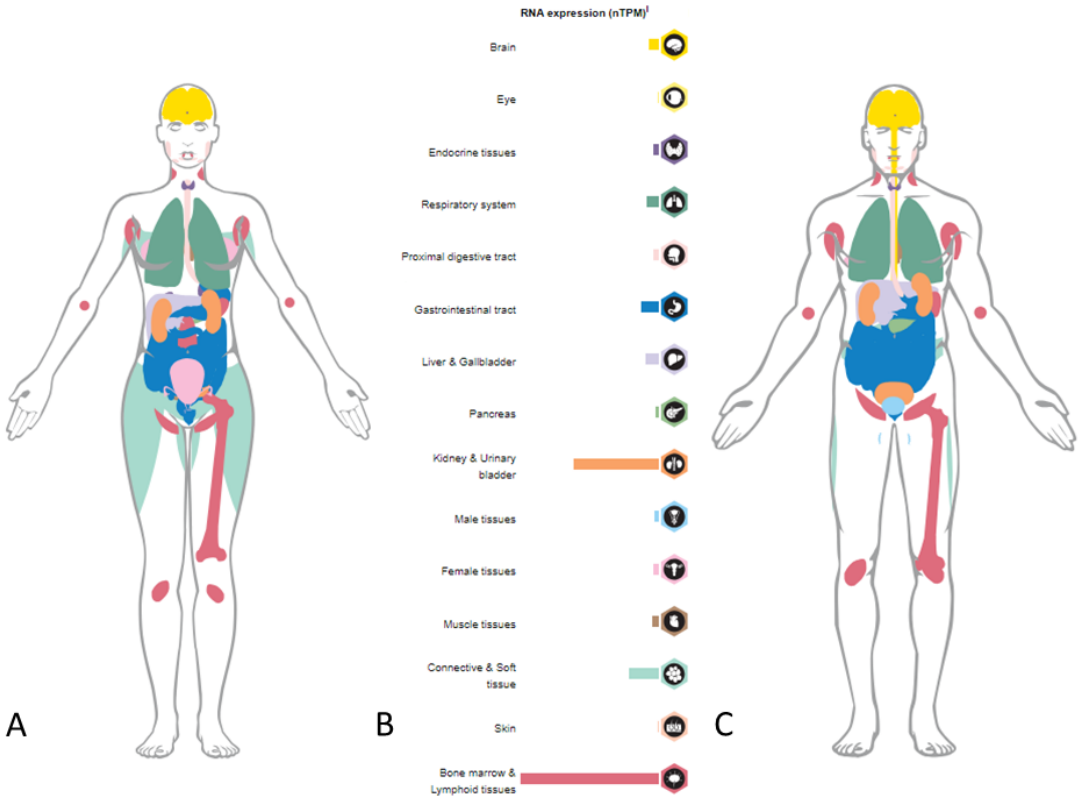

Figure 3.1: Organs expressing IL-1β in the human body. A) Expression in biological females, B)List of organs which express IL-1β and C) Expression of IL-1β in biological males. Adapted from the Human Protein Atlas [404]

IL-1β has several pathways in which it helps mediate host response to infection: it recruits neutrophils to inflammatory sites [405], induces several downstream cytokines and chemokines [388], and stimulates production of adaptive immunity [406, 407].

3.1.2.2 IL-17C

The IL-17 subset of interleukin's are a family of cytokines involved with inflammatory conditions [408]. The family is comprised of 6 subsets of IL-17A to IL-17F. IL-17C is functionally distinct from the rest of the family and is selectively induced in epithelial cells when exposed to bacterial stimulation [409,

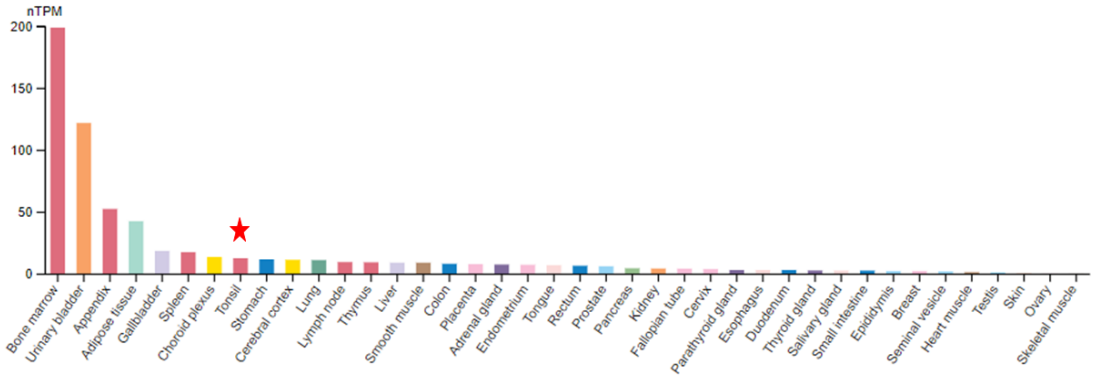

Figure 3.2: Organs expressing IL-1β in the human body. Bone marrow shows highest expression, tonsil is the 8th highest expressing organ, indicated by red star. Adapted from Human Protein Atlas [404]

410]. Some studies have linked expression and function of IL-17C to pathogenesis of disease in chronic rhinosinusitis [411, 412] and adenoiditis [413], however to date its presence in tonsils is unknown.

IL-17C is expressed in epithelial cells of both upper and lower respiratory organs upon stimulation by bacteria [413]. It is secreted extracellularly, functioning as an immunological mediator in innate immunity [414]. It is involved in host anti-microbial protective responses and plays a role in epithelial barrier maintenance in infection [409]. IL-17C is produced early in infection, due to its production at the interaction site of host and antigens, in contrast to most other ILs which are produced by immune cells [410]. Therefore, it acts as a rapid autocrine response to loss of integrity at the epithelial barrier. IL-17C is induced via a range of bacterial stimuli. Pattern recognition receptors (PRRs) are involved in immune surveillance at mucosal surfaces and recognise pathogen-associated molecular pathways (PAMPs), such as foreign DNA / RNA and flagella, or endogenous damage associated molecular pathways

(DAMPs) [415, 410]. Toll-like receptors (TLRs) are a subset of PRRs which detect and initiate immunity in response to microbial presence [409, 416]. Studies have shown that induction of TLRs promote production of IL-17C, providing evidence for its role in response to bacterial infection. In addition, IL-17C expression can also be regulated by various other cytokines. Tumor necrosis factor-alpha (TNF-α), a multi-functional cytokine involved in apoptosis and cell survival, is one such cytokine [417, 418]. Its synergistic relationship with IL-17A has been widely studied [419], and it has been shown that this synergy can enhance TNF-α mediated production of IL-17C [410]. IL-1β has also been shown to induce expression of IL-17C [409].

IL-17C has been shown to stimulate the production and release of other cytokines which enhance inflammatory responses. Some of these include IL-1β and TNF-α [410]. I previously mentioned that IL-17C expression is induced by IL-1β and TNF-α, this therefore shows that the communication and regulatory network between these three cytokines is complex. At the time of publication, very little research has been performed looking at the downstream cascades of IL-17C with its receptors.

IL-17C is a relatively understudied cytokine and its function in many organs remains undocumented, as shown in figure 3.3. Figure 3.4 shows the relative RNA expression in few organs, in comparison to IL-1β. IL-17C is known to be involved with urinary [421] and genital infections [422], and is known to be expressed in nasal epithelium [423, 420]. This, alongside its known involvement in adenoiditis and rhinosinusitis, leads to the question of its involvement in chronic tonsillitis and in OSA. I hypothesized that, due to its stimulation when exposed to bacteria, it should be both present in tonsillitis patients more than OSA, and should be released within close proximity to the bacteria and

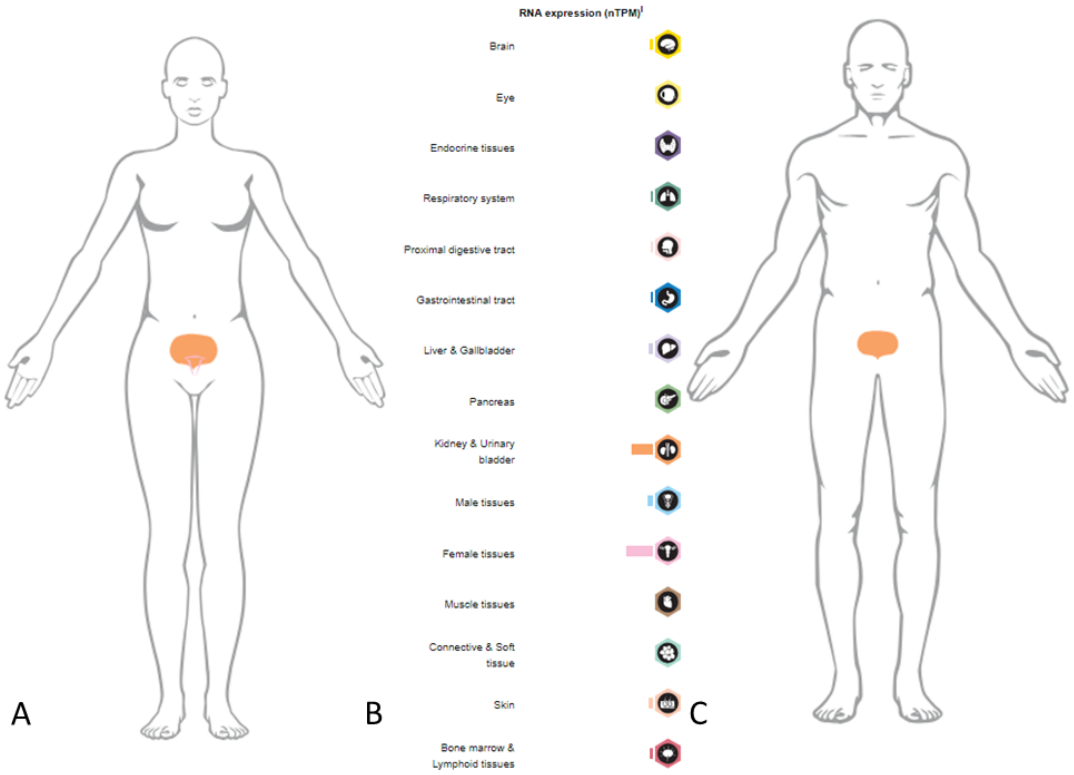

Figure 3.3: Organs expressing IL-17C in the human body. A) Expression in biological females, B)List of organs which express IL-17C and C) Expression of IL-17C in biological males. Adapted from Human Protein Atlas [420]

biofilms within the tonsil.

3.1.3 Immunofluorescence

Immunofluorescence (IF) is a common technique used to selectively visualise a target of interest within biological samples [424]. IF uses the specificity of an antibody to their particular antigen in order to label specific cellular targets. These targets are then visualised by the aid of fluorophores which have been linked to either the primary antibody or a secondary antibody. Using fluorescence microscopy, these fluorophores may be excited, revealing their spatial distribution amongst a sample [424]. This technique allows for various types

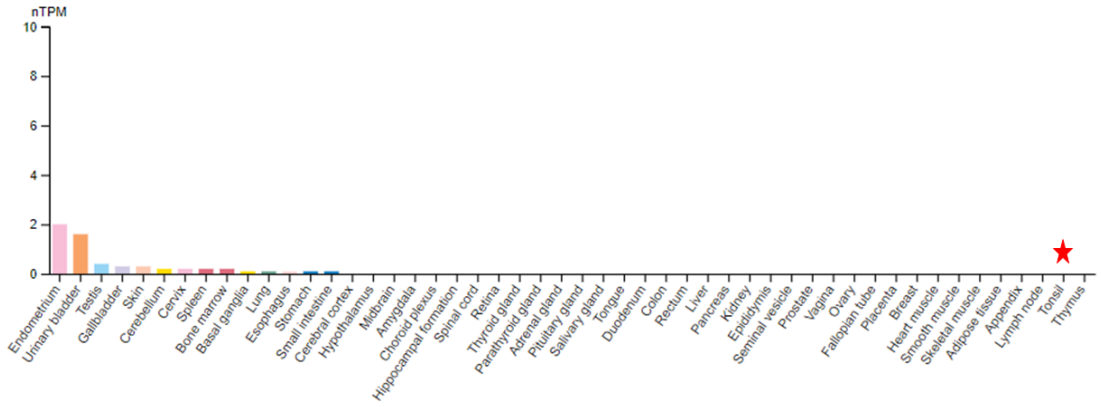

Figure 3.4: Organs expressing IL-17C in the human body. Endometrium shows highest expression, tonsil expression not detected by human protein atlas, shown by red star. Adapted from Human Protein Atlas [420]

of proteins to be studied including the indications of inflammation [425, 426, 427], deciphering mechanisms of tumour growth [428, 429, 430], and looking for biomarkers of infectious disease [431, 432]. The specificity of this technique will be discussed more in the subsequent sections.

3.1.3.1 Antibodies

An antibody, also known as immunoglobulin (Ig) is a protein used by the immune system to aid in the detection and subsequent neutralisation of antigens such as bacteria or viruses [433]. An antigen (Ag) is a molecule, moiety, foreign particle or allergen which binds to particular antibodies; the presence of these may induce an immune response [434, 435, 436]. These exist in normal and cancerous cells, parasites, viruses, fungi, and bacteria [424].

Antibodies are 'Y' shaped proteins, where each tip of the 'Y' contains antigen binding sites (paratopes), allowing for highly specific binding of the antibody - antigen complex [424]. This specific binding allows the antibody to 'tag' the

antigen and subsequently call upon other cells to aid in removing the exogenous agent. The arms of the 'Y' shaped region which binds to antigens is know as the 'Fab' domain, and the tail which is recognised by effector cells, immune proteins and antibodies is known as the 'Fc' domain [424].

For IF, a fluorophore is conjugated to an antibody [437]. The unique structure of the antibody allows for the targeting of antigens. There are two classes of conjugation, primary (direct) and secondary (indirect), represented by Fig 3.5 and further discussed in the below subsections.

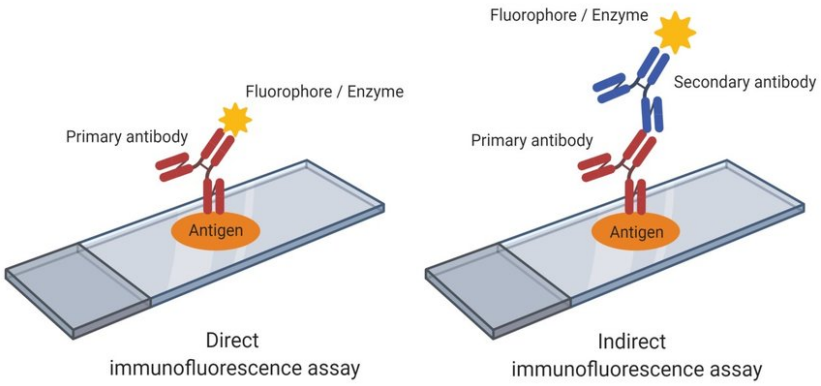

Figure 3.5: Overview of direct labelling (single tagged primary antibody) and indirect (primary plus tagged secondary antibody) antibody labelling of cells / tissue. Reproduced from [438]

Before performing IF labelling and adding antibodies, and important step is to block the tissue. Blocking prevents antibodies from binding to non-target Fc domains which may be present [437]. The reagents used for blocking typically have no affinity for the target Fc domains, instead they will have affinity for non-target domains. Blocking buffers typically fall into a few distinct categories including protein solutions and normal serums. Protein blocking solutions are buffers containing concentrated proteins which bind to all proteins in the sample; this means that antibodies have to compete with these proteins

and results in the reduction of nonspecific binding. Examples of these buffers include bovine serum albumin (BSA) [439, 440]. gelatin [439] and milk [441]. Conversely, normal serum contains antibodies from the same species as the secondary antibody host [440]; this blocks non-target sites to prevent the secondaries from binding there. A combination of both types is also commonly used [440].

3.1.3.2 Primary (direct) immunofluorescence

As demonstrated in Fig 3.5, primary (direct) immunofluorescence uses a single antibody to bind to its antigen, which has been chemically linked to a fluorophore [424]. The location of this binding can be elucidated by the use of fluorescence microscopy, where the correct excitation wavelength is chosen to excite the fluorophore of choice and the emission from this is detected.

Direct IF is the less common of the two IF classes, however, it does have a few advantages. One notable advantage is the simplicity of the sample preparation; with only one antibody to consider the steps needed for IF are reduced, this saves time and reduces the chance of non-specific background signal due to unbound secondaries, as well as limiting the possibility of cross-reactivities of the antibodies where they antibodies may not bind to their intended location.

There are also some disadvantages: direct IF is noticeably less sensitive than indirect due to the lower number of fluorescently tagged molecules which can bind to an individual site [424]. It is also more expensive than indirect due to the need to use more primary antibody.

3.1.3.3 Secondary (indirect) immunofluorescence

In comparison to direct labelling, secondary (indirect) labelling uses two antibodies. The primary antibody in this case has not been labelled with a fluorescence probe, and binds to the target within the cell [424]. The secondary antibody, which has been conjugated to a fluorophore, has specificity to the primary antibody Fc domain which is conserved amongst species, and binds there.

Specificity of the secondary antibody arises from the species upon which the primary antibodies are raised [437]. To prevent the secondary antibody from cross-reacting with endogenous Igs in the tissue or cells, the primary antibody should be raised in a different species from that of the sample. The secondary antibody should then be raised in yet another species, with targeting capabilities for the host of the primary antibody.

An advantage of this technique arises from the fact that multiple secondary antibodies can bind to an individual primary antibody, providing much better signal than direct IF by increasing the ratio of fluorophores per antigen. In addition, multiple different secondary antibodies may be used to target a particular primary, which is in contrast to that of direct IF [442]. This much increased amplification comes at the disadvantage of a more complex and time-consuming sample preparation.

3.1.4 Immunoblotting

Western blotting is a common molecular biology procedure used for the detection of proteins within samples, first introduced by Towbin *et al* in 1979 [443]. The process of 'blotting' involves the transfer of proteins from a gel matrix to

a membrane, generally using electrophoretic transfer [443, 444], an example of this can be seen in Figure 3.6.

Proteins may be manually transferred via manual sample deposition as well as through gel transfer [444]. General practice involves the electrophoretic transfer method mentioned above.

The first step in a western blot involves separating the proteins in a sample using gel electrophoresis [446]. Gel electrophoresis involves the separation of proteins or DNA according to their size and charge, via an electric current. Proteins are commonly separated by using polyacrylamide gel electrophoresis (PAGE), allowing for detection of small proteins, proteins in complex samples, and multiple proteins within a single sample [447]. Combined alongside Western Blotting, PAGE provides information on the mass, charge, purity and general presence of a protein [444]. Sodium dodecyl sulfate-PAGE (SDS-PAGE) is a common type of page which separates proteins according to their mass due to the negative charge put upon proteins bound to the SDS detergent [444].

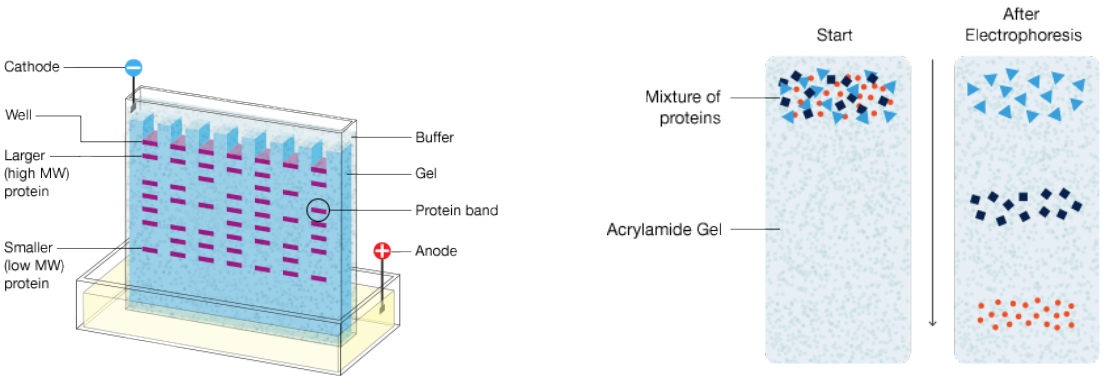

Figure 3.6: Schematic of electrophoretic protein separation using PAGE gel - Left depicts set-up of experiment, right depicts the separation of proteins by molecular weight (MW) after electrophoretic separation. Reproduced from [445]

These separated proteins are then transferred, or 'blotted', onto a second matrix which is typically a nitrocellulose membrane, once again via electrophoretic transfer [444]. Electrophoretic transfer of a protein includes placing the PAGE gel with protein into direct contact with a nitrocellulose (or other suitable) membrane and 'sandwiching' these, using porous pads and filter paper, between two electrodes within a conducting solution. After application of electric field, the proteins migrate from gel to membrane surface, where they tightly adhere to the membrane, resulting in a membrane with a 'copy' of protein which was in the gel. A diagram of this can be seen in Figure 3.7.

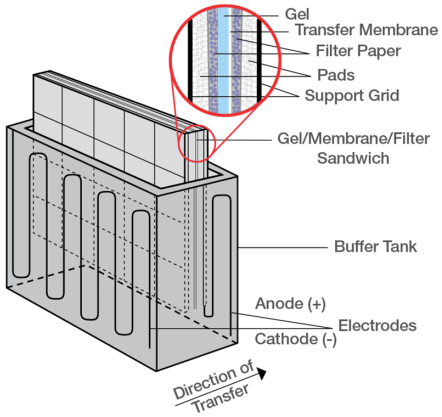

Figure 3.7: Western blot transfer schematic. Depicts standard sandwich composition and transfer direction for 'wet' transfer. Reproduced from [448]

Transferring of proteins from gel to membrane can be dramatically different between different proteins [444, 449]. This depends on various conditions including the gel composition, incomplete contact between gel and membrane, electrode position, transfer time, field strength and composition of the transfer buffer.

The membrane is then blocked to prevent subsequent non-specific binding of the chosen antibodies to the surface of the membrane [449]. The membranes

are then tagged with a chosen antibody to bind with the protein of interest. To detect the primary antibody, a second antibody which has affinity to the host-species of the primary is chosen. This secondary antibody is usually complexed with an enzyme which when combined with a particular reagent will produce a signal. Chemiluminescent substrates will react with the enzyme conjugated to the secondary antibody and produce light as a byproduct [450, 451]. The most popular chemiluminescent substrates used are luminol-based. Luminol oxidises in the presence of horseradish peroxidase and a peroxide buffer, forming an excited state product, 3-aminophthalate, emitting light at 425 nm when the excited state product decays to its ground state [450]. These emissions are typically captured on x-ray film and developed in a dark room [450]. The addition of enhanced chemiluminescence (ECL) substrates the reactions from luminol such that the light emission occurs over a several minutes, as opposed to seconds, allowing for more accurate and sensitive detection without significant light-output reduction.

3.1.5 Fluorescence *in situ* hybridisation

There are countless commercial and custom fluorescent dyes that offer a range of possibilities for selectively staining for bacteria [452, 453], fungi [454, 455], proteins [456] etc. However, many of these dyes have multiple targets. For example, to selectively stain bacteria on a section of tissue using DAPI [457, 458, 459], one would also stain the nuclei of mammalian cells present alongside the bacteria due to its binding to mammalian cell nuclei [458, 389, 460]. Wheat Germ Agglutinin (WGA) is a fluorophore often used for staining fungi [461, 462], but also has high binding affinity for tissue and will stain mammalian cell walls [463, 464]. One way to ensure high specificity of a fluorescent stain is to

use specifically targeted DNA probes using Fluorescent *in situ* Hybridisation (FISH) [465].

FISH is a technique which uses custom or commercially available fluorescent probes which target and bind to only specific regions of a nucleic acid sequence with a high degree of sequence complementary [465]. A relatively new technique, developed in the early 1980's to determine the presence or absence of sequences on chromosomes [466], it has adopted recent popularity due to its specificity and relative simplicity in the age of purchasable and customisable probes. For FISH, an RNA or DNA probe is constructed which is large enough to successfully hybridise with its target, but short enough to not directly interfere with the hybridisation process - approximately 20 oligonucleotide pairs. The probe is designed with a particular target in mind, such as a cellular protein or bacterial genomic region. In the case of this thesis, a target was made to bind with the conserved 16S rRNA region of the bacterial genome to target both Gram-Positive and Gram-negative bacteria [467]. The probe is tagged with a fluorophore of choice in order to selectively visualise on its own, or amongst other FISH [468, 453], IF [469] or cellular fluorescent stains [470]. FISH then occurs in three main steps: pre-hybridisation, hybridisation and post-hybridisation; or more colloquially, sample preparation, target binding, and washing. There are outlined in Figure 3.8 [471].

Tissue sections, or samples, are first fixed and frozen, or paraffin embedded. Fixation is generally performed with 4% PFA in PBS. After fixation, samples are permeabalised to allow penetration of both hybridisation reagents and probes. FISH is a sensitive procedure and optimisation of hybridisation temperature and time, pH, formamide concentration and salt concentrations is key before proceeding [472]. Once optimised, probe can be added to the sample

and hybridisation occurs via means similar to PCR mentioned in section 2.1.3. Multiplex FISH exists where it is possible to bind more than one probe at once [468, 453], but here I focus only on single-probe FISH. Signal amplification of in hybridisation is caused via a series of sequential hybridisation steps. After hybridisation, washing is performed to remove nonspecific hybridisation and unbound probes from the sample to reduce background signal. Samples are then mounted to be viewed under a fluorescence microscope.

FISH probes need to be approximately 20 oligonucleotides long to offer effective hybridisation, these cover a range of 40-50 base pairs on the target to, with the overlap of probes and target defining the resolution of the technique [326]. For example, if attempting to find a specific region of a sequence, then the window in which to find it would be defined by the overlap of the probes, or the degree to which one sequence is contained within the adjacent probes.

FISH has been extensively used in medical research to detect specific pathogens

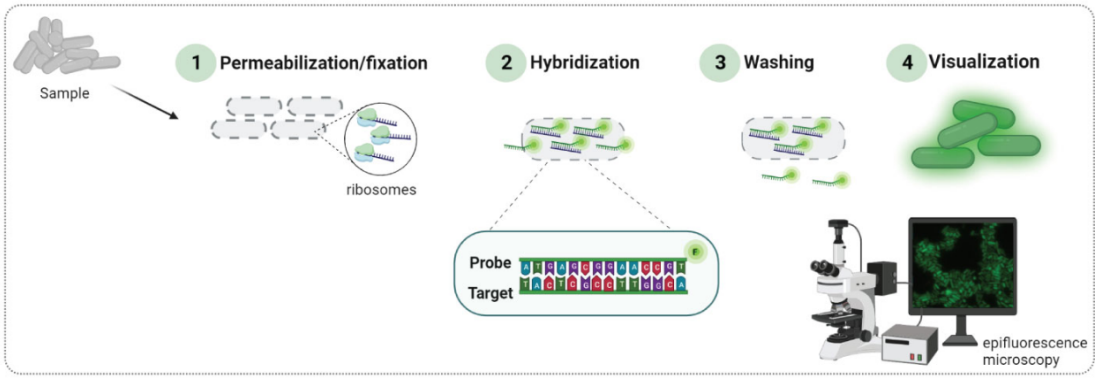

Figure 3.8: Steps in a standard FISH protocol. First, sample is fixed and permeabilised to both stabilise the sample and allow probe and reagents to penetrate. Fluorescently tagged probes are then added and allowed to hybridise with rRNA target. Excess probe is then washed away. Once hybridisation protocol complete, samples can be examined using a fluorescence microscope. Figure adapted from [471]

in medical microbiology [473, 474, 475, 476]. While it has proven both quick and useful, other techniques such as MALDI-TOF-MS (Matrix-assisted laser desorption / ionisation coupled to time-of-flight mass spectrometry) are more useful for the identification of a wider range of pathogens in a single sample compared to FISH [477, 478]. FISH for diagnostic purposes is of most use when identification of a particular species is needed, such as detecting malaria in blood cultures [479]. FISH is also widely applicable in researching biofilms [480]. With use of multiplex FISH or by applying a series of probes to target different bacteria, it is possible to determine the different species of bacteria which make up a biofilm and to study the distribution of different species therein. In the case of this thesis, FISH is used alongside IF to determine the spatial distribution of bacteria in relation to IL-1β and IL-17C within tonsillar tissue.

3.1.6 Colocalisation Analysis

Colocalisation analysis is frequently used on fluorescence microscopy images and is useful in investigating the spatial relationships between two or more structures [481]. In general, it aims to evaluate whether two or more structures are located close enough to each other to be interacting or functioning together. In fluorescence microscopy, this is evaluated by labelling the target structures with specific dyes, and is often performed in conjunction with antibody labelling or fluorescence *in situ* hybridisation. By analysing the fluorescence emission by these probes or dyes relative to each other, it is possible to determine the degree of overlap (colocalisation) between these labelled structures. This type of analysis is useful in a wide variety of biological settings: from the study of protein-protein interactions, to determining inflammatory

pathways [482, 483, 484], giving a greater understanding of the spatial relationships between different structures within cells and tissues.

Many colocalisation analyses are performed qualitatively, by assessing the overlap of two probes by eye [485, 486]. While this works as a quick check to determine if there is likely to be overlap, this does not provide any quantitative results.

Quantitative colocalisation may be performed by implementing image analyses software; Fiji has several pre-loaded plugins for performing such analyses. The method incorporated to this study is the use of the plugin JACoP [487]. The various plugins will calculate parameters such as Pearsons Correlation Coefficient and Manders Overlap Coefficients, amongst other statistical algorithms,these will be discussed in greater detail in the following sections. Both of these coefficients provide a quantitative analysis of the degree of correlation between the structures of interest.

3.1.6.1 Pearsons Correlation Coefficient

Pearsons correlation coefficient (PCC) is a measure of linear correlation between data of interest [488]. Originally formulated in 1896 by mathematician (and prominent eugenicist) Karl Pearson, it is one of the most common methods for quantifying correlation and is measured as a number ranging from -1 to +1, showing the strength and direction of the correlation between data. Simply put, it measures the degree of which variations in the intensity of two probes can be explained with a simple linear relationship.

The formula for PCC is shown below, where we assume two channels; one red and one green:

$$PCC = \frac{\Sigma_i(R_i - \bar{R}) \times (G_i - \bar{G})}{\sqrt{\Sigma_i(R_i - \bar{R})^2 \times \Sigma_i(G_i - \bar{G})^2)}} \tag{3.1}$$

Where R_i and G_i represent the intensity of the red and green channels, respectively, at pixel number i, while $\bar{R}$ and $\bar{G}$ represent the mean intensity of the red and green channels, respectively, for the whole image.

In the case of a perfectly correlated image where each channels fluorescence intensities are perfectly linearly related, the PCC value would be equal to 1. In the case where both channels fluorescence intensities are perfectly, but inversely, relate, the PCC value would be equal to -1. Finally, if the distribution of intensities show no correlation to one another the PCC value would be zero [489].

Due to the relatively simple linear relationship of PCC, tissue or cells to be analysed should be heterogeneous in order to not misrepresent results. In the case of high sample autofluorescence, or tissue not taking up full FOV of the microscope field, the mean signal may be artificially increased or decreased [489]. Thus, it is generally considered best practice to perform PCC analysis on ROIs containing the region or cell of interest. Additionally for samples where colocalisation of probes happen at different densities in different cellular or tissue compartments, PCC provides a poor measure of correlation due to the lack of heterogeneity across a single cell or tissue. Therefore, variations in heterogeneity occurring from the background as well as within the sample contribute to poor PCC measurements.

3.1.6.2 Manders Overlap Coefficient

Nearly 100 years after PCC was established, Manders characterised its use for fluorescent microscopy image analysis, and introduced a new coefficient to omit the perceived difficulty of interpreting negative PCC values [481]. This metric is closely related to PCC and is described as the Manders Overlap Coefficient (MOC):

$$MOC = \frac{\Sigma_i(R_i \times G_i)}{\sqrt{\Sigma_i R_i^2 \times \Sigma_i G_i^2}} \tag{3.2}$$

Where R_i and G_i represent the intensity of the red and green channels, respectively, at pixel number i.

MOC is implemented in many image processing software such as Imaris and Colocalizer Pro, or in the case of this Chapter, is implemented via an open source ImageJ plugin JACoP. [487].

The omission of subtracting mean fluorescence signal solves the issue of negative MOC values. This however can mean that MOC results may be artificially inflated or deflated due to, in the case of this Chapter, tissue autofluorescence or background signal. Since MOC can be taken as a measure of simply the spatial overlap of two channels, one way to circumvent this is by pre-processing. By thresholding the image above a certain minimum threshold it would then be possible to measure only the overlap of signal left from the fluorescent probes, discarding that of background and autofluorescence.

However, MOC potentially introduces more confusion. One study which was examining co-occurrence showed two datasets with $PCC_a = 0.73$ and $PCC_b = -0.71$, where a was positively correlated and b was negatively correlated [489].

When determining the overlap with MOC, $MOC_a = 0.99$ for the correlated data, still showing correlation. However, for the negatively correlated data, $MOC_b = 0.92$, suggesting that it is actually highly correlated. This discrepancy arises since MOC is mostly independent of signal proportionality and is instead sensitive to the overlap of the probes on any value above the given threshold.

By not taking into consideration signal proportionality, one might consider that MOC is superior to PCC, since its main focus is the overlap of signal. However, since it is not exactly a measure of only overlap and there are some additional steps, it is not perfect, and many articles have advised against its use in favour of more appropriate alternatives [489, 490, 491, 492, 493]. Instead, it may be more appropriate to perform an analysis of the fractional overlap of pixels with values above background of one channel with another.

3.1.6.3 Manders Colocalisation Coefficient (M_1 & M_2)

While both of the aforementioned correlation analyses provide a measure of the overall association of two channel signals, they miss a fundamental calculation: the fractional overlap of the two signals. In simple terms PCC and MOC measure general correlation of data, while taking into consideration the signal proportions while Manders Colocalisation Coefficient (MCC) is a measure of the fractional overlap of one channel to another, irrespective of signal intensity [494]. This measurement is commonly used in biological image analysis and is again found in the JACoP plugin, alongside other image analysis software.

Assuming again two channels, one red (R) and one green (G), we determine two different values of MCC: M_1, the fraction of R in regions containing G, and

M_2, the fraction of G in regions containing R.The coefficients are calculated as follows:

$$M_1 = \frac{\Sigma_i R_{i,colocal}}{\Sigma_i R_i} \tag{3.3}$$

Where $R_{i,colocal} = R_i$ if $G_i > 0$ and $R_{i,colocal} = 0$ if $G_i = 0$, and

$$M_2 = \frac{\Sigma_i G_{i,colocal}}{\Sigma_i G_i} \tag{3.4}$$

Where $G_{i,colocal} = G_i$ if $R_i > 0$ and $G_{i,colocal} = 0$ if $R_i = 0$

MCC provides an intuitive indication of colocalisation for most biological studies. Unlike PCC and MOC, MCC required pre-processing before application, i.e by choosing an appropriate threshold to remove background or unwanted fluorescence signal [489]. Many methods exist for choosing the appropriate threshold of an image. JACoP includes the Costes thresholding method. This method for Costes thresholding is as follows: PCC is measured for all pixels in an image, then again for serially reducing threshold values in both channels, repeated till PCC values drop to below or equal to zero [495]. The values of signal from each channel at this point is used for the threshold. MCC is then calculated on any points above this set threshold and these points are considered colocalised. While this method works well for many cases, there are circumstances wherein it will not produce a threshold at all, or not produce a reliable threshold [489]. For example, it struggles to identify thresholds in images where there is high labelling density or images with low signal intensity [489]. In addition, it struggles in circumstances where the background varies

spatially, for example in images where probes are being measured against tissue, and that tissue is against a background [489]. The Costes method of automatic thresholding in JACoP in theory would produce different thresholds for different images due to inhomogeneity in tissue autofluorescence or background fluorescence. Since it is important to keep thresholding consistent for colocalisation measurements in biological specimens [496], manually thresholding based upon the signal of the background, tissue autofluorescence or tissue staining is more appropriate.

3.1.7 Tissue Autofluorescence

Tissue autofluorescence refers to the emission of fluorescence after excitation from endogenous fluorophores within these tissues using the same mechanisms described in section 1.1.5. The most common sources of autofluorescence in tissues arise from nicotinamide adenine dinucleotide phosphate (NADPH), flavins as well as connective structures such as collagen and elastin [497, 498].

In many imaging experiments tissue autofluorescence is considered a hindrance, and care is taken to ensure that autofluorescence in minimised [499, 500]. This is because it can add unwanted signal when staining tissues with fluorohpores, However, there are cases in which autofluorescence can be useful, such as when structural information can be obtained without the use of exogenous fluorophores [501, 502, 503]. This is also useful in medical research in a variety of settings, including using autofluorescence to study morphological changes in diseased tissue [503], to assess malignant lesions [497], and for acne assessment [504]. Chemical fixation can cause increased levels of autofluorescence in a sample. Since many studies use fixed tissues and cells this can make deciphering signal of fluorescent probes from the tissue difficult. To circumvent

this issue, one may use a chemical quenching agent [505], alternative stains [506], photobleaching [506], or a combination of several. It is also possible to use image processing techniques such that thresholds are set to the value of autofluorescence and only signal above this is counted.

3.1.8 Experimental Aims

Using a combination of immunofluorescence and mesoscopic imaging, I aimed to for the first time demonstrate the spatial distribution and characterise the expression of IL-17C in patient tissue sections. Alongside this I aimed to examine the spatial distribution and expression of IL-1β within the same samples. By using a custom fluorescence *in situ* hybridisation probe to target both Gram-Positive and Gram-Negative bacteria, I aimed to determine if the cytokines had spatial overlap with the bacteria, and if this correlation was linked to levels of expression. This work was performed with the aim to determine if either IL-17C or IL-1β expression could be used as a biomarker for ART.

3.2 Methods

3.2.1 Specimen Preparation

3.2.1.1 Sample Acquisition, patient exclusions

This study was approved by Biorepository Management Committee of NHS Greater Glasgow and Clyde, UK (Biorep 548). Seventeen tonsils were collected after routine tonsillectomy at the Royal Hospital for Children, Glasgow, UK. The tonsils collected for use in this chapter differ from those of the previous chapter. No information of patient age, sex or socio-economic status was provided. The institutional review board approval (Biorep 548) was awarded to allow anonymous patient tissue use, waiving the need for individual level patient consent. Whole tonsils were rapidly transported in sterile saline solution (0.9% Sodium Chloride, Baxter Healthcare Ltd, UK) to the Strathclyde Institute of Pharmacy and Biomedical Sciences at the University of Strathclyde after the completion of a surgical list.

Specimens were blinded for the purposes of preventing bias throughout the duration of the study. A total of 8 tonsils from patients with ART and 9 tonsils from patients with OSA were collected across the duration of study, no patient tissues were excluded. For western blot analysis, 8 ART and 8 OSA patient tonsils were used. For IF, 3 ART and 6 OSA patient tissues were used.

3.2.1.2 Fixation

Prior to fixation, tonsils widths were measured by placing tonsils length-ways atop a ruler separated from the tissue by a petri dish, as shown in figure 3.9.

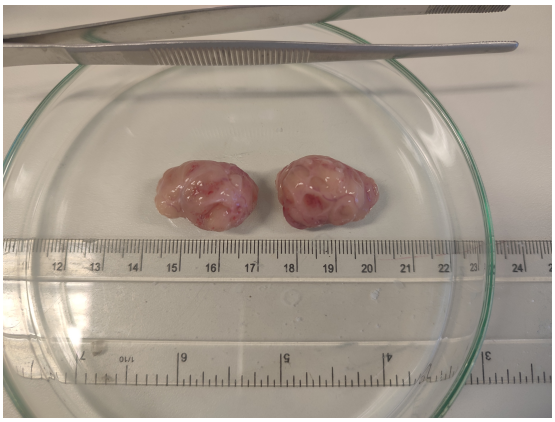

Figure 3.9: Fresh tonsils are placed length-ways next to a ruler, separated by a sterile petri dish in order to measure the length of the tonsils.

Tonsil size was measured by eye. If samples were too big to fit into cryo-moulds later used for cryo-sectioning, they were reserved for immunoblotting. This equated to samples over approximately 3.3 cm in length (the length of the diagonal of a 22 mm cryo-mould). One sample was kept for fixation, and from patient 14 onwards, one sample was homogenised for further research. In the case where one tonsil of a pair was greater than 3.3 cm and one was smaller, the smaller tonsil was used for imaging and the larger was used for homogenisation, to minimise patient tissue wastage. Otherwise, it was a random choice.

4% paraformaldehyde,which had been previously mixed fresh from powder (158127, Sigma-Aldrich, USA) and stored for long term storage in a -20° freezer, was defrosted in the fridge if tonsils were to be collected that day. Once samples had been washed, they were placed into fresh 15ml universal tubes and covered with PFA to double the volume of saline solution that was originally in the tube. Samples were then left to fix overnight in the fridge at 4°C, for between 12-18 hours.

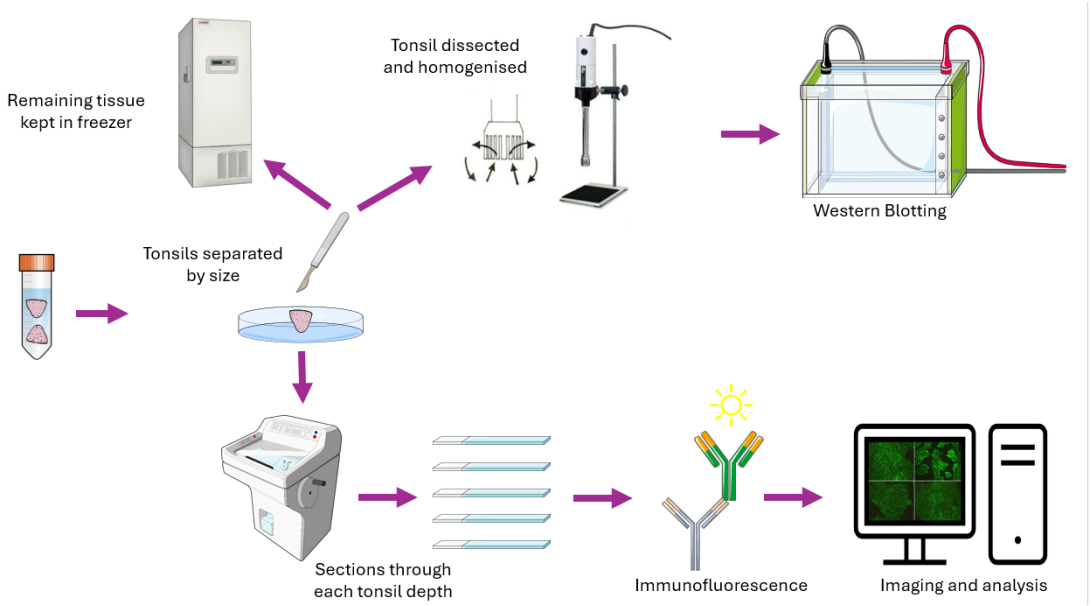

Figure 3.10: Graphical representation of methods. Tonsils were measured, with the larger specimen partially homogenised and analysed using a western blot, and the smaller specimen was sectioned to provide 10 slices at regular intervals throughout the whole thickness of the tonsil. These sections were immunolabelled with antibodies against IL-1β and IL-17C and were imaged using widefield fluorescence mesoscopy with the Mesolens. Image assembled using icons from Wikimedia commons and BioIcons (CC-BY license)

3.2.1.3 Tissue Sectioning

Prior to cryosectioning of tissue, slides (Z692255, Sigma-Aldrich, USA) were coated with 200 µl of a 0.1% solution of Poly-L-Lysine (P4832, Sigma-Aldrich, USA) to aid in tissue adhesion. The coating was left for 20 minutes to dry, and slides were subsequently rinsed with sterile PBS. Slides were air dried in a laminar flow cabinet overnight before use.

Freshly excised tonsils reserved for immunofluorescence were fixed overnight

in 4% paraformaldehyde at 4°C. After fixation, tonsils were rinsed 3 x 5 minutes with 1X PBS (10010023, ThermoFisher Scientific, USA) without agitation. Once washed, tonsils were placed into 22 mm x 22 mm x 20 mm square cryomoulds (Peel-A-Way™embedding moulds, E6032-1cs, Sigma-Aldrich, USA) and covered with optical cutting temperature (OCT) embedding matrix for frozen tissue (KMA-0100-00A, Cell Path, UK). Blocks were snap-frozen on dry ice before being stored at -80°C prior to use.

Cryosectioning (CM1950, Leica Microsystems, Germany) of the tonsil tissue was performed with the optimised ambient temperature of cryostat set to -12 °C and the temperature at the specimen holder set to -12 °C. A new blade was inserted for each tonsil to ensure reliable sectioning. Ten tissue sections, each of 10 μm thickness, were taken at regular intervals through the tonsil depth to sample through the tonsil mass. Sections were lifted to the Poly-L-Lysine coated slides and immediately stored at - 80 °C for long term storage, or, if used straight away, allowed to dry, and adhere to coverslips for up to 48 hours. Sampling at such intervals allowed for a reasonable amount of tissue to be processed, otherwise hundreds of slides would be generated per tonsil sample. Optimisation of section thickness was performed by taking a series of sections of varying thicknesses and visually assessing their structure after sectioning.

An additional three tissue sections were taken for each patient and processed without the addition of antibodies. This was to facilitate the measurement of autofluorescence arising from the tissue and sample processing such that it could be accounted for when performing intensity-based analysis as described in section.

3.2.2 Immunoblotting

3.2.2.1 Tissue homogenisation

Seventeen patients tonsils were used for western blotting, approximately 1/4 of the tonsil was dissected for homogenisation. For each patient (n = 16) there was one homogenate created. Tonsil tissue of approximate equal size was taken for each sample and mechanically homogenized in 300-500 μl of lysis buffer containing cOmplete™Protease Inhibitor Cocktail on ice using a X 120 Portable Homogenizer (CAT Scientific, Germany). Samples were kept at 4°C on ice, vortexed and syringed through a 23 G needle as part of the lysis process and then centrifuged at 16,000 x g for 10 minutes for sample clarification prior to protein determination.

3.2.2.2 Protein Extraction

Protein concentrations across all samples were normalised to the same protein concentration (500 μg/ml) with protein determination quantified using the well-established Pierce BCA Protein Assay (Thermo Fisher) following the recommended guidelines provided by the manufacturer. An equal volume of NuPAGE™LDS Sample Buffer (2X) containing 100 mM DTT was add to the normalised tissue homogenate sample to create a 1x sample for SDS-PAGE (with 250 μg/mL protein, 50 mM DTT). Samples were stored at -80°C until processed by immunoblotting.

3.2.2.3 Antibodies

All antibodies used are described in Figure 3.11. Primary antibodies targeting IL-1β and IL-17C were used for both blotting and IF imaging. A GAPDH

primary antibody was used for immunoblotting as a housekeeping protein loading control for signal normalisation between samples. An AlexaFluor-350 conjugated secondary antibody was used for targeting IL-1β primary, and an AlexaFluor-594 conjugated secondary antibody for IL-17C primary for IF. For western blotting (WB), Goat anti rabbit and donkey anti mouse secondary antibodies were used for targeting IL-17C and IL-1β primary antibodies, respectively.

Antibody	Target	Primary / Secondary	Used for	Dilution / concentration	Manufacturer details
Mouse monoclonal IL-1β	Human	Primary	WB / IF	1:3000 (WB) 1:100 (IF)	2801, Invitrogen, ThermoFisher Scientific, USA
Rabbit polyclonal IL-17C	Human	Primary	WB / IF	1:3000 (WB) 1:100 (IF)	ab153896, Abcam, UK
GAPDH	Human	Primary	WB	1:100,000	ab8245 Abcam, UK
Goat anti-rabbit	Rabbit	Secondary	WB	1:7000	111-035-133, Jackson Laboratories
Donkey anti-mouse	Mouse	Secondary	WB	1:7000	715-035-150, Jackson Laboratories, USA
Goat anti-mouse (alexafluor 350)	Mouse	Secondary	IF	2 µg/ml	A-11045, ThermoFisher Scientific, USA
Goat anti-rabbit (alexafluor 594)	Rabbit	Secondary	IF	2 µg/ml	8889, Cell Signalling Technology, USA

Figure 3.11: Containing information regarding which antibodies were used in WB / IF, their targets, use, dilutions and manufacturer information

3.2.2.4 Western Blotting

15% SDS-Page gels were loaded with 20 μl of each sample, alongside 5 μl of protein ladder (26619, ThermoFisher Scientific, UK). Gel electrophoresis was performed at 120 V for 1 hour 30 minutes, or until the sample ran off the gel, before being transferred onto nitrocellulose membrane (10600002, Amersham plc, UK) for 2 hour 30 minutes at 295 mA. Membranes were subsequently blocked in 3% BSA (81-003-3, MilliporeSigma, USA) and then diluted in Tris

buffered saline with Tween20 (TBS-T) for 2 hours with constant agitation. Primary antibodies were both diluted 1 in 3000 in 0.3% BSA, added to the membranes, and incubated overnight with constant agitation. Membranes were washed 3 x 5 minutes with TBS-T then incubated with secondary antibodies for 1 hour then washed again for 3 x 5 minutes with TBS-T.

Membranes were placed in (4 ml each) enhanced chemiluminescence (ECL) buffers for 2 minutes, and fluorescence emission was detected with X-ray film. Film was developed in a dark room.

Following development, the membranes were stripped at 60C at 60 RPM for 25 minutes in stripping buffer, and then blocked again for 2 hours in 3% BSA. The newly stripped and blocked membranes were incubated with 1 in 100,000 dilution GAPDH housekeeping primary antibody (ab8245 Abcam, UK) in 0.3% BSA, and the above process was repeated using the mouse secondary antibody.

For each patient (n = 17 total) and each antibody, n = 3 repeats were performed. Analysis of blots was performed using ImageJ, where analysis replicates were performed at n = 3 for each sample. Data was presented using GraphPad Prism (GraphPad Prism v.8.0.2 for Windows, GraphPad Software, USA).

3.2.3 Fluorescence *in situ* hybridisation

3.2.3.1 Designing FISH probe

A custom general eubacteria FISH probe was used for detection of bacteria within human palatine tonsil. The probe was adapted from Amann *et al* [507], with a modification of an ATTO 488 dye at the 5′ region. The adapted and custom EUB-488 probe, with sequence 5′ - GCTGCCTCCCGTAGGAGT - 3′ (16S

[338-355]) was synthesized by Eurogentec (Eurogentec, Belgium), with IEX-HPLC purification, the probe specifications can be seen in figure 3.12. Probe specificity was tested on *S.aureus* and *P.aeruginosa* ESKAPE bacteria as positive controls, and *candida albicans* for negative controls. Probes were optimised using previously published methods [472], it was found that a formamide concentration of 30% was optimal.

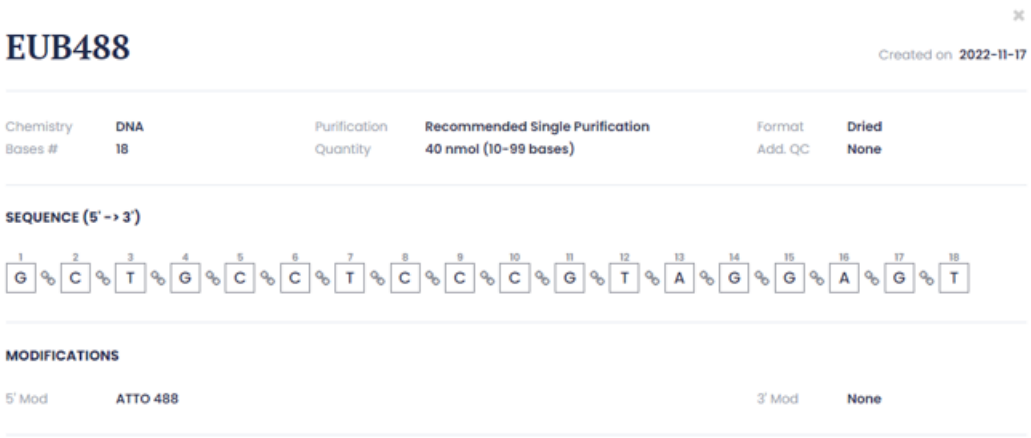

Figure 3.12: EUB488 probe design using Eurogentec

3.2.3.2 FISH

Hydrophobic rings were drawn around each tonsil sample to provide a retaining barrier to added liquids using an A-PAP pen (Z672548, Sigma-Aldrich, USA). *In situ* hybridisation buffer and FISH wash buffer were made to the concentrations required for the optimised 30% formamide concentration [472], buffer compositions can be seen in Table 3.1. 36 μl of FISH buffer and 4 μl of EUB488 probe working stock solution was mixed then added to each slide, the slide was gently agitated to distribute probe mix. After probe addition, each slide was placed horizontally into a 50 ml centrifuge tube (430290, Corning, USA), or horizontal slide tray, alongside a folded Kimwipe (13258179, Thermo

Buffer	Composition
In situ hybridisation buffer	300 μl 5M NaCl, 40 μl 1M Tris-HCL (pH 8), 600 μl Formamide, 1060 μl dH_2O, 2 μl SDS
FISH wash buffer	1 ml 1M Tris-HCL, 1020 μl 5M NaCl, 500 μl 0.5M EDTA, 47.5 ml dH_2O, 50 μl 10% SDS

Table 3.1: Compositions and component supplier for FISH buffers, all reagents were purchased from Sigma-Aldrich or ThermoFisher Scientific

Fisher Scientific, USA) saturated with 200 μl of FISH buffer. Keeping horizontal, the falcons were placed into a hybridisation oven set to 47°C overnight, protected from light. Prior to removal from the oven, FISH wash buffer was warmed to 47°C in a water bath. Slides were removed from the oven and rapidly transported to wash station, where they were rinsed with pre warmed wash buffer, then incubated with wash buffer for 10 minutes. Samples were then rinsed with dH_2O, and dried at room temperature in dark for at least 2 hours before performing antibody labelling.

Formamide concentration of FISH buffers was found to be optimal with the designed EUB488 probe at 30%. This was determined via empirically measuring fluorescence from control samples which were treated with increasing concentrations of formamide in the buffer, ranging from 0-50%.

3.2.3.3 Bacterial / Fungal Culture

Yeast cells were used for negative controls for the FISH probes designed to target any bacteria. The targets bind to the 16S rRNA section of the bacterial genome, which is conserved across all bacterial species, but not evident in fungi. Yeast plates were cultured and kindly gifted from Dr Katherine Baxter

(University of Strathclyde). Both *S.aureus* and *P.aeruginosa* ESKAPE bacteria were used as positive controls for FISH probes.

Frozen stocks of *P. aeruginosa* and *S. aureus* were streaked onto petri dishes with LB agar and incubated at 37°C for 48 hours. After incubation, a single colony was picked from each plate with a sterile inoculation loop, and diluted into 5 ml of LB broth in 15 ml universal tubes. These suspensions were left to incubate overnight at 37°C in a shaking incubator. The following morning, rebound cultures were created by making a 1 in 100 dilution of overnight culture into fresh LB broth, then further incubating in 37°C shaking incubator for 3-4 hours. 1 ml of each rebound culture was placed in a 1.5 ml eppendorf tube and centrifuged at 4500 rpm for 5 minutes. The supernatent was discarded and pellet washed and resuspended with 1 ml of PBS. Suspension was again centrifuged at 4500 rpm for 5 minutes, and the wash steps repeated to have a total of 3 washes. After removing supernatant, 250 μl of PBS and 750 μl of 4% PFA was added to each eppendorf, ensuring the pellet was thoroughly re-suspended, then incubated on ice for 2 hours. Eppendorfs were centrifuged at 4500 rpm for 5 minutes, discarding of the PFA supernatent waste. Pellets resuspended in PBS and a total of 2 washes were performed. After washing, pellets were resuspended in 1 ml of 50% ethanol (diluted in PBS), ensuring homogenous re-suspension. If not using right away, suspensions were stored at -20°. *Candida Albicans* plates, gifted by Dr Katherine Baxter (University of Strathclyde), were used for negative controls of FISH stain. The same preparation steps as mentioned above were performed.

3.2.3.4 FISH control using bacteria and fungi

Samples were vortexed to ensure thorough resuspension and were mixed 1:1 with each other to provide mixed Gram samples, the stock of fungal cultures was used on its own. 20 μl of sample was added to a type 1.5 coverslip and allowed to thoroughly air dry (for approximately 2 hours). Hybridisation oven was set to 47° and allowed to come to temperature before the following steps. FISH probes were mixed 1:10 with hybridisation buffer from the working stock solution and 10 μl of this mix were added to slides containing fixed and dried mixed bacteria. A Kimwipe™(13258179, Fisher Scientific, USA) saturated with 200 μl of wash buffer was placed in the bottom of a slide box, slides with probes were sat atop these wipes, with sample facing away from wipe. Slides in box were kept horizontal to prevent the probe solution displacing from the target. Keeping horizontal, box was placed in the hybridisation oven overnight, protected from light. The following day, FISH wash buffer was pre-heated to 47° in a water bath. Subsequent wash steps were performed in a fume hood. After hybridisation time complete, samples were transferred to fume hood and washed 3 times with the pre-warmed FISH wash buffer. One final wash was performed with cooled (2-8°C) dH_2O. All FISH buffers and run off wash fluids were disposed of via the same system.

Slides were dried for 2 hours on the bench, protected from light. Approximately 10 μl of VectaMount (H-5000, Vector Laboratories) was placed onto each slide and coverslips were gently angled down to adhere. Gentle force was applied to ensure even distribution of mounting media and to avoid bubbles. Slides were left to cure overnight.

3.2.4 Immunofluorescence

3.2.4.1 Primary Antibodies

Mouse monoclonal IL-1β antibody (2801, Invitrogen, ThermoFisher Scientific, USA) was chosen for targeting IL-1β production in human palatine tonsil. Rabbit polyclonal to IL-17C antibody (AB153896, Abcam, UK) was chosen for targeting IL-17C production in human palatine tonsil.

3.2.4.2 Immunofluorescence staining

Tonsil slides were blocked with 100 μL of antibody blocking buffer (see Appendix B for reagent compositions) for two hours at room temperature. The blocking buffer was aspirated, primary antibodies were diluted to 1:100 in antibody dilution buffer, and 100 μL of each primary antibody solution was added to each specimen. Slides were placed in a humidity chamber and incubated overnight at 4°C. Slides were rinsed 3 x 5 minutes in PBS, aspirating waste. Information about antibodies used for IF can be found in Figure 3.11. Goat anti-Mouse IgG (H+L) cross-absorbed secondary antibody conjugated with AlexaFluor 350 was diluted to 2 μg/ml in antibody dilution buffer and added at 100 μL volume to slides to target the IL-1β primary antibody, and was incubated for 2 hours at room temperature in the dark. Slides were rinsed 3 x 5 minutes with PBS, aspirating waste. Anti-rabbit IgG (H+L), F(ab')$_2$ fragment conjugated with the fluorescent label Alexa Fluor 594 was diluted to 2 μg/ml in antibody dilution buffer and was added at 100 μL volume to slides to target the IL-17C primary antibody. This was incubated for 2 hours at room temperature in the dark. Secondary antibodies were sequentially added to minimise potential cross-reactivity, though order of sequence was of no effect.

Slides were rinsed 3 x 5 minutes with PBS, with the last rinse step being performed at 37°C in a hot cupboard. Samples were then mounted onto type 1.5 coverslips using VectaMount (H-5000, Vector Laboratories).

Mammalian cells known to express the cytokine of interest were used as controls for antibody labelling. Fungi was used as negative control for FISH labelling and known Gram-positive and Gram-negative bacteria co-culture was used as positive control for FISH probes.

The concentration of the IF secondary antibody was optimised by imaging a range of dilutions and found that a 1:100 dilution was optimal and yielded the greatest results in the control HeLa cells. The IL-17C primary antibody used did not have published recommended dilutions for IF use, but was chosen due to limited options at the time of purchase. Therefore, optimisation on both primary dilution (1:100) and a high concentration of secondary had to be used to yield best results.

IL-1β antibody dilution was recommended by manufacturers for IF, these dilutions were followed after also checking for specificity of staining. Both antibodies specificities were verified using control cells of HeLa cells for IL-17C and HMC3 cells for IL-1β. These can be seen in Figure 3.13

The use of a negative control for immunofluorescence staining by applying only the secondary antibody without the primary was omitted in this study. This presents a potential limitation, but the use of positive controls, with appropriate blocking agents applied to the tissues mitigates potential problems arising from this.

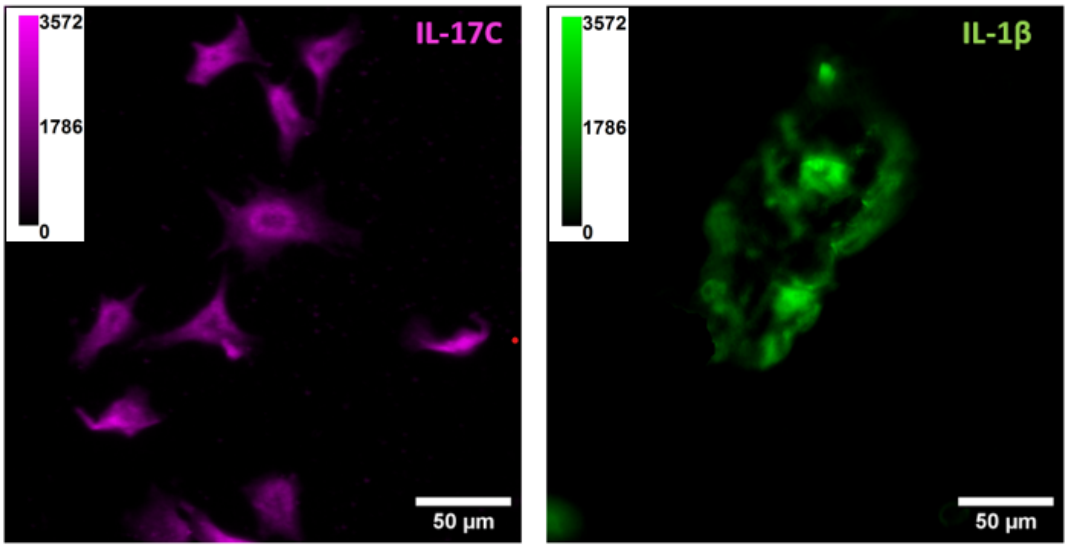

Figure 3.13: IL-17C Control: HeLa Cells labelled with 1:100 dilution of rabbit anti human IL-17C primary antibody. Contrast achieved by addition of goat anti rabbit IgG secondary antibody tagged with AlexaFluor594. IL-1β control labelled with 1;100 dilution of mouse anti human IL-1β primary antibody. Contrast achieved by addition of goat anti mouse secondary antibody tagged with AlexaFluor350.

3.2.4.3 Culture of HMC3

HMC3 cells were used as a positive control for IL-1β expression. HMC3 cells are an immortalised microglial cell line, isolated from the brain of a patient, established in 1995. Microglia are known to express IL-1β. These cells were kindly gifted by Holly Brown, SIPBS, Strathclyde

HMC3 cells were cultured in D++++ media, consisting of DMEM, 10% v/v Heat Inactivated FBS, 1% v/v penicillin-streptomycin, 1% L-glutamine and 1% non-essential amino acids. Cells were kept in a 5% CO_2 cell culture incubator at 37°C. Cells were split at 75% confluency to a 1 in 10 dilution into fresh media and allowed to grow, time to 75% confluency was approximately 48 hours, growth curves were not conducted as cell dynamics were not of concern. At

the next split, cells were seeded onto sterile 13 mm coverslips which had been treated with fibronectin (2.6 μg/μL) to aid in cell adhesion, then allowed to grow overnight in the incubator. The following day, cells were washed twice with pre-warmed PBS and then fixed with cold 4% PFA in the fridge for 20 minutes. Coverslips were then rinsed again with PBS and stored long term in PBS at 4°C. Cells were stained to the same concentrations described in section 3.2.4.2.

3.2.4.4 Culture of HeLa cells

HeLa cells were used as a positive control for IL-17C expression. HeLa cells are an immortalised human cervical cancer epithelial cell line, isolated from Henrietta Lacks in 1951. Epithelial cells are known to express IL-17C in response to antigen stimulation. HeLa cells were exposed to non-sterile air prior to fixation to induce IL-17C expression.

HeLa cells were cultured in D+++ media, consisting of DMEM, 10% v/v Heat Inactivated FBS, 1% v/v penicillin-streptomycin, and 1% L-glutamine. Cells were kept in a 5% CO_2 cell culture incubator at 37°C. Cells were split at 75% confluency to a 1 in 10 dilution into fresh media and allowed to grow, time to 75% confluency was approximately 72 hours, growth curves were not conducted as cell dynamics were not of concern. At the next split, cells were seeded onto sterile 13 mm coverslips which had been treated with fibronectin (2.6 μg/μL) to aid in cell adhesion, then allowed to grow overnight in the incubator. The following day, cells were washed twice with pre-warmed PBS and then fixed with cold 4% PFA in the fridge for 20 minutes. Coverslips were then rinsed again with PBS and stored long term in PBS at 4°C. Cells were stained to the same concentrations described in section 3.2.4.2.

3.2.5 Imaging

3.2.5.1 Mesolens brightfield

Brightfield transmission and widefield fluorescence images of tissue sections were obtained using the Mesolens and data were captured using a chip-shifting camera sensor (VNP-29MC, Vieworks, Republic of Korea). Brightfield transmission mesoscopic images were taken with exposure time set to 20 ms and a gain of 1.

3.2.5.2 Mesolens widefield epifluorescence

Widefield mesoscopy was performed with the Mesolens correction collars set for water immersion (n = 1.33) to reduce spherical aberration.

Fluorescence excitation was achieved by use of 405 nm , 490 nm or 585 nm LEDs from a pE-4000 LED illuminator (CoolLED, UK) to excite the IL-1β, EUB488 and IL-17C antibodies and probes, respectively. All fluorescence images taken with an exposure time of 500 ms and gain of 15. The 405 nm LED was used at 70% power, the 490 nm at 90% and the 585 at 80% throughout all imaging experiments. Measurements of tissue autofluorescence was taken for each wavelength used for excitation using unlabelled specimens. Widefield mesoscopy was performed with the Mesolens correction collars set for water immersion (n = 1.33). The choice of fluorescent secondary antibodies was informed by the Pinkel-type [508] barrier filters used for Mesolens imaging [114], which had emission bands at 417 ± 10 nm, 525 $\pm$ 25 nm and 635 ± 20 nm.

3.2.6 Image Analysis

3.2.6.1 Analysis of Western Blots

Blots were quantified to show relative intensities against the house-keeping protein GAPDH, relative band intensity was measured and compared using FIJI. Band intensity was measured with 3 replicates for each band. Relative intensity of each band with respect to GAPDH was recorded and means taken for each patient over n = 3 biological repeats per patient. Relative intensity was plotted for both IL-17C and IL-1β in both patient groups.

3.2.6.2 Measurement of autofluorescence

An image analysis pipeline was developed to reduce the contribution of tissue autofluorescence in the quantification of image data. The autofluorescence signal intensity was measured from n = 3 unlabelled tissue sections obtained from the top, centre, and bottom of each of the n = 16 tonsil specimens. These were imaged as described above, with data acquired at emission wavelengths of 417 $\pm$ 10 nm, 525 $\pm$ 25 nm and 635 $\pm$ 20 nm. Within each image, n = 9 regions of interest (ROIs) were selected using Fiji [106] and the mean intensity value of these n = 9 ROIs was used as the mean value of tissue autofluorescence signal intensity for each data channel for each tonsil. This was required due to the difference in autofluorescence that was detected patient to patient.

3.2.6.3 Analysis of IL-17C and IL-1β expression

Brightfield transmission images were thresholded using Otsu thresholding in the FIJI 'threshold' tool, to create a mask for intensity measurements. Tonsil epithelium was visually distinguished from the rest of the tissue by assessing

its histological features and was evaluated to be between 0.2 mm and 1 mm thick. This agreed with the measurements of Olofsson *et al* [509]. Using Fiji, a freehand selection ROI was drawn to create masks of the epithelial and the core tissues. over the core tissues and extracting these data. The mean fluorescence signal intensity within each ROI for each channel was measured using the 'measure' tool in Fiji.

Data was plotted using Prism (GraphPad Prism v.8.0.2 for Windows, GraphPad Software, USA). Values of mean fluorescence signal intensity, and the ratio of fluorescence intensities in the epithelium to core tissues for both ART and OSA were plotted. For the ratio measurements, outliers were removed using Prism 'Identify Outliers' tool, choosing the ROUT (robust regression and outlier removal) [510] method with Q = 1%. Data were normalised for presentation purposes, using the 'Normalise' function in Prism.

All quantitative analysis used raw data. However, for presentation purposes, IF images were contrast adjusted using the Contrast Limited Adaptive Histogram Equalisation (CLAHE) function in FIJI [511] with the default parameters (block size = 127, histogram bins = 256, maximum slope = 3).

3.2.6.4 Colocalisation using JACoP

Colocalisation analysis was accomplished using an ImageJ plugin, JACoP [487]. JACoP offers a collection of colocalisation, correlation and visualisation tools within a simple package controlled by a user-friendly interface.

MCC was chosen for colocalisation analysis, with threshold being set on a per-patient basis. Blank specimens, which had been through the process of IF and FISH, but without the conjugated fluorescence probes or antibodies, were

used to guide baseline autofluorescence on a patient-by-patient basis used for thresholding

Heatmaps displaying the colocalisation results per disease type, at different spatial locations and depths throughout the tonsil were produced in Inkscape (Inkscape 1.1 (c68e22c387, 2021-05-23), Inkscape Project, USA), using the results generated with JACoP.

3.2.6.5 Statistical Analysis

Statistical analysis was performed using Prism. For western blot analysis, data were normally distributed and therefore an unpaired t-test was used to assess significance with $\alpha = 0.05$. For the analysis of all other data, a Mann-Whitney U test ($\alpha = 0.05$) was used in the case of non-normally distributed data. No multiple comparisons were made, focusing only on the inter-disease statistics. In all cases, raw data were analysed. Where data has been normalised, it has been re-distributed to fit between a 0 - 1 scale, with 0 corresponding to the minimum data value and 1 corresponding to the maximum data value.

3.3 Results

3.3.1 Optimisation

3.3.1.1 Section thickness

A series of sections of varying thicknesses were assessed to determine the optimal section thickness. It was found that 10 μm section thicknesses had minimal tearing and tissue folding. Sections taken below this thickness at 8 μm and 5 μm had a high degree of folding and tearing as can be seen in Figure **??**

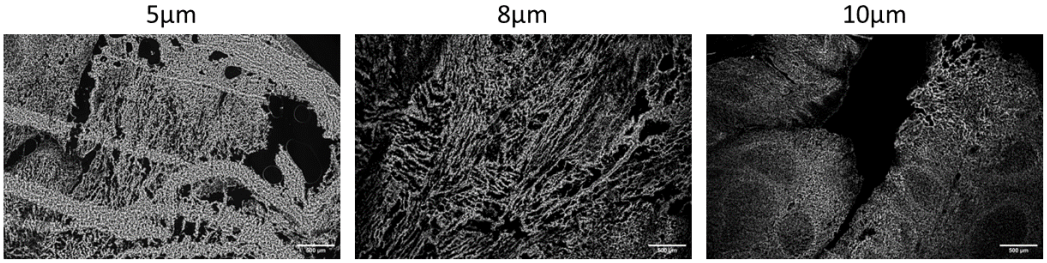

Figure 3.14: Tonsil sectioned at different thicknesses using Leica cryotome. 5um slicing yielded too many tears and tissue folding, 8um yielded too many tears, 10um was determined to be optimal thickness for this protocol. Scale Bar = 500um

3.3.1.2 Fluorescence *in situ* hybridisation

The optimised FISH probes can be seen positively staining bacteria within tonsil sections in Figure 3.15.

It was found that hybridising the large samples overnight provided optimal [471, 512]. This was assessed empirically and confirmed by literature. The diffusion of probes in solution, through a cell and through tissue is slow [513]. The probe length did not influence the incubation time as it was relatively short, however, there was a chance of small number of targets due to loss of

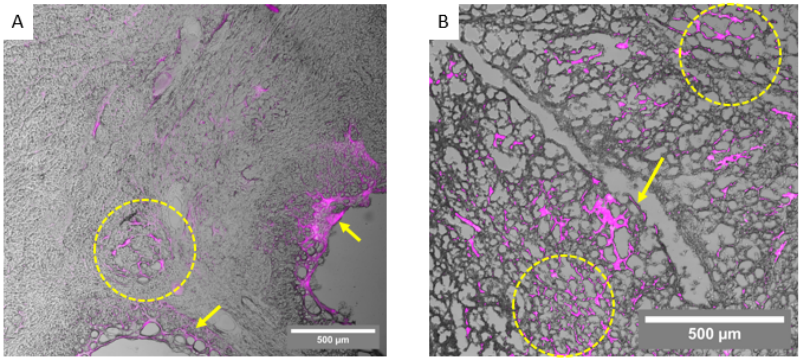

Figure 3.15: Staining of bacterial cells by FISH staining using EUB488 (magenta) on tonsil tissue (grey). Data presented as WF epifluorescence image (FISH) overlayed on top of a BF transmission image (tissue). A) Bacteria can be seen on tonsil epithelia (crypt epithelia) as shown with arrows, and can be found within the tonsillar tissue (dotted yellow circle). B) Bacteria found both somewhat lining tonsillar crypt (arrows) and spread more widely within tonsillar tissue (yellow circles).

bacteria due to long fixation times. Data were generated by thresholding image above value of autofluorescence in Fiji, creating a mask over the thresholded image and applying this mask to the raw data, taking the value of mean fluorescence. This was repeated for n = 4 of the 2 hour hybridisations and n = 8 of the overnight. It was found that there was an almost 4 times increase in mean normalised (re-distributed between 0 - 1 with 0 being the minimum data value and 1 being maximum data value) with 2-hour hybridisation having a mean normalised gray value of 0.14 and overnight increasing to 0.47.

3.3.2 IL-17C is expressed in both ART and OSA tonsils

Through analysis of western blots, the expression levels of IL-17C in human paediatric palatine tonsils was characterised, for the first time. It was found that IL-17C (approximately 15-20 kDa) was expressed in all patients (n = 16,

with n = 3 repeats per patient), as was IL-1β (approximately 30-35 kDa), these results can be seen in Figure 3.16.

Blots were quantified to show relative intensities against the house-keeping protein GAPDH, relative band intensity was measured and compared using FIJI. Relative intensity was plotted for both IL-17C and IL-1β in both patient groups. Tissue from patients with ART (n = 8) and OSA (n = 8) both showed expression of IL-17C. ART tissue homogenates had significantly higher expression levels of IL-17C (mean = 1.45) than the OSA patients (mean = 0.77), p = 0.05. Conversely, patients with ART typically had lower expression of IL-1β (mean = 0.35) while OSA had higher expression (mean = 0.66), but these data were not statistically significant.

3.3.3 IL-17C is expressed in the epithelium of patients with ART

IL-17C was shown to be predominantly concentrated in the epithelia of tissues from patients with ART, though expression likely from germinal cells and cell secretions can be seen less concentrated throughout the tissue. This was initially verified by qualitative examination of images. Figure 3 shows example Mesolens images of tonsil tissue from patients with OSA (Fig 3.A-C) and ART (Fig 3.D-F). IL-1β is widely spread throughout the tonsil tissues in tissue irrespective of disease, but IL-17C is mainly expressed in the tonsil epithelium of tissue from patients with ART, while tissue from patients with OSA does not show the same level of expression in this region.

Through analysis of the imaging data, it was shown that the ratio of expression of IL-17C in the epithelial to core tissue was significantly higher in tissue from

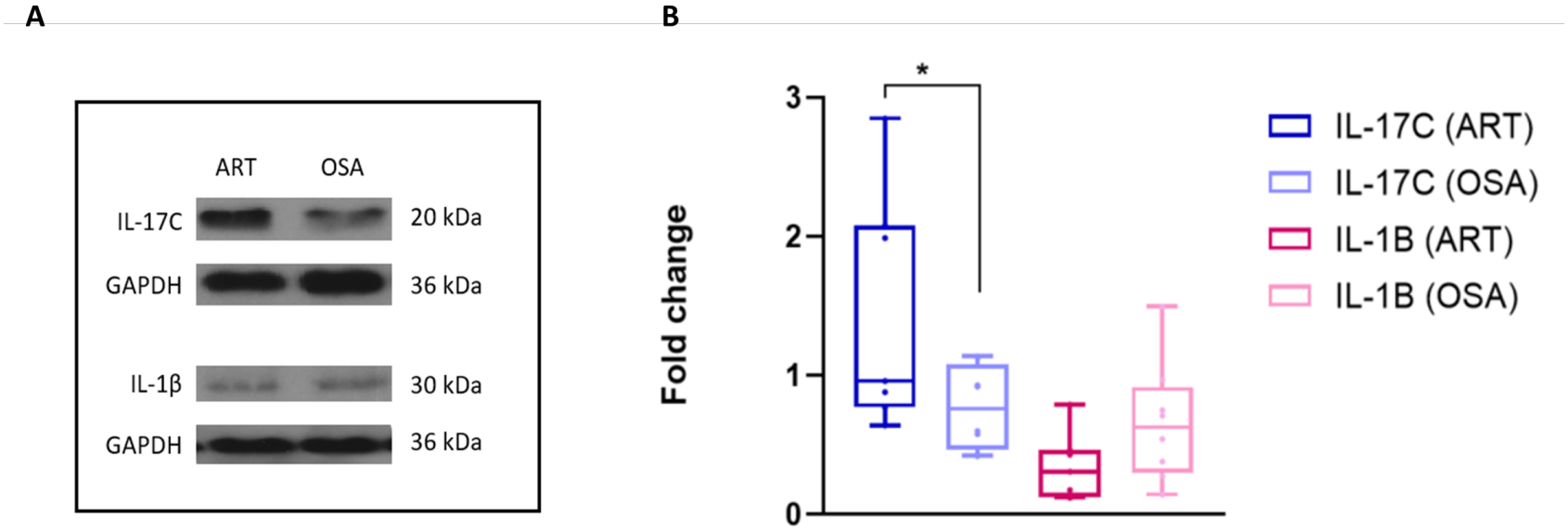

Figure 3.16: Protein quantification by western blot confirmed presence of IL-17C in both ART and OSA patient tonsil tissues over a total of n = 16 patient tissues (n = 8 ART and n = 8 OSA). A) Representative western blots of tonsil homogenates showing increase in expression of IL-17C in ART compared to OSA, with no difference in IL-1β expression. B) Graph shows relative band intensity against GAPDH, confirming that tissue from patients with ART have increased expression of IL-17C compared to tissue from patients with OSA (unpaired t-test, p = 0.05), whereas the levels of IL-1β in both patient groups showed similar expression.

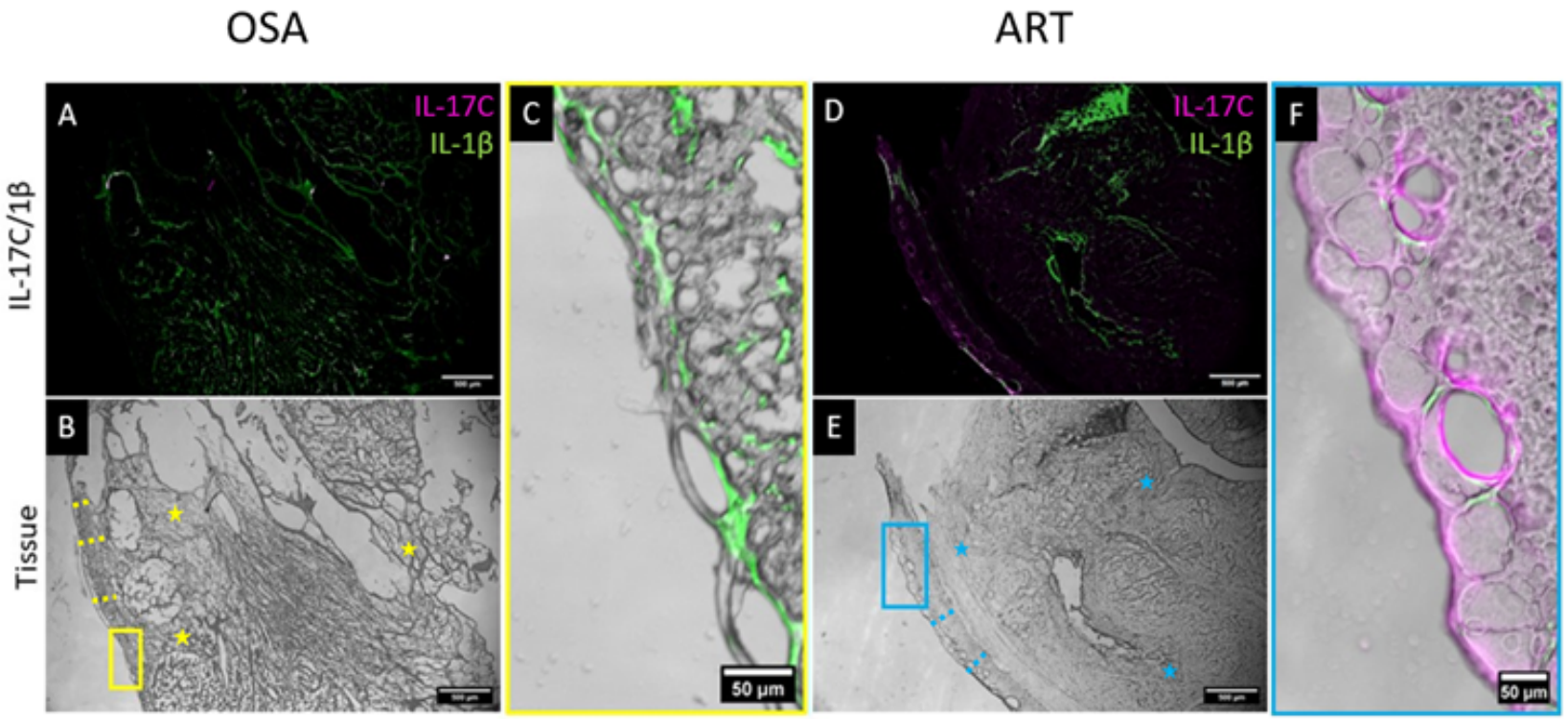

Figure 3.17: Representative Mesolens images of tonsil tissue. IL-17C is shown in magenta, and IL-1β is shown in green. Dotted lines represent regions considered epithelial tissue, and stars indicate regions considered core tissue (tissue comprising of lymphoid follicles, extrafollicular region and connective tissues) (A) shows a full field of view image of a tonsil section from a patient with OSA imaged with widefield fluorescence mesoscopy. (B) is a brightfield transmission image of the same region shown in (A). A yellow box highlights a small region of interest (ROI). (C) shows a digital zoom of the ROI highlighted in (B). No expression of IL-17C is present, although IL-1β is clearly visible. (D) shows a full field of view image of a tonsil section from a patient with ART imaged with widefield fluorescence mesoscopy. (E) is a brightfield transmission image of the same region shown in (D). A cyan box highlights a small ROI. (F) shows a digital zoom of the ROI indicated by the cyan box in (E). Unlike (C), almost no IL-1β expression is observed, but IL-17C is clearly visible in the surface epithelium of the tonsil.

patients with ART compared to tissue from patients with OSA. Figure 3.18 shows a graphical representation of the distribution of the ratios of epithelial expression to core expression of IL-17C in both ART and OSA. The mean ratio in ART was 1.37 (n = 28 images, n = 3 patients) while in OSA was 1.07 (n = 54 images, n = 6 patients), p = 0.004. This indicates that the difference in expression of IL-17C in the epithelial tissues compared to the core of ART patients is greater than that of OSA. IL-17C in OSA patient tissue is more dispersed throughout the tissue whereas it is more localised to the surface epithelial tissues in tissue from patients with ART.

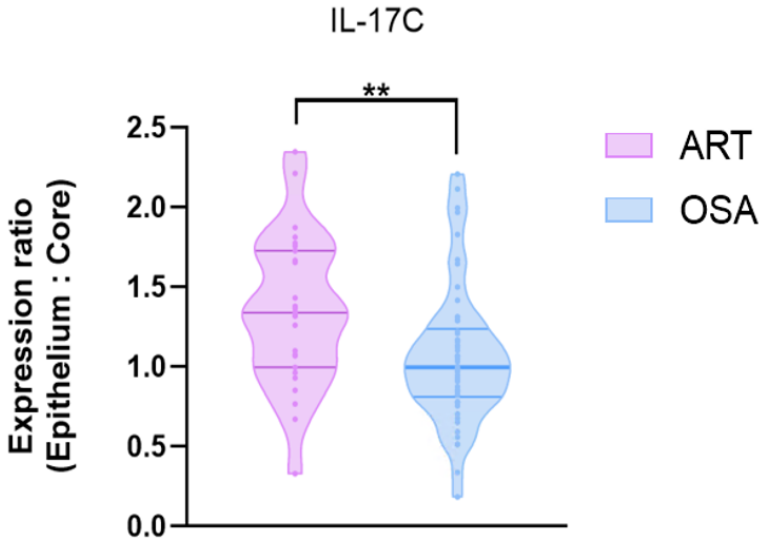

Figure 3.18: Ratio of expression of IL-17C in the epithelial tissue to core tissue of ART (pink) patient tissue and OSA (blue) patient tissue. Ratio is significantly greater in the ART tissues than OSA tissues (Mann-Whitney test, p = 0.004).

3.3.4 Expression of IL-17C and IL-1β is significantly higher in ART compared to expression levels in OSA

Through the same segmentation-based analysis, the values of mean fluorescence signal intensity were assessed in both diseases at the epithelium and core of the tonsils. Data were normalised for presentation purposes and can be seen in Figure 3.19. Through the detailed and region specific analysis, it was found that IL-17C expression was significantly higher in the epithelial tissues of tissue from patients with ART (mean = 0.19, n = 28) compared to tissue from patients with OSA (mean = 0.06, n = 54), $p < 0.0001$. IL-17C was also more highly expressed in the core tissue sections of tonsils from patients with ART (mean = 0.12, n = 28) when compared to tissue from the same tonsillar region from patients with OSA (mean = 0.06, n = 54), $p = 0.0007$. In addition, IL-1β expression was significantly higher in ART epithelial tissue (mean = 0.38, n = 28) than OSA (mean = 0.13, n = 54), $p = 0.002$. This increase in expression was not apparent in the Western Blots due to the nature of the blots encompassing a mix of homogenised tissue from various regions of the tonsil. In comparison, this method examines tonsillar regions with greater specificity, measuring the counts on only the epithelia or interior tissues.

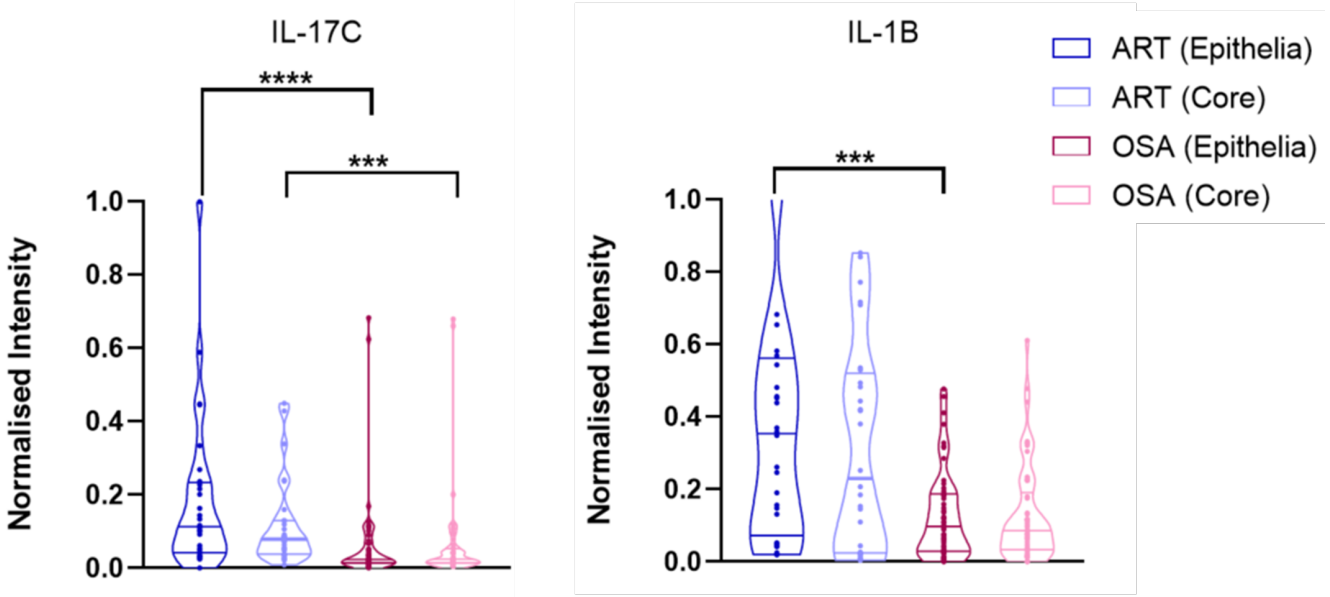

Figure 3.19: Normalised mean fluorescence intensities for epithelial and core tissues for patients with ART or OSA demonstrates that IL-17C is significantly higher expressed throughout the tonsil tissue in ART vs OSA. Each dot represents a single data set. A) Expression of IL-17C is significantly higher in the epithelia of tissue from patients with ART (dark blue) than in the epithelia of tissue from patients with OSA (dark pink), $p < 0.0001$. Additionally, expression of IL-17C is significantly higher in the core of the tonsil in patients with ART (light blue) compared with the expression level of the same interleukin in the core of the tonsil of patients with OSA (light pink), $p = 0.0007$. B) Expression of IL-1β is significantly higher in the tonsil epithelia of patients with ART compared to patients with OSA, $p = 0.002$. No significant difference in levels of IL-1β expression was found in the core of tonsils from patients with either ART or OSA. These data indicate that IL-17C expression is higher overall in the ART tissue than OSA tissue, with considerably higher expression levels in the tonsil epithelium. Mann Whitney U test, $\alpha = 0.05$, no multiple comparisons used, statistical tests performed on raw data.

3.3.5 Expression of IL-1β and IL-17C is spatially correlated with bacteria in OSA

Figure 3.20 demonstrates the distribution of bacteria within tonsillar tissue using fluorescence *in situ* hybridisation relative to the expression of both ILs (imaged using FISH).

Colocalisation analyses was performed using the JACoP ImageJ plugin, where M_1 was recorded to demonstrate the fractional overlap of IL-17C or IL-1β with bacteria, results were saved for figure preparation. Data is shown as heatmaps depicting degree of colocalisation measured on a colour scale ranging from 0 (deep magenta) to 1 (dark green). These data are shown for image location (left / centre / right) and slice depth through tonsil on figures 3.21 and 3.22.

No statistical significance was generated in these heat-map graphs, eluding that colocalisation was no different between location or depth of sample.

ART tissues had less colocalisation between IL-1β or IL-17C and bacteria when examining with Manders one-way colocalisation (the overlap of the IL of interest to bacteria). This is likely to be because ART patients have higher IL-17C and IL-1β expression than OSA patients and therefore the ratio of IL expression to EUB488 probe is greater in the ART patient tissue. Therefore, the probability of IL spatially overlapping with bacteria is lower in these patient tissues. Given there is little epithelia within the central tissues (except from the occasional crypt), it may be expected that IL-17C is also generally not colocalised with bacteria in the central tissue sections.

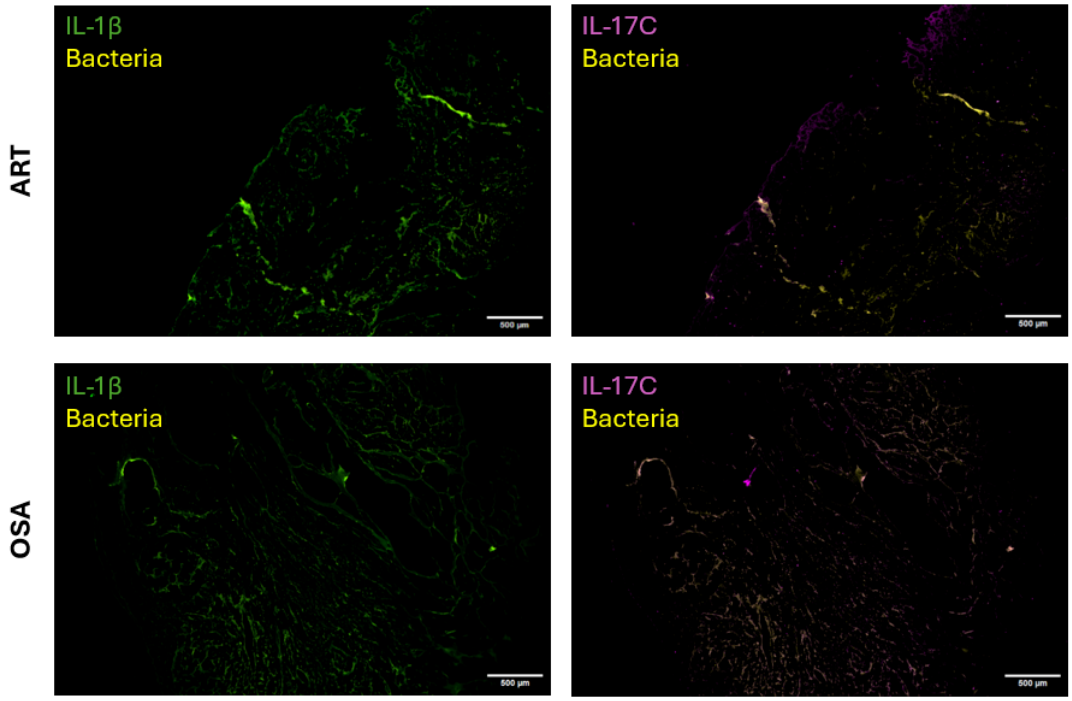

Figure 3.20: Distribution of bacteria (yellow), IL-17C (magenta) and IL-1β (green) on tonsillar tissue. Representative overlap of IL-1β to bacteria and IL-17C to Bacteria for ART (top row) and OSA (bottom row). Representative for n = 3 ART patient tissues and n = 6 OSA patient tissues.

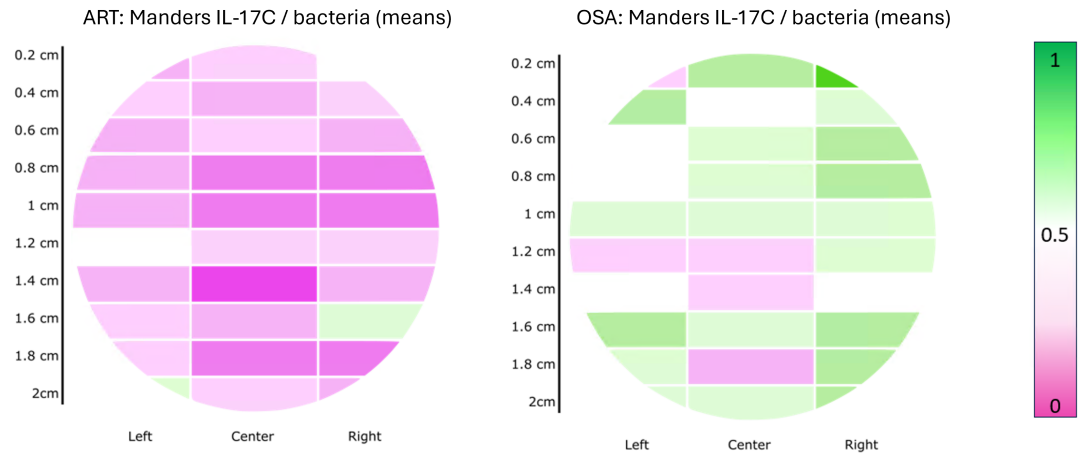

Figure 3.21: Magenta represents no or little colocalisation, green represents varying degrees of colocalisation. Left, centre, right represent locations of image on a single section as described in section 3.2. The cm scale represents the distance from the upper tonsil surface 0.2 cm is the location of the first cryosection, 2 cm is the location of the final cryosection. Left shows colocalisation of IL-1β to bacteria in ART patients, right is for OSA.

3.4 Discussion

This work shows that IL-17C is expressed at significantly higher levels throughout the tonsil mass in ART patient tissue than in OSA, with its increased expression in the epithelium of patients with ART being higher than the core expression on a patient-by-patient basis. IL-17C is a marker of bacterial infection and has been extensively studied in other tissues [413, 414, 514], but here the potential of IL-17C as a biomarker for diagnosis of ART has been shown.

These findings are consistent with other studies involving IL-17C in similar tissue types. For example, IL-17C has been shown to be expressed in adenoid tissues [413] and nasal epithelia [414]. This work is the first to demonstrate and

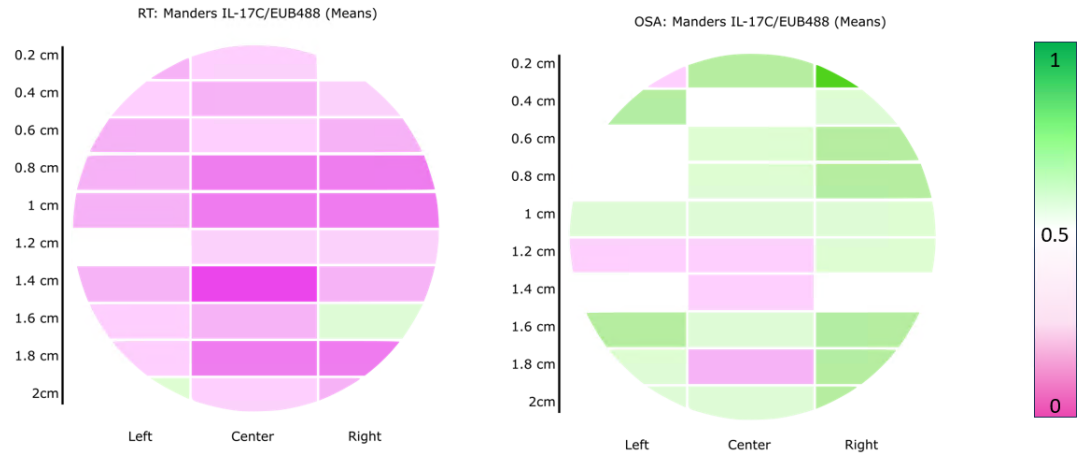

Figure 3.22: Magenta represents no or little colocalisation, green represents varying degrees of colocalisation. Left, centre, right represent locations of image on a single section as described in section 3.2. The cm scale represents the distance from the upper tonsil surface 0.2 cm is the location of the first cryosection, 2 cm is the location of the final cryosection. Left shows colocalisation of IL-17C to bacteria in ART patients, right is for OSA.

quantify its presence in tonsillar epithelia, and the first to successfully characterise the difference in protein expression between tonsils from patients with ART and patients with OSA. IL-17C plays a critical role in early infection defence; its synergistic role with TNF-α upregulates other cytokines, chemokines, and antimicrobial clearance agents [410, 514]. Therefore high expression is indicative of active microbial infection [410].

The ability to use IL-1β as a biomarker for tonsillar disease has conflicting evidence in current literature. Agren *et al* showed that IL-1β is expressed at significantly higher levels in ART patients than hypertrophy patients [515], however, Huang et al have shown that IL-1β is significantly more expressed in tonsillar hypertrophy patients when compared to 'control' and to patients with

co-morbid hypertrophy and infection [516]. Spikermann *et al* examined serum and saliva samples from ART patients compared to 'healthy' control volunteers and found that IL-1β expression was higher in the ART cases [517]. To conflate this further, Babakurban *et al* showed no difference between expression of IL-1β between OSA and ART patients [518]. Therefore, it is difficult to determine whether IL-1β may be used as a marker for either OSA or ART from searching literature. It has been demonstrated in this study that there a significant increase in expression of IL-1β in the tonsillar epithelial tissues of tissue from patients with ART compared to OSA patient tissue, somewhat confirming the results of Agren *et al*, however, no such difference is seen in the core tissues. This is a subtle but potentially important finding; the sensitivity allowed by analysis of IF images to determine expression between different tissue regions allowed for such significance in results to be achieved in comparison to blots where large volume of mixed tonsil tissue homogenates were analysed. The work of Agren *et al* considered expression levels throughout the tonsil, but the data in this Chapter shows that the expression level varies significantly in different regions the tonsil. Significant differences in expression at the protein level between ART homogenates and OSA homogenates with western blots has not been shown. Therefore concluding that IL-1β is not as strong a candidate as IL-17C as a potential biomarker for ART.

The potential to use expression of IL-17C as a biomarker for ART has been explored, however, the methods used in this Chapter currently do not facilitate pre-operative detection of these cytokines. One proposed method to detect pre-operatively would be to take swabs from the tonsil epithelia, which would contain detached epithelial cells, and stain these for IL-17C. This method would likely be restricted to sampling from the tonsil epithelium, but as the results in

the measurement of IL-17C in the tonsil epithelia shows, this may be adequate for assessment. Another proposed method would be to perform protein extraction from tonsillar swabbed cells, from tonsil exudate, or from saliva samples. IL-17C has been shown to be secreted extracellularly in adenoid tissue, therefore it is highly likely to be secreted from palatine tonsils due to their immunological similarities [413]. Saliva has been previously used to determine expression levels of biomarkers of tonsillar diseases [518, 519] and others have demonstrated its use in delineating between ART and tonsillar abscess [520]. It is however worth noting that using saliva introduces the risk that the signals of inflammation or disease have originated elsewhere in the oral cavity. Within this study, due to restrictions surrounding ethical approval, it was not possible to perform pre-operative assessments with saliva or exudates, limiting this study to being purely post-operative detection. Further work in assessing the presence of IL-17C in pre-operative saliva / exudates [519, 517], would be essential for determining if these cytokines can be used as a pre-operative biomarker of disease.

Interestingly, *S. pyogenes*, thought to be one of the main contributors to bacterial tonsillitis infections, contributes to IL-1β secretion. *S. pyogenes* produces streptolysin O, a pore-forming toxin, which induces a cascade of protein activation resulting in the secretion of IL-1β [521]. Therefore, a significant increase in IL-1β expression within the tonsillar tissue of ART patients compared to OSA was expected, however this was only found to be the case in ART tissue epithelia when examined with IF. Recent studies have shown that many patients are asymptomatic carriers of *S. pyogenes* [522, 523, 524], which may contribute to the similar expression profile in the 'uninfected' OSA tonsillar tissue. This is further evidenced by Viciani *et al* who found an association

with *S. pyogenes* in patient tissue extracted due to OSA [525]. Therefore, general bacterial presence within tonsils may not lead to the increased expression of immune markers, and instead is likely to be more complicated by multiple species, specific bacterial colonisation or to the degree of colonisation of a particular species within a patient.

In Chapter 2, it was noted noted that fixation of tissue results in degradation of total bacterial bio-volume. This is why imaging on fresh *ex vivo* tissue was performed. Within this chapter though, fixed tissue was used. While IF and FISH on fresh tissue is possible, it is in its infancy. Standard protocols for IF and FISH were used rather than further developing live-FISH / IF, as such, it is likely that the work in this chapter is not detecting the full bacterial burden that would have been present prior to fixation. Therefore, the degree of colocalisation in this study may be lower than the truth if tissue had not been fixed.

The number of specimens made available in this study limit it to having an exploratory nature. Due to limitations in sample size, we make postulations on the ability of these cytokines to be used as biomarkers; this would have to be followed up with robust studies on expression in both diseased and healthy patients. In addition, as an indicator of biomarker status, further study would have to be performed on if detection of either cytokine furthered disease treatment such that its detection led to a more positive patient outcome than if it had not been detected. In addition, it was not possible to gather control tissue for our study. Control tissue in such a study may involve the use of post-mortem tissues where ART / OSA was not implicated in the patients recent medical history. This was not possible due to the ethics approvals in place. In addition, there would be no guarantee that such tonsils would be absent of

pathogens and may have evidence of increased cytokine production. Instead, it may be possible to use a primary tonsillar epithelial cell line to demonstrate a baseline level of expression of IL-17C to compare to the ART and OSA levels of expression. However, this was not possible to achieve during the study. Despite this study limitation, we have shown a significant increase in the expression of IL-17C in ART patient tissues, indicating that there is involvement in the pathophysiology of ART. With this knowledge, further study into it's suitability as a biomarker is warranted, but outwith the scope of this study.

It was found that there was no correlation between bacterial location and the spatial expression of either IL-17C or IL-1β within the ART tonsil sections. However, there was evidence of correlation between these for the OSA patient tissue sections.In the heat-map data from Figures 3.21 and 3.22, it was shown that in both cases, there was higher colocalisation between the studied ILs and bacterial staining in the OSA cases. Due to the relative lower abundance of the ILs in the case of OSA, this initially came as a surprising result. However, this result may be explained in a few ways. Firstly, the work in Chapter 2 demonstrated that ART and OSA have similar biofilm abundance [110]. Therefore, with similar levels of biofilm / bacterial presence between samples, but relative lower expression of antibodies, it is to be expected that the fractional overlap of IL to bacteria would be higher in the case of OSA. For ART, with a significantly higher expression of ILs, the fractional overlap of IL to bacteria would be lower. Secondly, it would be safe to assume from a naïve perspective that since IL-17C is expressed in response to bacterial stimulation, then it should be expressed where the bacteria is located. However, IL-17C is not released exactly due to the presence of bacteria, rather, it is expressed as a consequence of bacterial insult and is also stimulated by other cytokines. Some

of these include TLRs, TNF-α and IL-1β. Due to this, the expression of IL-17C may occur at regions further afield from the exact location of the bacterial insult. Therefore, with widely spread and significantly increased expression of IL-17C, sometimes across the whole epithelia, in ART patients it is reasonable to expect that the colocalisation of interleukins and bacteria is lower in ART than OSA.

3.5 Conclusion

In this chapter, the potential of using IL-17C as a biomarker for ART has been explored using a combination of molecular biology, imaging and imaging analysis.

Using immunoblotting of homogenised tonsillar tissue, it was shown that IL-17C is expressed significantly higher in the homogenates from ART patient tissue in comparison to OSA patient tissue. Meanwhile, IL-1β expression was not statistically significant between disease. Immunofluorescence staining was used to determine the spatial distribution of the cytokines in excised patient tissue, confirming that IL-17C was expressed predominantly in tonsillar epithelia, but could also be found throughout. The levels of expression of IL-17C in both the epithelial and core regions in ART patient tissues were significantly higher than OSA patient tissues. In addition, IL-1β was found to be spread throughout the tonsillar mass, but was generally less evident in the epithelia of ART patients when compared to IL-17C expression which dominated in the epithelial tissue. An important finding brought about by the analysis of IF images was that IL-1β is expressed at significantly higher levels in the epithelia of ART in comparison to OSA patient tissues, despite appearing visually more dispersed across tissue.

By looking at the data mentioned in the previous paragraph, the expression of IL-17C in the tonsillar epithelia compared to the core were examined on a patient by patient basis. This analysis showed that the ART patient tissue had a higher ratio of expression of IL-17C in the epithelia compared to core than that of the OSA tissue. This indicates that expression of IL-17C in the epithelia of tissues of patients afflicted with recurring infection is higher than those with

hypertrophied tonsils.

Chapter 2 showed that biofilms were present throughout patient tissue in both ART and OSA with approximately equal volume. By using FISH alongside IF the spatial distribution of bacteria could be seen in relation to the expression of ILs. By using MCC, with the minimum threshold being taken as the value for autofluorescence in the relative data channels, it was possible to determine the fractional overlap of an IL of interest with the bacteria within the sample. It was found that there was very little to no spatial overlap of both ILs with bacteria in the ART patients, likely due to the relative high abundance of cytokines in relation to bacteria reducing the probability of overlap. In comparison, the OSA patients which had overall lower expression of both ILs compared to the ART tissue, with the same level of bacteria, demonstrated medium to high spatial overlap of both ILs to probes. This demonstrated that while both disease types have bacteria and biofilms present, it is not the bacterial abundance that dictate the level of cytokine presence within the tissue, and is likely due to various immune cascades contributing to expression of both cytokines in the chronically infected patients.

The presence of IL-17C and IL-1β in ART and OSA using a combination of molecular biology and imaging techniques, and has demonstrated the promise of IL-17C as a potential biomarker for ART, and demonstrates that it plays a role in the pathophysiology of ART. This work was performed on a relatively small cohort of patients (n = 17), therefore in order to further test this hypothesis it would be useful for this to be tested on a much larger cohort of patients. In addition, by testing for IL-17C or IL-1β patients on perfect controls, such as primary tonsillar cell lines, it may be possible to elucidate a baseline of expression in non-diseased patients upon which an increase of expression

indicative of disease could be bench-marked to. The obvious extension of this work would be to perform more specific blotting to selectively blot on tissue homogenates from exclusive regions of the tonsil such as epithelia or core in order to further verify the specificity of expression that was demonstrated in the IF. Additionally, after verification of biomarker status, it would be interesting to determine if the expression was detectable in patient saliva, tonsillar exudates / washes, or via tonsillar swabs, at a point of care setting. Finally, comparison of IL-17C expression levels between viral and bacterial infected tonsils would be of interest, once again to determine if the expression profiles were different. This would potentially allow for a biomarker to detect if infection was due to one or the other, and to help guide antibiotic prescribing to help with the reduction of antibiotic prescribing which is contributing to antibiotic resistance.

Chapter 4

Fluorescence lifetime microscopy can distinguish ART from OSA

4.1 Introduction

In the previous chapters, fluorescent dyes have been used to delineate between ART and OSA patient tissue. In this chapter, I aim to use the properties of endogenous fluorophores in tonsillar tissue to determine if there are intrinsic differences in the lifetimes of these fluorophores within different diseased states. To study this, Fluorescence Lifetime Imaging Microscopy (FLIM) was applied to examine the lifetimes of endogenous fluorophores within tonsillar tissue. To our knowledge, FLIM has not been implemented in the study of ART or OSA in tonsillar tissues. To date, tonsillar studies using FLIM have involved tumour and cancer studies [526, 527, 528]. Being able to assess ART and OSA via lifetime imaging would potentially allow for differentiating between disease with minimal sample preparation - only freezing and sectioning of the tissue prior to imaging would be required. *In vivo* FLIM has been performed in the past and may be applicable to the diagnosis of ART and OSA if differences in

lifetime were apparent *in vivo* FLIM measurements [529, 530, 531, 39].

First, the FLIM system used was calibrated using known methods of diluting fluorescent dye with a known lifetime into an ascending glycerol series [532]. The ability to use frozen tissue in place of fresh tissue was then assessed and compared to fixed tissue to determine if the lifetimes were similar. After further optimisation, FLIM was performed using a high magnification objective lens on a time-correlated single photon counting PicoQuant MicroTime 200 system. Three regions within three tissue sections of 10 μm thickness were imaged from a total of 16 tonsils (9 ART, 7 OSA). Lifetimes were fitted using n-exponential reconvolution fitting models, and individual lifetime components were compared between ART and OSA to determine if different lifetimes were measured.

4.1.1 Fluorescence Lifetime Imaging Microscopy

Fluorescence lifetime imaging measures the lifetime of fluorophores within a sample, and, in contrast to intensity based imaging, is generally insensitive to fluorophore concentration. It can be applied in different imaging modalities such as endoscopy and tomography [533], however, in this thesis its application in microscopy is of interest.

Applications of fluorescence lifetime imaging microscopy presents images which are generally false colour coded such that the colour of each pixel represents lifetimes and the intensity of these colours represent the number of objects with these lifetimes [98]. Both time-domain (TD) and frequency domain (FD) measurements are possible for recovering lifetime parameters [534]. TD and FD measurements have similar temporal resolution, and are related by the Fourier Transform [534]. While similar in nature, they are better suited to different applications. FD-FLIM is better suited to the study of short lifetime measurements and is possible with any continuous wave light source [33]. TD-FLIM, however, is better suited for large temporal-range systems or measurements where long lifetimes are expected [33].

TD-FLIM involves reconstructing the (multi-)exponential decay of fluorescence intensity over time and is achieved via time-gated FLIM and time-correlated-single-photon-counting (TCSPC) FLIM [535]. TCSPC-FLIM was used in the work in this chapter.

4.1.1.1 Excitation

To excite fluorophores and subsequently detect their lifetimes in TD-FLIM, ultrafast pulsed lasers are required [535]. Ultrafast in laser terminology typically

refers to lasers with pulses shorter than 1 ps [536] in duration. The earliest ultrafast lasers were dye laser systems whose gain materials were made of jets of organic dyes which were dissolved in viscous solvents and were pumped by argon ion lasers [537, 538]. These systems were physically large, relatively unreliable and complicated to use and maintain, therefore their use was limited to few labs where they were operated by laser experts.

Developments into ultrafast lasers have happened rapidly in recent years, with ultrafast solid state and fiber lasers becoming possible due to advancements in the fields of optics and semiconductor physics [539, 540]. Common ultrafast lasers used for biophotonics applications are femtosecond Ti:sapphire lasers which are widely tunable over wavelength ranges [541]. In addition, other ultrafast diode pumped solid-state lasers are available which are doped with other rare earth materials (such as neodymium and ytterbium), however, these have limited emission bandwidths and have slightly longer pulse durations in comparison to the Ti:sapphire lasers [542]. Ultrafast fiber lasers are also used for biophotonic applications, with their inherent design meaning that they take up a small footprint on an optical table with their ability to be coiled [543, 544].

4.1.1.2 TCSPC

The first TCSPC-FLIM scanning microscope was developed in 1988 at the Friedrich Schiller University Jena in Germany and used an ultrashort (picosecond) pulsed laser for excitation [545].

TCSPC-FLIM requires the recording of the time-dependent intensity profiles of emitted light after excitation from a pulsed source [98]. Endogenous fluorophores have extremely short lifetimes: using ultrafast pulsed lasers and collecting emission over multiple cycles of excitation and emission, it is possible

to reliably reconstruct fluorescence decay profiles from many cycles of single photon events.

In a sample with high quantum yield, each single excitation pulse would generate a detectable fluorescence decay, however, this is rarely the case in practice [33]. The reasons for this range from using relatively low excitation power to limit effects of photodamage, to weakly fluorescing samples. To overcome these limitations, time differences between excitation and emission per pixel per cycle is measured by the imaging system, similarly to a stopwatch [98]. These 'stopwatch' readings are sorted into histograms showing the range of lifetimes per image or pixel. TCSPC therefore requires highly sensitive detectors capable of detecting single photons such as photomultiplier tubes (PMT), micro channel plates (MCP) or single photon avalanche diodes (SPAD) [33, 98, 535]. SPAD detectors are frequently used in TCSPC-FLIM due to their relative low costs, high quantum efficiencies and resistance to damage by high light levels. However, they have comparatively small active sensor areas of up to a few hundred micrometers (compared to several millimeters afforded by PMTs and MCPs) [546].

In a TCSPC measurement, the detector records each excitation pulse to which produces the starting signal which triggers the voltage ramp of a time-to-amplitude converter (TAC) (start of stopwatch), when stops after a photon is then detected (end of stopwatch) [33]. This provides an output pulse which has a voltage proportional to a time channel using an analogue to digital converter (ADC) and multichannel analyser (MCA) to allocate the count to its time channel [546]. Samples are excited at MHz rates to build a probability distribution histogram of photon arrival time in the MCA. This information is used to compile the fluorescence decay curve [546].

Within a TCSPC FLIM system, many cycles of excitation and photon detection are required. This is to facilitate a low photon count at the detector of < 10% of the excitation repetition rate [98]. This is to avoid an effect known as the pile-up effect where, due to instrument dead time, many of the emitted photons will not be detected [547]. The result of this effect is that only photons with shorter arrival times will be recorded, creating an overall shortening of the fluorescence lifetimes detected in the system. The signal-to-noise ratio of FLIM in a TCSPC arrangement (SNR_{FLIM}) is dependent upon the number of photons detected per pixel (N) [548]:

$$SNR_{FLIM} \propto \sqrt{N} \tag{4.1}$$

Thus, improvements in the SNR_{FLIM} are made by repeating the photon detection process thousands of times in order to create a histogram of the fluorescence lifetimes. It is important, however, to consider the sample when performing TCSPC. Autofluorescence FLIM typically has a lower photon count than labelled FLIM, therefore it may be necessary to increase the photons detected per pixel. To do this, increasing the pixel dwell time, repeating imaging over multiple frames or a combination of both may be used to generate adequate photon statistics.

The temporal resolution of a TCSPC system is given by the Instrument Response Function (IRF) [547]. A perfect system with no loss, infinitely short laser pulse, and infinitely accurate detection would have an infinitely small (or narrow) IRF. Deviations from this result in a broadening of the IRF. Sources which contribute to the IRF can be from the detector (timing accuracy when

converting photon to electrical pulse), excitation source (from syncing the timing of pulse to detection), and timing jitter of components (phase noise from signal interference in electronics). The total system IRF is the convolution of all component IRFs [547].

Mathematically, the measured decay intensity *D(t)* is a convolution of the IRF, *R(t)* and the fluorescence decay function *(F(t)*:

$$D(t) = \int_0^t F(t')R(t-t')dt' \tag{4.2}$$

Therefore, to determine the fluorescence decay (or lifetime) at a particular pixel, the excitation pulse must be deconvolved from the measured decay [547, 33, 98]. The methods upon how this is performed is discussed in the following section.

4.1.1.3 Curve fitting

FLIM measurements provide 3D data containing spatio (xy) -temporal (lifetime) information. Methods of 3D spatial (x,y,,z) FLIM exist, introducing the ability to produce 4D-FLIM data. Therefore, analysis can be more complicated in FLIM than when considering fluorescence intensity. In FLIM, firstly the IRF is either imported to the analysis software, or in the case of this thesis, reconstructed within the software by evaluating the onset of the fluorescence decay. The decay curve is then analysed via various methods depending on availability of methods in the software, and which method is most applicable to the experiment. Methods of analysing or fitting decay curves include:

1. rapid lifetime determination (RLD) and analytical least-squares algorithms: useful for time-gated FLIM data analysis, not for TCSPC [549].

2. n-exponential reconvolution fitting (iterative least-squares analysis with multi-exponential fitting): this is the method used in this thesis and will be discussed in greater detail below [550, 551, 547].

3. phasor plot analysis: originally optimised for FD FLIM, now applicable to TD FLIM. Produces a plot where every molecular species present has a unique phasor vector which allows for their identification on the plot [98, 552]. Again this was limited by software restraints, so was not used in this thesis.

The iterative least-squares analysis mentioned above, and henceforth referred to as n-exponential reconvolution, is applicable to the analysis of TCSPC FLIM data, and remains one of the most reliable methods for TD-FLIM analysis [553].

During n-exponential reconvolution fitting, the fluorescence decay is estimated by lifetime distribution [554]:

$$\frac{F(t)}{F_0} = F_N(t) = \int_0^\infty p(\tau) e^{-\frac{t}{\tau}} dt \tag{4.3}$$

where τ is the lifetime and $p(\tau)$ is the corresponding probability amplitude. In most cases, multi-exponential fitting is used, in which case $p(\tau)$ is represented by a weighted sum of lifetime components τ_i:

$$p(\tau) = \sum_{i=1}^{n} \alpha_i \delta(\tau - \tau_i) \tag{4.4}$$

giving:

$$F_n(t) = \sum_{i=1}^{n} = \alpha_i e^{-\frac{t}{\tau_i}} \tag{4.5}$$

where α_i is the contribution from the ith lifetime component. The resulting decay function is convolved with an IRF to allow for comparison against the measured decay. Fitting parameters (α and τ) are iteratively improved by increasing exponential fit until a good fit is made. Goodness of fit is determined via a least-squares analysis performed using the chi squared (χ^2) statistic:

$$\chi^2 = \sum_{j=1}^{n_c} \left[\frac{D_{obs}(j) - D_{calc}(j)}{\sqrt{D_{obs}(j)}} \right]^2 \tag{4.6}$$

where j represents the channel number, n_c is the total number of channels used in the fit, D_{obs} is the measured decay and D_{calc} is the calculated decay after convolution with the IRF. The residuals of the fit, r, are given by:

$$r(j) = \frac{D_{obs}(j) - D_{calc}(j)}{\sqrt{D_{obs}(j)}} \tag{4.7}$$

χ^2 is usually normalised by the degrees of freedom in the fit, v, in order to account for the number of fitting parameters within the model n_p:

$$\chi^2_R = \frac{\chi^2}{v} = \frac{\chi^2}{N_c - n_p - 1} \tag{4.8}$$

The goodness of fit may be interpreted in the following way:

1. $\chi^2_R \gg 1$ is a poor fit
2. $\chi^2_R > 1$ suggests the fit is not adequate
3. $\chi^2_R \approx 1$ suggests that the observed fluorescence decay has been adequately matched to the model
4. $\chi^2_R < 1$ suggests the data is *over-fitted*

In most cases, over-fitting occurs due to the model having too many parameters or due to an inappropriate fitting range. The χ^2 informs the overall quality of the fit by indicating the magnitude of the residuals.

In a single-lifetime source sample (i.e single fluorescent dye on a coverslip), a single-exponential fit would be adequate for fitting and would return a $\chi^2_R \approx 1$. Adding complexities to the sample such as inhomogenous distribution of a probe, or multiple probes introduces the need for additional exponents and results in poorer fitting χ^2_Rs [555]. Therefore, in FLIM experiments involving complex samples or autofluorescent tissue with many lifetime contributors, a $\chi^2_R \approx 1$ and $\chi^2_R \leq 1.5$ is considered appropriate [555, 556, 557]. Throughout this chapter χ^2_R was generally found to be between 1 and 1.3 ns. If fit residuals are found to be randomly distributed around zero [558, 559], and the χ^2 is within the defined accepted range, the decay has been well matched to the model.

The multi-exponential fitting model produces lifetime components corresponding to the number of exponents used, i.e a 3-exponential fit generates 3 lifetime components. Studies which examine, for example, NADH and FAD often use two-exponential decay fitting to accurately map lifetimes to those individual components [560]. However, it becomes more complex in samples with unknown lifetime contributors (and sometimes with known), where increasing exponents increases the risk of overlap in components. This overlap often occurs in the τ_2/τ_3 lifetime components [561, 562], and was something found to also happen within the work in this chapter.

4.1.1.4 Microscopy

In general, two microscopy techniques are employed in FLIM imaging, namely CLSM and WF. Within a microscope geared for FLIM, an appropriate light

source for illumination and highly sensitive detectors must be present alongside the electronic components required for detecting the fluorescence lifetimes [98].

WF FLIM may be used in the time domain: after exciting a sample with an ultrashort laser pulse, time-gated images of fluorescence emission are taken at various time delays (in the order of nanoseconds) WF FLIM has several advantages: comparatively lower photobleaching [544] to CLSM and higher frame rates as all pixels are acquired in parallel [563]. The high frame rates are advantageous as this method allows for rapid acquisition of FLIM data (100 Hz FLIM has been reported [564]). However, this methodology has several disadvantages: they do not have single-photon sensitivity, are less precise than CLSM methods and have a limited temporal resolution of approximately 80 ps [33].

CLSM has several advantages over WF epifluorescence microscope, as were discussed in the introductory chapter. TCSPC is considered the best method for TD FLIM: it has the best signal to noise ratio of any FLIM technique, single photon sensitivity and wide dynamic ranges which allow visualisation of fluorescence decays. A schematic overview of a TCSPC CLSM FLIM system may be seen in Figure 4.1.

4.1.2 Fluorescence lifetimes as a diagnostic aid

Fluorescence lifetime imaging may be used to guide disease detection based on the characteristically different lifetimes exhibited by different molecules. A few examples of these are discussed below.

Fluorescence lifetime imaging ophthalmoscopy (FLIO) is a technique used to

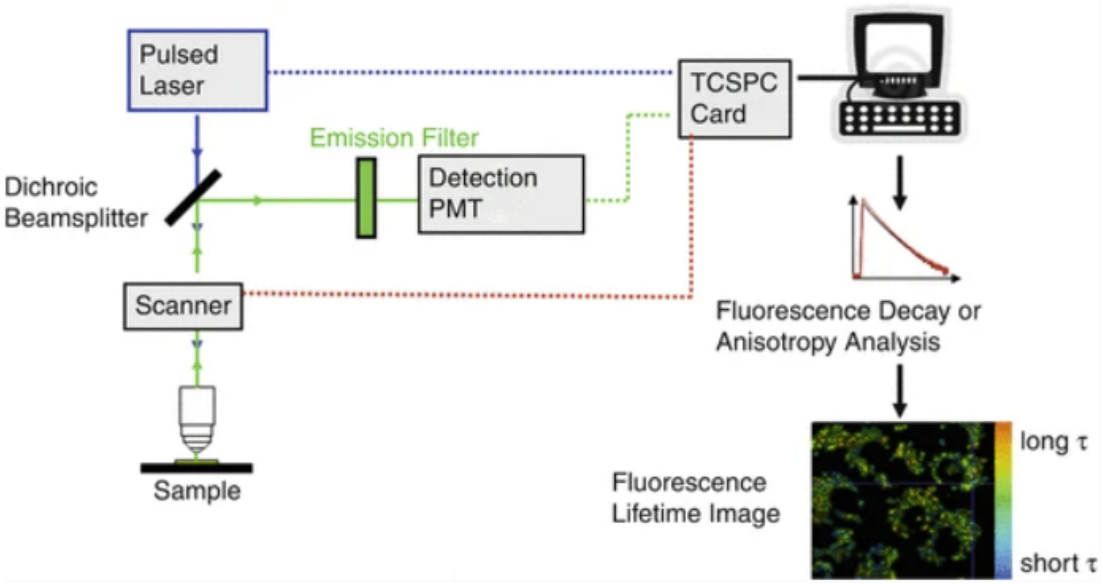

Figure 4.1: A schematic of a TCSPC based scanning FLIM setup. A pulsed laser is scanned across the sample, the pulse time is recorded through TCSPC electronics. Once excited, emitted photons are guided to a detector (PMT in this diagram) and the time of photon arrival collected. The 'TCSPC' card depicts location of the FLIM electronics responsible for the 'stopwatch' component of a FLIM system. The fluorescence decays are sorted into time bins and analysis is performed to extract the measured decay. FLIM images are displayed as false colour images where the colour corresponds to lifetime. Figure reproduced with permission (License number: 5705971060078) [546]

assess FLs *in vivo*, by applying a laser pulse to the retina to excite endogenous fluorophores within the tissue[530]. The differences in decay times of these excited fluorophores can be measured, and quantitative images of the retina can be formed using a false-colour look-up table that indicates the different lifetimes present [565]. FLIO can detect retinal abnormalities at early stages, and has been shown to be useful in detecting early Alzheimer's disease markers [566].

Secondly, a research group examining cancerous and non-cancerous breast tissues found that malignancy-associated stromal regions decay more quickly than benign stromal regions, although the specific molecular mechanisms were not elucidated [567]. Another study analysed the efficacy of cancer treatments *in vivo* using FLIM, and showed that there was a significant difference in observed lifetimes pre- and post-treatments [568].

Several studies have used FLIM as a tool for studying host response to viral infection [569, 570, 571], bacteria [572, 573] and infection by parasites [574]. However, at the time of writing, no study involving ART and OSA has been performed using FLIM.

4.1.3 Endogenous fluorophores in tonsils

As discussed in previous chapters, autofluorescence is present in tonsillar tissues and can serve as both advantageous and a hindrance depending on the study. In Chapter 2, autofluorescence was of little consequence. In chapter 3, however, autofluorescence was a problem, due to the need to image the fluorescent probes and not the endogenous fluorophores within. In this chapter, the aim is to use autofluorescence, or the fluorescence emission from endogenous fluorophores, to determine if the autofluorescence lifetime of tissues can

be used as a diagnostic aid.

Biological specimens have an abundance of endogenous fluorophores which have been exploited for label-free imaging [575, 37]. Examples of endogenous fluorophores with known lifetimes are displayed in Table 4.1. Endogenous fluorophores which may be present in tonsillar tissue involve amino acids including phenylalanine [576], tyrosine [577] and tryptophan [578, 579], connective tissue proteins such as collagen [580] and elastin [579], and metabolic co-enzymes such as nictinamide adenine dinucleotide phosphate (NAD(P)H) [39, 581], flavin mononucleotide (FMN) and flavin adenine dinucleotide (FAD) [580]. Imaging endogenous fluorophores is advantageous as their emission properties are often indicative of sample microenvironment, metabolic state and pathological sample condition. Alongside this, minimal sample preparation is required since the addition of exogenous fluorophores is not required.

Nicotinamide adenine dinucleotide (NAD) and flavin adenine dinucleotide (FAD) are two commonly examined endogenous fluorophores which are co-enzymes involved in cellular metabolism [98]. The reduced form of NAD, NADH, is fluorescent, alongside the reduced NAD phosphate (NADPH), however, their fluorescence signals are difficult to distinguish and therefore they are often referred to by their combined fluorescence as NAD(P)H [98]. FAD is also fluorescent. Due to the crucial roles they play in cellular metabolism, NADH, NADPH and FAD these molecules have been extensively studied for their use in monitoring redox reactions (NAD carries electrons from one reaction to another in the cell) [98, 585], cellular metabolism [39, 586] and as indicators of disease [586, 587, 39]. The wavelength used within this study to excite fluorophores was not sufficient to excite NAD(P)H, however, it was suitable for excitation of FAD, alongside other molecules as indicated within

Endogenous Fluorophore	Excitation (nm)	Emission (nm)	Lifetime (ns)	Ref	Can be excited by 480nm?
NAD(P)H	300 - 380	450 - 500	0.3 (free), 2-2.3 (bound)	[533]	N
FAD	420 - 500	520 - 570	2.91	[533]	Y
FMN	420 - 500	520 - 570	4.27 - 4.67	[582]	Y
Collagen	280 - 350 / 450	370 - 440 / > 480	0.2 - 5.3	[533]	Y
Elastin	300 - 370	420 - 460	0.2 - 2.5	[533]	N
Riboflavin	420 - 500	520 - 570	4.12	[582]	Y
Melanin	300 - 800	520	1.9	[533]	Y
Protoporhorphyrin IX	400 - 450	630	up to 15	[533]	Y
Lipofuscin	340 - 395	540	1.34	[583]	N
Phenylalanine	240-270	540	7.5	[576]	N
Tyrosine	250 - 290	300	2.5	[577]	N
Tryptophan	250 - 310	350	3.03	[584]	N

Table 4.1: Endogenous fluorescence lifetimes

Table 4.1.

4.1.4 The effects of fixation on fluorescence lifetimes

As discussed in previous chapters, fixation is often used within biological studies to preserve samples to be imaged or assessed at later dates. Aldehyde-based fixation is the most commonly used fixative in microscopy studies. This type of sample preparation is necessary for studies involving immunofluorescence based assays or fluorescence *in situ* hybridisation. It in generally considered that due to changes in protein conformations invoked by aldehyde based fixation, that the fluorescence lifetimes of fluorophores would be changed [588]. However, very few studies have been performed to analyse the effects of fixation on the specific lifetime of endogenous fluorophores in biological samples.

A study by Chacko *et al* demonstrated that NAD(P)H lifetimes in various different cell lines showed a consistent increase in fluorescent lifetime after formaldehyde fixation, and that the degree at which the lifetime increased was not conserved between different cell types [589]. Poulon *et al* also demonstrated that NADH and FAD lifetimes increased after sample fixation [590]. Contrarily, Ganguly *et al* demonstrated that the fluorescence lifetimes of the fluorescent protein EYFP in hamster ovarian cells (CHO cells) was reduced in fixed cells compared to fresh [591]. More recently, Wang *et al* have demonstrated that fixation of HeLa cells increases the fluorescence lifetime of both NADH and FAD, with the increase in lifetime lengthening over fixation time [592].

Therefore, due to lack of consensus in the literature, and in general a lack of

study on the biochemical changes that proteins undergo during chemical fixation which may alter FL, it is generally considered desirable to avoid fixation within FLIM studies.

4.2 Methods

4.2.1 Sample Acquisition

This study was approved by Biorepository Management Committee of NHS Greater Glasgow and Clyde, UK (Biorep 548). Seventeen tonsils were collected after routine tonsillectomy at the Royal Hospital for Children, Glasgow, UK. A total of 7 new patient tonsils were collected for this study, using 9 tonsils collected in the patient cohort of the previous chapter. The tonsils collected previously had been frozen in OCT and stored at -80°C prior to use. The patients tonsils were used for FLIM, with n = 9 specimens from patients with ART and n = 7 tonsils from patients with OSA. The study was blinded until all analysis was complete. No information of patient age, sex or socio-economic status was provided. The institutional review board approval (Biorep 548) was awarded to allow anonymous patient tissue use, waiving the need for individual level patient consent. Whole tonsils were rapidly transported in sterile saline solution (0.9% Sodium Chloride, Baxter Healthcare Ltd, UK) to the Strathclyde Institute of Pharmacy and Biomedical Sciences at the University of Strathclyde after the completion of a surgical list.

4.2.2 Effects of freezing and fixation on FL

Fixation is known to cause effects on the fluorescence lifetime of endogenous fluorophores within a sample, but little study has been performed to determine differences in lifetimes between fresh and frozen tissue. Therefore, I aimed first to determine the difference in FL between fresh, frozen and fixed tonsil samples.

Fixation allows for tissue to be stored and imaged at a later date: this was something that was of interest within this study to allow imaging of stored (frozen) patient tissue, as well as to allow thin sections of tissue to be imaged. Freezing tissue is an alternative way to preserve tissue for medium to long term and to allow for cryo-sectioning to produce thin sections of tissue. Therefore, the effects on lifetime of freezing tissue was examined compared to fresh tissue. These tissue mounts were directly compared such that the same tissues were freshly imaged, frozen then imaged then finally, fixed and imaged.

For analysis of the fresh vs frozen vs fixed tonsillar tissue sections, an 2 or 3-exponential reconvolution was used. The intensity weighted average lifetime is plotted for this data in agreement with the study of Wang *et al* in order to compare results [592].

4.2.2.1 Fresh tissue

Whole tonsils were gently washed to remove blood on the outside of tissue which may present obstacles to image through if smeared on mount. To accurately compare the results, whole mounts of tissue were used of approximately 0.5 cm^3 since fresh tissue could not be sectioned. Tissue was then placed into 35 mm diameter dishes with a coverslip glass bottom (IB-81158, Thistle Scientific, UK) and was mounted in PBS for imaging.

4.2.2.2 Frozen tissue

Whole tonsil tissue was frozen and stored at -80◦C for long term storage. Frozen tissue was used in this chapter in two ways: as whole mounts of frozen tissue, or as thin sections.

For whole mounts of frozen tissue, tissue was placed into 30 mm diameter dishes with a coverslip glass bottom (IB-81158, Thistle Scientific, UK) and was mounted in PBS for imaging to test the differences in lifetime between fresh and frozen tissue.

4.2.2.3 Fixed tissue

The same pieces of tissue which had been imaged fresh (Sec. 4.2.2.1) and then frozen (Sec. 4.2.2.2) was fixed for 4 hours at 4°C in 4% PFA. Tissue was rinsed 3 times in PBS. These tissue mounts were then imaged in the same way as previous tissue sections to determine the effects of fixation on fluorescence lifetime.

4.2.3 Fluorescence Lifetime Imaging Microscopy

4.2.3.1 Sample preparation

A total of 16 tonsils removed for ART (n = 9) and OSA (n = 7) were examined in this study. A total of nine images were analysed for each tonsil (n = 3 areas within n = 3 sections per tonsil), giving a total of n = 62 OSA tissue section images and n = 81 for ART.

Whole tonsils were placed into 22 mm x 22 mm x 20 mm square cryo-moulds (Peel-A-Way™embedding moulds, E6032-1cs, Sigma-Aldrich, USA) and covered with optical cutting temperature (OCT) embedding matrix for frozen tissue (KMA-0100-00A, Cell Path, UK). Blocks were snap-frozen on dry ice before being stored at -80°C prior to use. Sectioning was performed as described in Section 3.2.1.3. Coverslips with tonsil tissue were mounted in PBS and the edges sealed with nail polish. Imaging was performed directly after sectioning.

4.2.3.2 FLIM imaging system

FLIM was performed using a MicroTime 200 Time-resolved Fluorescence Microscope system (PicoQuant). Ultrashort excitation pulses from a LDH-D-C-485S Laser head at 485 $\pm$ 10 nm were available with picosecond pulses (912483, PicoQuant). The 485 nm LDH-D-C-485S laser had a maximum possible repetition rate of 40 MHz. The high average power was 5 mW and low average power was 0.7 mW. The laser was used at 70% power as set in the SymPhoTime 64 control software. A 485 nm excitation filter set (75224, PicoQuant) was used, consisting of a 475/28 nm clean-up filter, a 485 nm and 640 nm dualband dichroic filter and a 520/35 nm emission bandpass filter was used to detect fluorescence output within the range of 503 - 538 nm. Imaging was performed using an inverted Olympus IX 73 microscope equipped with a 60$\times$ (1.2 NA, 0.28 mm working distance) water immersion objective lens (UPLSAPO60XW, Olympus Life Science) for tissue sections and a 10$\times$ (0.25 NA, 10.6 mm working distance) air objective (PLN 10X, Olympus Life Science) for the whole tissue mounts to account for the uneven contact between whole mounts at coverslips. Widefield illumination was achieved with an Xcite-120 halide based widefield illuminator (75010, PicoQuant).

TCSPC was possible using the MultiHarp 150 4P TCSPC module and event timer (930043, PicoQuant) in time-tagged time-resolved (TTTR) mode. TCSPC was performed with a maximum temporal resolution of 5 ps. A pixel dwell time of 6 μs was used over an average of 20 frames, taking a total of 65 seconds per acquisition to allow for adequate photon statistics from the autofluorescent tissue. The microscope was equipped with a FLIMbee beam scanner upgrade (973260, PicoQuant) and the relevant FLIMbee adapter (75309, PicoQuant) to allow for high precision scanning and controllable scan speeds.

A single photon counting module (SPAD) was used for FLIM detection (76040, PicoQuant). The SPAD detector had a quantum efficiency of 40-50% within the emission regime chosen for this study, which was at the maximum range of its performance capabilities. Raw images were recorded by scanning an area of 512 x 512 pixels at 3 pixels per μm. Nyquist sampling was not performed; the resolution of the microscope system was determined to be 213 nm, due to limitations in acquisition the data in this chapter was sampled every 300 nm. To conform to Nyquist sampling theorem, sampling would have to be performed every 108 nm [16].

4.2.4 Calibration of MicroTime 200

Suhling *et al* demonstrated that green fluorescent protein (GFP) in dilutions of glycerol exhibits lifetimes which are a function of the local refractive index of the GFP environment [532]. They demonstrated that lifetime of GFP gradually decreases as glycerol content (and therefore refractive index) increases. This method was implemented here to calibrate the FLIM microscope.

Fluorescein was diluted in dH_20 to a concentration of 10 $\mu g ml^{-1}$. The stock solution was then diluted in a series of glycerol dilutions in PBS from 0 - 100% in increments of 10%. A total volume of 1 ml was prepared in an eppindorf tube for each dilution, and was vortexed to ensure mixing of the dye throughout the solution. 100 μl of each mixture was placed onto a coverslip and added to a slide, using clear nail polish to seal the edges of the coverslip to the slide. Imaging was performed as described in Section 4.2.3.2, with a 1.3 μs pixel dwell time. The low dwell time used allowed for adequate photon statistics in comparison to the autofluorescence FLIM performed on tissue. Expected τ_1 of fluorescein in PBS is approximately 4 nanoseconds [593, 594].

The fluorescence lifetime was fitted using a single-exponential tailfit, this can be seen in Figure 4.2. Single exponential fit was appropriate due to the lifetime contribution being from a single source within the sample. It was found that the fluorescence lifetime of Fluorescein in glycerol decreased from 3.95 ns at 0% glycerol to 3.4 ns at 100 % glycerol. The fractional decrease in lifetime observed is consistent with that observed by Suhling *et al* [532].

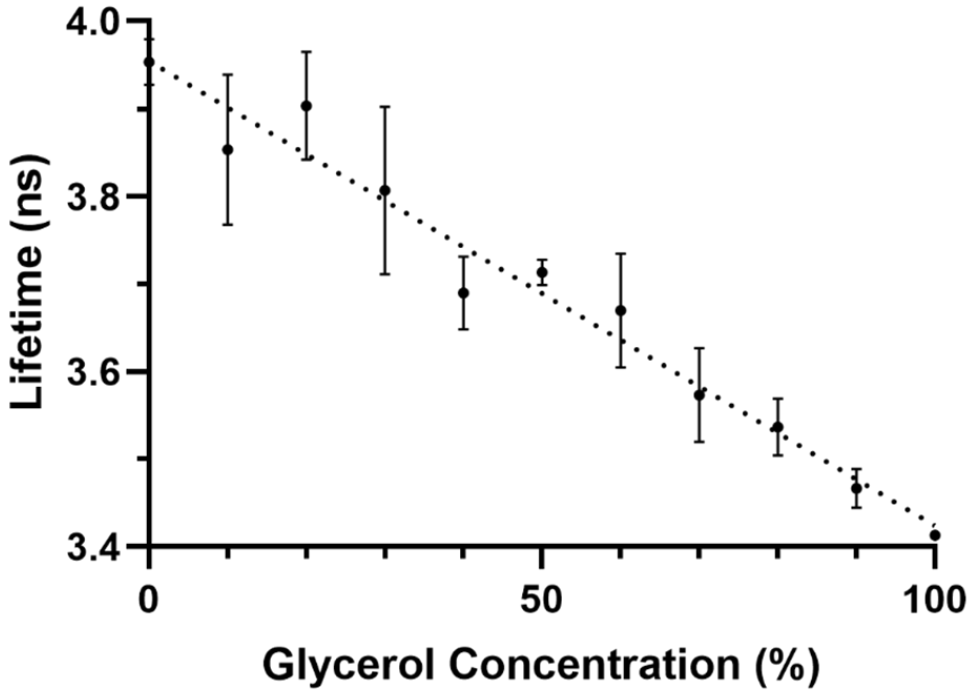

Figure 4.2: Calibration of Micro Time 200 system for FLIM imaging. Fluorescein lifetime decreases in an increasing glycerol concentration gradient. Data presented as mean with standard error. Line fit with linear regression (GraphPad Prism) with an R^2=0.97. The lifetime in PBS (0% glycerol) is 3.95 ns, and decreases to 3.4 ns in 100% glycerol. This data is in agreement with the findings of Suhling *et al* [532].

4.2.5 Data Analysis

Analysis was performed using the SymPhoTime 64 software with the FLIM analysis algorithm. This algorithm produces a 'Fast FLIM' image displayed in a colour scale with the image brightness encoding intensity (number of counts) and the false colour encoding the average lifetime (the mean arrival time of photons after pulse).

For analysis of glycerol series with a single known lifetime, a single exponential tailfit was used for fitting lifetimes, as was performed by Suhling *et al* [532]. In all cases, a χ^2 $\leq$1.3 and approaching 1 was considered a good fit. The software recommends that users choose reconvolution fit due to the fitting of the full decay curve with this method, in contrast to the tailfit method where the beginning of the curve fitting is somewhat arbitrary [595].

Once appropriate fitting parameters were chosen, the FLIM-Fit algorithm was performed to increase the quality of the fit. In this algorithm, several assumptions are made:

1. The excitation pulse does not shift within the acquisition time in the TC-SPC window: this is almost always valid in such an experiment.

2. Background values before and after decay are approaching 0.

3. Fix the fitted lifetimes, i.e, if a 3-exponential fit is chosen, an assumption is made that there are 3 components within that contribute to lifetime. This is valid when a sample has the exact number of fluorophore sources that the exponential fit has, but it more complicated in samples with both unknown lifetimes and unknown number of lifetime sources.

FLIM-Fit then performs the chosen n-exponential reconvolution fit (or tailfit, if chosen) on each pixel within the image resulting in an updated FLIM image and an update lifetime frequency histogram containing histograms for each lifetime parameter (if 3-exponents chosen, 3 lifetime histograms are present).

For statistical analysis of data, numerical values were exported to Prism (GraphPad Software, USA). Plots for presentation purposes were created using Prism. Outliers were removed using ROUT with Q=1%. All data were non-normally distributed, therefore a Mann-Whitney two-tailed U test was used for significance testing, with $\alpha = 0.05$.

The IRF consistency was examined by assessing n = 3 randomly selected patient data sets (within these, n = 9 images), resulting in analysis of n = 27 IRFs. These data were analysed using Excel (Microsoft ®Excel ®for Microsoft 365 MSO (Version 2311 Build 16.0.17029.20028) 64-bit).

4.2.6 Lifetime of specific tissue morphologies

Very little is published on FLIM-based imaging of tonsillar tissues, and as such, I measured lifetime properties of specific tonsillar tissue types. Images were grouped into sub-types after analysis of the previous sections and similarities in lifetime profiles compared.

It is important to note that while suggestions can be made as to where the lifetime components arise from according to findings in the literature (Table 4.1), it is not possible to say for certain where the lifetime components arise from. Further work including measurement of known samples or selective staining of known endogenous fluorophores to correlatively image the fluorescence lifetime of endogenous fluorophore and corresponding intensity of

exogenous staining would be required to draw exact conclusions. However, this was outwith this scope of this thesis. With this in mind, tissue sections were examined and split into three categories which had distinct similarities in morphologies between tissue: lymphoid tissues [219], tissue with bacteria present [250] and tissue which exhibited fibrous structures resembling collagen [219]. Within these sections, similarities in lifetime profiles are discussed and suggestions as to where the components arise from are made..

4.3 Results

4.3.1 IRF Measurement

The IRF was measured to be 0.94 ± 0.1 ns, with a range of 0.75 ns to 1 ns. An example IRF can be seen in Figure 4.3. This was in good agreement with the expected performance. The published IRF for this instrument is 1 ± 0.5 ns [596, 597].

4.3.2 Fresh and Frozen tissue exhibit similar lifetime profiles

It is known that aldehyde fixation induces changes in fluorescent lifetimes of samples, making the lifetimes longer than is expected. This has been verified here in tonsil tissue mounts, demonstrating that there is a significant increase in observed mean lifetime of fixed tissue sections when compared to both fresh and frozen sections ($p = 0.03$, Mann Whitney U test), fitted using a 2 or 3 exponential reconvolution with $\chi^2 \leq 1.3$, as can be seen in Figure 4.4 and in agreement with that observed by Wang *et al* [592].

It was found that there was not significant difference in lifetimes of the frozen tissue when compared to fresh tissue, indicating that frozen tissue was appropriate to use in this study.

Representative images of these data can be seen in Figure 4.5. These images were acquired with comparatively poorer resolution than the images presented in subsequent sections. This was due to the use of whole mounts of tissue, meaning that millimeter (or more) thick pieces of tissue were imaged on top of a coverslip, rather than thinly sectioned tissue. Due to this, a longer working

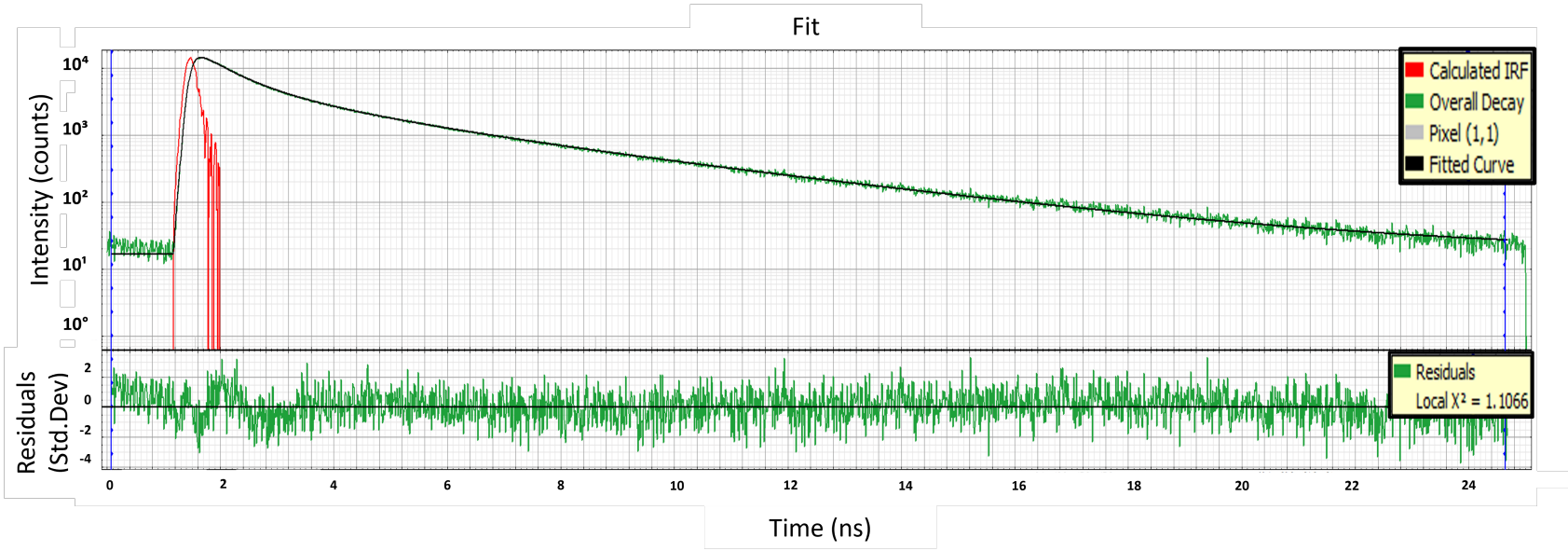

Figure 4.3: Representative example of IRF (red) generated in SymPhoTime FLIM analysis. Shown on the measured (green) and fitted (black) decay curve in the top figure, with the corresponding residuals on the bottom figure. In this representative figure, χ^2 = 1.066, for all figures examined, a $\chi^2 \leq 1.3$ was considered a good fit.

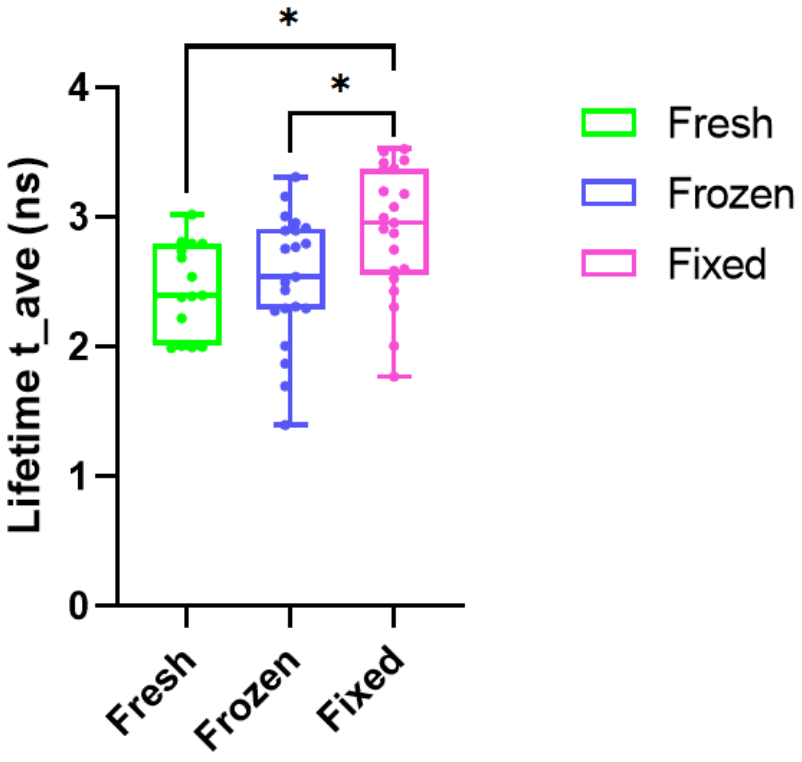

Figure 4.4: Fresh, frozen and fixed tissue sections were assessed to determine average lifetime before and after freezing and fixation. Fresh tissue had a τ_{ave} of 2.45 $\pm$ 0.09 ns, frozen tissue had a τ_{ave} of 2.53 $\pm$ 0.11 ns, and fixed tissue had a τ_{ave} of 2.9 $\pm$ 0.11 ns. There was no significant difference in lifetime between fresh and frozen tissues. However, there was a significant increase in lifetime between both fresh and fixed (p = 0.02) and frozen and fixed (p = 0.03), indicating that frozen tissue could be used in place of fresh, but fixed tissue could not be reliably used to to increased lifetime.

distance objective lens was used with a lower magnification to collect sufficient photon statistics for analysis since not all tissue was in contact with the coverslip.

4.3.3 τ_1 lifetime component is longer in ART patient tissue than in tissue from patients with OSA

Median τ_1 for OSA patients was 3.65 $\pm$ 0.85 ns (median $\pm$ standard deviation), and for ART was 3.90 $\pm$ 0.35 ns. The increase in lifetime in ART was considered significant with p = 0.003. Median τ_2 lifetime for OSA patient tissue was 1.02 $\pm$ 0.54 ns, and for ART was 0.98 $\pm$ 0.58 ns: these data were not significant. Median τ_3 for OSA was 1.12 $\pm$ 1.07 ns, and for ART was 0.67 $\pm$ 0.71 ns: these data were not statistically significant. The extremely high standard deviations present in the τ_1 and τ_2 lifetime components indicate that they are not reliable measures in this case in comparison to the low standard deviation present in the τ_1 component.

Using an ordinary ANOVA multiple comparisons test, all data were compared and can be seen with the blue and magenta significance lines in Figure 4.6. It was found that in both OSA and ART, the lifetime components τ_1 were significantly higher than τ_2 components ($p < 0.0001$ for both). Similarly, the τ_1 components were significantly higher than τ_3 components for both OSA ($p < 0.0001$) and ART ($p < 0.0001$). No such significance was found when comparing τ_2 components to τ_3 components, indicating that these components may overlap or be coming from similar molecular sources between measurements.

The range in lifetimes is high amongst all lifetime components in both ART

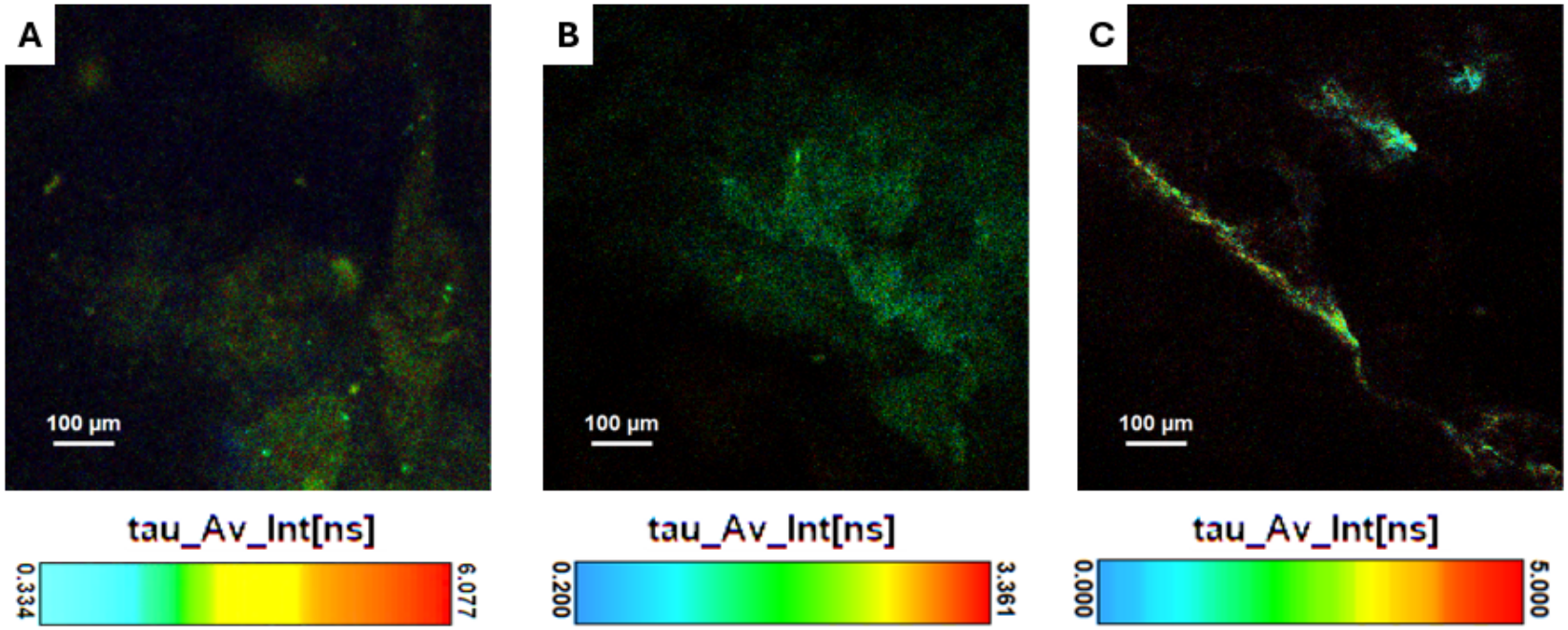

Figure 4.5: Representative images of whole mounts of (A) fresh, (B) frozen and (C) fixed tonsil tissue. Data presented as false colour images where colour is representative of average lifetime per pixel, individual colour scales are seen below each subfigure.

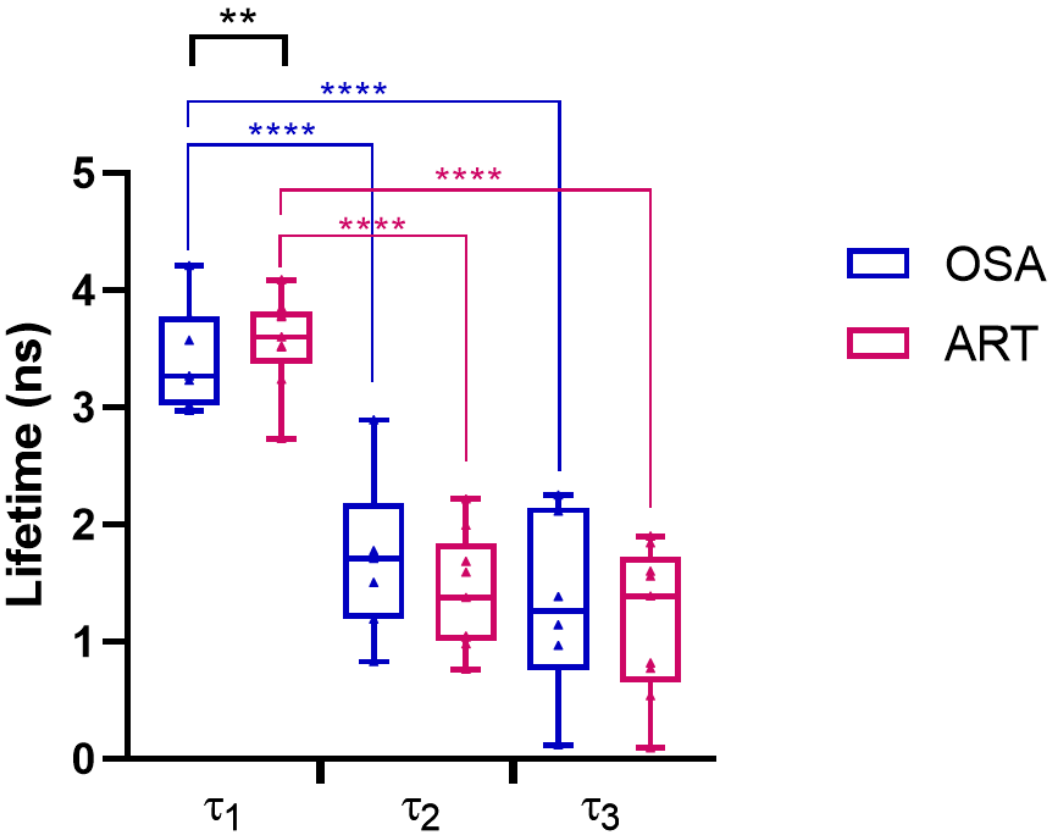

Figure 4.6: τ_1, τ_2 and τ_3 lifetime components of frozen tissue sections fitted by a 3-exponential reconvolution. The data from 16 patients are represented, with each dot representing the average lifetime component from a total of n = 9 images from n = 3 tissue sections from each (n = 16) patients. τ_1 is significantly higher in ART patient tissues (Outliers removed using ROUT method with Q = 1%, Mann Whiteny U Test for non-normally distributed data with α = 0.05, p = 0.003), no such significance is found in the τ_2 and τ_3 components. There is a significant difference between the τ_1 lifetime components compared to both τ_2 and τ_3 components for ART and OSA (Ordinary Anova with correction for multiple comparisons). No such significance is seen between τ_2 and τ_3 components.

and OSA, suggesting that the lifetimes do not generalise well between different anatomies present within a single tonsil image. Overall, OSA presented lower mean lifetime than ART in the τ_1 lifetime component, were approximately equal for τ_2, and was increased in τ_3. Therefore, it is not appropriate to draw a conclusion that all OSA lifetime components are shorter. However, these results do indicate a significant shortening of lifetime in the τ_1 lifetime in tissue from patients with OSA compared to tissue from patients with ART, indicating it may be used as an indicator of disease type.

4.3.4 Lifetimes of specific tissue components

4.3.4.1 Lymphoid tissues

A set of 4 FLIM images from 4 separate patients were characterised based on their morphologies as having predominantly lymphoid tissues, as can be seen in Figure 4.7. It was found that all 4 had similar τ_1 lifetime components (Figure 4.8), with a range of 4.05 - 4.2 ns with a median of 4.12 $\pm$ 0.06, corresponding with the expected lifetimes of Riboflavin and potentially collagen. τ_2 fell within the range of 1.62- 1.69 ns with a median of 1.66 $\pm$ 0.03 ns. τ_3 lifetime components were again similar, with a range of 0.58 - 0.62 ns and median of 0.6 $\pm$ 0.01 ns. But as seen in the previous sections, there is in general high overlap in the $\tau_{2/3}$ lifetime components and therefore more emphasis should be placed on the τ_1 component.

4.3.4.2 Connective tissues

Images which contained collagen-like connective tissues were examined next. A total of 17 images from 6 patients were considered to have these structures, which are seen as the fibrous components in Figure 4.9. These images were

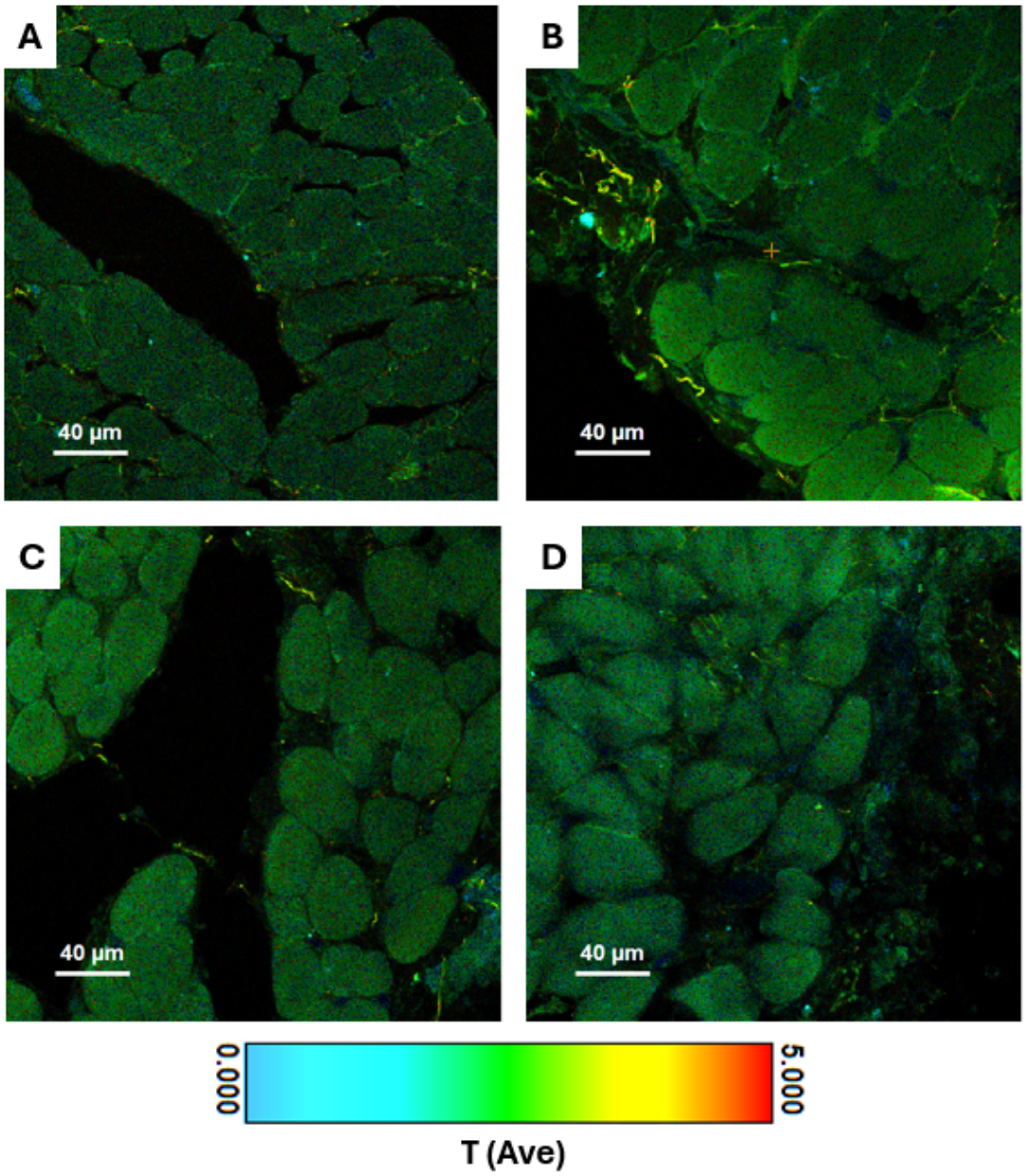

Figure 4.7: FLIM images of the total of 4 tonsillar sections which exhibited morphology of lymphoid tissues. A) lymphoid cells (green) surrounding a tissue void which may be a tonsillar crypt. B) lymphoid cells (green) surrounding a crypt where the crypt epithelium is present (bottom left) with discontinuous collagenous fibers present (yellow). C) lymphoid cells (green) with discontinuous collagenous fibers (yellow) around a likely tonsil crypt. D) lymphoid tissues (green) present through most of image. Lifetimes all presented within a 0 - 5 ns range, with the average lifetime per pixel displayed.

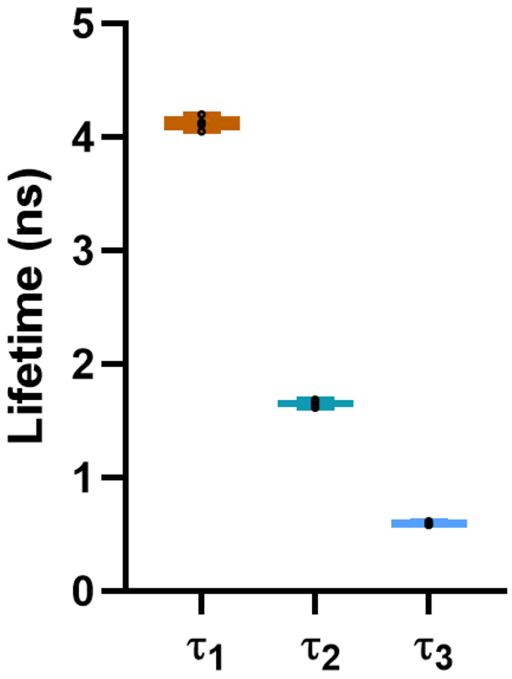

Figure 4.8: Graphical representation of distribution of τ_1 and τ_2 lifetime components in the lymphoid tissue FLIM data (n = 4 samples). The median τ_1 was 4.12 $\pm$ 0.06 ns, median τ_2 was 1.66 $\pm$ 0.03 ns and median τ_3 was 0.6 $\pm$ 0.01 ns.

taken in close proximity to the epithelia of the sample, where collagenous material is to be expected [219]. The τ_1 lifetime components (Figure 4.10) were similar, ranging from 3.81 - 4.34 ns with a median of 4.03 $\pm$ 0.14 ns, which falls within the range of expected lifetime for collagen as exhibited in Table 4.1. The τ_2 components once again are more varied from 0.52 - 1.87 ns, with a median of 1 $\pm$ 0.43 ns, as is τ_3, which varies between 0.67 - 1.5 ns with a median of 0.73 $\pm$ 0.35 ns. There is much crossover in the range of lifetimes found in the τ_2 and τ_3 components, with these lifetimes falling within the ranges expected for the lower end of collagen lifetimes, Protoporphyrin IX and lipofuscin. Previous studies have excited and detected collagen in autofluorescence intensity based imaging at the wavelengths used in this study [135], therefore, it is likely that the long lifetime component detected here arises from collagenous structures.

4.3.4.3 Bacteria

Images which appeared to contain bacteria were then examined. Here, bacterial presence was classed as a section containing more than 5 objects which are between 1 - 3 μm in diameter (to allow for abnormally large bacteria), which appear as small round and usually cyan (within the colour coded FLIM images) objects within the representative images in Figure 4.12. A total of 29 images were found to contain object morphology that corresponded to the category of bacteria, data from only these images were used within the analysis of this section. It was found that the long τ_1 lifetime components ranged from 3.46 - 4.38 ns with a median of 4 $\pm$ 0.23 ns. The τ_2 lifetime ranged from 0.56 to 1.83 ns with a median of 0.87 $\pm$ 0.37 ns. The τ_3 lifetime ranged from 0.6 to 1.6 ns with a median of 0.68 $\pm$ 0.55 ns. There were few cases where a τ_3 component emerged within these data, only 3 of the 29 cases required a 3-exponential

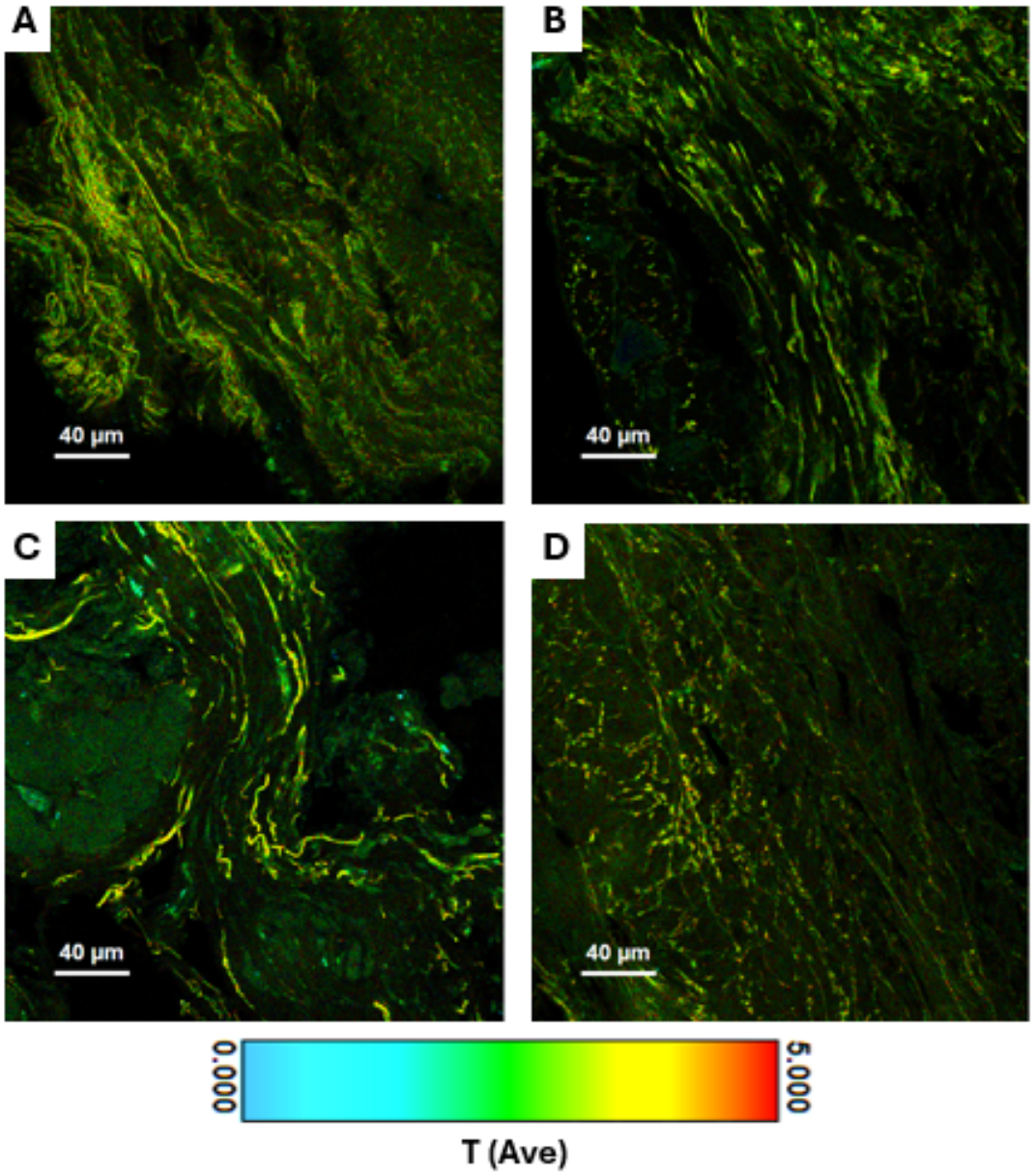

Figure 4.9: Representative 4 (of n = 10 total) FLIM images of tonsil sections which had collagenous structures present. A) continuous collagenous fibers present (yellow) mixed with other unknown tissue types. B) fewer collagenous fibers (yellow) present which appear to be intertwined between lymph follicles (circular dim green region on left). C) discontinuous collagenous fibers (yellow) surrounding lymphoid cells (green). D) discontinuous collagenous fibers (yellow) spread throughout image. Lifetimes all presented within a 0 - 5 ns range, with the average lifetime per pixel displayed.

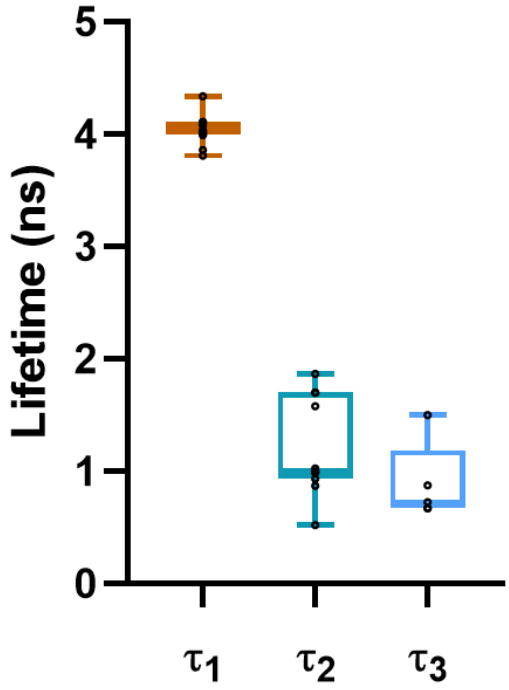

Figure 4.10: Graphical representation of distribution of τ_1 and τ_2 lifetime components in the connective tissue FLIM data (n = 10 samples). The median τ_1 was 4.03 $\pm$ 0.14 ns, median τ_2 was 1 $\pm$ 0.43 ns and median τ_3 was 0.73 $\pm$ 0.35 ns.

fitting. Therefore, it is best in this scenario to disregard the τ_3 component and instead assess τ_1 and τ_2 which were evident in all (n = 29) images examined.

Interestingly, not all images used within this study contained objects fitting the defined criteria of bacteria. This is likely due to the comparatively much smaller FOV used in this Chapter in comparison to Chapter 2, approximately 25 $\times$ smaller than the FOV of the Mesolens, with a comparable resolution.

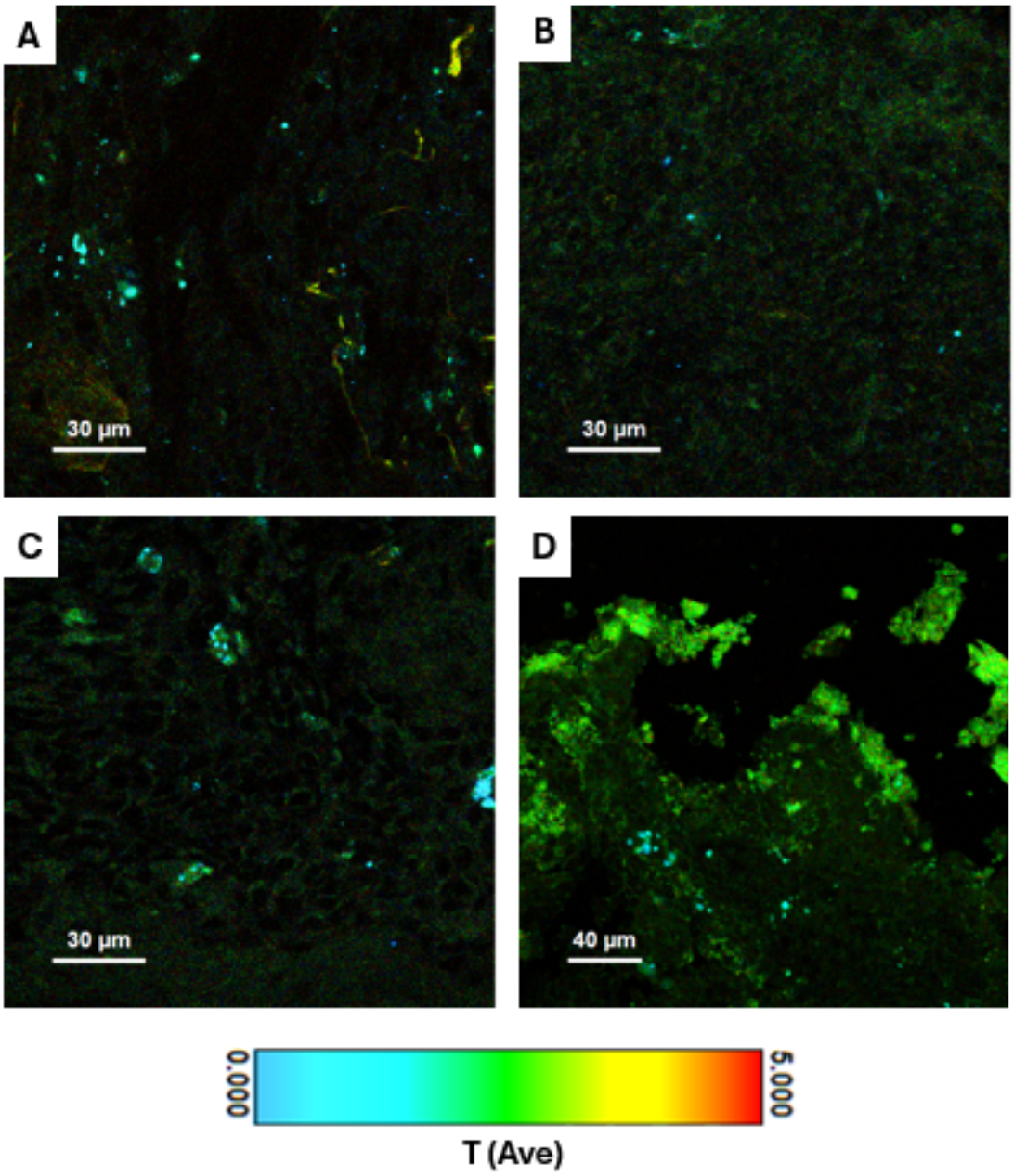

Figure 4.11: Representative 4 (of n = 29 total) FLIM images of tonsil sections which appeared to have bacteria within. A) bacteria (cyan) spread amongst a variety of tissue types. B) bacteria (cyan) present amongst tissue (green). C) bacteria (cyan) seen spread amongst tissue (green) and can be seen to cluster in small colonies of several cells. D) bacteria (cyan) again seen clustering together in small numbers and spread amongst tissue (green). Lifetimes all presented within a 0 - 5 ns range, with the average lifetime per pixel displayed.

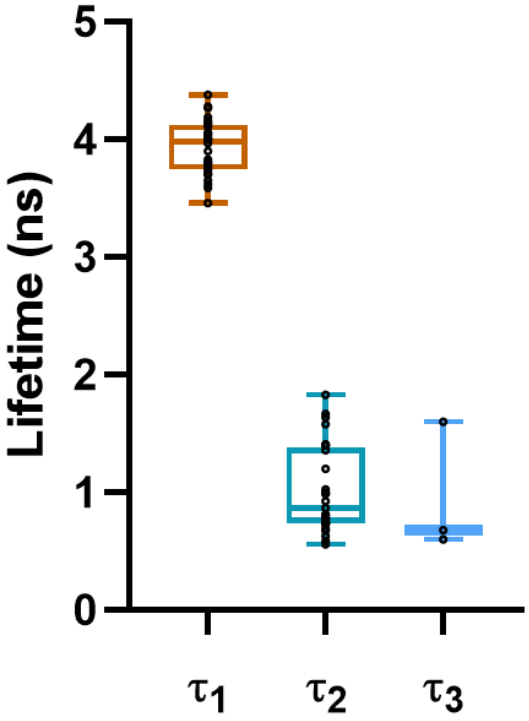

Figure 4.12: Graphical representation of distribution of τ_1 and τ_2 lifetime components in the bacterial FLIM data (n = 29 samples). The median τ_1 was 4 $\pm$ 0.23 ns, median τ_2 was 0.87 $\pm$ 0.37 ns and median τ_3 was 0.68 $\pm$ 0.55 ns.

4.4 Discussion

Within this work, it has been shown that there is a statistically significant difference in fluorescence lifetime in tissue from patients with ART compared with tissue from patients with OSA. These results suggest that ART tissue sections contain a long lifetime component which is significantly longer than those of OSA tissues. It has also been shown that this lifetime component is conserved through different tonsillar tissue structures via analysis of tonsil sections from different patients.

The few published studies involving FLIM of tonsillar tissue [526, 527, 528], and tissue in general, use ultraviolet emitting lasers for excitation. Therefore, there is limited published information on the properties of fluorescence lifetimes of endogenous fluorophores excited at longer wavelengths. Since FL is dependent upon local microenvironment, it is difficult to compare fluorescence lifetimes generated within this study to ground truth measurements of lifetimes which have been performed in fundamentally different tissues or on molecules in solution [98]. Therefore, within this thesis, only observations upon where the lifetimes arise from are made, and are not stated with absolute certainty. This work aimed to examine whether it was possible to delineate ART and OSA tonsillar tissue from one another using lifetime components: the data show that the long lifetime component τ_1 could be used for this purpose.

With many endogenous fluorophores having overlapping lifetime profiles, disentangling them through analysis pipelines can prove difficult. Prime examples of these are the overlapping values of NADH, NADPH, FAD and FMN [598, 98]. In addition, several drugs have known fluorescence lifetimes which

may overlap with the lifetimes of endogenous fluorphores of interest, potentially introducing unknown lifetime sources into the sample if prior knowledge of patient drug intake is not known [599, 600, 601]. These factors contribute to the reason that only suggestions of where the FLs detected in this thesis arise from, as without additional exogenous staining it is not possible to determine contributors of FLs.

Within this work, it has been shown that there is a significant difference in τ_1 lifetime component in sections of freshly frozen ART tonsil tissue compared to OSA tissue. While other studies have been performed involving FLIM and tonsillar cancer [526, 527, 528], none have been performed to examine differences in lifetimes between ART and OSA. Recent studies have been performed using FLIM for investigating infections: Szaszák *et al* used FLIM to examine host-pathogen interaction during intracellular *Chlamydia trachomatis* infection, enabling study of the infectious cellular metabolism independently of the host cell metabolism [602]. In addition, Bhattacharjee *et al* successfully demonstrated a method for metabolic fingerprinting of 5 bacterial species using FLIM [603]. While Qazi *et al* have more recently developed a method for identifying up to 12 separate species using a combination of FLIM and intensity based imaging [604]. These methods are in their relative infancy, however, there would be great interest in applying these methods alongside *in vivo* FLIM methods [605, 606] to determine bacterial species within infected tissues (such as tonsils) *in situ*.

The imaging setup used within this Chapter has a smaller FOV than those used in the previous chapters. The Micro Time 200 FLIM imaging system was used with a 60$\times$ objective lens to achieve comparable resolution to that used in previous chapters. This reduced the FOV by over 600$\times$ (from 2.5 x $10^7 \mu m^2$ to 4 x

$10^4 \mu m^2$) and greatly limited the throughput of the imaging system, achieving images of approximately 200 μm by 200 μm in comparison to the Mesolens images which were several mm in diameter. For example, assuming the same set-up was possible with a Mesolens objective lens, a single image would capture over 600 $\times$ the imaging area possible with the FLIM set-up used in this chapter, greatly increasing the sampling area within a single acquisition. Due to the complex instrumentation required for FLIM, applying it to the Mesolens would be costly both financially and in time to set up. Therefore, it was outwith the scope of this work. However, this work has identified a need for mesoscale FLIM using the Mesolens, where it would be possible to perform FLIM across much larger regions of tissue or sample and greatly increase the throughput of FLIM imaging. Alfonso-Garcia *et al*'s recent review article covered current methodologies in mesoscale FLIM, however, no methods had imaging specifications which were similar to that afforded by the Mesolens, instead having generally high FOVs but with comparatively low resolution [607].

It was found that while the τ_1 lifetime component was able to be used as a method for differentiating between ART and OSA, the τ_2 and τ_3 components were not. There was high overlap between the τ_2 and τ_3 components which was apparent in both ART and OSA. This finding is not isolated to this study, but has been observed by others [561, 562].

4.5 Conclusion

Within this chapter, FLIM was used to determine if a difference in fluorescence lifetime of endogenous fluorescent molecules present in tonsillar tissue from ART and OSA patients was observed, with the aim of identifying a new method to discriminate between these diseases.

First, whole mounts of tissue were imaged fresh, then fixed, then frozen to determine the effects of freezing and fixation on the lifetimes of endogenous fluorophores within using a commercial FLIM system. It was found that there was no significant difference in FL between fresh and frozen tissue, but there was a significant increase in FL in fixed tissue when compared to fresh and frozen. Therefore, it was decided to proceed with frozen tissue such that thin sections could be prepared using a cryostat in order to minimise scattering within the sample.

Thin sections of frozen tonsils were examined per disease type (n = 9 images per patient, n = 9 ART patients, n = 7 OSA patients) using the same commercial system. The FLs were extracted from the multi-exponential decay curve using an n-exponential reconvolution fit on the proprietary software. The shorter τ_2 and τ_3 lifetime components had a large degree of overlap in measured lifetimes and did not show differences between disease type. However, interestingly, the long lifetime component, τ_1 was shown to be significantly different between ART and OSA tissue sections. This work suggests that the τ_1 lifetime component therefore may be used as a label-free diagnostic to differentiate between the two tonsillar diseases studied.

Chapter 5

Concluding remarks and directions for future work

This Chapter will summarise and contextualise the results of Chapters 2,3 and 4. Recommendations for future work are also discussed.

5.1 Summary

The work presented within this thesis centred around applying advanced optical microscopy for the study of infected and hypertrophied paediatric palatine tonsils. This was achieved by performing various sample staining methods including fluorescently-conjugated antibiotics, immunofluorescence, fluorescence *in situ* hybridisation alongside imaging of endogenous fluorophores within the tonsil tissue. Imaging was performed both on the micro and mesoscale, using the Mesolens to image large tissue sections and volumes, as well as using a Micro Time 200 FLIM system for examination of tonsil tissue. Image analysis tools were used throughout this work to quantify differences within ART and OSA sample. The work performed aimed to determine if there are differences between the examined disease types that may be used to discriminate between ART and OSA.

In Chapter 2, a methodology for imaging and quantifying the presence of Gram-positive biofilms on whole mounts of fresh tonsil tissue using the Mesolens was established. Microbiological assessment of swabs taken from tonsillar tissues were first performed to determine the distribution of bacteria on samples. It was found that the tonsillar microbiome within this study contained predominantly Gram-positive bacteria consisting of *Streptococcal* and *Staphylococcal spp.*, with only a single Gram-negative species, *M. nonliquiefaciens*, detected. Whole mounts of fresh tonsil tissue were used for imaging as it was found that both formaldehyde and Carnoy fixation of whole tonsils left little to no bacteria after. The Mesolens was then used to image whole mounts of fresh tonsil tissue stained with Vancomycin BODIPY to visualise Gram-positive biofilms and using reflection contrast to image the tonsillar tissue. Imaris was used for

quantification of the 3D confocal dual-colour datasets, where the number of biofilms present, the relative biofilm volume and the mean biofilm sizes were measured. It was found that there was no difference in biofilm abundance between ART and OSA tissue mounts, suggesting that biofilms may be an inherent property of a tonsil with ART or OSA. In addition, it was found that the distribution of biofilms did not vary in a location dependent matter, that is to say that the biofilm distribution at the surface and the interior of the tonsillar tissue did not change. In contrast to previous studies who detected biofilms in small regions of fixed tonsil tissue, this study detected biofilms in 100% of tonsils analysed using this method.

In Chapter 3, the presence of IL-17C was found in the epithelium of tonsillar tissues for the first time. The presence of IL-17C and IL-1β were first confirmed using Western Blot analysis of tonsil tissue homogenates. This indicated that IL-17C expression at the protein level was significantly higher in ART patient tissues compared to OSA. At the time of publication, no other studies could be found which had analysed the expression levels of IL-17C within tonsil tissue. In contrast, IL-1β showed no difference in expression level between disease type. Nonetheless, IL-1βs spatial distribution within tonsil had not been previously studied. Therefore, using immunofluorescence the distribution of both IL-17C and IL-1β within tonsil tissue was analysed using the Mesolens. The immunofluorescence staining was quantified using image analysis to verify expression in two tissue regions: the epithelia and the core tissues. It was found that the expression of IL-1β was significantly higher in the epithelia of ART patients compared to OSA, but no difference was found for internal tissues. However, IL-17C expressed was significantly higher in both the epithelia

and core of tissue from patients with ART compared to OSA. This further evidenced the promising capability of IL-17C as a potential biomarker for ART, however, further work would be required to establish this for certain. Further to this work, FISH was used to examine the distribution of bacteria and biofilms within the tonsil tissue sections. Through colocalisation analysis, it was found that there was little colocalisation of both interleukins to bacteria within the ART patient tissues. There was, however, medium to high levels of colocalisation between the interleukins and bacteria within the OSA patient tissues, though these data were not significant.

Finally, Chapter 4 presented a label-free methodology for determining differences in ART and OSA tissues using the measured fluorescence lifetime of endogenous fluorophores. This work was performed on a Micro Time 200 system equipped for FLIM and was the first study to use FLIM in the analysis of tonsillitis or tonsillar hypertrophy. The ability to use frozen tissue in place of fresh tissue was first examined, and showed little difference in detected average fluorescence lifetime. When examining fixed tissue, there was a significant lengthening of fluorescence lifetime observed, as was consistent with literature. After determining the suitability of frozen tissue, thin sections of tonsillar tissue from patient tissues with ART or OSA were examined. It was found that there was a significant increase in the τ_1 lifetime component of ART compared to OSA. The other exponential lifetime components (τ_2 and τ_3) were found to have no significant difference and were highly overlapping in their lifetimes. The work performed in this Chapter demonstrated the suitability of the τ_1 fluorescence lifetime component as a label-free indicator of disease type.

5.2 Recommendations for future work.

The central theme of this thesis is investigating infected and hypertrophied tonsils using advanced optical microscopy to determine imaging-based indications of disease type. The presence and spatial distribution of Gram-positive biofilms in fresh *ex vivo* tonsillar tissue was first investigated in Chapter 2 using multimodal optical mesoscopy and image analysis paired alongside microbiological assessment. Chapter 3 involved using optical mesoscopy and image analysis to quantify the presence of bacteria and IL-17C / IL-1β in tonsil slices, paired with western blot analysis to examine protein expression of the ILs. Chapter 3 introduced FLIM-based imaging using a different microscope system and involved the label-free imaging and analysis of tonsillar tissue based on the inherent fluorescence lifetimes of endogenous fluorophores within.

The work presented in Chapter 2 would be further improved by searching for Gram-negative bacteria alongside Gram-positive. This could be achieved by designing a targeted FISH probe for Gram-negative bacteria. It is, however, important to note that live cell FISH is still in its infancy, and the volume of probe required to perform FISH on whole mounts of tonsillar tissue would be extremely costly. At the time of this study, this work was not possible due to the high financial cost involved in designing and using such probes, and due to the additional time that imaging a 3rd channel would involve. Imaging of *ex vivo* tonsil tissue involved a delicate balance of time to image and volume of imaging required such that the tissue would not become necrotic within the time frame. Imaging of more patient samples would have potentially introduced significance in the results presented, however, due to the COVID-19 pandemic the sample collection in this thesis was inherently limited. Increased

sample size may have introduced trends in the presence and spatial distribution of biofilms depending upon disease type.

The work presented in Chapter 3 would have benefited from tissue-location dependent blotting to further evidence the use of IL-17C as a biomarker of ART. In addition, this would potentially open the possibility of IL-1β as a biomarker: IL-1β was found to be more highly expressed in the epithelial regions of ART tissue sections using IF, but no difference in expression was found in blots. By blotting specifically on homogenates taken from tonsil epithelium and core, it would be possible to correlate the blotting and IF performed in this chapter. In addition, it would be of great interest use patient derived tonsil cells to determine a baseline of expression of both ILs. This would then allow for a baseline of normal expression from which increased expression would be considered indicative of disease, rather than comparatively between ART and OSA tissues. Furthermore, performing blotting and / or IF on patient saliva or tonsil exudates to determine if the expression in these components were comparable to that of the tissue could prove useful, especially for the epithelia-produced IL-17C. By detecting this in saliva or tonsil exudate, it would be possible to test for infection in patients who had not yet had their tonsils removed. If this could also be compared to a baseline, it would be possible to determine expression of the cytokines at a point of care level. Finally, it would be of interest to compare the expression of IL-17C in tonsils which had bacterial tonsillitis compared to viral tonsillitis, to determine if the levels of expression could be indicative of particular infection type. This would be of great interest as being able to accurately detect bacterial or viral tonsillitis at a point of care level would prevent antibiotic mis-prescribing, which is a major contributing factor in the growing epidemic of antibiotic resistance.

The differences in the τ_1 fluorescence lifetime component presented in Chapter 4 introduces a label-free method of differentiating between ART and OSA patient tissues. The obvious extension of this work is to perform endoscopy based FLIM on tonsils *in vivo*, to determine if it may be used as a method of differentiating between disease. In addition, comparing the lifetimes of bacterial and viral based tonsil infections would again be of great interest in order to have a point of care method of delineating between disease. Endoscope based FLIM methods have already been established; these methods however are generally limited by the trade-off in resolution and field of view that plagues optical imaging. Generally, these systems operate at a large FOV with poor resolution, or a small FOV with high resolution. While the Mesolens itself would not be possible to fit in the oral cavity of humans (approximately 20 cm in diameter), the development of a Meso-FLIM system could prove useful in high throughput investigation of *ex vivo* human tissues. This would allow for comparable resolution to what was achieved in this chapter, but over a much increased FOV (200 μm to 5 mm in diameter) and would allow for the study of lifetime distribution over a large region of tonsil tissue at once. The development of such a system was outwith the scope of this study.

The work presented within this thesis is focussed around the palatine tonsil, but many of the methods developed and applied would be relevant to the study of similar tissues such as adenoids, or other MALT tissues such as the gut. The methods applied and developed here add the ability to examine biomarkers of disease type over a much larger scale than is conventionally performed and adds to the wealth of applications of advanced optical microscopy

for the study of human disease. In particular, I have demonstrated two indicators for ART (IL-17C and the fluorescence lifetime of endogenous fluorophores), and shown for the first time that biofilms are present throughout the tonsil mass at equal volume regardless of disease type. The findings within this thesis further our understanding of ART and OSA in terms of biofilm spatial presence, and indicators of disease type. These finding could inform the investigation of biofilms in other tissues using the Mesolens, as well as provide the baseline for *in vivo* studies of IL-17C / fluorescence lifetimes as diagnostic aids of ART.

"With writing like this, Megan will never make it to university."

Mrs Bell (*Clydebank High School*)

Appendix A

Appendix A

A.1 Bacterial Culture Media Recipes

Molecular grade reagents were purchased from Merck (Germany,), ThermoFisher Scientific (UK) and Melford (UK). Broth and Agar media were prepared in 500 ml Duran bottled using distilled water to the desired volume. Media was sterilised in the facility autoclave suite at 121 °C at 100 kPA. When required, agar media was melted using a laboratory grade microwaved and cooled in a 55 °C water bath till use. All bottles were opened and closed in an aseptic environment to maintain media sterility.

Name	**Components**
LB Broth (/ Agar)	10 g/L tryptone, 5 g/L yeast extract, 10 g/L NaCl, (20 g/L agar)
Sheeps Blood Agar	40 g/L blood agar base, 70 ml/L defibrinated sheeps blood

Table A.1: Bacterial culture growth media recipes used in this work.

A.2 Cell Culture Media Recipes

Cell culture media was purchased from Thermofisher Scientific (UK). Media was prepared and aliquoted into 50 ml sterile falcons in a cell culture hood. Stock solutions of HI-FBS, P/S, L/G and NEAA were kept in sterile frozen 5 ml aliquots prior to use.

Media	**Components**
D+++ media	500 ml sterile bottle DMEM, 50 ml HI FBS, 5 ml penicillin / streptomycin, 5 ml L-glutamine
D++++ media	500 ml sterile bottle DMEM, 50 ml HI FBS, 5 ml penicillin / streptomycin, 5 ml L-glutamine, 5 ml non-essential amino acids

Table A.2: Cell culture growth media recipes used in this work.

Appendix B

Appendix B

The information required for making buffers for use in Chapter 3 can be found here.

Application	Reagent	Recipe	Manufacturer
Tonsil Homogenisation	Lysis Buffer	50 mM Tris-HCL pH 7.4 1 % v/v Triton X-100	Sigma-Aldrich (10812846001) Sigma-Aldrich (X-100)
SDS-Page	15% Resolving Gel	6 ml H_2O 6 ml Buffer 1 12 ml Acrylamide Solution 200 µl APS 20 µl TEMED	 Roth (A124.1) ThermoFisher Scientific (17874) ThermoFisher Scientific (17919)
	Buffer 1	90 g Tris Base 2 g SDS 400 µl dH_2O pH to 8.8 Make to 500 ml with dH_2O	FisherScientific (10103203) Sigma-Aldrich (L3771)
	Stacking Gel	9.75 ml dH_2O 3.75 ml Buffer 2 1.5 ml Acrylamide Solution 250 µl APS 40 µl TEMED	 Roth (A124.1) ThermoFisher Scientific (17874) ThermoFisher Scientific (17919)
	Buffer 2	30.25 g Tris Base 2 g SDS 400 µl dH_2O pH to 6.8 Make to 500 ml with dH_2O	FisherScientific (10103203) Sigma-Aldrich (L3771)
Western Blotting	Running Buffer	3 g Tris Base 14.4 g Glycine 1 g SDS 1 L dH_2O	Sigma-Aldrich (77-86-1) Sigma-Aldrich (G8898) Sigma-Aldrich (L3771)
	Transfer Buffer	3 g Tris Base 14.4 g Glycine 200 ml methanol 800 ml dH_2O	FisherScientific (10103203) Sigma-Aldrich (G8898) Fisher Scientific (10245850)
	TBS-T	8.76 g NaCl 2.4 g Tris Base 1 L dH_2O	VWR (27810.295) FisherScientific (10103203)

		1 ml Tween 20 pH 7.5	Sigma-Aldrich (P9416)
	Stripping Buffer	3.8 g Tris Base 10 g SDS 400 µl dH_2O pH to 6.7 Make to 500 ml with dH_2O	FisherScientific (10103203) Sigma-Aldrich (L3771)
	ECL-1	88.5 ml dH_2O 1 ml Luminol 480 µl Coumeric Acid 10 ml Tris (1M)	 Sigma-Aldrich (A8511) Sigma-Aldrich (C9008) ThermoFisher Scientific (AM9856)
	ECL-2	90 ml dH_2O 64 µl H_2O_2 10 ml Tris (1M)	 Fisher Scientific (10185790) ThermoFisher Scientific (AM9856)
Fluorescence *in situ* hybridisation	In situ Hybridisation Buffer	300 µl 5M NaCl 40 µl 1M Tris-HCl (pH 8) 600 µl Formamide 1060 µl dH_2O 2 µl SDS	Sigma-Aldrich (31434) Sigma-Aldrich (10812846001) ThermoFisher Scientific (17889) Sigma-Aldrich (71736)
	FISH wash buffer	1 ml 1M Tris-HCl 1020 µl 5M NaCl 500 µl 0.5M EDTA 47.5 ml dH_2O 50 µl 10% SDS	Sigma-Aldrich (10812846001) Sigma-Aldrich (31434) Sigma-Aldrich (E7889) Sigma-Aldrich (71736)
Antibody Labelling	Dilution Buffer	4 ml 10x PBS 120 µl Triton X-100 0.4 g BSA 15 ml dH_2O	FisherScientific (AM9624) Sigma-Aldrich (X-100) Sigma-Aldrich (10735086001)
	Blocking Buffer	2.5 ml 10x PBS 1.25 ml FBS 21.25 ml dH_2O 0.025 ml Saponin	FisherScientific (AM9624) ThermoFisher Scientific (A5256701)) Sigma-Aldrich (SAE0073)

Bibliography

[1] Douglas B. Murphy. *Fundamentals of light microscopy and electronic imaging*. en. New York: Wiley-Liss, 2001. ISBN: 978-0-471-25391-4.

[2] Karel Zuiderveld. "Contrast Limited Adaptive Histogram Equalization". en. In: *Graphics Gems*. Elsevier, 1994, pp. 474–485. ISBN: 978-0-12-336156-1. DOI: 10.1016/B978-0-12-336156-1.50061-6. URL: https://linkinghub.elsevier.com/retrieve/pii/B9780123361561500616 (visited on 02/24/2023).

[3] Max Born and Emil Wolf. *Principles of optics: electromagnetic theory of propagation, interference and diffraction of light*. 6th ed. Oxford ; New York: Pergamon Press, 1980. ISBN: 978-0-08-026481-3 978-0-08-026482-0.

[4] *The Numerical Aperture*. URL: https://spie.org/publications/fg06_p16_na?SSO=1 (visited on 11/06/2023).

[5] *Olympus FluoView Resource Center: Resolution and Contrast in Confocal Microscopy*. URL: http://www.olympusconfocal.com/theory/resolutionintro.html (visited on 11/06/2023).

[6] Daniel Schmolze et al. "Advances in Microscopy Techniques". In: *Archives of pathology & laboratory medicine* 135 (Feb. 2011), pp. 255–63. DOI: 10.1043/1543-2165-135.2.255.

[7] Raymond A. Serway, John W. Jewett, and Vahé Peroomian. *Physics for scientists and engineers: technology update*. eng. Ninth edition. Boston, MA: Cengage Learning, 2016. ISBN: 978-1-305-11640-5.

[8] "Beyond the diffraction limit". en. In: *Nature Photonics* 3.7 (July 2009), pp. 361–361. ISSN: 1749-4893. DOI: 10.1038/nphoton.2009.100. URL: https://www.nature.com/articles/nphoton.2009.100 (visited on 11/06/2023).

[9] Shiraz S Kaderuppan et al. "Smart Nanoscopy: A Review of Computational Approaches to Achieve Super-Resolved Optical Microscopy". In: *IEEE Access* 8 (Dec. 2020), pp. 214801–214831. DOI: 10.1109/ACCESS.2020.3040319.

[10] E. Abbe. "Beiträge zur Theorie des Mikroskops und der mikroskopischen Wahrnehmung". de. In: *Archiv für Mikroskopische Anatomie* 9.1 (Dec. 1873), pp. 413–468. ISSN: 0176-7364. DOI: 10.1007/BF02956173. URL: https://doi.org/10.1007/BF02956173 (visited on 11/06/2023).

[11] *The Diffraction Barrier in Optical Microscopy*. URL: https://www.microscopyu.com/techniques/super-resolution/the-diffraction-barrier-in-optical-microscopy (visited on 11/06/2023).

[12] Rayleigh. "XXXI. *Investigations* in optics, with special reference to the spectroscope". en. In: *The London, Edinburgh, and Dublin Philosophical Magazine and Journal of Science* 8.49 (Oct. 1879), pp. 261–274. ISSN: 1941-5982, 1941-5990. DOI: 10.1080/14786447908639684. URL: https://www.tandfonline.com/doi/full/10.1080/14786447908639684 (visited on 11/06/2023).

[13] James B. Pawley, ed. *Handbook of biological confocal microscopy*. 3rd ed. New York, NY: Springer, 2006. ISBN: 978-0-387-25921-5.

[14] Filippo Piccinini et al. "Extended depth of focus in optical microscopy: Assessment of existing methods and a new proposal". en. In: *Microscopy Research and Technique* 75.11 (2012), pp. 1582–1592. ISSN: 1097-0029. DOI: 10.1002/jemt.22104. URL: https://onlinelibrary.wiley.com/doi/abs/10.1002/jemt.22104 (visited on 12/07/2023).

[15] David S.C. Biggs. "3D Deconvolution Microscopy". en. In: *Current Protocols in Cytometry* 52.1 (Apr. 2010). ISSN: 1934-9297, 1934-9300. DOI: 10.1002/0471142956.cy1219s52. URL: https://currentprotocols.onlinelibrary.wiley.com/doi/10.1002/0471142956.cy1219s52 (visited on 12/07/2023).

[16] C.E. Shannon. "Communication in the Presence of Noise". In: *Proceedings of the IRE* 37.1 (Jan. 1949), pp. 10–21. ISSN: 0096-8390. DOI: 10.1109/JRPROC.1949.232969.

[17] Harald H. Rose. "Historical aspects of aberration correction". In: *Journal of Electron Microscopy* 58.3 (June 2009), pp. 77–85. ISSN: 0022-0744. DOI: 10.1093/jmicro/dfp012. URL: https://doi.org/10.1093/jmicro/dfp012 (visited on 11/14/2023).

[18] Erin E. Diel, Jeff W. Lichtman, and Douglas S. Richardson. "Tutorial: avoiding and correcting sample-induced spherical aberration artifacts in 3D fluorescence microscopy". eng. In: *Nature Protocols* 15.9 (Sept. 2020), pp. 2773–2784. ISSN: 1750-2799. DOI: 10.1038/s41596-020-0360-2.

[19] M. Kozubek and P. Matula. "An efficient algorithm for measurement and correction of chromatic aberrations in fluorescence microscopy". en. In: *Journal of Microscopy* 200.3 (2000), pp. 206–217. ISSN: 1365-2818. DOI: 10.1046/j.1365-2818.2000.00754.x. URL: https://onlinelibrary.

wiley.com/doi/abs/10.1046/j.1365-2818.2000.00754.x (visited on 11/14/2023).

[20] Soon-Wook Chung, Byoung-Kwang Kim, and Woo-Jin Song. "Removing chromatic aberration by digital image processing". In: *Optical Engineering* 49.6 (June 2010), p. 067002. ISSN: 0091-3286, 1560-2303. DOI: 10.1117/1.3455506. URL: https://www.spiedigitallibrary.org/journals/optical-engineering/volume-49/issue-6/067002/Removing-chromatic-aberration-by-digital-image-processing/10.1117/1.3455506.full (visited on 11/14/2023).

[21] Joonyoung Chang, Hee Kang, and Moon Gi Kang. "Correction of Axial and Lateral Chromatic Aberration With False Color Filtering". In: *IEEE Transactions on Image Processing* 22.3 (Mar. 2013), pp. 1186–1198. ISSN: 1941-0042. DOI: 10.1109/TIP.2012.2228489. URL: https://ieeexplore.ieee.org/abstract/document/6357254 (visited on 11/14/2023).

[22] S. Bradbury and P. J. Evennett. *Contrast Techniques in Light Microscopy*. en. Garland Science, Aug. 2020. ISBN: 978-1-00-014460-4.

[23] P. C. Cheng and A. Kriete. "Image Contrast in Confocal Light Microscopy". en. In: *Handbook of Biological Confocal Microscopy*. Ed. by James B. Pawley. Boston, MA: Springer US, 1995, pp. 281–310. ISBN: 978-1-4757-5348-6. DOI: 10.1007/978-1-4757-5348-6_17. URL: https://doi.org/10.1007/978-1-4757-5348-6_17 (visited on 12/01/2023).

[24] Gary W. Gill. "Köhler Illumination". en. In: *Cytopreparation: Principles & Practice*. Ed. by Gary W. Gill. Essentials in Cytopathology. New York, NY: Springer, 2013, pp. 309–323. ISBN: 978-1-4614-4933-1. DOI: 10.1007/978-1-4614-4933-1_19. URL: https://doi.org/10.1007/978-1-4614-4933-1_19 (visited on 11/06/2023).

[25] RW Horobin. "Biological staining: mechanisms and theory". In: *Biotechnic & Histochemistry* 77.1 (Jan. 2002), pp. 3–13. ISSN: 1052-0295. DOI: 10.1080/bih.77.1.3.13. URL: https://doi.org/10.1080/bih.77.1.3.13 (visited on 11/06/2023).

[26] Andrew H. Fischer et al. "Hematoxylin and Eosin Staining of Tissue and Cell Sections". en. In: *Cold Spring Harbor Protocols* 2008.5 (May 2008), pdb.prot4986. ISSN: 1940-3402, 1559-6095. DOI: 10.1101/pdb.prot4986. URL: http://cshprotocols.cshlp.org/content/2008/5/pdb.prot4986 (visited on 11/06/2023).

[27] Richard Horobin and John Kiernan. *Conn's Biological Stains: A Handbook of Dyes, Stains and Fluorochromes for Use in Biology and Medicine*. en. Taylor & Francis, Aug. 2020. ISBN: 978-1-00-014461-1.

[28] Bernard Valeur and Mário N. Berberan-Santos. "A Brief History of Fluorescence and Phosphorescence before the Emergence of Quantum Theory". en. In: *Journal of Chemical Education* 88.6 (June 2011), pp. 731–738. ISSN: 0021-9584, 1938-1328. DOI: 10.1021/ed100182h. URL: https://pubs.acs.org/doi/abs/10.1021/ed100182h (visited on 11/06/2023).

[29] Joseph R. Lakowicz. "Introduction to Fluorescence". en. In: *Principles of Fluorescence Spectroscopy*. Ed. by Joseph R. Lakowicz. Boston, MA: Springer US, 1999, pp. 1–23. ISBN: 978-1-4757-3061-6. DOI: 10.1007/978-1-4757-3061-6_1. URL: https://doi.org/10.1007/978-1-4757-3061-6_1 (visited on 11/06/2023).

[30] Thorsten Schweizer, Heiko Kubach, and Thomas Koch. "Investigations to characterize the interactions of light radiation, engine operating media and fluorescence tracers for the use of qualitative light-induced

fluorescence in engine systems". en. In: *Automotive and Engine Technology* 6.3-4 (Dec. 2021), pp. 275–287. ISSN: 2365-5127, 2365-5135. DOI: 10.1007/s41104-021-00092-3. URL: https://link.springer.com/10.1007/s41104-021-00092-3 (visited on 12/01/2023).

[31] Ewa M. Goldys. *Fluorescence Applications in Biotechnology and Life Sciences*. en. John Wiley & Sons, Aug. 2009. ISBN: 978-0-470-08370-3.

[32] D Phillips. "Luminescence lifetimes in biological systems". In: *Analyst* 119.4 (1994). Publisher: The Royal Society of Chemistry, pp. 543–550.

[33] Klaus Suhling et al. "Fluorescence lifetime imaging (FLIM): Basic concepts and some recent developments". en. In: *Medical Photonics* 27 (May 2015), pp. 3–40. ISSN: 22138846. DOI: 10.1016/j.medpho.2014.12.001. URL: https://linkinghub.elsevier.com/retrieve/pii/S2213884614000033 (visited on 01/07/2024).

[34] Elizabeth Baggaley et al. "Long-lived metal complexes open up microsecond lifetime imaging microscopy under multiphoton excitation: from FLIM to PLIM and beyond". en. In: *Chem. Sci.* 5.3 (2014), pp. 879–886. ISSN: 2041-6520, 2041-6539. DOI: 10.1039/C3SC51875B. URL: http://xlink.rsc.org/?DOI=C3SC51875B (visited on 01/16/2024).

[35] Yingying Ning et al. "Fluorescence lifetime imaging of upper gastrointestinal pH *in vivo* with a lanthanide based near-infrared probe". en. In: *Chemical Science* 10.15 (2019), pp. 4227–4235. ISSN: 2041-6520, 2041-6539. DOI: 10.1039/C9SC00220K. URL: http://xlink.rsc.org/?DOI=C9SC00220K (visited on 01/16/2024).

[36] Rupsa Datta et al. "Recent innovations in fluorescence lifetime imaging microscopy for biology and medicine". In: *Journal of Biomedical Optics* 26.07 (July 2021). ISSN: 1083-3668. DOI: 10.1117/1.JBO.26.7.070603.

URL: https://www.spiedigitallibrary.org/journals/journal-of-biomedical-optics/volume-26/issue-07/070603/Recent-innovations-in-fluorescence-lifetime-imaging-microscopy-for-biology-and/10.1117/1.JBO.26.7.070603.full (visited on 01/07/2024).

[37] Riccardo Cicchi and Francesco Saverio Pavone. "Non-linear fluorescence lifetime imaging of biological tissues". en. In: *Analytical and Bioanalytical Chemistry* 400.9 (July 2011), pp. 2687–2697. ISSN: 1618-2642, 1618-2650. DOI: 10.1007/s00216-011-4896-4. URL: http://link.springer.com/10.1007/s00216-011-4896-4 (visited on 01/07/2024).

[38] R Cicchi et al. "Multidimensional non-linear laser imaging of Basal Cell Carcinoma". In: *Optics Express* 15.16 (2007). Publisher: Optica Publishing Group, pp. 10135–10148.

[39] Melissa C. Skala et al. "In vivo multiphoton fluorescence lifetime imaging of protein-bound and free nicotinamide adenine dinucleotide in normal and precancerous epithelia". en. In: *Journal of Biomedical Optics* 12.2 (2007), p. 024014. ISSN: 10833668. DOI: 10.1117/1.2717503. URL: http://biomedicaloptics.spiedigitallibrary.org/article.aspx?doi=10.1117/1.2717503 (visited on 01/07/2024).

[40] Jean-Christophe Meile et al. "Systematic localisation of proteins fused to the green fluorescent protein in Bacillus subtilis: Identification of new proteins at the DNA replication factory". en. In: *PROTEOMICS* 6.7 (2006), pp. 2135–2146. ISSN: 1615-9861. DOI: 10.1002/pmic.200500512. URL: https://onlinelibrary.wiley.com/doi/abs/10.1002/pmic.200500512 (visited on 11/14/2023).

[41] Bruce H. Davis et al. "Validation of cell-based fluorescence assays: Practice guidelines from the ICSH and ICCS – part I – rationale and aims". en. In: *Cytometry Part B: Clinical Cytometry* 84.5 (2013), pp. 282–285. ISSN: 1552-4957. DOI: 10.1002/cyto.b.21104. URL: https://onlinelibrary.wiley.com/doi/abs/10.1002/cyto.b.21104 (visited on 11/14/2023).

[42] A. C. Croce and G. Bottiroli. "Autofluorescence spectroscopy and imaging: a tool for biomedical research and diagnosis". eng. In: *European journal of histochemistry: EJH* 58.4 (Dec. 2014), p. 2461. ISSN: 2038-8306. DOI: 10.4081/ejh.2014.2461.

[43] J. H. Simons and L. P. Block. "FLUOROCARBONS". en. In: *Journal of the American Chemical Society* 59.7 (July 1937), pp. 1407–1407. ISSN: 0002-7863, 1520-5126. DOI: 10.1021/ja01286a512. URL: https://pubs.acs.org/doi/abs/10.1021/ja01286a512 (visited on 11/14/2023).

[44] D. M. McClure. "The Development of Fluorescence Microscopy for Tubercle Bacilli and its Use as an Adjunct to Histological Routine". In: *Journal of Clinical Pathology* 6.4 (Nov. 1953), pp. 273–281. ISSN: 0021-9746. URL: https://www.ncbi.nlm.nih.gov/pmc/articles/PMC1023644/ (visited on 11/14/2023).

[45] Albert H Coons. "Histochemistry with labeled antibody". In: *International review of cytology*. Vol. 5. Elsevier, 1956, pp. 1–23.

[46] Roger Y. Tsien and Alan Waggoner. "Fluorophores for Confocal Microscopy: Photophysics and Photochemistry". en. In: *Handbook of Biological Confocal Microscopy*. Ed. by James B. Pawley. Boston, MA: Springer US, 1990, pp. 169–178. ISBN: 978-1-4615-7133-9. DOI: 10.1007/978-1-4615-7133-9_16. URL: https://doi.org/10.1007/978-1-4615-7133-9_16 (visited on 11/14/2023).

[47] Igor Buchwalow et al. "Non-specific binding of antibodies in immunohistochemistry: fallacies and facts". en. In: *Scientific Reports* 1.1 (July 2011), p. 28. ISSN: 2045-2322. DOI: 10.1038/srep00028. URL: https://www.nature.com/articles/srep00028 (visited on 11/14/2023).

[48] M Barzan and F Hajiesmaeilbaigi. "Investigation the concentration effect on the absorption and fluorescence properties of Rhodamine 6G dye". In: *Optik* 159 (Apr. 2018), pp. 157–161. ISSN: 0030-4026. DOI: 10.1016/j.ijleo.2018.01.075. URL: https://www.sciencedirect.com/science/article/pii/S0030402618300871 (visited on 11/14/2023).

[49] *The Application of the Beer-Lambert Law to Optically Anisotropic Systems*. en. DOI: 10.1126/science.110.2845.41.b. URL: https://www.science.org/doi/10.1126/science.110.2845.41.b (visited on 11/14/2023).

[50] Sebastian Van De Linde, Mike Heilemann, and Markus Sauer. "Live-Cell Super-Resolution Imaging with Synthetic Fluorophores". en. In: *Annual Review of Physical Chemistry* 63.1 (May 2012), pp. 519–540. ISSN: 0066-426X, 1545-1593. DOI: 10.1146/annurev-physchem-032811-112012. URL: https://www.annualreviews.org/doi/10.1146/annurev-physchem-032811-112012 (visited on 01/09/2024).

[51] Jaroslav Icha et al. "Phototoxicity in live fluorescence microscopy, and how to avoid it". en. In: *BioEssays* 39.8 (2017), p. 1700003. ISSN: 1521-1878. DOI: 10.1002/bies.201700003. URL: https://onlinelibrary.wiley.com/doi/abs/10.1002/bies.201700003 (visited on 11/14/2023).

[52] Tom K. L. Meyvis et al. "Fluorescence Recovery After Photobleaching: A Versatile Tool for Mobility and Interaction Measurements in Pharmaceutical Research". en. In: *Pharmaceutical Research* 16.8 (Aug. 1999),

pp. 1153–1162. ISSN: 1573-904X. DOI: 10.1023/A:1011924909138. URL: https://doi.org/10.1023/A:1011924909138 (visited on 11/14/2023).

[53] Jay M. Enoch. "In Search of the Earliest Known Lenses (Dating Back 4500 Years)". en. In: *Optics and Lasers in Biomedicine and Culture*. Ed. by Costas Fotakis, Theodore G. Papazoglou, and Costas Kalpouzos. Series of the International Society on Optics Within Life Sciences. Berlin, Heidelberg: Springer, 2000, pp. 3–13. ISBN: 978-3-642-56965-4. DOI: 10.1007/978-3-642-56965-4_1.

[54] Nasser Pouyan. "MESOPOTAMIA, THE CRADLE OF CIVILIZATION AND MEDICINE". In: *World Journal of Pharmaceutical Research* 5 (Jan. 2016), pp. 192–225. DOI: 10.20959/wjpr20164-5895.

[55] Austen Henry Layard. *Discoveries in the Ruins of Nineveh and Babylon: With Travels in Armenia, Kurdistan, and the Desert : Being the Result of a Second Expedition Undertaken for the Trustees of the British Museum*. en. Harper & Brothers, 1859.

[56] *Pliny the Elder, The Natural History, BOOK I.\textbackslashtextlessa id="note-link1" href="#note1"\textbackslashtextgreater1\textbackslashtextless/a\textbackslashtextgr DEDICATION. \textbackslashtextlessa href="#note-link1"\textbackslashtextgreater1\textl Lemaire informs us, in his title-page, that the two first books of the Natural History are edited by M. Alexandre, in his edition.\textbackslashtextless/p\textbackslashtextg* URL: https://www.perseus.tufts.edu/hopper/text?doc=Plin.+Nat.+toc (visited on 11/06/2023).

[57] 965-1039 Alhazen. "The optics of Ibn al-Haytham : Books I-III : on direct vision / translated with introduction and commentary by A.I. Sabra." en. In: (). URL: https://commons.warburg.sas.ac.uk/concern/published_works/r494vk17h?locale=en (visited on 11/06/2023).

[58] Vincent Ilardi. *Renaissance Vision from Spectacles to Telescopes*. en. American Philosophical Society, 2007. ISBN: 978-0-87169-259-7.

[59] David Bardell. "Eyeglasses and the Discovery of the Microscope". In: *The American Biology Teacher* 43.3 (1981), pp. 157–159. ISSN: 0002-7685. DOI: 10.2307/4447190. URL: https://www.jstor.org/stable/4447190 (visited on 11/06/2023).

[60] &Na; "The evolution of microscope design from its invention to the present days:" en. In: *The American Journal of Surgical Pathology* 7.1 (Jan. 1983), pp. 95–102. ISSN: 0147-5185. DOI: 10.1097/00000478-198301000-00010. URL: http://journals.lww.com/00000478-198301000-00010 (visited on 11/06/2023).

[61] Stillman Drake. "Galileo's First Telescopic Observations". In: *Journal for the History of Astronomy* 7.3 (Oct. 1976), pp. 153–168. ISSN: 0021-8286. DOI: 10.1177/002182867600700301. URL: https://doi.org/10.1177/002182867600700301 (visited on 11/06/2023).

[62] Russell L. Haden. "Galileo and the Compound Microscope". In: *Bulletin of the History of Medicine* 12.2 (1942), pp. 242–247. ISSN: 0007-5140. URL: https://www.jstor.org/stable/44446268 (visited on 11/06/2023).

[63] *Microscope - Optics, Magnification, Invention \textbackslashtextbar Britannica*. en. URL: https://www.britannica.com/technology/microscope/History-of-optical-microscopes (visited on 11/06/2023).

[64] Clara Sue Ball. "The Early History of the Compound Microscope". In: *Bios* 37.2 (1966), pp. 51–60. ISSN: 0005-3155. URL: https://www.jstor.org/stable/4606667 (visited on 11/06/2023).

[65] *Robert Hooke type microscope \textbackslashtextbar Science Museum Group Collection*. en. URL: https://collection.sciencemuseumgroup.org.

uk/objects/co8592773/robert-hooke-type-microscope-compound-microscope (visited on 11/06/2023).

[66] Iml Donaldson. "Robert Hooke's Micrographia of 1665 and 1667". en. In: *The Journal of the Royal College of Physicians of Edinburgh* 40.4 (Dec. 2010), pp. 374–376. ISSN: 14782715. DOI: 10.4997/JRCPE.2010.420. URL: http://www.rcpe.ac.uk/journal/issue/journal_40_4/ex-libris.pdf (visited on 11/06/2023).

[67] Daniela P. Flores and Timothy C. Marzullo. "The construction of high-magnification homemade lenses for a simple microscope: an easy "DIY" tool for biological and interdisciplinary education". In: *Advances in Physiology Education* 45.1 (Mar. 2021), pp. 134–144. ISSN: 1043-4046. DOI: 10.1152/advan.00127.2020. URL: https://www.ncbi.nlm.nih.gov/pmc/articles/PMC9186497/ (visited on 11/06/2023).

[68] *Model of Leeuwenhoek's microscope \textbackslashtextbar Science Museum Group Collection*. en. URL: https://collection.sciencemuseumgroup.org.uk/objects/co119600/model-of-leeuwenhoeks-microscope-microscope (visited on 11/06/2023).

[69] Nick Lane. "The unseen world: reflections on Leeuwenhoek (1677) 'Concerning little animals'". In: *Philosophical Transactions of the Royal Society B: Biological Sciences* 370.1666 (Apr. 2015), p. 20140344. ISSN: 0962-8436. DOI: 10.1098/rstb.2014.0344. URL: https://www.ncbi.nlm.nih.gov/pmc/articles/PMC4360124/ (visited on 08/02/2023).

[70] P. Smit and J. Heniger. "Antoni van Leeuwenhoek (1632–1723) and the discovery of bacteria". en. In: *Antonie van Leeuwenhoek* 41.1 (Dec. 1975), pp. 217–228. ISSN: 1572-9699. DOI: 10.1007/BF02565057. URL: https://doi.org/10.1007/BF02565057 (visited on 11/06/2023).

[71] Wolfgang Wimmer. "Carl Zeiss, Ernst Abbe, and Advances in the Light Microscope". en. In: *Microscopy Today* 25.4 (July 2017), pp. 50–57. ISSN: 1551-9295, 2150-3583. DOI: 10.1017/S155192951700058X. URL: https://www.cambridge.org/core/journals/microscopy-today/article/carl-zeiss-ernst-abbe-and-advances-in-the-light-microscope/AB7931A055A6AA1399E3DD731DDAC960 (visited on 11/06/2023).

[72] *VII.—On the Estimation of Aperture in the Microscope. - Abbe - 1881 - Journal of the Royal Microscopical Society - Wiley Online Library*. URL: https://onlinelibrary.wiley.com/doi/10.1111/j.1365-2818.1881.tb05909.x (visited on 11/06/2023).

[73] E. Allen and J. L. Turk. "Microscopes in the Hunterian Museum." In: *Annals of The Royal College of Surgeons of England* 64.6 (Nov. 1982), pp. 414–418. ISSN: 0035-8843. URL: https://www.ncbi.nlm.nih.gov/pmc/articles/PMC2494086/ (visited on 11/06/2023).

[74] Maurice Daumas. *Scientific instruments of the seventeenth and eighteenth centuries and their makers*. eng. London: Portman Books, 1989. ISBN: 978-0-7134-0727-3.

[75] Subhash Chandra Parija. "Microscopy". en. In: *Textbook of Microbiology and Immunology*. Ed. by Subhash Chandra Parija. Singapore: Springer Nature, 2023, pp. 21–25. ISBN: 978-981-19331-5-8. DOI: 10.1007/978-981-19-3315-8_3. URL: https://doi.org/10.1007/978-981-19-3315-8_3 (visited on 11/06/2023).

[76] Richard L. Ornberg, B. Mark Woerner, and Dorothy A. Edwards. "Analysis of Stained Objects in Histological Sections by Spectral Imaging and Differential Absorption". In: *Journal of Histochemistry & Cytochemistry* 47.10 (Oct. 1999), pp. 1307–1313. ISSN: 0022-1554. DOI: 10.1177/

002215549904701010. URL: https://doi.org/10.1177/002215549904701010 (visited on 11/06/2023).

[77] Kazuya Kabayama and Ryugo Tero. "Optical Microscopy". en. In: *Compendium of Surface and Interface Analysis*. Ed. by The Surface Science Society of Japan. Singapore: Springer, 2018, pp. 413–417. ISBN: 978-981-10-6156-1. DOI: 10.1007/978-981-10-6156-1_68. URL: https://doi.org/10.1007/978-981-10-6156-1_68 (visited on 11/06/2023).

[78] Ruiyun Chen et al. "Electron Transfer-Based Single Molecule Fluorescence as a Probe for Nano-Environment Dynamics". In: *Sensors (Basel, Switzerland)* 14 (Feb. 2014), pp. 2449–67. DOI: 10.3390/s140202449.

[79] Ulrich Kubitscheck. *Fluorescence microscopy: from principles to biological applications*. John Wiley & Sons, 2017.

[80] Claire M. Brown, Andrew Reilly, and Richard W. Cole. "A Quantitative Measure of Field Illumination". In: *Journal of Biomolecular Techniques : JBT* 26.2 (July 2015), pp. 37–44. ISSN: 1524-0215, 1943-4731. DOI: 10.7171/jbt.15-2602-001. URL: https://www.ncbi.nlm.nih.gov/pmc/articles/PMC4365985/ (visited on 01/08/2024).

[81] Biagio Mandracchia et al. "Fast and accurate sCMOS noise correction for fluorescence microscopy". en. In: *Nature Communications* 11.1 (Jan. 2020), p. 94. ISSN: 2041-1723. DOI: 10.1038/s41467-019-13841-8. URL: https://www.nature.com/articles/s41467-019-13841-8 (visited on 11/09/2023).

[82] Hongtao Chen, Gerhard Holst, and Enrico Gratton. "Modulated CMOS camera for fluorescence lifetime microscopy". en. In: *Microscopy Research and Technique* 78.12 (2015), pp. 1075–1081. ISSN: 1097-0029. DOI:

10.1002/jemt.22587. URL: https://onlinelibrary.wiley.com/doi/abs/10.1002/jemt.22587 (visited on 11/09/2023).

[83] Lexy von Diezmann, Yoav Shechtman, and W. E. Moerner. "Three-Dimensional Localization of Single Molecules for Super-Resolution Imaging and Single-Particle Tracking". In: *Chemical Reviews* 117.11 (June 2017), pp. 7244–7275. ISSN: 0009-2665. DOI: 10.1021/acs.chemrev.6b00629. URL: https://doi.org/10.1021/acs.chemrev.6b00629 (visited on 11/09/2023).

[84] Kenneth R. Spring. "Cameras for Digital Microscopy". In: *Methods in Cell Biology*. Vol. 81. Digital Microscopy, 3rd Edition. Academic Press, Jan. 2007, pp. 171–186. DOI: 10.1016/S0091-679X(06)81010-1. URL: https://www.sciencedirect.com/science/article/pii/S0091679X06810101 (visited on 12/08/2023).

[85] Shinya Inoué. *Video microscopy*. Springer Science & Business Media, 2013.

[86] Talley J. Lambert and Jennifer C. Waters. "Chapter 3 - Assessing camera performance for quantitative microscopy". In: *Methods in Cell Biology*. Ed. by Jennifer C. Waters and Torsten Wittman. Vol. 123. Quantitative Imaging in Cell Biology. Academic Press, Jan. 2014, pp. 35–53. DOI: 10.1016/B978-0-12-420138-5.00003-3. URL: https://www.sciencedirect.com/science/article/pii/B9780124201385000033 (visited on 12/08/2023).

[87] Albert Einstein. "Über einem die Erzeugung und Verwandlung des Lichtes betreffenden heuristischen Gesichtspunkt". de. In: *Annalen der Physik* vol. 4, t. 17 (1905). URL: http://sedici.unlp.edu.ar/handle/10915/2784 (visited on 12/08/2023).

[88] Paul Jerram et al. "The LLCCD: low-light imaging without the need for an intensifier". In: *Sensors and camera systems for scientific, industrial, and digital photography applications ii*. Vol. 4306. SPIE, 2001, pp. 178–186.

[89] Craig D. Mackay et al. "Subelectron read noise at MHz pixel rates". In: *Sensors and Camera Systems for Scientific, Industrial, and Digital Photography Applications II*. Vol. 4306. SPIE, May 2001, pp. 289–298. DOI: 10.1117/12.426988. URL: https://www.spiedigitallibrary.org/conference-proceedings-of-spie/4306/0000/Subelectron-read-noise-at-MHz-pixel-rates/10.1117/12.426988.full (visited on 12/08/2023).

[90] M. Minsky. "Memoir on inventing the confocal scanning microscope". en. In: *Scanning* 10.4 (1988), pp. 128–138. ISSN: 1932-8745. DOI: 10.1002/sca.4950100403. URL: https://onlinelibrary.wiley.com/doi/abs/10.1002/sca.4950100403 (visited on 11/09/2023).

[91] Minsky Marvin. "Microscopy apparatus". US3013467A. Dec. 1961. URL: https://patents.google.com/patent/US3013467A/en (visited on 11/09/2023).

[92] Paul Davidovits and M. David Egger. "Scanning Laser Microscope". en. In: *Nature* 223.5208 (Aug. 1969), pp. 831–831. ISSN: 1476-4687. DOI: 10.1038/223831a0. URL: https://www.nature.com/articles/223831a0 (visited on 11/09/2023).

[93] J G White, W B Amos, and M Fordham. "An evaluation of confocal versus conventional imaging of biological structures by fluorescence light microscopy." en. In: *The Journal of cell biology* 105.1 (July 1987), pp. 41–48. ISSN: 0021-9525, 1540-8140. DOI: 10.1083/jcb.105.1.41. URL: https:

//rupress.org/jcb/article/105/1/41/28932/An-evaluation-of-confocal-versus-conventional (visited on 11/09/2023).

[94] W.b. Amos and J.g. White. "How the Confocal Laser Scanning Microscope entered Biological Research". en. In: *Biology of the Cell* 95.6 (2003), pp. 335–342. ISSN: 1768-322X. DOI: 10.1016/S0248-4900(03)00078-9. URL: https://onlinelibrary.wiley.com/doi/abs/10.1016/S0248-4900%2803%2900078-9 (visited on 11/09/2023).

[95] Coralie Fouquet et al. "Improving Axial Resolution in Confocal Microscopy with New High Refractive Index Mounting Media". en. In: *PLOS ONE* 10.3 (Mar. 2015). Ed. by Tom Waigh, e0121096. ISSN: 1932-6203. DOI: 10.1371/journal.pone.0121096. URL: https://dx.plos.org/10.1371/journal.pone.0121096 (visited on 01/09/2024).

[96] R. Foord et al. "The Use of Photomultiplier Tubes for Photon Counting". EN. In: *Applied Optics* 8.10 (Oct. 1969), pp. 1975–1989. ISSN: 2155-3165. DOI: 10.1364/AO.8.001975. URL: https://opg.optica.org/ao/abstract.cfm?uri=ao-8-10-1975 (visited on 11/09/2023).

[97] Ching-Wei Chang, Dhruv Sud, and Mary-Ann Mycek. "Fluorescence Lifetime Imaging Microscopy". en. In: *Methods in Cell Biology*. Vol. 81. Elsevier, 2007, pp. 495–524. ISBN: 978-0-12-374025-0. DOI: 10.1016/S0091-679X(06)81024-1. URL: https://linkinghub.elsevier.com/retrieve/pii/S0091679X06810241 (visited on 12/01/2023).

[98] Rupsa Datta et al. "Fluorescence lifetime imaging microscopy: fundamentals and advances in instrumentation, analysis, and applications". In: *Journal of Biomedical Optics* 25.7 (May 2020), p. 071203. ISSN: 1083-3668, 1560-2281. DOI: 10.1117/1.JBO.25.7.071203. URL: https://www.spiedigitallibrary.org/journals/journal-of-biomedical-

optics/volume-25/issue-7/071203/Fluorescence-lifetime-imaging-microscopy--fundamentals-and-advances-in-instrumentation/10.1117/1.JBO.25.7.071203.full (visited on 09/05/2023).

[99] Thomas Knapp et al. "Evaluation of tile artifact correction methods for multiphoton microscopy mosaics of whole-slide tissue sections". In: *Three-Dimensional and Multidimensional Microscopy: Image Acquisition and Processing XXIX*. Vol. 11966. SPIE, Mar. 2022, pp. 74–86. DOI: 10.1117/12.2609634. URL: https://www.spiedigitallibrary.org/conference-proceedings-of-spie/11966/119660D/Evaluation-of-tile-artifact-correction-methods-for-multiphoton-microscopy-mosaics/10.1117/12.2609634.full (visited on 11/21/2023).

[100] F.b. Legesse et al. "Seamless stitching of tile scan microscope images". pt. In: *Journal of Microscopy* 258.3 (2015), pp. 223–232. ISSN: 1365-2818. DOI: 10.1111/jmi.12236. URL: https://onlinelibrary.wiley.com/doi/abs/10.1111/jmi.12236 (visited on 11/21/2023).

[101] Sebastian Munck et al. "Challenges and advances in optical 3D mesoscale imaging". en. In: *Journal of Microscopy* 286.3 (June 2022), pp. 201–219. ISSN: 0022-2720, 1365-2818. DOI: 10.1111/jmi.13109. URL: https://onlinelibrary.wiley.com/doi/10.1111/jmi.13109 (visited on 03/08/2023).

[102] Gail McConnell et al. "A novel optical microscope for imaging large embryos and tissue volumes with sub-cellular resolution throughout". en. In: *eLife* 5 (Sept. 2016), e18659. ISSN: 2050-084X. DOI: 10.7554/eLife.18659. URL: https://elifesciences.org/articles/18659 (visited on 02/24/2023).

[103] *PLAN 4x/0,10*. en. URL: https://www.leica-microsystems.com/objectivefinder/objective/613240/ (visited on 11/14/2023).

[104] *ZEISS Primostar 3 iPlan Achromat 4x Objective Lens 415501-1600-000*. URL: https://www.microscopeworld.com/p-1116-zeiss-iplan-achromat-4x-objective-lens.aspx (visited on 11/14/2023).

[105] *4X Objective, Nikon CFI Plan Fluor \textbackslashtextbar Edmund Optics*. en. URL: https://www.edmundoptics.co.uk/p/4x-objective-nikon-cfi-plan-fluor/30636/ (visited on 11/14/2023).

[106] Johannes Schindelin et al. "Fiji: an open-source platform for biological-image analysis". en. In: *Nature Methods* 9.7 (July 2012), pp. 676–682. ISSN: 1548-7091, 1548-7105. DOI: 10.1038/nmeth.2019. URL: http://www.nature.com/articles/nmeth.2019 (visited on 02/24/2023).

[107] G. Mcconnell and W.B. Amos. "Application of the Mesolens for sub-cellular resolution imaging of intact larval and whole adult *Drosophila*: CONFOCAL MESOSCOPY OF *DROSOPHILA*". en. In: *Journal of Microscopy* 270.2 (May 2018), pp. 252–258. ISSN: 00222720. DOI: 10.1111/jmi.12693. URL: https://onlinelibrary.wiley.com/doi/10.1111/jmi.12693 (visited on 02/24/2023).

[108] Liam M. Rooney et al. "Intra-colony channels in E. coli function as a nutrient uptake system". en. In: *The ISME Journal* 14.10 (Oct. 2020), pp. 2461–2473. ISSN: 1751-7362, 1751-7370. DOI: 10.1038/s41396-020-0700-9. URL: http://www.nature.com/articles/s41396-020-0700-9 (visited on 07/26/2022).

[109] B. Bottura et al. "Intra-colony channel morphology in Escherichia coli biofilms is governed by nutrient availability and substrate stiffness". en. In: *Biofilm* 26 (2022), p. 100084.

[110] Megan Clapperton et al. *Multimodal optical mesoscopy reveals the quantity and spatial distribution of gram-positive biofilms in ex vivo tonsils*. en. preprint. Biophysics, July 2023. DOI: 10.1101/2023.07.03.547470. URL: http://biorxiv.org/lookup/doi/10.1101/2023.07.03.547470 (visited on 11/14/2023).

[111] S. Foylan et al. "Towards widefield multiphoton mesoscopy with the Mesolens". In: *Multiphoton Microscopy in the Biomedical Sciences XXIII*. Vol. 12384. SPIE, Apr. 2023, p. 1238402. DOI: 10.1117/12.2648753. URL: https://www.spiedigitallibrary.org/conference-proceedings-of-spie/12384/1238402/Towards-widefield-multiphoton-mesoscopy-with-the-Mesolens/10.1117/12.2648753.full (visited on 11/14/2023).

[112] Shannan Foylan et al. "Mesoscale standing wave imaging". en. In: *Journal of Microscopy* n/a.n/a (). ISSN: 1365-2818. DOI: 10.1111/jmi.13189. URL: https://onlinelibrary.wiley.com/doi/abs/10.1111/jmi.13189 (visited on 11/14/2023).

[113] Eliana Battistella, Juan F. Quintana, and Gail McConnell. "Application of Light-Sheet Mesoscopy to Image Host-Pathogen Interactions in Intact Organs". In: *Frontiers in Cellular and Infection Microbiology* 12 (June 2022), p. 903957. ISSN: 2235-2988. DOI: 10.3389/fcimb.2022.903957. URL: https://www.frontiersin.org/articles/10.3389/fcimb.2022.903957/full (visited on 02/24/2023).

[114] S. Foylan et al. *MesoTIRF: a Total Internal Reflection Fluorescence illuminator for axial super-resolution membrane imaging at the mesoscale*. en. preprint. Biophysics, Aug. 2022. DOI: 10.1101/2022.08.19.504513. URL: http://biorxiv.org/lookup/doi/10.1101/2022.08.19.504513 (visited on 02/24/2023).

[115] T. Ichimura et al. "Exploring rare cellular activity in more than one million cells by a transscale scope". en. In: *Scientific Reports* 11.1 (Aug. 2021), p. 16539. ISSN: 2045-2322. DOI: 10.1038/s41598-021-95930-7. URL: https://www.nature.com/articles/s41598-021-95930-7 (visited on 11/15/2023).

[116] Taro Ichimura et al. *Volumetric trans-scale imaging of massive quantity of heterogeneous cell populations in centimeter-wide tissue and embryo*. en. Aug. 2023. DOI: 10.1101/2023.08.21.553997. URL: https://www.biorxiv.org/content/10.1101/2023.08.21.553997v1 (visited on 11/15/2023).

[117] Nicholas James Sofroniew et al. "A large field of view two-photon mesoscope with subcellular resolution for in vivo imaging". In: *eLife* 5 (June 2016). Ed. by Fred Rieke, e14472. ISSN: 2050-084X. DOI: 10.7554/eLife.14472. URL: https://doi.org/10.7554/eLife.14472 (visited on 11/15/2023).

[118] Rongwen Lu et al. "Rapid mesoscale volumetric imaging of neural activity with synaptic resolution". en. In: *Nature Methods* 17.3 (Mar. 2020), pp. 291–294. ISSN: 1548-7105. DOI: 10.1038/s41592-020-0760-9. URL: https://www.nature.com/articles/s41592-020-0760-9 (visited on 11/15/2023).

[119] Omar E. Olarte et al. "Light-sheet microscopy: a tutorial". EN. In: *Advances in Optics and Photonics* 10.1 (Mar. 2018), pp. 111–179. ISSN: 1943-8206. DOI: 10.1364/AOP.10.000111. URL: https://opg.optica.org/aop/abstract.cfm?uri=aop-10-1-111 (visited on 11/14/2023).

[120] Eliana Battistella et al. "Light-sheet mesoscopy with the Mesolens provides fast sub-cellular resolution imaging throughout large tissue volumes". en. In: *iScience* 25.9 (Sept. 2022), p. 104797. ISSN: 25890042. DOI: 10.1016/j.isci.2022.104797. URL: https://linkinghub.elsevier.com/retrieve/pii/S2589004222010690 (visited on 05/05/2023).

[121] Ernst H. K. Stelzer et al. "Light sheet fluorescence microscopy". en. In: *Nature Reviews Methods Primers* 1.1 (Nov. 2021), pp. 1–25. ISSN: 2662-8449. DOI: 10.1038/s43586-021-00069-4. URL: https://www.nature.com/articles/s43586-021-00069-4 (visited on 11/30/2023).

[122] Michael Weber and Jan Huisken. "Light sheet microscopy for real-time developmental biology". In: *Current Opinion in Genetics & Development*. Developmental mechanisms, patterning and evolution 21.5 (Oct. 2011), pp. 566–572. ISSN: 0959-437X. DOI: 10.1016/j.gde.2011.09.009. URL: https://www.sciencedirect.com/science/article/pii/S0959437X11001444 (visited on 11/14/2023).

[123] Bin Yang et al. "DaXi—high-resolution, large imaging volume and multi-view single-objective light-sheet microscopy". en. In: *Nature Methods* 19.4 (Apr. 2022), pp. 461–469. ISSN: 1548-7105. DOI: 10.1038/s41592-022-01417-2. URL: https://www.nature.com/articles/s41592-022-01417-2 (visited on 11/14/2023).

[124] Liuba Dvinskikh et al. "High-speed 2D light-sheet fluorescence microscopy enables quantification of spatially varying calcium dynamics in ventricular cardiomyocytes". In: *Frontiers in Physiology* 14 (2023). ISSN: 1664-042X. URL: https://www.frontiersin.org/articles/10.3389/fphys.2023.1079727 (visited on 11/14/2023).

[125] Oluwatofunmi Sodimu et al. "Light sheet imaging and interactive analysis of the cardiac structure in neonatal mice". en. In: *Journal of Biophotonics* 16.5 (2023), e202200278. ISSN: 1864-0648. DOI: 10.1002/jbio.202200278. URL: https://onlinelibrary.wiley.com/doi/abs/10.1002/jbio.202200278 (visited on 11/14/2023).

[126] Xinyi Guo et al. "Rapid 3D isotropic imaging of whole organ with double-ring light-sheet microscopy and self-learning side-lobe elimination". EN. In: *Biomedical Optics Express* 14.12 (Dec. 2023), pp. 6206–6221. ISSN: 2156-7085. DOI: 10.1364/BOE.505217. URL: https://opg.optica.org/boe/abstract.cfm?uri=boe-14-12-6206 (visited on 11/14/2023).

[127] Hans-Ulrich Dodt et al. "Ultramicroscopy: three-dimensional visualization of neuronal networks in the whole mouse brain". eng. In: *Nature Methods* 4.4 (Apr. 2007), pp. 331–336. ISSN: 1548-7091. DOI: 10.1038/nmeth1036.

[128] Dongyue Wang et al. "Tiling light sheet selective plane illumination microscopy using discontinuous light sheets". en. In: *Optics Express* 27.23 (Nov. 2019), p. 34472. ISSN: 1094-4087. DOI: 10.1364/OE.27.034472. URL: https://opg.optica.org/abstract.cfm?URI=oe-27-23-34472 (visited on 11/15/2023).

[129] Fabian F. Voigt et al. "The mesoSPIM initiative: open-source light-sheet microscopes for imaging cleared tissue". en. In: *Nature Methods* 16.11 (Nov. 2019), pp. 1105–1108. ISSN: 1548-7091, 1548-7105. DOI: 10.1038/s41592-019-0554-0. URL: https://www.nature.com/articles/s41592-019-0554-0 (visited on 11/15/2023).

[130] K. F. A. Ross. "The Size of Living Bacteria". In: *Journal of Cell Science* s3-98.44 (Dec. 1957), pp. 435–454. ISSN: 0021-9533. DOI: 10.1242/jcs.s3-

98.44.435. URL: https://doi.org/10.1242/jcs.s3-98.44.435 (visited on 11/21/2023).

[131] Heide N. Schulz and Bo Barker Jørgensen. "Big Bacteria". In: *Annual Review of Microbiology* 55.1 (2001), pp. 105–137. DOI: 10.1146/annurev.micro.55.1.105. URL: https://doi.org/10.1146/annurev.micro.55.1.105 (visited on 11/21/2023).

[132] Anjum N. Bandarkar et al. "Tonsil ultrasound: technical approach and spectrum of pediatric peritonsillar infections". en. In: *Pediatric Radiology* 46.7 (June 2016), pp. 1059–1067. ISSN: 1432-1998. DOI: 10.1007/s00247-015-3505-7. URL: https://doi.org/10.1007/s00247-015-3505-7 (visited on 11/14/2023).

[133] Takahiro Hosokawa et al. "Evaluation of the Normal Tonsils in Pediatric Patients With Ultrasonography". en. In: *Journal of Ultrasound in Medicine* 36.5 (2017), pp. 1029–1036. ISSN: 1550-9613. DOI: 10.7863/ultra.16.05083. URL: https://onlinelibrary.wiley.com/doi/abs/10.7863/ultra.16.05083 (visited on 11/14/2023).

[134] Gargi Sharma et al. "A Proposal to Perform High Contrast Imaging of Human Palatine Tonsil with Cross Polarized Optical Coherence Tomography". en. In: *Photonics* 9.4 (Apr. 2022), p. 259. ISSN: 2304-6732. DOI: 10.3390/photonics9040259. URL: https://www.mdpi.com/2304-6732/9/4/259 (visited on 11/14/2023).

[135] Hamid Pahlevaninezhad et al. "Optical Coherence Tomography and Autofluorescence Imaging of Human Tonsil". en. In: *PLoS ONE* 9.12 (Dec. 2014). Ed. by Sunil Singhal, e115889. ISSN: 1932-6203. DOI: 10.1371/journal.pone.0115889. URL: https://dx.plos.org/10.1371/journal.pone.0115889 (visited on 02/24/2023).

[136] Karl-Heinz Herrmann et al. "High-resolution MRI of the human palatine tonsil and its schematic anatomic 3D reconstruction". en. In: *Journal of Anatomy* 240.1 (Jan. 2022), pp. 166–171. ISSN: 0021-8782, 1469-7580. DOI: 10.1111/joa.13532. URL: https://onlinelibrary.wiley.com/doi/10.1111/joa.13532 (visited on 11/14/2023).

[137] J. Heikkinen et al. "MRI Findings in Acute Tonsillar Infections". en. In: *American Journal of Neuroradiology* 43.2 (Feb. 2022), pp. 286–291. ISSN: 0195-6108, 1936-959X. DOI: 10.3174/ajnr.A7368. URL: https://www.ajnr.org/content/43/2/286 (visited on 11/14/2023).

[138] A D King, K I K Lei, and A T Ahuja. "MRI of primary non-Hodgkin's lymphoma of the palatine tonsil". en. In: *The British Journal of Radiology* 74.879 (Mar. 2001), pp. 226–229. ISSN: 0007-1285, 1748-880X. DOI: 10.1259/bjr.74.879.740226. URL: http://www.birpublications.org/doi/10.1259/bjr.74.879.740226 (visited on 02/24/2023).

[139] "Observations, communicated to the publisher by Mr. Antony van Leewenhoeck, in a dutch letter of the 9th Octob. 1676. here English'd: concerning little animals by him observed in rain-well-sea- and snow water; as also in water wherein pepper had lain infused". en. In: *Philosophical Transactions of the Royal Society of London* 12.133 (Mar. 1677), pp. 821–831. ISSN: 0261-0523, 2053-9223. DOI: 10.1098/rstl.1677.0003. URL: https://royalsocietypublishing.org/doi/10.1098/rstl.1677.0003 (visited on 08/02/2023).

[140] C. Prigent-Combaret et al. "Abiotic surface sensing and biofilm-dependent regulation of gene expression in Escherichia coli". eng. In: *Journal of Bacteriology* 181.19 (Oct. 1999), pp. 5993–6002. ISSN: 0021-9193. DOI: 10.1128/JB.181.19.5993-6002.1999.

[141] P. Becker et al. "Detection of differential gene expression in biofilm-forming versus planktonic populations of Staphylococcus aureus using micro-representational-difference analysis". eng. In: *Applied and Environmental Microbiology* 67.7 (July 2001), pp. 2958–2965. ISSN: 0099-2240. DOI: 10.1128/AEM.67.7.2958-2965.2001.

[142] *Electron Microscopic Study of a Slime Layer \textbackslashtextbar Journal of Bacteriology*. URL: https://journals.asm.org/doi/abs/10.1128/jb.99.1.316-325.1969 (visited on 03/31/2023).

[143] *How Bacteria Stick on JSTOR*. URL: https://www.jstor.org/stable/24955617 (visited on 03/31/2023).

[144] Luanne Hall-Stoodley, J William Costerton, and Paul Stoodley. "Bacterial biofilms: from the natural environment to infectious diseases". In: *Nature reviews microbiology* 2.2 (2004), pp. 95–108.

[145] Karin Sauer et al. "The biofilm life cycle: expanding the conceptual model of biofilm formation". en. In: *Nature Reviews Microbiology* (Aug. 2022). ISSN: 1740-1526, 1740-1534. DOI: 10.1038/s41579-022-00767-0. URL: https://www.nature.com/articles/s41579-022-00767-0 (visited on 09/05/2022).

[146] Paul Stoodley et al. "Biofilms as complex differentiated communities". In: *Annual Reviews in Microbiology* 56.1 (2002), pp. 187–209.

[147] Kasper Nørskov Kragh et al. "The Inoculation Method Could Impact the Outcome of Microbiological Experiments". In: *Applied and Environmental Microbiology* 84.5 (Feb. 2018), e02264–17. DOI: 10.1128/AEM.02264-17. URL: https://journals.asm.org/doi/full/10.1128/aem.02264-17 (visited on 11/09/2023).

[148] David Schleheck et al. “Pseudomonas aeruginosa PAO1 Preferentially Grows as Aggregates in Liquid Batch Cultures and Disperses upon Starvation”. en. In: *PLOS ONE* 4.5 (May 2009), e5513. ISSN: 1932-6203. DOI: 10.1371/journal.pone.0005513. URL: https://journals.plos.org/plosone/article?id=10.1371/journal.pone.0005513 (visited on 11/09/2023).

[149] Peter Ø. Jensen et al. “Microenvironmental characteristics and physiology of biofilms in chronic infections of CF patients are strongly affected by the host immune response”. en. In: *APMIS* 125.4 (2017), pp. 276–288. ISSN: 1600-0463. DOI: 10.1111/apm.12668. URL: https://onlinelibrary.wiley.com/doi/abs/10.1111/apm.12668 (visited on 11/09/2023).

[150] E. Somekh et al. “Concentration and bactericidal activity of fusidic acid and cloxacillin in serum and synovial fluid”. In: *Journal of Antimicrobial Chemotherapy* 43.4 (Apr. 1999), pp. 593–596. ISSN: 0305-7453. DOI: 10.1093/jac/43.4.593. URL: https://doi.org/10.1093/jac/43.4.593 (visited on 11/09/2023).

[151] Marc Habash and Gregor Reid. “Microbial Biofilms: Their Development and Significance for Medical Device—Related Infections”. en. In: *The Journal of Clinical Pharmacology* 39.9 (1999), pp. 887–898. ISSN: 1552-4604. DOI: 10.1177/00912709922008506. URL: https://onlinelibrary.wiley.com/doi/abs/10.1177/00912709922008506 (visited on 11/29/2023).

[152] Wen Yin et al. “Biofilms: The Microbial “Protective Clothing” in Extreme Environments”. en. In: *International Journal of Molecular Sciences* 20.14 (Jan. 2019), p. 3423. ISSN: 1422-0067. DOI: 10.3390/ijms20143423. URL: https://www.mdpi.com/1422-0067/20/14/3423 (visited on 11/29/2023).

[153] Matthew R Parsek and Pradeep K Singh. "Bacterial biofilms: an emerging link to disease pathogenesis". In: *Annual Reviews in Microbiology* 57.1 (2003), pp. 677–701.

[154] Gebreselema Gebreyohannes et al. "Challenges of intervention, treatment, and antibiotic resistance of biofilm-forming microorganisms". en. In: *Heliyon* 5.8 (Aug. 2019), e02192. ISSN: 24058440. DOI: 10.1016/j.heliyon.2019.e02192. URL: https://linkinghub.elsevier.com/retrieve/pii/S2405844019358529 (visited on 11/15/2023).

[155] Oana Ciofu et al. "Tolerance and resistance of microbial biofilms". en. In: *Nature Reviews Microbiology* (Feb. 2022). ISSN: 1740-1526, 1740-1534. DOI: 10.1038/s41579-022-00682-4. URL: https://www.nature.com/articles/s41579-022-00682-4 (visited on 09/05/2022).

[156] Karishma Bisht and Catherine Ann Wakeman. "Discovery and Therapeutic Targeting of Differentiated Biofilm Subpopulations". In: *Frontiers in Microbiology* 10 (2019). ISSN: 1664-302X. URL: https://www.frontiersin.org/articles/10.3389/fmicb.2019.01908 (visited on 11/29/2023).

[157] Claudia Michaelis and Elisabeth Grohmann. "Horizontal Gene Transfer of Antibiotic Resistance Genes in Biofilms". en. In: *Antibiotics* 12.2 (Feb. 2023), p. 328. ISSN: 2079-6382. DOI: 10.3390/antibiotics12020328. URL: https://www.mdpi.com/2079-6382/12/2/328 (visited on 11/29/2023).

[158] D.E. Salcedo et al. "The effects of antibiotics on the biofilm formation and antibiotic resistance gene transfer". In: *Desalination and Water Treatment* 54.13 (June 2015), pp. 3582–3588. ISSN: 1944-3994. DOI: 10.1080/

19443994.2014.923206. URL: https://doi.org/10.1080/19443994.2014.923206 (visited on 11/29/2023).

[159] Søren Molin and Tim Tolker-Nielsen. "Gene transfer occurs with enhanced efficiency in biofilms and induces enhanced stabilisation of the biofilm structure". In: *Current Opinion in Biotechnology* 14.3 (June 2003), pp. 255–261. ISSN: 0958-1669. DOI: 10.1016/S0958-1669(03)00036-3. URL: https://www.sciencedirect.com/science/article/pii/S0958166903000363 (visited on 11/29/2023).

[160] Jonas Stenløkke Madsen et al. "The interconnection between biofilm formation and horizontal gene transfer". In: *FEMS Immunology & Medical Microbiology* 65.2 (July 2012), pp. 183–195. ISSN: 0928-8244. DOI: 10.1111/j.1574-695X.2012.00960.x. URL: https://doi.org/10.1111/j.1574-695X.2012.00960.x (visited on 11/29/2023).

[161] Don Monroe. "Looking for chinks in the armor of bacterial biofilms". In: *PLoS biology* 5.11 (2007), e307.

[162] Waldemar Vollmer and Petra Born. "Chapter 2 - Bacterial cell envelope peptidoglycan". In: *Microbial Glycobiology*. Ed. by Otto Holst et al. San Diego: Academic Press, Jan. 2010, pp. 15–28. ISBN: 978-0-12-374546-0. DOI: 10.1016/B978-0-12-374546-0.00002-X. URL: https://www.sciencedirect.com/science/article/pii/B978012374546000002X (visited on 10/30/2023).

[163] *The Bacterial Cell Envelope - PMC*. URL: https://www.ncbi.nlm.nih.gov/pmc/articles/PMC2857177/ (visited on 10/30/2023).

[164] Omeed Sizar, Stephen W. Leslie, and Chandrashekhar G. Unakal. "Gram-Positive Bacteria". eng. In: *StatPearls*. Treasure Island (FL): StatPearls

Publishing, 2023. URL: http://www.ncbi.nlm.nih.gov/books/NBK470553/ (visited on 10/30/2023).

[165] Junio Oliveira and Wanda C. Reygaert. "Gram-Negative Bacteria". eng. In: *StatPearls*. Treasure Island (FL): StatPearls Publishing, 2023. URL: http://www.ncbi.nlm.nih.gov/books/NBK538213/ (visited on 10/30/2023).

[166] Christian Gram. "Ueber die isolirte Farbung der Schizomyceten in Schnitt- und Trockenpraparaten". In: *Fortschritte der Medicin* 2 (1884), pp. 185–189.

[167] *Gram-positive bacteria*. en. Oct. 2023. URL: https://en.wikipedia.org/w/index.php?title=Gram-positive_bacteria&oldid=1178944171 (visited on 10/30/2023).

[168] Dr Graham Beards. *English: Bacillus subtilis bacteria, Gram stain*. May 2021. URL: https://commons.wikimedia.org/wiki/File:Bacillus_subtilis_2.jpg (visited on 10/30/2023).

[169] *Gram-negative bacteria*. en. Oct. 2023. URL: https://en.wikipedia.org/w/index.php?title=Gram-negative_bacteria&oldid=1181952387 (visited on 10/30/2023).

[170] T J Marrie, J Nelligan, and J W Costerton. "A scanning and transmission electron microscopic study of an infected endocardial pacemaker lead." In: *Circulation* 66.6 (Dec. 1982), pp. 1339–1341. DOI: 10.1161/01.CIR.66.6.1339. URL: https://www.ahajournals.org/doi/abs/10.1161/01.CIR.66.6.1339 (visited on 11/09/2023).

[171] David A. Smith and Sara M. Nehring. "Bacteremia". eng. In: *StatPearls*. Treasure Island (FL): StatPearls Publishing, 2023. URL: http://www.ncbi.nlm.nih.gov/books/NBK441979/ (visited on 11/09/2023).

[172] Lei Yang et al. *In situ growth rates and biofilm development of Pseudomonas aeruginosa populations in chronic lung infections*. 2008.

[173] Drew J. Schwartz et al. "Population Dynamics and Niche Distribution of Uropathogenic Escherichia coli during Acute and Chronic Urinary Tract Infection". en. In: *Infection and Immunity* 79.10 (Oct. 2011). Ed. by S. M. Payne, pp. 4250–4259. ISSN: 0019-9567, 1098-5522. DOI: 10.1128/IAI.05339-11. URL: https://journals.asm.org/doi/10.1128/IAI.05339-11 (visited on 11/10/2023).

[174] Leah M. Feazel et al. "Microbiome complexity and Staphylococcus aureus in chronic rhinosinusitis". en. In: *The Laryngoscope* 122.2 (Feb. 2012), pp. 467–472. ISSN: 0023852X. DOI: 10.1002/lary.22398. URL: https://onlinelibrary.wiley.com/doi/10.1002/lary.22398 (visited on 11/10/2023).

[175] David Lebeaux et al. "From in vitro to in vivo Models of Bacterial Biofilm-Related Infections". en. In: *Pathogens* 2.2 (May 2013), pp. 288–356. ISSN: 2076-0817. DOI: 10.3390/pathogens2020288. URL: http://www.mdpi.com/2076-0817/2/2/288 (visited on 03/21/2023).

[176] Gabriel Carvalho et al. "How do environment-dependent switching rates between susceptible and persister cells affect the dynamics of biofilms faced with antibiotics?" eng. In: *NPJ biofilms and microbiomes* 4 (2018), p. 6. ISSN: 2055-5008. DOI: 10.1038/s41522-018-0049-2.

[177] Steven L Percival et al. "Healthcare-associated infections, medical devices and biofilms: risk, tolerance and control". In: *Journal of medical microbiology* 64.4 (2015). Publisher: Microbiology Society, pp. 323–334.

[178] J William Costerton et al. "Bacterial biofilms in nature and disease". In: *Annual Reviews in Microbiology* 41.1 (1987). Publisher: Annual Reviews

4139 El Camino Way, PO Box 10139, Palo Alto, CA 94303-0139, USA, pp. 435–464.

[179] Hong Wu et al. "Strategies for combating bacterial biofilm infections". en. In: *International Journal of Oral Science* 7.1 (Mar. 2015), pp. 1–7. ISSN: 2049-3169. DOI: 10.1038/ijos.2014.65. URL: https://www.nature.com/articles/ijos201465 (visited on 11/10/2023).

[180] Priscilla L. Phillips and Gregory S. Schultz. "Molecular Mechanisms of Biofilm Infection: Biofilm Virulence Factors". In: *Advances in Wound Care* 1.3 (June 2012), pp. 109–114. ISSN: 2162-1918. DOI: 10.1089/wound.2011.0301. URL: https://www.liebertpub.com/doi/abs/10.1089/wound.2011.0301 (visited on 11/10/2023).

[181] Federico Marchetti et al. "Early antibiotic treatment of pseudomonas aeruginosa colonisation in cystic fibrosis: a critical review of the literature". en. In: *European Journal of Clinical Pharmacology* 60.2 (Apr. 2004), pp. 67–74. ISSN: 1432-1041. DOI: 10.1007/s00228-004-0735-2. URL: https://doi.org/10.1007/s00228-004-0735-2 (visited on 11/10/2023).

[182] S. Monecke et al. "Molecular epidemiology of Staphylococcus aureus in asymptomatic carriers". en. In: *European Journal of Clinical Microbiology & Infectious Diseases* 28.9 (Sept. 2009), pp. 1159–1165. ISSN: 1435-4373. DOI: 10.1007/s10096-009-0752-2. URL: https://doi.org/10.1007/s10096-009-0752-2 (visited on 11/10/2023).

[183] A Vanbelkum et al. "Co-evolutionary aspects of human colonisation and infection by Staphylococcus aureus". en. In: *Infection, Genetics and Evolution* 9.1 (Jan. 2009), pp. 32–47. ISSN: 15671348. DOI: 10.1016/j.meegid.2008.09.012. URL: https://linkinghub.elsevier.com/retrieve/pii/S1567134808001779 (visited on 11/10/2023).

[184] Tanya Golubchik et al. "Within-Host Evolution of Staphylococcus aureus during Asymptomatic Carriage". en. In: *PLOS ONE* 8.5 (May 2013), e61319. ISSN: 1932-6203. DOI: 10.1371/journal.pone.0061319. URL: https://journals.plos.org/plosone/article?id=10.1371/journal.pone.0061319 (visited on 11/10/2023).

[185] Gregory P DeMuri et al. "Dynamics of Bacterial Colonization With Streptococcus pneumoniae, Haemophilus influenzae, and Moraxella catarrhalis During Symptomatic and Asymptomatic Viral Upper Respiratory Tract Infection". In: *Clinical Infectious Diseases* 66.7 (Mar. 2018), pp. 1045–1053. ISSN: 1058-4838. DOI: 10.1093/cid/cix941. URL: https://doi.org/10.1093/cid/cix941 (visited on 11/10/2023).

[186] Agnieszka Sulikowska et al. "Characteristics of Streptococcus pneumoniae, Haemophilus influenzae, and Moraxella catarrhalis Isolated from the Nasopharynges of Asymptomatic Children and Molecular Analysis of S. pneumoniae and H. influenzae Strain Replacement in the Nasopharynx". In: *Journal of Clinical Microbiology* 42.9 (Sept. 2004), pp. 3942–3949. DOI: 10.1128/jcm.42.9.3942-3949.2004. URL: https://journals.asm.org/doi/full/10.1128/jcm.42.9.3942-3949.2004 (visited on 11/10/2023).

[187] Ji Lam et al. "Production of mucoid microcolonies by Pseudomonas aeruginosa within infected lungs in cystic fibrosis". In: *Infection and immunity* 28.2 (1980), pp. 546–556.

[188] Klaus Kirketerp-Møller et al. "Distribution, organization, and ecology of bacteria in chronic wounds". In: *Journal of clinical microbiology* 46.8 (2008), pp. 2717–2722.

[189] Dirk de Beer, Paul Stoodley, and Zbigniew Lewandowski. "Measurement of local diffusion coefficients in biofilms by microinjection and confocal microscopy". In: *Biotechnology and bioengineering* 53.2 (1997), pp. 151–158.

[190] Luanne Hall-Stoodley et al. "Characterization of biofilm matrix, degradation by DNase treatment and evidence of capsule downregulation in Streptococcus pneumoniae clinical isolates". In: *BMC microbiology* 8 (2008), pp. 1–16.

[191] CA Fux, Suzanne Wilson, and Paul Stoodley. *Detachment characteristics and oxacillin resistance of Staphyloccocus aureus biofilm emboli in an in vitro catheter infection model*. 2004.

[192] Giorgia Borriello et al. "Oxygen limitation contributes to antibiotic tolerance of Pseudomonas aeruginosa in biofilms". In: *Antimicrobial agents and chemotherapy* 48.7 (2004), pp. 2659–2664.

[193] Devang Shah et al. "Persisters: a distinct physiological state of E. coli". In: *BMC microbiology* 6.1 (2006), pp. 1–9.

[194] Kimberly K Jefferson, Donald A Goldmann, and Gerald B Pier. "Use of confocal microscopy to analyze the rate of vancomycin penetration through Staphylococcus aureus biofilms". In: *Antimicrobial agents and chemotherapy* 49.6 (2005), pp. 2467–2473.

[195] Tiebin Wang, Imane El Meouche, and Mary J. Dunlop. "Bacterial persistence induced by salicylate via reactive oxygen species". eng. In: *Scientific Reports* 7 (Mar. 2017), p. 43839. ISSN: 2045-2322. DOI: 10.1038/srep43839.

[196] Thomas K. Wood, Stephen J. Knabel, and Brian W. Kwan. "Bacterial Persister Cell Formation and Dormancy". In: *Applied and Environmental*

Microbiology 79.23 (Dec. 2013), pp. 7116–7121. ISSN: 0099-2240. DOI: 10.1128/AEM.02636-13. URL: https://www.ncbi.nlm.nih.gov/pmc/articles/PMC3837759/ (visited on 11/15/2023).

[197] *Intracellular Bacterial Biofilm-Like Pods in Urinary Tract Infections \textbackslashtextbar Science*. URL: https://www.science.org/doi/full/10.1126/science.1084550 (visited on 11/15/2023).

[198] Luanne Hall-Stoodley and Paul Stoodley. "Evolving concepts in biofilm infections". en. In: *Cellular Microbiology* 11.7 (2009), pp. 1034–1043. ISSN: 1462-5822. DOI: 10.1111/j.1462-5822.2009.01323.x. URL: https://onlinelibrary.wiley.com/doi/abs/10.1111/j.1462-5822.2009.01323.x (visited on 11/15/2023).

[199] Beatrice Bottura et al. *Fractal complexity of Escherichia coli nutrient transport channels is influenced by cell shape and growth environment*. en. preprint. Microbiology, Nov. 2023. DOI: 10.1101/2023.11.29.569150. URL: http://biorxiv.org/lookup/doi/10.1101/2023.11.29.569150 (visited on 12/01/2023).

[200] Katherine J. Baxter et al. *Time-lapse mesoscopy of Candida albicans and Staphylococcus aureus dual-species biofilms reveals a structural role for the hyphae of C. albicans in biofilm formation*. en. Sept. 2023. DOI: 10.1101/2023.08.31.555792. URL: https://www.biorxiv.org/content/10.1101/2023.08.31.555792v3 (visited on 10/20/2023).

[201] Smrithi Santosh. *The Tonsils (Waldeyer's Ring)*. Dec. 2022. (Visited on 07/08/2023).

[202] Glenis K Scadding. "Immunology of the tonsil: a review". In: *Journal of the Royal Society of Medicine* 83.2 (1990), pp. 104–107.

[203] F. Rubin et al. "Transoral lateral oropharyngectomy". en. In: *European Annals of Otorhinolaryngology, Head and Neck Diseases* 134.6 (Dec. 2017), pp. 419–422. ISSN: 18797296. DOI: 10.1016/j.anorl.2017.06.002. URL: https://linkinghub.elsevier.com/retrieve/pii/S1879729617300996 (visited on 08/07/2023).

[204] Alexandra Arambula, Jason R. Brown, and Laura Neff. "Anatomy and physiology of the palatine tonsils, adenoids, and lingual tonsils". In: *World Journal of Otorhinolaryngology- Head and Neck Surgery* 07.03 (July 2021), pp. 155–160. DOI: 10.1016/j.wjorl.2021.04.003. URL: https://mednexus.org/doi/full/10.1016/j.wjorl.2021.04.003 (visited on 11/29/2023).

[205] *HA 235 - Histology - Lymphoid Tissues II*. URL: http://lecannabiculteur.free.fr/SITES/UNIV%20W.AUSTRALIA/mb140/CorePages/Lymphoid2/Lymph2.htm (visited on 11/10/2023).

[206] H. Nave, A. Gebert, and R. Pabst. "Morphology and immunology of the human palatine tonsil". In: *Anatomy and Embryology* 204.5 (Nov. 2001), pp. 367–373. ISSN: 03402061. DOI: 10.1007/s004290100210. URL: http://link.springer.com/10.1007/s004290100210 (visited on 07/28/2023).

[207] G. Siegel, Ruthild Linse, and Sigrun Macheleidt. "Factors of tonsillar involution: Age-dependent changes in B-cell activation and Langerhans' cell density". en. In: *Archives of Oto-Rhino-Laryngology* 236.3 (Dec. 1982), pp. 261–269. ISSN: 0302-9530, 1434-4726. DOI: 10.1007/BF00454218. URL: http://link.springer.com/10.1007/BF00454218 (visited on 07/28/2023).

[208] Margaretha L. Casselbrant. "What is wrong in chronic adenoiditis/tonsillitis anatomical considerations". en. In: *International Journal of Pediatric Otorhinolaryngology* 49 (Oct. 1999), S133–S135. ISSN: 01655876. DOI: 10.1016/S0165-5876(99)00147-0. URL: https://linkinghub.elsevier.com/retrieve/pii/S0165587699001470 (visited on 07/28/2023).

[209] K. Y. Jung et al. "Age-related changes of IgA immunocytes and serum and salivary IgA after tonsillectomy". eng. In: *Acta Oto-Laryngologica. Supplementum* 523 (1996), pp. 115–119. ISSN: 0365-5237.

[210] Alejandro Prados et al. "Characterization of mesenchymal stem/stromal cells with lymphoid tissue organizer cell potential in tonsils from children". en. In: *European Journal of Immunology* 48.5 (2018), pp. 829–843. ISSN: 1521-4141. DOI: 10.1002/eji.201746963. URL: https://onlinelibrary.wiley.com/doi/abs/10.1002/eji.201746963 (visited on 11/30/2023).

[211] Svetlana Glushakova et al. "Infection of human tonsil histocultures: A model for HIV pathogenesis". en. In: *Nature Medicine* 1.12 (Dec. 1995), pp. 1320–1322. ISSN: 1546-170X. DOI: 10.1038/nm1295-1320. URL: https://www.nature.com/articles/nm1295-1320 (visited on 11/30/2023).

[212] Prosper N. Boyaka et al. "Human Nasopharyngeal-Associated Lymphoreticular Tissues: Functional Analysis of Subepithelial and Intraepithelial B and T Cells from Adenoids and Tonsils". In: *The American Journal of Pathology* 157.6 (Dec. 2000), pp. 2023–2035. ISSN: 0002-9440. DOI: 10.1016/S0002-9440(10)64841-9. URL: https://www.sciencedirect.com/science/article/pii/S0002944010648419 (visited on 11/30/2023).

[213] Birgit K Van Staaij et al. "Effectiveness of adenotonsillectomy in children with mild symptoms of throat infections or adenotonsillar hypertrophy: open, randomised controlled trial". en. In: *BMJ* 329.7467 (Sept.

2004), p. 651. ISSN: 0959-8138, 1468-5833. DOI: 10.1136/bmj.38210.827917.7C. URL: https://www.bmj.com/lookup/doi/10.1136/bmj.38210.827917.7C (visited on 11/30/2023).

[214] Ron B. Mitchell et al. "Clinical Practice Guideline: Tonsillectomy in Children (Update)". en. In: *Otolaryngology–Head and Neck Surgery* 160.1_suppl (Feb. 2019), S1–S42. ISSN: 0194-5998. DOI: 10.1177/0194599818801757. URL: https://doi.org/10.1177/0194599818801757 (visited on 09/28/2023).

[215] Ronald Alastair McNeill. "A History of Tonsillectomy: Two Millenia of Trauma, Hæmorrhage and Controversy". In: *The Ulster Medical Journal* 29.1 (June 1960), pp. 59–63. ISSN: 0041-6193. URL: https://www.ncbi.nlm.nih.gov/pmc/articles/PMC2384338/ (visited on 11/30/2023).

[216] Brian W. Blakley. "Post-tonsillectomy bleeding: How much is too much?" en. In: *Otolaryngology–Head and Neck Surgery* 140.3 (Mar. 2009), pp. 288–290. ISSN: 0194-5998. DOI: 10.1016/j.otohns.2008.12.005. URL: https://doi.org/10.1016/j.otohns.2008.12.005 (visited on 11/22/2023).

[217] J. Alison Glover. "The Incidence of Tonsillectomy in School Children". en. In: *Proceedings of the Royal Society of Medicine* 31.10 (Aug. 1938), pp. 1219–1236. ISSN: 0035-9157. DOI: 10.1177/003591573803101027. URL: https://doi.org/10.1177/003591573803101027 (visited on 11/30/2023).

[218] Louis Dwyer-Hemmings. "'A Wicked Operation'? Tonsillectomy in Twentieth-Century Britain". en. In: *Medical History* 62.2 (Apr. 2018), pp. 217–241. ISSN: 0025-7273, 2048-8343. DOI: 10.1017/mdh.2018.5. URL: https://www.cambridge.org/core/journals/medical-history/article/wicked-operation-tonsillectomy-in-twentiethcentury-britain/18C27C3E6911014BCA5AA13F16F6C736 (visited on 11/30/2023).

[219] M. E. Perry. "The specialised structure of crypt epithelium in the human palatine tonsil and its functional significance". eng. In: *Journal of Anatomy* 185 (Pt 1) (Aug. 1994), pp. 111–127. ISSN: 0021-8782.

[220] Sung Yoon Catherine Kang et al. "Characterization of Epithelial Progenitors in Normal Human Palatine Tonsils and Their HPV16 E6/E7-Induced Perturbation". en. In: *Stem Cell Reports* 5.6 (Dec. 2015), pp. 1210–1225. ISSN: 22136711. DOI: 10.1016/j.stemcr.2015.09.020. URL: https://linkinghub.elsevier.com/retrieve/pii/S2213671115002829 (visited on 01/16/2024).

[221] Kazuya Abbey and Isuzu Kawabata. "Computerized Three-dimensional Reconstruction of the Crypt System of the Palatine Tonsil". en. In: *Acta Oto-Laryngologica* 105.sup454 (Jan. 1988), pp. 39–42. ISSN: 0001-6489, 1651-2251. DOI: 10.3109/00016488809125002. URL: http://www.tandfonline.com/doi/full/10.3109/00016488809125002 (visited on 07/28/2023).

[222] Valentino Natoli, Luca Viganò, and Cinzia Casu. "Cryptic Tonsils and Halitosis: An Overview of the Literature and a Clinical Image". In: *Cross Current International Journal of Medical and Biosciences* 1.5 (Oct. 2019), pp. 117–121. ISSN: 26632446. DOI: 10.36344/ccijmb.2019.v01i05.001. URL: https://www.easpublisher.com/media/features_articles/CCIJMB_15_117-121.pdf (visited on 07/28/2023).

[223] M. Ann Clark et al. "Differential cytokeratin and glycoconjugate expression by the surface and crypt epithelia of human palatine tonsils". en. In: *Histochemistry and Cell Biology* 114.4 (Oct. 2000), pp. 311–321. ISSN: 0948-6143, 1432-119X. DOI: 10.1007/s004180000198. URL: http://link.springer.com/10.1007/s004180000198 (visited on 07/28/2023).

[224] A. Gebert. "M cells in the rabbit palatine tonsil: the distribution, spatial arrangement and membrane subdomains as defined by confocal lectin histochemistry". In: *Anatomy and Embryology* 195.4 (Mar. 1997), pp. 353–358. ISSN: 03402061. DOI: 10.1007/s004290050055. URL: http://link.springer.com/10.1007/s004290050055 (visited on 07/28/2023).

[225] A. Gebert. "Identification of M-cells in the rabbit tonsil by vimentin immunohistochemistry and in vivo protein transport". en. In: *Histochemistry and Cell Biology* 104.3 (Sept. 1995), pp. 211–220. ISSN: 0948-6143, 1432-119X. DOI: 10.1007/BF01835154. URL: http://link.springer.com/10.1007/BF01835154 (visited on 07/28/2023).

[226] A. Gebert. "The role of M cells in the protection of mucosal membranes". In: *Histochemistry and Cell Biology* 108.6 (Dec. 1997), pp. 455–470. ISSN: 0948-6143, 1432-119X. DOI: 10.1007/s004180050186. URL: http://link.springer.com/10.1007/s004180050186 (visited on 07/28/2023).

[227] Marian R. Neutra, Andreas Frey, and Jean-Pierre Kraehenbuhl. "Epithelial M Cells: Gateways for Mucosal Infection and Immunization". en. In: *Cell* 86.3 (Aug. 1996), pp. 345–348. ISSN: 00928674. DOI: 10.1016/S0092-8674(00)80106-3. URL: https://linkinghub.elsevier.com/retrieve/pii/S0092867400801063 (visited on 07/28/2023).

[228] P. Brandtzaeg. "The B-cell development in tonsillar lymphoid follicles". eng. In: *Acta oto-laryngologica Supplementum* 523 (Jan. 1996), pp. 55–59. ISSN: 0365-5237.

[229] K. Agren et al. "The production of immunoregulatory cytokines is localized to the extrafollicular area of human tonsils". eng. In: *Acta Oto-Laryngologica* 116.3 (May 1996), pp. 477–485. ISSN: 0001-6489. DOI: 10.3109/00016489609137876.

[230] D. R. Dunlop. "The Life and Work of Louis Pasteur". In: *Canadian Medical Association Journal* 18.3 (Mar. 1928), pp. 297–303. ISSN: 0008-4409. URL: https://www.ncbi.nlm.nih.gov/pmc/articles/PMC1710086/ (visited on 11/29/2023).

[231] Gina R. Lewin et al. "Application of a quantitative framework to improve the accuracy of a bacterial infection model". In: *Proceedings of the National Academy of Sciences* 120.19 (May 2023), e2221542120. DOI: 10.1073/pnas.2221542120. URL: https://www.pnas.org/doi/10.1073/pnas.2221542120 (visited on 08/09/2023).

[232] Maartje van Seijen et al. "Impact of delayed and prolonged fixation on the evaluation of immunohistochemical staining on lung carcinoma resection specimen". In: *Virchows Archiv* 475.2 (2019), pp. 191–199. ISSN: 0945-6317. DOI: 10.1007/s00428-019-02595-9. URL: https://www.ncbi.nlm.nih.gov/pmc/articles/PMC6647403/ (visited on 11/15/2023).

[233] Fatemeh Mahjoub et al. "Comparison of formalin and FineFIX in preserving DNA material in small biopsies". en. In: *Pathology International* 58.10 (2008), pp. 678–680. ISSN: 1440-1827. DOI: 10.1111/j.1440-1827.2008.02290.x. URL: https://onlinelibrary.wiley.com/doi/abs/10.1111/j.1440-1827.2008.02290.x (visited on 11/15/2023).

[234] Kim S Suvarna, Christopher Layton, and John D Bancroft. *Bancroft's theory and practice of histological techniques*. Elsevier health sciences, 2018.

[235] Christophe Casteleyn et al. "The Tonsils Revisited: Review of the Anatomical Localization and Histological Characteristics of the Tonsils of Domestic and Laboratory Animals". en. In: *Journal of Immunology Research* 2011 (Aug. 2011), e472460. ISSN: 2314-8861. DOI: 10.1155/2011/472460.

URL: https://www.hindawi.com/journals/jir/2011/472460/ (visited on 11/15/2023).

[236] J. P. PRACY et al. "The comparative anatomy of the pig middle ear cavity: a model for middle ear inflammation in the human?" In: *Journal of Anatomy* 192.Pt 3 (Apr. 1998), pp. 359–368. ISSN: 0021-8782. DOI: 10.1046/j.1469-7580.1998.19230359.x. URL: https://www.ncbi.nlm.nih.gov/pmc/articles/PMC1467780/ (visited on 11/15/2023).

[237] Zhixue Liu et al. "Histological and Ultrastructural Examinations of Porcine Tonsils". en. In: *The Anatomical Record* 295.4 (2012), pp. 686–690. ISSN: 1932-8494. DOI: 10.1002/ar.21534. URL: https://onlinelibrary.wiley.com/doi/abs/10.1002/ar.21534 (visited on 11/15/2023).

[238] D M Williams and A C Rowland. "The palatine tonsils of the pig–an afferent route to the lymphoid tissue." In: *Journal of Anatomy* 113.Pt 1 (Oct. 1972), pp. 131–137. ISSN: 0021-8782. URL: https://www.ncbi.nlm.nih.gov/pmc/articles/PMC1271372/ (visited on 11/15/2023).

[239] Han Kyung Kim et al. "Generation of human tonsil epithelial organoids as an ex vivo model for SARS-CoV-2 infection". In: *Biomaterials* 283 (Apr. 2022), p. 121460. ISSN: 0142-9612. DOI: 10.1016/j.biomaterials.2022.121460. URL: https://www.sciencedirect.com/science/article/pii/S0142961222000990 (visited on 11/15/2023).

[240] Lisa E. Wagar et al. "Modeling human adaptive immune responses with tonsil organoids". en. In: *Nature Medicine* 27.1 (Jan. 2021), pp. 125–135. ISSN: 1546-170X. DOI: 10.1038/s41591-020-01145-0. URL: https://www.nature.com/articles/s41591-020-01145-0 (visited on 11/15/2023).

[241] Gillian L. Knight et al. "A cyclin-binding motif in human papillomavirus type 18 (HPV18) E1^E4 is necessary for association with CDK-cyclin complexes and G2/M cell cycle arrest of keratinocytes, but is not required for differentiation-dependent viral genome amplification or L1 capsid protein expression". In: *Virology* 412.1 (Mar. 2011), pp. 196–210. ISSN: 0042-6822. DOI: 10.1016/j.virol.2011.01.007. URL: https://www.ncbi.nlm.nih.gov/pmc/articles/PMC3722429/ (visited on 11/15/2023).

[242] Daniel Anacker and Cary Moody. "Generation of Organotypic Raft Cultures from Primary Human Keratinocytes". In: *Journal of Visualized Experiments : JoVE* 60 (Feb. 2012), p. 3668. ISSN: 1940-087X. DOI: 10.3791/3668. URL: https://www.ncbi.nlm.nih.gov/pmc/articles/PMC3376940/ (visited on 11/15/2023).

[243] Sally Roberts et al. "Modelling human papillomavirus biology in oropharyngeal keratinocytes". en. In: *Philosophical Transactions of the Royal Society B: Biological Sciences* 374.1773 (May 2019), p. 20180289. ISSN: 0962-8436, 1471-2970. DOI: 10.1098/rstb.2018.0289. URL: https://royalsocietypublish org/doi/10.1098/rstb.2018.0289 (visited on 05/10/2023).

[244] Sreejata Chatterjee et al. "Tissue-Specific Gene Expression during Productive Human Papillomavirus 16 Infection of Cervical, Foreskin, and Tonsil Epithelium". In: *Journal of Virology* 93.17 (Aug. 2019), 10.1128/jvi.00915–19. DOI: 10.1128/jvi.00915-19. URL: https://journals.asm.org/doi/full/10.1128/jvi.00915-19 (visited on 11/15/2023).

[245] Catriona M. Douglas et al. "A 20-year observational cohort of a 5 million patient population-Tonsillectomy rates in the context of two national policy changes". en. In: *Clinical Otolaryngology* 44.1 (Jan. 2019),

pp. 7–13. ISSN: 17494478. DOI: 10.1111/coa.13233. URL: https://onlinelibrary.wiley.com/doi/10.1111/coa.13233 (visited on 02/24/2023).

[246] *Group A Streptococci, Mycoplasmas, and Viruses Associated With Acute Pharyngitis \textbackslashtextbar JAMA \textbackslashtextbar JAMA Network*. URL: https://jamanetwork.com/journals/jama/article-abstract/336080 (visited on 11/22/2023).

[247] Markus Lilja, Simo Räisänen, and Lars-Eric Stenfors. "Initial events in the pathogenesis of acute tonsillitis caused by Streptococcus pyogenes1This paper was presented in part at the XVI World Congress of Otorhinolaryngology, Head and Neck Surgery, Sydney, Australia, March 2–7, 1997.1". In: *International Journal of Pediatric Otorhinolaryngology* 45.1 (Sept. 1998), pp. 15–20. ISSN: 0165-5876. DOI: 10.1016/S0165-5876(98)00071-8. URL: https://www.sciencedirect.com/science/article/pii/S0165587698000718 (visited on 11/22/2023).

[248] Jukka Ylikoski and Jouko Karjalainen. "Acute Tonsillitis in Young Men: Etiological Agents and Their Differentiation". In: *Scandinavian Journal of Infectious Diseases* 21.2 (Jan. 1989), pp. 169–174. ISSN: 0036-5548. DOI: 10.3109/00365548909039965. URL: https://doi.org/10.3109/00365548909039965 (visited on 11/22/2023).

[249] Richard A. Chole and Brian T. Faddis. "Anatomical Evidence of Microbial Biofilms in Tonsillar Tissues: A Possible Mechanism to Explain Chronicity". en. In: *Archives of Otolaryngology–Head & Neck Surgery* 129.6 (June 2003), p. 634. ISSN: 0886-4470. DOI: 10.1001/archotol.129.6.634. URL: http://archotol.jamanetwork.com/article.aspx?doi=10.1001/archotol.129.6.634 (visited on 02/24/2023).

[250] R. R. Diaz et al. "Relevance of biofilms in pediatric tonsillar disease". en. In: *European Journal of Clinical Microbiology & Infectious Diseases* 30.12 (Dec. 2011), pp. 1503–1509. ISSN: 0934-9723, 1435-4373. DOI: 10.1007/s10096-011-1249-3. URL: http://link.springer.com/10.1007/s10096-011-1249-3 (visited on 07/26/2022).

[251] Saad Musbah Alasil et al. "Evidence of Bacterial Biofilms among Infected and Hypertrophied Tonsils in Correlation with the Microbiology, Histopathology, and Clinical Symptoms of Tonsillar Diseases". en. In: *International Journal of Otolaryngology* 2013 (2013), pp. 1–11. ISSN: 1687-9201, 1687-921X. DOI: 10.1155/2013/408238. URL: http://www.hindawi.com/journals/ijoto/2013/408238/ (visited on 02/24/2023).

[252] Joo Hyun Woo et al. "Comparison of tonsillar biofilms between patients with recurrent tonsillitis and a control group". en. In: *Acta Oto-Laryngologica* 132.10 (Oct. 2012), pp. 1115–1120. ISSN: 0001-6489, 1651-2251. DOI: 10.3109/00016489.2012.689859. URL: http://www.tandfonline.com/doi/full/10.3109/00016489.2012.689859 (visited on 02/24/2023).

[253] Sara Torretta et al. "Recurrences in chronic tonsillitis substained by tonsillar biofilm-producing bacteria in children. Relationship with the grade of tonsillar hyperplasy". en. In: *International Journal of Pediatric Otorhinolaryngology* 77.2 (Feb. 2013), pp. 200–204. ISSN: 01655876. DOI: 10.1016/j.ijporl.2012.10.018. URL: https://linkinghub.elsevier.com/retrieve/pii/S0165587612005897 (visited on 08/24/2022).

[254] Marina Kostić et al. "Analysis of Tonsil Tissues from Patients Diagnosed with Chronic Tonsillitis—Microbiological Profile, Biofilm-Forming Capacity and Histology". en. In: *Antibiotics* 11.12 (Dec. 2022), p. 1747. ISSN:

2079-6382. DOI: 10.3390/antibiotics11121747. URL: https://www.mdpi.com/2079-6382/11/12/1747 (visited on 05/05/2023).

[255] K. N. Brahmadathan, P. Anitha, and P. Gladstone. "Increasing erythromycin resistance among group A streptococci causing tonsillitis in a tertiary care hospital in southern India". In: *Clinical Microbiology and Infection* 11.4 (Apr. 2005), pp. 335–337. ISSN: 1198-743X. DOI: 10.1111/j.1469-0691.2005.01100.x. URL: https://www.sciencedirect.com/science/article/pii/S1198743X14622485 (visited on 11/22/2023).

[256] Maryam Kardooni et al. "Study of common bacterial agents and antibiotic susceptibility in patients with chronic and repeated tonsillitis". In: (May 2020).

[257] Amity L Roberts et al. "Detection of group A Streptococcus in tonsils from pediatric patients reveals high rate of asymptomatic streptococcal carriage". en. In: *BMC Pediatrics* 12.1 (Dec. 2012), p. 3. ISSN: 1471-2431. DOI: 10.1186/1471-2431-12-3. URL: https://bmcpediatr.biomedcentral.com/articles/10.1186/1471-2431-12-3 (visited on 07/26/2022).

[258] Ericka L. Anderson et al. "The Fibrinogen-binding M1 Protein Reduces Pharyngeal Cell Adherence and Colonization Phenotypes of M1T1 Group A Streptococcus*". In: *Journal of Biological Chemistry* 289.6 (Feb. 2014), pp. 3539–3546. ISSN: 0021-9258. DOI: 10.1074/jbc.M113.529537. URL: https://www.sciencedirect.com/science/article/pii/S0021925819747449 (visited on 11/22/2023).

[259] Artemis Gogos and Michael J. Federle. "Modeling Streptococcus pyogenes Pharyngeal Colonization in the Mouse". In: *Frontiers in Cellular and Infection Microbiology* 9 (May 2019), p. 137. ISSN: 2235-2988. DOI:

10.3389/fcimb.2019.00137. URL: https://www.ncbi.nlm.nih.gov/pmc/articles/PMC6507483/ (visited on 11/22/2023).

[260] *Overview \textbackslashtextbar Sore throat (acute): antimicrobial prescribing \textbackslashtextbar Guidance \textbackslashtextbar NICE*. eng. Jan. 2018. URL: https://www.nice.org.uk/guidance/ng84 (visited on 11/01/2023).

[261] Itzhak Brook and Ronald Hirokawa. "Treatment of Patients with a History of Recurrent Tonsillitis Due to Group A Beta-hemolytic Streptococci: A Prospective Randomized Study Comparing Penicillin, Erythromycin, and Clindamycin". en. In: *Clinical Pediatrics* 24.6 (June 1985), pp. 331–336. ISSN: 0009-9228. DOI: 10.1177/000992288502400606. URL: https://doi.org/10.1177/000992288502400606 (visited on 11/22/2023).

[262] Marta Katkowska et al. "Genetic diversity and antimicrobial resistance of Staphylococcus aureus from recurrent tonsillitis in children". en. In: *APMIS* 128.3 (2020), pp. 211–219. ISSN: 1600-0463. DOI: 10.1111/apm.13007. URL: https://onlinelibrary.wiley.com/doi/abs/10.1111/apm.13007 (visited on 11/22/2023).

[263] I. J. Mitchelmore et al. "Tonsil surface and core cultures in recurrent tonsillitis: Prevalence of anaerobes and beta-lactamase producing organisms". en. In: *European Journal of Clinical Microbiology and Infectious Diseases* 13.7 (July 1994), pp. 542–548. ISSN: 1435-4373. DOI: 10.1007/BF01971304. URL: https://doi.org/10.1007/BF01971304 (visited on 11/23/2023).

[264] David J. Waxman and Jack L. Strominger. "Penicillin-Binding Proteins and the Mechanism of Action of Beta-Lactam Antibiotics". In: *Annual Review of Biochemistry* 52.1 (1983), pp. 825–869. DOI: 10.1146/annurev.

bi.52.070183.004141. URL: https://doi.org/10.1146/annurev.bi.52.070183.004141 (visited on 11/23/2023).

[265] Vincent Cattoir. "Mechanisms of Antibiotic Resistance". eng. In: *Streptococcus pyogenes: Basic Biology to Clinical Manifestations*. Ed. by Joseph J. Ferretti, Dennis L. Stevens, and Vincent A. Fischetti. Oklahoma City (OK): University of Oklahoma Health Sciences Center, 2016. URL: http://www.ncbi.nlm.nih.gov/books/NBK333414/ (visited on 11/23/2023).

[266] Anthony M. Smith and Keith P. Klugman. "Alterations in PBP 1A Essential for High-Level Penicillin Resistance in Streptococcus pneumoniae". In: *Antimicrobial Agents and Chemotherapy* 42.6 (June 1998), pp. 1329–1333. ISSN: 0066-4804. URL: https://www.ncbi.nlm.nih.gov/pmc/articles/PMC105597/ (visited on 11/23/2023).

[267] Peter A. Lambert. "Bacterial resistance to antibiotics: modified target sites". eng. In: *Advanced Drug Delivery Reviews* 57.10 (July 2005), pp. 1471–1485. ISSN: 0169-409X. DOI: 10.1016/j.addr.2005.04.003.

[268] D Passàli et al. "Group A Streptococcus and its antibiotic resistance". In: *Acta Otorhinolaryngologica Italica* 27.1 (Feb. 2007), pp. 27–32. ISSN: 0392-100X. URL: https://www.ncbi.nlm.nih.gov/pmc/articles/PMC2640020/ (visited on 11/23/2023).

[269] C.M. Douglas et al. "The effect of tonsillectomy on the morbidity from recurrent tonsillitis". en. In: *Clinical Otolaryngology* 42.6 (Dec. 2017), pp. 1206–1210. ISSN: 17494478. DOI: 10.1111/coa.12850. URL: https://onlinelibrary.wiley.com/doi/10.1111/coa.12850 (visited on 02/24/2023).

[270] TM Cook et al. "Major complications of airway management in the UK: results of the Fourth National Audit Project of the Royal College

of Anaesthetists and the Difficult Airway Society. Part 1: anaesthesia". In: *British journal of anaesthesia* 106.5 (2011), pp. 617–631.

[271] A. Williamson, H. Coleman, and C. Douglas. "Does infection play a role in post-tonsillectomy haemorrhage? A narrative review". en. In: *The Journal of Laryngology & Otology* 137.7 (July 2023), pp. 710–717. ISSN: 0022-2151, 1748-5460. DOI: 10.1017/S0022215122002547. URL: https://www.cambridge.org/core/journals/journal-of-laryngology-and-otology/article/does-infection-play-a-role-in-posttonsillectomy-haemorrhage-a-narrative-review/D9A8FA66BB1D5F8611C4CBAFA281B4A4 (visited on 11/23/2023).

[272] Denise Howel et al. "The impact of recurrent throat infection on children and their families". In: *Family practice* 19.3 (2002), pp. 242–246.

[273] Tejs Ehlers Klug et al. "Peritonsillar Abscess: Complication of Acute Tonsillitis or Weber's Glands Infection?" en. In: *Otolaryngology–Head and Neck Surgery* 155.2 (Aug. 2016), pp. 199–207. ISSN: 0194-5998. DOI: 10.1177/0194599816639551. URL: https://doi.org/10.1177/0194599816639551 (visited on 11/23/2023).

[274] Steven Powell et al. "Paediatric obstructive sleep apnoea". en. In: *BMJ* 340 (Apr. 2010), p. c1918. ISSN: 0959-8138, 1468-5833. DOI: 10.1136/bmj.c1918. URL: https://www.bmj.com/content/340/bmj.c1918 (visited on 11/23/2023).

[275] Christopher M. Cielo and Carole L. Marcus. "Obstructive sleep apnoea in children with craniofacial syndromes". In: *Paediatric Respiratory Reviews* 16.3 (June 2015), pp. 189–196. ISSN: 1526-0542. DOI: 10.1016/j.prrv.2014.11.003. URL: https://www.sciencedirect.com/science/article/pii/S1526054214001420 (visited on 11/23/2023).

[276] C. Gonzaga et al. "Obstructive sleep apnea, hypertension and cardiovascular diseases". en. In: *Journal of Human Hypertension* 29.12 (Dec. 2015), pp. 705–712. ISSN: 1476-5527. DOI: 10.1038/jhh.2015.15. URL: https://www.nature.com/articles/jhh201515 (visited on 11/23/2023).

[277] Sogol Javaheri, Shahrokh Javaheri, and Ali Javaheri. "Sleep Apnea, Heart Failure, and Pulmonary Hypertension". en. In: *Current Heart Failure Reports* 10.4 (Dec. 2013), pp. 315–320. ISSN: 1546-9549. DOI: 10.1007/s11897-013-0167-3. URL: https://doi.org/10.1007/s11897-013-0167-3 (visited on 11/23/2023).

[278] P.c. Zhang et al. "Comparison of histology between recurrent tonsillitis and tonsillar hypertrophy". en. In: *Clinical Otolaryngology & Allied Sciences* 28.3 (2003), pp. 235–239. ISSN: 1365-2273. DOI: 10.1046/j.1365-2273.2003.00697.x. URL: https://onlinelibrary.wiley.com/doi/abs/10.1046/j.1365-2273.2003.00697.x (visited on 11/23/2023).

[279] Jacopo Galli et al. "Pediatric oropharyngeal microbiome: Mapping in chronic tonsillitis and tonsillar hypertrophy". en. In: *International Journal of Pediatric Otorhinolaryngology* 139 (Dec. 2020), p. 110478. ISSN: 01655876. DOI: 10.1016/j.ijporl.2020.110478. URL: https://linkinghub.elsevier.com/retrieve/pii/S0165587620306212 (visited on 07/26/2022).

[280] James Johnston et al. "Paired analysis of the microbiota between surface tissue swabs and biopsies from pediatric patients undergoing adenotonsillectomy". en. In: *International Journal of Pediatric Otorhinolaryngology* 113 (Oct. 2018), pp. 51–57. ISSN: 01655876. DOI: 10.1016/j.ijporl.2018.07.024. URL: https://linkinghub.elsevier.com/retrieve/pii/S0165587618303392 (visited on 07/26/2022).

[281] Bing Quan Huang and Edward C. Yeung. "Chemical and Physical Fixation of Cells and Tissues: An Overview". en. In: *Plant Microtechniques and Protocols*. Ed. by Edward Chee Tak Yeung et al. Cham: Springer International Publishing, 2015, pp. 23–43. ISBN: 978-3-319-19943-6 978-3-319-19944-3. DOI: 10.1007/978-3-319-19944-3_2. URL: https://link.springer.com/10.1007/978-3-319-19944-3_2 (visited on 08/02/2023).

[282] Michael J Taylor et al. "New approaches to cryopreservation of cells, tissues, and organs". In: *Transfusion Medicine and Hemotherapy* 46.3 (2019). Publisher: S. Karger AG Basel, Switzerland, pp. 197–215.

[283] Richard T. Giberson and Richard S. Demaree Jr. *Microwave Techniques and Protocols*. en. Springer Science & Business Media, May 2008. ISBN: 978-1-59259-128-2.

[284] *CYTOCHEMISTRY AND ELECTRON MICROSCOPY - PMC*. URL: https://www.ncbi.nlm.nih.gov/pmc/articles/PMC2106262/ (visited on 08/02/2023).

[285] Rooban Thavarajah et al. "Chemical and physical basics of routine formaldehyde fixation". en. In: *Journal of Oral and Maxillofacial Pathology* 16.3 (2012), p. 400. ISSN: 0973-029X. DOI: 10.4103/0973-029X.102496. URL: https://journals.lww.com/10.4103/0973-029X.102496 (visited on 01/08/2024).

[286] C. H. Fox et al. "Formaldehyde fixation". eng. In: *The Journal of Histochemistry and Cytochemistry: Official Journal of the Histochemistry Society* 33.8 (Aug. 1985), pp. 845–853. ISSN: 0022-1554. DOI: 10.1177/33.8.3894502.

[287] H. Puchtler and S. N. Meloan. "On the chemistry of formaldehyde fixation and its effects on immunohistochemical reactions". en. In: *Histochemistry* 82.3 (May 1985), pp. 201–204. ISSN: 1432-119X. DOI: 10.1007/BF00501395. URL: https://doi.org/10.1007/BF00501395 (visited on 08/02/2023).

[288] David D. Sabatini, Klaus Bensch, and Russell J. Barrnett. "CYTOCHEMISTRY AND ELECTRON MICROSCOPY". In: *The Journal of Cell Biology* 17.1 (Apr. 1963), pp. 19–58. ISSN: 0021-9525. URL: https://www.ncbi.nlm.nih.gov/pmc/articles/PMC2106262/ (visited on 08/02/2023).

[289] P Tagliaferro et al. "Immunofluorescence and glutaraldehyde fixation. A new procedure based on the Schiff-quenching method". en. In: *Journal of Neuroscience Methods* 77.2 (Dec. 1997), pp. 191–197. ISSN: 0165-0270. DOI: 10.1016/S0165-0270(97)00126-X. URL: https://www.sciencedirect.com/science/article/pii/S016502709700126X (visited on 08/02/2023).

[290] Hans F. Wehrl et al. "Assessment of murine brain tissue shrinkage caused by different histological fixatives using magnetic resonance and computed tomography imaging". eng. In: *Histology and Histopathology* 30.5 (May 2015), pp. 601–613. ISSN: 1699-5848. DOI: 10.14670/HH-30.601.

[291] Nancy W. Troiano, Wendy A. Ciovacco, and Melissa A. Kacena. "The Effects of Fixation and Dehydration on the Histological Quality of Undecalcified Murine Bone Specimens Embedded in Methylmethacrylate". In: *Journal of histotechnology* 32.1 (Mar. 2009), pp. 27–31. ISSN: 0147-8885. URL: https://www.ncbi.nlm.nih.gov/pmc/articles/PMC2770706/ (visited on 08/02/2023).

[292] Sara Jonmarker et al. "Tissue shrinkage after fixation with formalin injection of prostatectomy specimens". eng. In: *Virchows Archiv: An International Journal of Pathology* 449.3 (Sept. 2006), pp. 297–301. ISSN: 0945-6317. DOI: 10.1007/s00428-006-0259-5.

[293] H. Boonstra et al. "Cervical tissue shrinkage by formaldehyde fixation, paraffin wax embedding, section cutting and mounting". eng. In: *Virchows Archiv. A, Pathological Anatomy and Histopathology* 402.2 (1983), pp. 195–201. ISSN: 0174-7398. DOI: 10.1007/BF00695061.

[294] Shailja Chatterjee. "Artefacts in histopathology". In: *Journal of Oral and Maxillofacial Pathology : JOMFP* 18.Suppl 1 (Sept. 2014), S111–S116. ISSN: 0973-029X. DOI: 10.4103/0973-029X.141346. URL: https://www.ncbi.nlm.nih.gov/pmc/articles/PMC4211218/ (visited on 08/02/2023).

[295] G. F. Bahr, G. Bloom, and U. Friberg. "Volume changes of tissues in physiological fluids during fixation in osmium tetroxide or formaldehyde and during subsequent treatment". en. In: *Experimental Cell Research* 12.2 (Aug. 1957), pp. 342–355. ISSN: 0014-4827. DOI: 10.1016/0014-4827(57)90148-9. URL: https://www.sciencedirect.com/science/article/pii/0014482757901489 (visited on 08/02/2023).

[296] A Penttila, E M McDowell, and B F Trump. "Effects of fixation and postfixation treatments on volume of injured cells;." In: *Journal of Histochemistry & Cytochemistry* 23.4 (Apr. 1975), pp. 251–270. ISSN: 0022-1554. DOI: 10.1177/23.4.805169. URL: https://doi.org/10.1177/23.4.805169 (visited on 08/02/2023).

[297] Malin E. V. Johansson and Gunnar C. Hansson. "Preservation of Mucus in Histological Sections, Immunostaining of Mucins in Fixed Tissue, and Localization of Bacteria with FISH". en. In: *Mucins: Methods and*

Protocols. Ed. by Michael A. McGuckin and David J. Thornton. Methods in Molecular Biology. Totowa, NJ: Humana Press, 2012, pp. 229–235. ISBN: 978-1-61779-513-8. DOI: 10.1007/978-1-61779-513-8_13. URL: https://doi.org/10.1007/978-1-61779-513-8_13 (visited on 08/02/2023).

[298] Marc Rüger, Mandy Ackermann, and Udo Reichl. "Species-specific viability analysis of Pseudomonas aeruginosa, Burkholderia cepacia and Staphylococcus aureus in mixed culture by flow cytometry". en. In: *BMC Microbiology* 14.1 (2014), p. 56. ISSN: 1471-2180. DOI: 10.1186/1471-2180-14-56. URL: http://bmcmicrobiol.biomedcentral.com/articles/10.1186/1471-2180-14-56 (visited on 08/01/2023).

[299] Christian Falter and Christian A. Voigt. "The Eurotiomycete Apinisia graminicola as the causal agent of a leaf spot disease on the energy crop Miscanthus x giganteus in Northern Germany". en. In: *European Journal of Plant Pathology* 149.4 (Dec. 2017), pp. 797–806. ISSN: 0929-1873, 1573-8469. DOI: 10.1007/s10658-017-1226-5. URL: http://link.springer.com/10.1007/s10658-017-1226-5 (visited on 08/01/2023).

[300] Juan Yang et al. "Transcriptomic profiling of Alternaria longipes invasion in tobacco reveals pathogenesis regulated by AlHK1, a group III histidine kinase". en. In: *Scientific Reports* 7.1 (Nov. 2017), p. 16083. ISSN: 2045-2322. DOI: 10.1038/s41598-017-16401-6. URL: https://www.nature.com/articles/s41598-017-16401-6 (visited on 08/01/2023).

[301] Girishkumar Kaitholil Kumaran and Israel Hanukoglu. "Identification and classification of epithelial cells in nephron segments by actin cytoskeleton patterns". en. In: *The FEBS Journal* 287.6 (Mar. 2020), pp. 1176–1194. ISSN: 1742-464X, 1742-4658. DOI: 10.1111/febs.15088. URL: https:

//onlinelibrary.wiley.com/doi/10.1111/febs.15088 (visited on 08/01/2023).

[302] Lip Nam Loh, Geli Gao, and Elaine I. Tuomanen. "Dissecting Bacterial Cell Wall Entry and Signaling in Eukaryotic Cells: an Actin-Dependent Pathway Parallels Platelet-Activating Factor Receptor-Mediated Endocytosis". en. In: *mBio* 8.1 (Mar. 2017). Ed. by Jorge Eugenio Vidal and Larry S. McDaniel, e02030–16. ISSN: 2161-2129, 2150-7511. DOI: 10.1128/mBio.02030-16. URL: https://journals.asm.org/doi/10.1128/mBio.02030-16 (visited on 08/01/2023).

[303] "Expression, Localization and Functional Activity of the Major Na+/H+ Exchange Isoforms Expressed in the Intestinal Cell Line Caco-2BBe". In: *Cellular Physiology and Biochemistry* 52.2 (Apr. 2019), pp. 1017–1038. ISSN: 10158987, 14219778. DOI: 10.33594/000000070. URL: https://www.cellphysiolbiochem.com/Articles/000070/ (visited on 08/01/2023).

[304] T. Kent Gartner and T.R. Podieski. "Evidence that a membrane bound lectin mediates fusion of L6 myoblasts". en. In: *Biochemical and Biophysical Research Communications* 67.3 (Dec. 1975), pp. 972–978. ISSN: 0006291X. DOI: 10.1016/0006-291X(75)90770-6. URL: https://linkinghub.elsevier.com/retrieve/pii/0006291X75907706 (visited on 08/01/2023).

[305] I. Ofek, D. Mirelman, and N. Sharon. "Adherence of Escherichia coli to human mucosal cells mediated by mannose receptors". en. In: *Nature* 265.5595 (Feb. 1977), pp. 623–625. ISSN: 0028-0836, 1476-4687. DOI: 10.1038/265623a0. URL: https://www.nature.com/articles/265623a0 (visited on 08/01/2023).

[306] R. J. Doyle and D. C. Birdsell. "Interaction of Concanavalin A with the Cell Wall of *Bacillus* subtilis". en. In: *Journal of Bacteriology* 109.2 (Feb. 1972), pp. 652–658. ISSN: 0021-9193, 1098-5530. DOI: 10.1128/jb.109.2.652-658.1972. URL: https://journals.asm.org/doi/10.1128/jb.109.2.652-658.1972 (visited on 08/01/2023).

[307] Kenneth D. Noonan and Max M. Burger. "THE RELATIONSHIP OF CONCANAVALIN A BINDING TO LECTIN-INITIATED CELL AGGLUTINATION". en. In: *The Journal of Cell Biology* 59.1 (Oct. 1973), pp. 134–142. ISSN: 1540-8140, 0021-9525. DOI: 10.1083/jcb.59.1.134. URL: https://rupress.org/jcb/article/59/1/134/18198/THE-RELATIONSHIP-OF-CONCANAVALIN-A-BINDING-TO (visited on 08/01/2023).

[308] Anika C. Jahns, Hinnerk Eilers, and Oleg A. Alexeyev. "Transcriptomic analysis of Propionibacterium acnes biofilms in vitro". en. In: *Anaerobe* 42 (Dec. 2016), pp. 111–118. ISSN: 10759964. DOI: 10.1016/j.anaerobe.2016.10.001. URL: https://linkinghub.elsevier.com/retrieve/pii/S1075996416301202 (visited on 08/01/2023).

[309] Milton M. Weiser. "Concanavalin A Agglutination of Intestinal Cells from the Human Fetus". en. In: *Science* 177.4048 (Aug. 1972), pp. 525–526. ISSN: 0036-8075, 1095-9203. DOI: 10.1126/science.177.4048.525. URL: https://www.science.org/doi/10.1126/science.177.4048.525 (visited on 08/01/2023).

[310] S. V. Lynch et al. "Role of the *rapA* Gene in Controlling Antibiotic Resistance of *Escherichia* coli Biofilms". en. In: *Antimicrobial Agents and Chemotherapy* 51.10 (Oct. 2007), pp. 3650–3658. ISSN: 0066-4804, 1098-6596. DOI: 10.1128/AAC.00601-07. URL: https://journals.asm.org/doi/10.1128/AAC.00601-07 (visited on 08/01/2023).

[311] Michael J. Boersma et al. "Minimal Peptidoglycan (PG) Turnover in Wild-Type and PG Hydrolase and Cell Division Mutants of Streptococcus pneumoniae D39 Growing Planktonically and in Host-Relevant Biofilms". en. In: *Journal of Bacteriology* 197.21 (Nov. 2015). Ed. by P. De Boer, pp. 3472–3485. ISSN: 0021-9193, 1098-5530. DOI: 10.1128/JB.00541-15. URL: https://journals.asm.org/doi/10.1128/JB.00541-15 (visited on 08/01/2023).

[312] Natalya Doroshenko et al. "Extracellular DNA Impedes the Transport of Vancomycin in Staphylococcus epidermidis Biofilms Preexposed to Subinhibitory Concentrations of Vancomycin". en. In: *Antimicrobial Agents and Chemotherapy* 58.12 (Dec. 2014), pp. 7273–7282. ISSN: 0066-4804, 1098-6596. DOI: 10.1128/AAC.03132-14. URL: https://journals.asm.org/doi/10.1128/AAC.03132-14 (visited on 08/01/2023).

[313] Burke A. Cunha. "Vancomycin". en. In: *Medical Clinics of North America* 79.4 (1995), pp. 817–831. ISSN: 00257125. DOI: 10.1016/S0025-7125(16)30041-4. URL: https://linkinghub.elsevier.com/retrieve/pii/S0025712516300414 (visited on 08/02/2023).

[314] Maham A Mehmood, Madanmohan Patel, and Harshavardhan Sanekommu. "Methicillin-Resistant Staphylococcus Aureus: A Very Rare Cause of Meningitis". en. In: *Cureus* (Sept. 2020). ISSN: 2168-8184. DOI: 10.7759/cureus.10370. URL: https://www.cureus.com/articles/40986-methicillin-resistant-staphylococcus-aureus-a-very-rare-cause-of-meningitis (visited on 08/02/2023).

[315] Nicholas M Brown et al. "Treatment of methicillin-resistant *Staphylococcus* aureus (MRSA): updated guidelines from the UK". en. In: *JAC-Antimicrobial Resistance* 3.1 (Jan. 2021), dlaa114. ISSN: 2632-1823. DOI:

10.1093/jacamr/dlaa114. URL: https://academic.oup.com/jacamr/article/doi/10.1093/jacamr/dlaa114/6127118 (visited on 08/02/2023).

[316] D. W. Gump. "Vancomycin for treatment of bacterial meningitis". eng. In: *Reviews of Infectious Diseases* 3 suppl (1981), S289–292. ISSN: 0162-0886.

[317] Yanguang Cong, Sijin Yang, and Xiancai Rao. "Vancomycin resistant Staphylococcus aureus infections: A review of case updating and clinical features". en. In: *Journal of Advanced Research* 21 (Jan. 2020), pp. 169–176. ISSN: 20901232. DOI: 10.1016/j.jare.2019.10.005. URL: https://linkinghub.elsevier.com/retrieve/pii/S2090123219301638 (visited on 08/02/2023).

[318] Manfred Rohde. "The Gram-Positive Bacterial Cell Wall". en. In: *Microbiology Spectrum* 7.3 (May 2019). Ed. by Vincent A. Fischetti et al., p. 7.3.10. ISSN: 2165-0497. DOI: 10.1128/microbiolspec.GPP3-0044-2018. URL: https://journals.asm.org/doi/10.1128/microbiolspec.GPP3-0044-2018 (visited on 08/02/2023).

[319] C. Watanakunakorn. "Mode of action and in-vitro activity of vancomycin". en. In: *Journal of Antimicrobial Chemotherapy* 14.suppl D (Jan. 1984), pp. 7–18. ISSN: 0305-7453, 1460-2091. DOI: 10.1093/jac/14.suppl_D.7. URL: https://academic.oup.com/jac/article-lookup/doi/10.1093/jac/14.suppl_D.7 (visited on 08/02/2023).

[320] Michael Ford. "5.4 Bacterial Pathogens". In: *Medical microbiology*. Oxford University Press, 2019.

[321] Henry A. Erlich, ed. *PCR Technology: Principles and Applications for DNA Amplification*. en. London: Palgrave Macmillan UK, 1989. ISBN: 978-0-333-48948-2 978-1-349-20235-5. DOI: 10.1007/978-1-349-20235-5.

URL: http://link.springer.com/10.1007/978-1-349-20235-5 (visited on 11/09/2023).

[322] *Polymerase chain reaction (PCR) (article)*. en. URL: https://www.khanacademy.org/science/ap-biology/gene-expression-and-regulation/biotechnology/a/polymerase-chain-reaction-pcr (visited on 10/30/2023).

[323] Soo Hyun Eom, Jimin Wang, and Thomas A. Steitz. "Structure of Taq polymerase with DNA at the polymerase active site". en. In: *Nature* 382.6588 (July 1996), pp. 278–281. ISSN: 1476-4687. DOI: 10.1038/382278a0. URL: https://www.nature.com/articles/382278a0 (visited on 11/09/2023).

[324] C R Woese. "Bacterial evolution". en. In: *Microbiological Reviews* 51.2 (June 1987), pp. 221–271. ISSN: 0146-0749. DOI: 10.1128/mr.51.2.221-271.1987. URL: https://journals.asm.org/doi/10.1128/mr.51.2.221-271.1987 (visited on 01/08/2024).

[325] C.R. Woese et al. "A Phylogenetic Definition of the Major Eubacterial Taxa". en. In: *Systematic and Applied Microbiology* 6.2 (Sept. 1985), pp. 143–151. ISSN: 07232020. DOI: 10.1016/S0723-2020(85)80047-3. URL: https://linkinghub.elsevier.com/retrieve/pii/S0723202085800473 (visited on 01/08/2024).

[326] Alistair Boettiger and Sedona Murphy. "Advances in Chromatin Imaging at Kilobase-Scale Resolution". en. In: *Trends in Genetics* 36.4 (Apr. 2020), pp. 273–287. ISSN: 01689525. DOI: 10.1016/j.tig.2019.12.010. URL: https://linkinghub.elsevier.com/retrieve/pii/S0168952519302719 (visited on 12/18/2023).

[327] Enrico Tortoli. "Impact of Genotypic Studies on Mycobacterial Taxonomy: the New Mycobacteria of the 1990s". en. In: *Clinical Microbiology Reviews* 16.2 (Apr. 2003), pp. 319–354. ISSN: 0893-8512, 1098-6618. DOI:

10.1128/CMR.16.2.319-354.2003. URL: https://journals.asm.org/doi/10.1128/CMR.16.2.319-354.2003 (visited on 01/08/2024).

[328] Kumiko Ueda et al. "Two Distinct Mechanisms Cause Heterogeneity of 16S rRNA". en. In: *Journal of Bacteriology* 181.1 (Jan. 1999), pp. 78–82. ISSN: 0021-9193, 1098-5530. DOI: 10.1128/JB.181.1.78-82.1999. URL: https://journals.asm.org/doi/10.1128/JB.181.1.78-82.1999 (visited on 01/08/2024).

[329] Christopher P Kolbert and David H Persing. "Ribosomal DNA sequencing as a tool for identification of bacterial pathogens". en. In: *Current Opinion in Microbiology* 2.3 (June 1999), pp. 299–305. ISSN: 13695274. DOI: 10.1016/S1369-5274(99)80052-6. URL: https://linkinghub.elsevier.com/retrieve/pii/S1369527499800526 (visited on 01/08/2024).

[330] Nurnabila Syafiqah Muhamad Rizal et al. "Advantages and Limitations of 16S rRNA Next-Generation Sequencing for Pathogen Identification in the Diagnostic Microbiology Laboratory: Perspectives from a Middle-Income Country". en. In: *Diagnostics* 10.10 (Oct. 2020), p. 816. ISSN: 2075-4418. DOI: 10.3390/diagnostics10100816. URL: https://www.mdpi.com/2075-4418/10/10/816 (visited on 01/08/2024).

[331] Ramya Srinivasan et al. "Use of 16S rRNA Gene for Identification of a Broad Range of Clinically Relevant Bacterial Pathogens". en. In: *PLOS ONE* 10.2 (Feb. 2015). Ed. by Markus M. Heimesaat, e0117617. ISSN: 1932-6203. DOI: 10.1371/journal.pone.0117617. URL: https://dx.plos.org/10.1371/journal.pone.0117617 (visited on 01/08/2024).

[332] Jill E. Clarridge. "Impact of 16S rRNA Gene Sequence Analysis for Identification of Bacteria on Clinical Microbiology and Infectious Diseases". en. In: *Clinical Microbiology Reviews* 17.4 (Oct. 2004), pp. 840–862. ISSN:

0893-8512, 1098-6618. DOI: 10.1128/CMR.17.4.840-862.2004. URL: https://journals.asm.org/doi/10.1128/CMR.17.4.840-862.2004 (visited on 01/08/2024).

[333] David A. Relman. "The Search for Unrecognized Pathogens". en. In: *Science* 284.5418 (May 1999), pp. 1308–1310. ISSN: 0036-8075, 1095-9203. DOI: 10.1126/science.284.5418.1308. URL: https://www.science.org/doi/10.1126/science.284.5418.1308 (visited on 01/08/2024).

[334] Dennis A. Benson et al. "GenBank". en. In: *Nucleic Acids Research* 41.D1 (Nov. 2012), pp. D36–D42. ISSN: 0305-1048, 1362-4962. DOI: 10.1093/nar/gks1195. URL: http://academic.oup.com/nar/article/41/D1/D36/1068219/GenBank (visited on 01/08/2024).

[335] H. Munck, W.W. Jørgensen, and T.E. Klug. "Antibiotics for recurrent acute pharyngo-tonsillitis: systematic review". en. In: *Eur. J. Clin. Microb. Inf. Dis* 37 (2018), pp. 1221–1230.

[336] Hetal Harish Patel et al. "Indications for tonsillectomy: A 10 year retrospective review". en. In: *International Journal of Pediatric Otorhinolaryngology* 78.12 (Dec. 2014), pp. 2151–2155. ISSN: 01655876. DOI: 10.1016/j.ijporl.2014.09.030. URL: https://linkinghub.elsevier.com/retrieve/pii/S0165587614005503 (visited on 05/05/2023).

[337] L.Normal Anatomy Michaels and Histology. *Inflammatory Diseases. Ear, Nose and Throat Histopath*. da. Springer, 1997. ISBN: 978-1-4471-3332-2.

[338] A. Swidinski. "Spatial organisation of microbiota in quiescent adenoiditis and tonsillitis". et. In: *J. Clin. Pathol* 60 (2006), pp. 253–260.

[339] R. W. Mazzone, S. Kornblau, and C. M. Durand. "Shrinkage of lung after chemical fixation for analysis of pulmonary structure-function relations". en. In: *Journal of Applied Physiology* 48.2 (Feb. 1980), pp. 382–385.

ISSN: 8750-7587, 1522-1601. DOI: 10.1152/jappl.1980.48.2.382. URL: https://www.physiology.org/doi/10.1152/jappl.1980.48.2.382 (visited on 05/05/2023).

[340] Y Suto, E Matsuda, and Y Inoue. "MRI of the pharynx in young patients with sleep disordered breathing". en. In: *The British Journal of Radiology* 69.827 (Nov. 1996), pp. 1000–1004. ISSN: 0007-1285, 1748-880X. DOI: 10.1259/0007-1285-69-827-1000. URL: http://www.birpublications.org/doi/10.1259/0007-1285-69-827-1000 (visited on 02/24/2023).

[341] Eugene Lin and Adam Alessio. "What are the basic concepts of temporal, contrast, and spatial resolution in cardiac CT?" en. In: *Journal of Cardiovascular Computed Tomography* 3.6 (Nov. 2009), pp. 403–408. ISSN: 19345925. DOI: 10.1016/j.jcct.2009.07.003. URL: https://linkinghub.elsevier.com/retrieve/pii/S1934592509004055 (visited on 02/24/2023).

[342] Karl-Heinz Herrmann et al. "High-resolution MRI of the human palatine tonsil and its schematic anatomic 3D reconstruction". eng. In: *Journal of Anatomy* 240.1 (Jan. 2022), pp. 166–171. ISSN: 1469-7580. DOI: 10.1111/joa.13532.

[343] *Management of sore throat and indications for tonsillectomy*. en-GB. URL: https://testing36.scot.nhs.uk (visited on 11/01/2023).

[344] Stephen F Altschul et al. "Basic local alignment search tool". In: *Journal of molecular biology* 215.3 (1990), pp. 403–410.

[345] K. Balaji, R. Thenmozhi, and S.K. Pandian. "Effect of subinhibitory concentrations of fluoroquinolones on biofilm production by clinical isolates of Streptococcus pyogenes". en. In: *Ind. J. Med. Res* 137 (2013), pp. 963–9711.

[346] Guido Werner, Birgit Strommenger, and Wolfgang Witte. "Acquired vancomycin resistance in clinically relevant pathogens". en. In: *Future Microbiology* 3.5 (Oct. 2008), pp. 547–562. ISSN: 1746-0913, 1746-0921. DOI: 10.2217/17460913.3.5.547. URL: https://www.futuremedicine.com/doi/10.2217/17460913.3.5.547 (visited on 11/30/2023).

[347] Taskeen Raza et al. "Vancomycin resistant Enterococci: A brief review". In: *Journal of the Pakistan Medical Association* 68 (May 2018), pp. 768–772.

[348] I Kühn et al. "Epidemiology and ecology of enterococci, with special reference to antibiotic resistant strains, in animals, humans and the environment: Example of an ongoing project within the European research programme*This ongoing project forms a part of the 4th framework of the European research programme for Agriculture and Fisheries (FAIR). The project started in January 1998, and will be finished in June 2001.*". In: *International Journal of Antimicrobial Agents* 14.4 (May 2000), pp. 337–342. ISSN: 0924-8579. DOI: 10.1016/S0924-8579(00)00146-1. URL: https://www.sciencedirect.com/science/article/pii/S0924857900001461 (visited on 11/30/2023).

[349] Liam Toner et al. "Vancomycin resistant enterococci in urine cultures: Antibiotic susceptibility trends over a decade at a tertiary hospital in the United Kingdom". en. In: *Investigative and Clinical Urology* 57.2 (2016), p. 129. ISSN: 2466-0493, 2466-054X. DOI: 10.4111/icu.2016.57.2.129. URL: https://icurology.org/DOIx.php?id=10.4111/icu.2016.57.2.129 (visited on 11/30/2023).

[350] Anders Jensen et al. "Molecular Mapping to Species Level of the Tonsillar Crypt Microbiota Associated with Health and Recurrent Tonsillitis". en. In: *PLoS ONE* 8.2 (Feb. 2013). Ed. by Ping Xu, e56418. ISSN:

1932-6203. DOI: 10.1371/journal.pone.0056418. URL: https://dx.plos.org/10.1371/journal.pone.0056418 (visited on 07/26/2022).

[351] Ignacio Arganda-Carreras et al. "Trainable Weka Segmentation: a machine learning tool for microscopy pixel classification". In: *Bioinformatics* 33.15 (Aug. 2017), pp. 2424–2426. ISSN: 1367-4803. DOI: 10.1093/bioinformatics/btx180. URL: https://doi.org/10.1093/bioinformatics/btx180 (visited on 11/30/2023).

[352] Loay George. "Comparative Study Using Weka for Red Blood Cells Classification". In: *International Journal of Medical, Health, Pharmaceutical and Biomedical Engineering* 9 (Jan. 2015), pp. 19–23.

[353] S. T. Clark et al. "Fluorescence in situ hybridisation in Carnoy's fixed tonsil tissue". eng. In: *Scientific Reports* 12.1 (July 2022), p. 12395. ISSN: 2045-2322. DOI: 10.1038/s41598-022-16309-w.

[354] Raimo Hartmann et al. "Quantitative image analysis of microbial communities with BiofilmQ". en. In: *Nature Microbiology* 6.2 (Jan. 2021), pp. 151–156. ISSN: 2058-5276. DOI: 10.1038/s41564-020-00817-4. URL: https://www.nature.com/articles/s41564-020-00817-4 (visited on 02/24/2023).

[355] T. Hartman. "BASIN: A semi-automatic workflow, with machine learning segmentation, for objective statistical analysis of biomedical and biofilm image datasets". en. In: *J. Mol. Biol* 435 (2023), p. 167895.

[356] Sébastien Herbert et al. "LocalZProjector and DeProj: a toolbox for local 2D projection and accurate morphometrics of large 3D microscopy images". en. In: *BMC Biology* 19.1 (Dec. 2021), p. 136. ISSN: 1741-7007. DOI: 10.1186/s12915-021-01037-w. URL: https://bmcbiol.biomedcentral.com/articles/10.1186/s12915-021-01037-w (visited on 02/28/2023).

[357] N. Sofronieuw. *napari: a multi-dimensional image viewer for Python*. en. DOI: 10.5281/zenodo.3555620..

[358] Z. Ciftci et al. "A new horizon in the treatment of biofilm-associated tonsillitis". en. In: *Ther. Adv. Respir. Dis* 8 (2014), pp. 78–83.

[359] L.K. Vestby et al. "Bacterial biofilm and its role in the pathogenesis of disease". en. In: *Antibiotics* 9 (2020), p. 59.

[360] W. Andrew Clement and John H. Dempster. "Implementation by Scottish otolaryngologists of the Scottish Intercollegiate Guidelines Network document *Management* of Sore Throats and the Indications for Tonsillectomy : four years on". en. In: *The Journal of Laryngology & Otology* 118.5 (May 2004), pp. 357–361. ISSN: 0022-2151, 1748-5460. DOI: 10.1258/002221504323086543. URL: https://www.cambridge.org/core/product/identifier/S0022215104000994/type/journal_article (visited on 02/24/2023).

[361] Megan Clapperton. "IL-17C plays a role in the pathophysiology of acute recurrent tonsillitis". In: *BioRxiv* (). DOI: doi:https://doi.org/10.1101/2024.02.08.578879.

[362] P Brandtzaeg. "Immunology of tonsils and adenoids: everything the ENT surgeon needs to know". In: *International Congress Series*. Advances in Pediatric ORL. Proceedings of the 8th International Congress of Pediatric Otorhinolaryngology 1254 (Nov. 2003), pp. 89–99. ISSN: 0531-5131. DOI: 10.1016/S0531-5131(03)00964-6. URL: https://www.sciencedirect.com/science/article/pii/S0531513103009646 (visited on 12/10/2023).

[363] Andreas Gebert and Reinhard Pabst. "M cells at locations outside the gut". In: *Seminars in Immunology* 11.3 (June 1999), pp. 165–170. ISSN:

1044-5323. DOI: 10.1006/smim.1999.0172. URL: https://www.sciencedirect.com/science/article/pii/S1044532399901720 (visited on 12/10/2023).

[364] Y. Fujimura. "Evidence of M cells as portals of entry for antigens in the nasopharyngeal lymphoid tissue of humans". en. In: *Virchows Archiv* 436.6 (June 2000), pp. 560–566. ISSN: 1432-2307. DOI: 10.1007/s004289900177. URL: https://doi.org/10.1007/s004289900177 (visited on 12/10/2023).

[365] Charles Janeway et al. *Immunobiology: the immune system in health and disease*. Vol. 2. Garland Pub. New York, 2001.

[366] David C. Dale, Laurence Boxer, and W. Conrad Liles. "The phagocytes: neutrophils and monocytes". en. In: *Blood* 112.4 (Aug. 2008), pp. 935–945. ISSN: 0006-4971, 1528-0020. DOI: 10.1182/blood-2007-12-077917. URL: https://ashpublications.org/blood/article/112/4/935/25254/The-phagocytes-neutrophils-and-monocytes (visited on 01/08/2024).

[367] Shashank Shekhar et al. "Review—Interleukins Profiling for Biosensing Applications: Possibilities and the Future of Disease Detection". en. In: *ECS Sensors Plus* 1.4 (Oct. 2022), p. 041601. ISSN: 2754-2726. DOI: 10.1149/2754-2726/ac9227. URL: https://dx.doi.org/10.1149/2754-2726/ac9227 (visited on 12/10/2023).

[368] Charles A. Dinarello. "Historical insights into cytokines". en. In: *European Journal of Immunology* 37.S1 (2007), S34–S45. ISSN: 1521-4141. DOI: 10.1002/eji.200737772. URL: https://onlinelibrary.wiley.com/doi/abs/10.1002/eji.200737772 (visited on 12/10/2023).

[369] W. Conrad Liles and Wesley C. Van Voorhis. "Review: Nomenclature and Biologic Significance of Cytokines Involved in Inflammation and the Host Immune Response". In: *The Journal of Infectious Diseases* 172.6

(Dec. 1995), pp. 1573–1580. ISSN: 0022-1899. DOI: 10.1093/infdis/172.6.1573. URL: https://doi.org/10.1093/infdis/172.6.1573 (visited on 12/10/2023).

[370] Piotr Wojdasiewicz, Łukasz A. Poniatowski, and Dariusz Szukiewicz. "The Role of Inflammatory and Anti-Inflammatory Cytokines in the Pathogenesis of Osteoarthritis". en. In: *Mediators of Inflammation* 2014 (Apr. 2014), e561459. ISSN: 0962-9351. DOI: 10.1155/2014/561459. URL: https://www.hindawi.com/journals/mi/2014/561459/ (visited on 12/10/2023).

[371] Nirmita Dutta et al. "Electrochemical Biosensors for Cytokine Profiling: Recent Advancements and Possibilities in the Near Future". en. In: *Biosensors* 11.3 (Mar. 2021), p. 94. ISSN: 2079-6374. DOI: 10.3390/bios11030094. URL: https://www.mdpi.com/2079-6374/11/3/94 (visited on 12/10/2023).

[372] Mohammad Hossein Pournaghi-Azar et al. "Direct and rapid electrochemical biosensing of the human interleukin-2 DNA in unpurified polymerase chain reaction (PCR)-amplified real samples". In: *Biosensors and Bioelectronics* 24.4 (Dec. 2008), pp. 524–530. ISSN: 0956-5663. DOI: 10.1016/j.bios.2008.05.008. URL: https://www.sciencedirect.com/science/article/pii/S0956566308002455 (visited on 12/10/2023).

[373] Shankar Subramanian Iyer and Genhong Cheng. "Role of Interleukin 10 Transcriptional Regulation in Inflammation and Autoimmune Disease". In: *Critical reviews in immunology* 32.1 (2012), pp. 23–63. ISSN: 1040-8401. URL: https://www.ncbi.nlm.nih.gov/pmc/articles/PMC3410706/ (visited on 12/10/2023).

[374] C A Dinarello and J W Mier. "Interleukins". In: *Annual Review of Medicine* 37.1 (1986), pp. 173–178. DOI: 10.1146/annurev.me.37.020186.001133. URL: https://doi.org/10.1146/annurev.me.37.020186.001133 (visited on 12/10/2023).

[375] Marcel van Deuren. *Acute meningococcal diseases: a study of clinical management, cytokine activation and regulation*. en. 1998. ISBN: 978-90-373-0416-9.

[376] Sarra Setrerrahmane and Hanmei Xu. "Tumor-related interleukins: old validated targets for new anti-cancer drug development". In: *Molecular Cancer* 16.1 (Sept. 2017), p. 153. ISSN: 1476-4598. DOI: 10.1186/s12943-017-0721-9. URL: https://doi.org/10.1186/s12943-017-0721-9 (visited on 12/10/2023).

[377] Daria Briukhovetska et al. "Interleukins in cancer: from biology to therapy". en. In: *Nature Reviews Cancer* 21.8 (Aug. 2021), pp. 481–499. ISSN: 1474-1768. DOI: 10.1038/s41568-021-00363-z. URL: https://www.nature.com/articles/s41568-021-00363-z (visited on 12/10/2023).

[378] Nathan L. Sanders and Anil Mishra. "Role of interleukin-18 in the pathophysiology of allergic diseases". In: *Cytokine & Growth Factor Reviews* 32 (Dec. 2016), pp. 31–39. ISSN: 1359-6101. DOI: 10.1016/j.cytogfr.2016.07.001. URL: https://www.sciencedirect.com/science/article/pii/S1359610116300715 (visited on 12/10/2023).

[379] C. M. Hawrylowicz and A. O'Garra. "Potential role of interleukin-10-secreting regulatory T cells in allergy and asthma". en. In: *Nature Reviews Immunology* 5.4 (Apr. 2005), pp. 271–283. ISSN: 1474-1741. DOI: 10.1038/nri1589. URL: https://www.nature.com/articles/nri1589 (visited on 12/10/2023).

[380] Guido Kroemer and Carlos Martínez-A. "Cytokines and autoimmune disease". In: *Clinical Immunology and Immunopathology* 61.3 (Dec. 1991), pp. 275–295. ISSN: 0090-1229. DOI: 10.1016/S0090-1229(05)80001-7. URL: https://www.sciencedirect.com/science/article/pii/S0090122905800017 (visited on 12/10/2023).

[381] Abdul Waheed Khan et al. "Autoimmune Neuroinflammatory Diseases: Role of Interleukins". en. In: *International Journal of Molecular Sciences* 24.9 (Jan. 2023), p. 7960. ISSN: 1422-0067. DOI: 10.3390/ijms24097960. URL: https://www.mdpi.com/1422-0067/24/9/7960 (visited on 12/10/2023).

[382] S Balamurugan et al. "Interleukins and cytokine biomarkers in uveitis". In: *Indian Journal of Ophthalmology* 68.9 (Sept. 2020), pp. 1750–1763. ISSN: 0301-4738. DOI: 10.4103/ijo.IJO_564_20. URL: https://www.ncbi.nlm.nih.gov/pmc/articles/PMC7690463/ (visited on 12/10/2023).

[383] Wanvisa Udomsinprasert et al. "Circulating Levels of Interleukin-6 and Interleukin-10, But Not Tumor Necrosis Factor-Alpha, as Potential Biomarkers of Severity and Mortality for COVID-19: Systematic Review with Meta-analysis". en. In: *Journal of Clinical Immunology* 41.1 (Jan. 2021), pp. 11–22. ISSN: 1573-2592. DOI: 10.1007/s10875-020-00899-z. URL: https://doi.org/10.1007/s10875-020-00899-z (visited on 12/10/2023).

[384] Paolo G. Arduino et al. "Possible role for interleukins as biomarkers for mortality and recurrence in oral cancer". en. In: *The International Journal of Biological Markers* 30.2 (Apr. 2015), pp. 262–266. ISSN: 0393-6155. DOI: 10.5301/jbm.5000142. URL: https://doi.org/10.5301/jbm.5000142 (visited on 12/10/2023).

[385] Stefan Ivanov and Anders Lindén. "Interleukin-17 as a drug target in human disease". English. In: *Trends in Pharmacological Sciences* 30.2 (Feb. 2009), pp. 95–103. ISSN: 0165-6147. DOI: 10.1016/j.tips.2008.11.004. URL: https://www.cell.com/trends/pharmacological-sciences/abstract/S0165-6147(09)00002-9 (visited on 12/10/2023).

[386] Chunlei Tang et al. "Interleukin-23: as a drug target for autoimmune inflammatory diseases". en. In: *Immunology* 135.2 (2012), pp. 112–124. ISSN: 1365-2567. DOI: 10.1111/j.1365-2567.2011.03522.x. URL: https://onlinelibrary.wiley.com/doi/abs/10.1111/j.1365-2567.2011.03522.x (visited on 12/10/2023).

[387] Natacha Ipseiz et al. "Tissue-resident macrophages actively suppress IL-1beta release via a reactive prostanoid/IL-10 pathway". In: *The EMBO Journal* 39.14 (July 2020), e103454. ISSN: 0261-4189. DOI: 10.15252/embj.2019103454. URL: https://www.embopress.org/doi/full/10.15252/embj.2019103454 (visited on 12/10/2023).

[388] Adekunle Babajide Rowaiye et al. "Attenuating the Effects of Novel COVID-19 (SARS-CoV-2) Infection-Induced Cytokine Storm and the Implications". In: *Journal of Inflammation Research* 14 (Apr. 2021), pp. 1487–1510. ISSN: null. DOI: 10.2147/JIR.S301784. URL: https://www.tandfonline.com/doi/abs/10.2147/JIR.S301784 (visited on 12/10/2023).

[389] Weiran Li, Shuanghong Luo, and Chaomin Wan. "Characterization of fever and sickness behavior regulated by cytokines during infection". eng. In: *Behaviour* 157.10-11 (Sept. 2020), pp. 855–878. ISSN: 0005-7959, 1568-539X. DOI: 10.1163/1568539X-bja10028. URL: https://brill.com/view/journals/beh/157/10-11/article-p855_1.xml (visited on 12/10/2023).

[390] Clarissa M. D. Mota and Christopher J. Madden. "Neural circuits mediating circulating interleukin-1-evoked fever in the absence of prostaglandin E2 production". In: *Brain, Behavior, and Immunity* 103 (July 2022), pp. 109–121. ISSN: 0889-1591. DOI: 10.1016/j.bbi.2022.04.008. URL: https://www.sciencedirect.com/science/article/pii/S0889159122001064 (visited on 12/10/2023).

[391] Palesa Mosili et al. "The Pathogenesis of Fever-Induced Febrile Seizures and Its Current State". en. In: *Neuroscience Insights* 15 (Jan. 2020), p. 2633105520956973. ISSN: 2633-1055. DOI: 10.1177/2633105520956973. URL: https://doi.org/10.1177/2633105520956973 (visited on 12/10/2023).

[392] Elizabeth S. Mayne, Jaya A. George, and Susan Louw. "Assessing Biomarkers in Viral Infection". en. In: *Application of Omic Techniques to Identify New Biomarkers and Drug Targets for COVID-19*. Ed. by Paul C. Guest. Advances in Experimental Medicine and Biology. Cham: Springer International Publishing, 2023, pp. 159–173. ISBN: 978-3-031-28012-2. DOI: 10.1007/978-3-031-28012-2_8. URL: https://doi.org/10.1007/978-3-031-28012-2_8 (visited on 12/10/2023).

[393] Laurie P Shornick et al. "Mice deficient in IL-1beta manifest impaired contact hypersensitivity to trinitrochlorobenzone." In: *The Journal of experimental medicine* 183.4 (1996), pp. 1427–1436.

[394] Mohamed Lamkanfi and Vishva M. Dixit. "Inflammasomes and Their Roles in Health and Disease". In: *Annual Review of Cell and Developmental Biology* 28.1 (2012), pp. 137–161. DOI: 10.1146/annurev-cellbio-101011-155745. URL: https://doi.org/10.1146/annurev-cellbio-101011-155745 (visited on 12/10/2023).

[395] Amer Siddiq et al. "Association of Pro-Inflammatory Cytokines with Vitamin D in Hashimoto's Thyroid Autoimmune Disease". en. In: *Medicina* 59.5 (May 2023), p. 853. ISSN: 1648-9144. DOI: 10.3390/medicina59050853. URL: https://www.mdpi.com/1648-9144/59/5/853 (visited on 12/10/2023).

[396] Alexandra-Chloé Villani et al. "Common variants in the NLRP3 region contribute to Crohn's disease susceptibility". en. In: *Nature Genetics* 41.1 (Jan. 2009), pp. 71–76. ISSN: 1061-4036, 1546-1718. DOI: 10.1038/ng.285. URL: https://www.nature.com/articles/ng.285 (visited on 12/10/2023).

[397] Mariia Aristova et al. "LP-203 The new markers of systemic lupus erythematosus activity: focus on interleukin (IL)-1b and soluble IL-2 receptor". en. In: *Lupus Science & Medicine* 10.Suppl 1 (July 2023). ISSN: 2053-8790. DOI: 10.1136/lupus-2023-KCR.147. URL: https://lupus.bmj.com/content/10/Suppl_1/A101.2 (visited on 12/10/2023).

[398] Sunny Malhotra et al. "NLRP3 inflammasome as prognostic factor and therapeutic target in primary progressive multiple sclerosis patients". In: *Brain* 143.5 (May 2020), pp. 1414–1430. ISSN: 0006-8950. DOI: 10.1093/brain/awaa084. URL: https://doi.org/10.1093/brain/awaa084 (visited on 12/10/2023).

[399] Claudia Tulotta et al. "IL-1B drives opposing responses in primary tumours and bone metastases; harnessing combination therapies to improve outcome in breast cancer". en. In: *npj Breast Cancer* 7.1 (July 2021), pp. 1–15. ISSN: 2374-4677. DOI: 10.1038/s41523-021-00305-w. URL: https://www.nature.com/articles/s41523-021-00305-w (visited on 12/10/2023).

[400] Lindi Masson et al. "Inflammatory cytokine biomarkers of asymptomatic sexually transmitted infections and vaginal dysbiosis: a multicentre validation study". en. In: *Sexually Transmitted Infections* 95.1 (Feb. 2019), pp. 5–12. ISSN: 1368-4973, 1472-3263. DOI: 10.1136/sextrans-2017-053506. URL: https://sti.bmj.com/content/95/1/5 (visited on 12/10/2023).

[401] James S. Griffiths et al. "Role for IL-1 Family Cytokines in Fungal Infections". In: *Frontiers in Microbiology* 12 (2021). ISSN: 1664-302X. URL: https://www.frontiersin.org/articles/10.3389/fmicb.2021.633047 (visited on 12/10/2023).

[402] Anuradha S. Tripathy et al. "Pro-inflammatory CXCL-10, TNF-, IL-1, and IL-6: biomarkers of SARS-CoV-2 infection". en. In: *Archives of Virology* 166.12 (Dec. 2021), pp. 3301–3310. ISSN: 1432-8798. DOI: 10.1007/s00705-021-05247-z. URL: https://doi.org/10.1007/s00705-021-05247-z (visited on 12/10/2023).

[403] Marta Bodro et al. "Increased CSF levels of IL-1, IL-6, and ACE in SARS-CoV-2–associated encephalitis". In: *Neurology® Neuroimmunology & Neuroinflammation* 7.5 (July 2020), e821. ISSN: 2332-7812. DOI: 10.1212/NXI.0000000000000821. URL: https://www.ncbi.nlm.nih.gov/pmc/articles/PMC7357418/ (visited on 12/10/2023).

[404] *IL-1Beta Expression*. Place: https://www.proteinatlas.org/ENSG00000125538-IL1B/tissue. (Visited on 12/18/2023).

[405] Ioannis Mitroulis, Konstantinos Kambas, and Konstantinos Ritis. "Neutrophils, IL-1, and gout: is there a link?" en. In: *Seminars in Immunopathology* 35.4 (July 2013), pp. 501–512. ISSN: 1863-2300. DOI: 10.1007/s00281-

013-0361-0. URL: https://doi.org/10.1007/s00281-013-0361-0 (visited on 12/10/2023).

[406] Alberto Mantovani et al. "IL-1 and related cytokines in innate and adaptive immunity in health and disease". In: *Immunity* 50.4 (Apr. 2019), pp. 778–795. ISSN: 1074-7613. DOI: 10.1016/j.immuni.2019.03.012. URL: https://www.ncbi.nlm.nih.gov/pmc/articles/PMC7174020/ (visited on 12/10/2023).

[407] Charles L. Evavold and Jonathan C. Kagan. "How Inflammasomes Inform Adaptive Immunity". In: *Journal of Molecular Biology*. Mechanisms of Inflammasome Activation 430.2 (Jan. 2018), pp. 217–237. ISSN: 0022-2836. DOI: 10.1016/j.jmb.2017.09.019. URL: https://www.sciencedirect.com/science/article/pii/S0022283617304709 (visited on 12/10/2023).

[408] Mio Kawaguchi et al. "IL-17 cytokine family". In: *Journal of Allergy and Clinical Immunology* 114.6 (Dec. 2004), pp. 1265–1273. ISSN: 0091-6749. DOI: 10.1016/j.jaci.2004.10.019. URL: https://www.sciencedirect.com/science/article/pii/S0091674904026429 (visited on 12/10/2023).

[409] Vladimir Ramirez-Carrozzi et al. "IL-17C regulates the innate immune function of epithelial cells in an autocrine manner". en. In: *Nature Immunology* 12.12 (Dec. 2011), pp. 1159–1166. ISSN: 1529-2916. DOI: 10.1038/ni.2156. URL: https://www.nature.com/articles/ni.2156 (visited on 09/28/2023).

[410] Stephanie Swedik, Abson Madola, and Alan Levine. "IL-17C in human mucosal immunity: More than just a middle child". en. In: *Cytokine* 146 (Oct. 2021), p. 155641. ISSN: 10434666. DOI: 10.1016/j.cyto.2021.155641. URL: https://linkinghub.elsevier.com/retrieve/pii/S1043466621002271 (visited on 11/20/2023).

[411] Anna C. Zemke and Keven M. Robinson. "Right on the Nose: IL-17C and Nasal Host Defense". In: *American Journal of Respiratory Cell and Molecular Biology* 62.1 (Jan. 2020), pp. 10–11. ISSN: 1044-1549. DOI: 10.1165/rcmb.2019-0236ED. URL: https://www.atsjournals.org/doi/full/10.1165/rcmb.2019-0236ED (visited on 12/10/2023).

[412] Kyla C. Jamieson et al. "Rhinovirus and Bacteria Synergistically Induce IL-17C Release from Human Airway Epithelial Cells To Promote Neutrophil Recruitment". In: *The Journal of Immunology* 202.1 (Jan. 2019), pp. 160–170. ISSN: 0022-1767. DOI: 10.4049/jimmunol.1800547. URL: https://doi.org/10.4049/jimmunol.1800547 (visited on 12/10/2023).

[413] Hyun Jin Min and Kyung Soo Kim. "IL-17C expression and its correlation with pediatric adenoids: a preliminary study". en. In: *International Journal of Medical Sciences* 17.17 (2020), pp. 2603–2610. ISSN: 1449-1907. DOI: 10.7150/ijms.49244. URL: https://www.medsci.org/v17p2603.htm (visited on 01/26/2023).

[414] Jun Jin et al. "IL-17C expression in nasal epithelial cells of chronic rhinosinusitis with nasal polyposis". en. In: *European Archives of Oto-Rhino-Laryngology* 271.5 (May 2014), pp. 1097–1105. ISSN: 1434-4726. DOI: 10.1007/s00405-013-2683-x. URL: https://doi.org/10.1007/s00405-013-2683-x (visited on 09/27/2023).

[415] Osamu Takeuchi and Shizuo Akira. "Pattern Recognition Receptors and Inflammation". en. In: *Cell* 140.6 (Mar. 2010), pp. 805–820. ISSN: 00928674. DOI: 10.1016/j.cell.2010.01.022. URL: https://linkinghub.elsevier.com/retrieve/pii/S0092867410000231 (visited on 12/10/2023).

[416] Eunok Im, Jane Jung, and Sang Hoon Rhee. "Toll-Like Receptor 5 Engagement Induces Interleukin-17C Expression in Intestinal Epithelial

Cells". In: *Journal of Interferon & Cytokine Research* 32.12 (Dec. 2012), pp. 583–591. ISSN: 1079-9907. DOI: 10.1089/jir.2012.0053. URL: https://www.liebertpub.com/doi/abs/10.1089/jir.2012.0053 (visited on 12/10/2023).

[417] Lynette A. Fouser et al. "Th17 cytokines and their emerging roles in inflammation and autoimmunity". en. In: *Immunological Reviews* 226.1 (Dec. 2008), pp. 87–102. ISSN: 0105-2896, 1600-065X. DOI: 10.1111/j.1600-065X.2008.00712.x. URL: https://onlinelibrary.wiley.com/doi/10.1111/j.1600-065X.2008.00712.x (visited on 12/10/2023).

[418] Remco Van Horssen, Timo L. M. Ten Hagen, and Alexander M. M. Eggermont. "TNF- in Cancer Treatment: Molecular Insights, Antitumor Effects, and Clinical Utility". en. In: *The Oncologist* 11.4 (Apr. 2006), pp. 397–408. ISSN: 1083-7159, 1549-490X. DOI: 10.1634/theoncologist.11-4-397. URL: https://academic.oup.com/oncolo/article/11/4/397/6397077 (visited on 12/10/2023).

[419] Karline Guilloteau et al. "Skin Inflammation Induced by the Synergistic Action of IL-17A, IL-22, Oncostatin M, IL-1, and TNF- Recapitulates Some Features of Psoriasis". en. In: *The Journal of Immunology* 184.9 (May 2010), pp. 5263–5270. ISSN: 0022-1767, 1550-6606. DOI: 10.4049/jimmunol.0902464. URL: https://journals.aai.org/jimmunol/article/184/9/5263/83302/Skin-Inflammation-Induced-by-the-Synergistic (visited on 12/10/2023).

[420] *IL-17C expression*. Place: https://www.proteinatlas.org/ENSG00000124391-IL17C. (Visited on 12/18/2023).

[421] Feng Wang et al. "IL-17C has a pathogenic role in kidney ischemia/reperfusion injury". en. In: *Kidney International* 97.6 (June 2020), pp. 1219–1229. ISSN:

00852538. DOI: 10.1016/j.kint.2020.01.015. URL: https://linkinghub.elsevier.com/retrieve/pii/S0085253820301137 (visited on 01/29/2024).

[422] Erin M. Garcia et al. *IL-17C is a driver of damaging inflammation during Neisseria gonorrhoeae infection of human Fallopian tube*. en. Nov. 2022. DOI: 10.1101/2022.11.28.518270. URL: https://www.biorxiv.org/content/10.1101/2022.11.28.518270v1 (visited on 12/10/2023).

[423] Yung Jin Jeon et al. "IL-17C Protects Nasal Epithelium from *Pseudomonas* aeruginosa Infection". en. In: *American Journal of Respiratory Cell and Molecular Biology* 62.1 (Jan. 2020), pp. 95–103. ISSN: 1044-1549, 1535-4989. DOI: 10.1165/rcmb.2018-0377OC. URL: https://www.atsjournals.org/doi/10.1165/rcmb.2018-0377OC (visited on 12/10/2023).

[424] Ian D. Odell and Deborah Cook. "Immunofluorescence Techniques". en. In: *Journal of Investigative Dermatology* 133.1 (Jan. 2013), pp. 1–4. ISSN: 0022202X. DOI: 10.1038/jid.2012.455. URL: https://linkinghub.elsevier.com/retrieve/pii/S0022202X15359546 (visited on 12/10/2023).

[425] Jonas Wizenty et al. "Autofluorescence: A potential pitfall in immunofluorescence-based inflammation grading". In: *Journal of Immunological Methods* 456 (May 2018), pp. 28–37. ISSN: 0022-1759. DOI: 10.1016/j.jim.2018.02.007. URL: https://www.sciencedirect.com/science/article/pii/S002217591730546X (visited on 12/10/2023).

[426] Nancy B. Kiviat et al. "Localization of Chlamydia trachomatis infection by direct immunofluorescence and culture in pelvic inflammatory disease". In: *American Journal of Obstetrics and Gynecology* 154.4 (Apr. 1986), pp. 865–873. ISSN: 0002-9378. DOI: 10.1016/0002-9378(86)90473-4. URL: https://www.sciencedirect.com/science/article/pii/0002937886904734 (visited on 12/10/2023).

[427] Işın Sinem Bağcı et al. "New-generation diagnostics in inflammatory skin diseases: Immunofluorescence and histopathological assessment using ex vivo confocal laser scanning microscopy in cutaneous lupus erythematosus". en. In: *Experimental Dermatology* 30.5 (2021), pp. 684–690. ISSN: 1600-0625. DOI: 10.1111/exd.14265. URL: https://onlinelibrary.wiley.com/doi/abs/10.1111/exd.14265 (visited on 12/10/2023).

[428] A. R. Currie et al. "Immunofluorescent localisation of a growth hormone-like factor in normal and abnormal syncytiotrophoblast". en. In: *The Journal of Pathology and Bacteriology* 92.2 (1966), pp. 395–399. ISSN: 1555-2039. DOI: 10.1002/path.1700920217. URL: https://onlinelibrary.wiley.com/doi/abs/10.1002/path.1700920217 (visited on 12/10/2023).

[429] Stephen Kershaw et al. "Optimisation of immunofluorescence methods to determine MCT1 and MCT4 expression in circulating tumour cells". In: *BMC Cancer* 15.1 (May 2015), p. 387. ISSN: 1471-2407. DOI: 10.1186/s12885-015-1382-y. URL: https://doi.org/10.1186/s12885-015-1382-y (visited on 12/10/2023).

[430] Y. D. Jung et al. "Effects of combination anti-vascular endothelial growth factor receptor and anti-epidermal growth factor receptor therapies on the growth of gastric cancer in a nude mouse model". In: *European Journal of Cancer* 38.8 (May 2002), pp. 1133–1140. ISSN: 0959-8049. DOI: 10.1016/S0959-8049(02)00013-8. URL: https://www.sciencedirect.com/science/article/pii/S0959804902000138 (visited on 12/10/2023).

[431] Anup Sood et al. "Comparison of Multiplexed Immunofluorescence Imaging to Chromogenic Immunohistochemistry of Skin Biomarkers in Response to Monkeypox Virus Infection". en. In: *Viruses* 12.8 (Aug.

2020), p. 787. ISSN: 1999-4915. DOI: 10.3390/v12080787. URL: https://www.mdpi.com/1999-4915/12/8/787 (visited on 12/10/2023).

[432] Dung Nguyen, Donal Skelly, and Niluka Goonawardane. "A Novel Immunofluorescence Assay for the Rapid Serological Detection of SARS-CoV-2 Infection". en. In: *Viruses* 13.5 (May 2021), p. 747. ISSN: 1999-4915. DOI: 10.3390/v13050747. URL: https://www.mdpi.com/1999-4915/13/5/747 (visited on 12/10/2023).

[433] Rodney Rhoades and Richard G. Pflanzer. *Human physiology*. eng. Australia ; Pacific Grove, Calif. : Thomson : Brooks/Cole, 2003. ISBN: 978-0-534-46251-2 978-0-534-42174-8 978-0-03-032129-0 978-0-534-39502-5. URL: http://archive.org/details/humanphysiologyw00rodn (visited on 12/10/2023).

[434] Emma Reeves and Edward James. "Antigen processing and immune regulation in the response to tumours". en. In: *Immunology* 150.1 (2017), pp. 16–24. ISSN: 1365-2567. DOI: 10.1111/imm.12675. URL: https://onlinelibrary.wiley.com/doi/abs/10.1111/imm.12675 (visited on 12/10/2023).

[435] Gonzalo de la Rosa et al. "Lactoferrin Acts as an Alarmin to Promote the Recruitment and Activation of APCs and Antigen-Specific Immune Responses12". In: *The Journal of Immunology* 180.10 (May 2008), pp. 6868–6876. ISSN: 0022-1767. DOI: 10.4049/jimmunol.180.10.6868. URL: https://doi.org/10.4049/jimmunol.180.10.6868 (visited on 12/10/2023).

[436] Tazio Storni et al. "Immunity in response to particulate antigen-delivery systems". In: *Advanced Drug Delivery Reviews*. Trends in Particulate Antigen and DNA Delivery Systems for Vaccines 57.3 (Jan. 2005), pp. 333–

355. ISSN: 0169-409X. DOI: 10.1016/j.addr.2004.09.008. URL: https://www.sciencedirect.com/science/article/pii/S0169409X04002066 (visited on 12/10/2023).

[437] Kyuseok Im et al. "An Introduction to Performing Immunofluorescence Staining". en. In: *Biobanking: Methods and Protocols*. Ed. by William H. Yong. Methods in Molecular Biology. New York, NY: Springer, 2019, pp. 299–311. ISBN: 978-1-4939-8935-5. DOI: 10.1007/978-1-4939-8935-5_26. URL: https://doi.org/10.1007/978-1-4939-8935-5_26 (visited on 12/10/2023).

[438] Malin Lager. *Molecular and serological tools for clinical diagnostics of Lyme borreliosis - can the laboratory analysis be improved?* en. Vol. 1744. Linköping University Medical Dissertations. Linköping: Linköping University Electronic Press, Nov. 2020. ISBN: 978-91-7929-833-3. DOI: 10.3384/diss.diva-170740. URL: http://urn.kb.se/resolve?urn=urn:nbn:se:liu:diva-170740 (visited on 12/18/2023).

[439] Sami Zaqout, Lena-Luise Becker, and Angela M. Kaindl. "Immunofluorescence Staining of Paraffin Sections Step by Step". In: *Frontiers in Neuroanatomy* 14 (2020). ISSN: 1662-5129. URL: https://www.frontiersin.org/articles/10.3389/fnana.2020.582218 (visited on 12/10/2023).

[440] Hendrik A. Messal et al. "Antigen retrieval and clearing for whole-organ immunofluorescence by FLASH". en. In: *Nature Protocols* 16.1 (Jan. 2021), pp. 239–262. ISSN: 1750-2799. DOI: 10.1038/s41596-020-00414-z. URL: https://www.nature.com/articles/s41596-020-00414-z (visited on 12/10/2023).

[441] Juan Cai et al. "Staphylococcus aureus facilitates its survival in bovine macrophages by blocking autophagic flux". en. In: *Journal of Cellular*

and Molecular Medicine 24.6 (2020), pp. 3460–3468. ISSN: 1582-4934. DOI: 10.1111/jcmm.15027. URL: https://onlinelibrary.wiley.com/doi/abs/10.1111/jcmm.15027 (visited on 12/10/2023).

[442] *Direct vs indirect immunofluorescence \textbackslashtextbar Abcam*. URL: https://www.abcam.com/secondary-antibodies/direct-vs-indirect-immunofluorescence (visited on 12/10/2023).

[443] H Towbin, T Staehelin, and J Gordon. "Electrophoretic transfer of proteins from polyacrylamide gels to nitrocellulose sheets: procedure and some applications." en. In: *Proceedings of the National Academy of Sciences* 76.9 (Sept. 1979), pp. 4350–4354. ISSN: 0027-8424, 1091-6490. DOI: 10.1073/pnas.76.9.4350. URL: https://pnas.org/doi/full/10.1073/pnas.76.9.4350 (visited on 12/11/2023).

[444] Christine Blancher and Adam Jones. "SDS -PAGE and Western Blotting Techniques". en. In: *Metastasis Research Protocols: Volume I: Analysis of Cells and Tissues*. Ed. by Susan A. Brooks and Udo Schumacher. Methods in Molecular Medicine. Totowa, NJ: Humana Press, 2001, pp. 145–162. ISBN: 978-1-59259-136-7. DOI: 10.1385/1-59259-136-1:145. URL: https://doi.org/10.1385/1-59259-136-1:145 (visited on 12/11/2023).

[445] *Western Blotting Electrophoresis Techniques \textbackslashtextbar Bio-Rad*. URL: https://www.bio-rad.com/en-uk/applications-technologies/western-blotting-electrophoresis-techniques?ID=PQEENTWDLBV5 (visited on 09/04/2023).

[446] Michael J. Dunn. *Gel Electrophoresis of Proteins*. en. Elsevier, May 2014. ISBN: 978-1-4831-9354-0.

[447] A. Chrambach and D. Rodbard. "Polyacrylamide Gel Electrophoresis". In: *Science* 172.3982 (Apr. 1971), pp. 440–451. DOI: 10.1126/science.172.3982.440. URL: https://www.science.org/doi/abs/10.1126/science.172.3982.440 (visited on 12/11/2023).

[448] *Overview of Western Blotting - UK*. en. URL: https://www.thermofisher.com/uk/en/home/life-science/protein-biology/protein-biology-learning-center/protein-biology-resource-library/pierce-protein-methods/overview-western-blotting.html (visited on 09/04/2023).

[449] Abdulhamid A. Al-Tubuly. "SDS-PAGE and Western Blotting". en. In: *Diagnostic and Therapeutic Antibodies*. Ed. by Andrew J. T. George and Catherine E. Urch. Methods in Molecular Medicine. Totowa, NJ: Humana Press, 2000, pp. 391–405. ISBN: 978-1-59259-076-6. DOI: 10.1385/1-59259-076-4:391. URL: https://doi.org/10.1385/1-59259-076-4:391 (visited on 12/11/2023).

[450] Alice Alegria-Schaffer, Andrew Lodge, and Krishna Vattem. "Chapter 33 Performing and Optimizing Western Blots with an Emphasis on Chemiluminescent Detection". In: *Methods in Enzymology*. Ed. by Richard R. Burgess and Murray P. Deutscher. Vol. 463. Guide to Protein Purification, 2nd Edition. Academic Press, Jan. 2009, pp. 573–599. DOI: 10.1016/S0076-6879(09)63033-0. URL: https://www.sciencedirect.com/science/article/pii/S0076687909630330 (visited on 12/11/2023).

[451] Rui Hai Liu, James Jacob, and Bud Tennant. "Chemiluminescent Detection of Protein Molecular Weight Markers in Western Blot Techniques". en. In: *BioTechniques* 22.4 (Apr. 1997), pp. 594–595. ISSN: 0736-6205, 1940-9818. DOI: 10.2144/97224bm01. URL: https://www.future-science.com/doi/10.2144/97224bm01 (visited on 12/11/2023).

[452] Zhizhong Yao and Rut Carballido-López. "Fluorescence Imaging for Bacterial Cell Biology: From Localization to Dynamics, From Ensembles to Single Molecules". en. In: *Annual Review of Microbiology* 68.1 (Sept. 2014), pp. 459–476. ISSN: 0066-4227, 1545-3251. DOI: 10.1146/annurev-micro-091213-113034. URL: https://www.annualreviews.org/doi/10.1146/annurev-micro-091213-113034 (visited on 12/18/2023).

[453] Tian Huang et al. "A rapid and sensitive, multiplex, whole mount RNA fluorescence in situ hybridization and immunohistochemistry protocol". en. In: *Plant Methods* 19.1 (Nov. 2023), p. 131. ISSN: 1746-4811. DOI: 10.1186/s13007-023-01108-9. URL: https://plantmethods.biomedcentral.com/articles/10.1186/s13007-023-01108-9 (visited on 12/18/2023).

[454] Marlene Chevalier, Stephane Ranque, and Isabelle Prêcheur. "Oral fungal-bacterial biofilm models in vitro: a review". en. In: *Medical Mycology* 56.6 (Aug. 2018), pp. 653–667. ISSN: 1369-3786, 1460-2709. DOI: 10.1093/mmy/myx111. URL: https://academic.oup.com/mmy/article/56/6/653/4714786 (visited on 12/18/2023).

[455] Katherine Lagree et al. "Microscopy of fungal biofilms". en. In: *Current Opinion in Microbiology* 43 (June 2018), pp. 100–107. ISSN: 13695274. DOI: 10.1016/j.mib.2017.12.008. URL: https://linkinghub.elsevier.com/retrieve/pii/S136952741730139X (visited on 12/18/2023).

[456] Robertas Ursache et al. "A protocol for combining fluorescent proteins with histological stains for diverse cell wall components". en. In: *The Plant Journal* 93.2 (Jan. 2018), pp. 399–412. ISSN: 0960-7412, 1365-313X. DOI: 10.1111/tpj.13784. URL: https://onlinelibrary.wiley.com/doi/10.1111/tpj.13784 (visited on 12/18/2023).

[457] Haw-Young Kwon et al. "Development of a Universal Fluorescent Probe for Gram-Positive Bacteria". en. In: *Angewandte Chemie International Edition* 58.25 (June 2019), pp. 8426–8431. ISSN: 1433-7851, 1521-3773. DOI: 10.1002/anie.201902537. URL: https://onlinelibrary.wiley.com/doi/10.1002/anie.201902537 (visited on 12/18/2023).

[458] Liyuan Lin et al. "Imaging Commensal Microbiota and Pathogenic Bacteria in the Gut". en. In: *Accounts of Chemical Research* 54.9 (May 2021), pp. 2076–2087. ISSN: 0001-4842, 1520-4898. DOI: 10.1021/acs.accounts.1c00068. URL: https://pubs.acs.org/doi/10.1021/acs.accounts.1c00068 (visited on 12/18/2023).

[459] S. Sutrave et al. "Effect of daptomycin and vancomycin on Staphylococcus epidermidis biofilms: An in vitro assessment using fluorescence in situ hybridization". en. In: *PLOS ONE* 14.8 (Aug. 2019). Ed. by Ulrich Nübel, e0221786. ISSN: 1932-6203. DOI: 10.1371/journal.pone.0221786. URL: https://dx.plos.org/10.1371/journal.pone.0221786 (visited on 12/18/2023).

[460] Andrew J. Stout et al. "Engineering carotenoid production in mammalian cells for nutritionally enhanced cell-cultured foods". en. In: *Metabolic Engineering* 62 (Nov. 2020), pp. 126–137. ISSN: 10967176. DOI: 10.1016/j.ymben.2020.07.011. URL: https://linkinghub.elsevier.com/retrieve/pii/S1096717620301208 (visited on 12/18/2023).

[461] Isabell Klawonn et al. "Intercomparison of Two Fluorescent Dyes to Visualize Parasitic Fungi (Chytridiomycota) on Phytoplankton". en. In: *Microbial Ecology* 85.1 (Jan. 2023), pp. 9–23. ISSN: 0095-3628, 1432-184X. DOI: 10.1007/s00248-021-01893-7. URL: https://link.springer.com/10.1007/s00248-021-01893-7 (visited on 12/18/2023).

[462] João Paulo Rodrigues Marques and Marli Kasue Misaki Soares. "Fungus Detection". en. In: *Handbook of Techniques in Plant Histopathology*. Cham: Springer International Publishing, 2022, pp. 51–66. ISBN: 978-3-031-14658-9 978-3-031-14659-6. DOI: 10.1007/978-3-031-14659-6_4. URL: https://link.springer.com/10.1007/978-3-031-14659-6_4 (visited on 12/18/2023).

[463] Ryosuke Nakamura et al. "Microscopic observation of human airway ciliary movement using wheat germ agglutinin". en. In: *Methods in Cell Biology*. Vol. 175. Elsevier, 2023, pp. 33–43. ISBN: 978-0-443-18586-1. DOI: 10.1016/bs.mcb.2022.07.019. URL: https://linkinghub.elsevier.com/retrieve/pii/S0091679X22001108 (visited on 12/18/2023).

[464] Maria A. Petkova and Halina Dobrzynski. "Do human sinoatrial node cells have t-tubules?" en. In: *Translational Research in Anatomy* 25 (Nov. 2021), p. 100131. ISSN: 2214854X. DOI: 10.1016/j.tria.2021.100131. URL: https://linkinghub.elsevier.com/retrieve/pii/S2214854X21000212 (visited on 12/18/2023).

[465] Alexander P. Young, Daniel J. Jackson, and Russell C. Wyeth. "A technical review and guide to RNA fluorescence in situ hybridization". en. In: *PeerJ* 8 (Mar. 2020), e8806. ISSN: 2167-8359. DOI: 10.7717/peerj.8806. URL: https://peerj.com/articles/8806 (visited on 12/18/2023).

[466] R H Singer and D C Ward. "Actin gene expression visualized in chicken muscle tissue culture by using in situ hybridization with a biotinated nucleotide analog." en. In: *Proceedings of the National Academy of Sciences* 79.23 (Dec. 1982), pp. 7331–7335. ISSN: 0027-8424, 1091-6490. DOI: 10.1073/pnas.79.23.7331. URL: https://pnas.org/doi/full/10.1073/pnas.79.23.7331 (visited on 12/18/2023).

[467] Jethro S. Johnson et al. "Evaluation of 16S rRNA gene sequencing for species and strain-level microbiome analysis". en. In: *Nature Communications* 10.1 (Nov. 2019), p. 5029. ISSN: 2041-1723. DOI: 10.1038/s41467-019-13036-1. URL: https://www.nature.com/articles/s41467-019-13036-1 (visited on 12/18/2023).

[468] Jolene Jie Lin Goh et al. "Highly specific multiplexed RNA imaging in tissues with split-FISH". en. In: *Nature Methods* 17.7 (July 2020), pp. 689–693. ISSN: 1548-7091, 1548-7105. DOI: 10.1038/s41592-020-0858-0. URL: https://www.nature.com/articles/s41592-020-0858-0 (visited on 12/18/2023).

[469] Dylan M. Parker et al. "Improved Methods for Single-Molecule Fluorescence *In* Situ Hybridization and Immunofluorescence in *Caenorhabditis* elegans Embryos". en. In: *Current Protocols* 1.11 (Nov. 2021), e299. ISSN: 2691-1299, 2691-1299. DOI: 10.1002/cpz1.299. URL: https://currentprotocols.onlinelibrary.wiley.com/doi/10.1002/cpz1.299 (visited on 12/18/2023).

[470] Jocelyn Y. Kishi et al. "SABER amplifies FISH: enhanced multiplexed imaging of RNA and DNA in cells and tissues". en. In: *Nature Methods* 16.6 (June 2019), pp. 533–544. ISSN: 1548-7091, 1548-7105. DOI: 10.1038/s41592-019-0404-0. URL: https://www.nature.com/articles/s41592-019-0404-0 (visited on 12/18/2023).

[471] Noelle James, Xiaochen Liu, and Alison Bell. "A fluorescence in situ hybridization (FISH) protocol for stickleback tissue". In: *Evolutionary ecology research* 17 (2016), pp. 603–617. ISSN: 1522-0613. URL: https://www.ncbi.nlm.nih.gov/pmc/articles/PMC5642962/ (visited on 12/14/2023).

[472] Laura Nistico et al. "Fluorescence "In Situ" Hybridization for the Detection of Biofilm in the Middle Ear and Upper Respiratory Tract Mucosa". In: *Auditory and Vestibular Research*. Ed. by John M. Walker and Bernd Sokolowski. Vol. 493. Totowa, NJ: Humana Press, 2009, pp. 191–213. ISBN: 978-1-934115-62-6 978-1-59745-523-7. DOI: 10.1007/978-1-59745-523-7_12. URL: http://link.springer.com/10.1007/978-1-59745-523-7_12 (visited on 12/18/2023).

[473] Elsa Prudent and Didier Raoult. "Fluorescence in situ hybridization, a complementary molecular tool for the clinical diagnosis of infectious diseases by intracellular and fastidious bacteria". en. In: *FEMS Microbiology Reviews* 43.1 (Jan. 2019), pp. 88–107. ISSN: 1574-6976. DOI: 10.1093/femsre/fuy040. URL: https://academic.oup.com/femsre/article/43/1/88/5173038 (visited on 12/18/2023).

[474] Nick Spindler et al. "Fluorescence in situ Hybridization (FISH) in the Microbiological Diagnostic of Deep Sternal Wound Infection (DSWI)". en. In: *Infection and Drug Resistance* Volume 14 (June 2021), pp. 2309–2319. ISSN: 1178-6973. DOI: 10.2147/IDR.S310139. URL: https://www.dovepress.com/fluorescence-in-situ-hybridization-fish-in-the-microbiological-diagnos-peer-reviewed-fulltext-article-IDR (visited on 12/18/2023).

[475] Simone Eichinger et al. "Fluorescence in situ hybridization for identification and visualization of microorganisms in infected heart valve tissue as addition to standard diagnostic tests improves diagnosis of endocarditis". en. In: *Interactive CardioVascular and Thoracic Surgery* 29.5 (Nov. 2019), pp. 678–684. ISSN: 1569-9285. DOI: 10.1093/icvts/ivz159.

URL: https://academic.oup.com/icvts/article/29/5/678/5528514 (visited on 12/18/2023).

[476] Felix Schoenrath et al. "Fluorescence In Situ Hybridization and Polymerase Chain Reaction to Detect Infections in Patients With Left Ventricular Assist Devices". en. In: *ASAIO Journal* 67.5 (May 2021), pp. 536–545. ISSN: 1058-2916. DOI: 10.1097/MAT.0000000000001260. URL: https://journals.lww.com/10.1097/MAT.0000000000001260 (visited on 12/18/2023).

[477] Mohammad Y. Ashfaq, Dana A. Da'na, and Mohammad A. Al-Ghouti. "Application of MALDI-TOF MS for identification of environmental bacteria: A review". en. In: *Journal of Environmental Management* 305 (Mar. 2022), p. 114359. ISSN: 03014797. DOI: 10.1016/j.jenvman.2021.114359. URL: https://linkinghub.elsevier.com/retrieve/pii/S030147972102421X (visited on 12/18/2023).

[478] Martin Welker et al. "An update on the routine application of MALDI-TOF MS in clinical microbiology". en. In: *Expert Review of Proteomics* 16.8 (Aug. 2019), pp. 695–710. ISSN: 1478-9450, 1744-8387. DOI: 10.1080/14789450.2019.1645603. URL: https://www.tandfonline.com/doi/full/10.1080/14789450.2019.1645603 (visited on 12/18/2023).

[479] Jyotsna Shah et al. "Fluorescence in situ hybridization (FISH) assays for diagnosing malaria in endemic areas". In: *PLoS One* 10.9 (2015), e0136726.

[480] Ana Barbosa et al. "Imaging biofilms using fluorescence in situ hybridization: seeing is believing". In: *Frontiers in Cellular and Infection Microbiology* 13 (May 2023), p. 1195803. ISSN: 2235-2988. DOI: 10.3389/

fcimb.2023.1195803. URL: https://www.frontiersin.org/articles/10.3389/fcimb.2023.1195803/full (visited on 12/18/2023).

[481] E. M. M. Manders et al. "Dynamics of three-dimensional replication patterns during the s-phase, analysed by double labelling of dna and confocal microscopy". en. In: *Journal of Cell Science* 103.3 (Nov. 1992), pp. 857–862. ISSN: 0021-9533, 1477-9137. DOI: 10.1242/jcs.103.3.857. URL: https://journals.biologists.com/jcs/article/103/3/857/23454/Dynamics-of-three-dimensional-replication-patterns (visited on 07/28/2023).

[482] Tord Berggård, Sara Linse, and Peter James. "Methods for the detection and analysis of protein–protein interactions". en. In: *PROTEOMICS* 7.16 (Aug. 2007), pp. 2833–2842. ISSN: 16159853, 16159861. DOI: 10.1002/pmic.200700131. URL: https://onlinelibrary.wiley.com/doi/10.1002/pmic.200700131 (visited on 07/28/2023).

[483] Anke Reinders et al. "Protein–Protein Interactions between Sucrose Transporters of Different Affinities Colocalized in the Same Enucleate Sieve Element". en. In: *The Plant Cell* 14.7 (July 2002), pp. 1567–1577. ISSN: 1040-4651, 1532-298X. DOI: 10.1105/tpc.002428. URL: https://academic.oup.com/plcell/article/14/7/1567-1577/6009781 (visited on 07/28/2023).

[484] Christian A Schaer et al. "Heme carrier protein (HCP-1) spatially interacts with the CD163 hemoglobin uptake pathway and is a target of inflammatory macrophage activation". en. In: *Journal of Leukocyte Biology* 83.2 (Feb. 2008), pp. 325–333. ISSN: 0741-5400, 1938-3673. DOI: 10.1189/jlb.0407226. URL: https://academic.oup.com/jleukbio/article/83/2/325/6975355 (visited on 07/28/2023).

[485] Jennifer A. Wambach et al. "Functional Characterization of *ATP*-Binding Cassette Transporter A3 Mutations from Infants with Respiratory Distress Syndrome". en. In: *American Journal of Respiratory Cell and Molecular Biology* 55.5 (Nov. 2016), pp. 716–721. ISSN: 1044-1549, 1535-4989. DOI: 10.1165/rcmb.2016-0008OC. URL: https://www.atsjournals.org/doi/10.1165/rcmb.2016-0008OC (visited on 07/28/2023).

[486] Jeremy Katzen et al. "A SFTPC BRICHOS mutant links epithelial ER stress and spontaneous lung fibrosis". en. In: *JCI Insight* (Feb. 2019). ISSN: 2379-3708. DOI: 10.1172/jci.insight.126125. URL: http://insight.jci.org/articles/view/126125 (visited on 07/28/2023).

[487] S. Bolte and F. P. Cordelières. "A guided tour into subcellular colocalization analysis in light microscopy". en. In: *Journal of Microscopy* 224.3 (Dec. 2006), pp. 213–232. ISSN: 0022-2720, 1365-2818. DOI: 10.1111/j.1365-2818.2006.01706.x. URL: https://onlinelibrary.wiley.com/doi/10.1111/j.1365-2818.2006.01706.x (visited on 07/28/2023).

[488] "VII. Mathematical contributions to the theory of evolution.—III. Regression, heredity, and panmixia". en. In: *Philosophical Transactions of the Royal Society of London. Series A, Containing Papers of a Mathematical or Physical Character* 187 (Dec. 1896), pp. 253–318. ISSN: 0264-3952, 2053-9258. DOI: 10.1098/rsta.1896.0007. URL: https://royalsocietypublishing.org/doi/10.1098/rsta.1896.0007 (visited on 07/28/2023).

[489] Kenneth W. Dunn, Malgorzata M. Kamocka, and John H. McDonald. "A practical guide to evaluating colocalization in biological microscopy". In: *American Journal of Physiology - Cell Physiology* 300.4 (Apr. 2011), pp. C723–C742. ISSN: 0363-6143. DOI: 10.1152/ajpcell.00462.2010. URL: https:

//www.ncbi.nlm.nih.gov/pmc/articles/PMC3074624/ (visited on 05/12/2023).

[490] Jeremy Adler and Ingela Parmryd. "Quantifying colocalization by correlation: the Pearson correlation coefficient is superior to the Mander's overlap coefficient". eng. In: *Cytometry. Part A: The Journal of the International Society for Analytical Cytology* 77.8 (Aug. 2010), pp. 733–742. ISSN: 1552-4930. DOI: 10.1002/cyto.a.20896.

[491] Jeremy Adler and Ingela Parmryd. "Quantifying colocalization: the MOC is a hybrid coefficient – an uninformative mix of co-occurrence and correlation". In: *Journal of Cell Science* 132.1 (Jan. 2019), jcs222455. ISSN: 0021-9533. DOI: 10.1242/jcs.222455. URL: https://doi.org/10.1242/jcs.222455 (visited on 12/12/2023).

[492] Jeremy Adler and Ingela Parmryd. "Quantifying colocalization: The case for discarding the Manders overlap coefficient". en. In: *Cytometry Part A* 99.9 (2021), pp. 910–920. ISSN: 1552-4930. DOI: 10.1002/cyto.a.24336. URL: https://onlinelibrary.wiley.com/doi/abs/10.1002/cyto.a.24336 (visited on 12/12/2023).

[493] P.G. Penarrubia, X.F. Ruiz, and J. Galvez. "Quantitative analysis of the factors that affect the determination of colocalization coefficients in dual-color confocal images". In: *IEEE Transactions on Image Processing* 14.8 (Aug. 2005), pp. 1151–1158. ISSN: 1941-0042. DOI: 10.1109/TIP.2005.851699. URL: https://ieeexplore.ieee.org/document/1468199 (visited on 12/12/2023).

[494] E. M. M. Manders, F. J. Verbeek, and J. A. Aten. "Measurement of co-localization of objects in dual-colour confocal images". en. In: *Journal of Microscopy* 169.3 (Mar. 1993), pp. 375–382. ISSN: 0022-2720, 1365-2818.

DOI: 10.1111/j.1365-2818.1993.tb03313.x. URL: https://onlinelibrary.wiley.com/doi/10.1111/j.1365-2818.1993.tb03313.x (visited on 12/12/2023).

[495] Sylvain V. Costes et al. "Automatic and Quantitative Measurement of Protein-Protein Colocalization in Live Cells". en. In: *Biophysical Journal* 86.6 (June 2004), pp. 3993–4003. ISSN: 00063495. DOI: 10.1529/biophysj.103.038422. URL: https://linkinghub.elsevier.com/retrieve/pii/S0006349504744392 (visited on 12/12/2023).

[496] James Jonkman et al. "Tutorial: guidance for quantitative confocal microscopy". en. In: *Nature Protocols* 15.5 (May 2020), pp. 1585–1611. ISSN: 1750-2799. DOI: 10.1038/s41596-020-0313-9. URL: https://www.nature.com/articles/s41596-020-0313-9 (visited on 12/12/2023).

[497] Monica Monici. "Cell and tissue autofluorescence research and diagnostic applications". In: *Biotechnology Annual Review*. Vol. 11. Elsevier, Jan. 2005, pp. 227–256. DOI: 10.1016/S1387-2656(05)11007-2. URL: https://www.sciencedirect.com/science/article/pii/S1387265605110072 (visited on 12/10/2023).

[498] I. Giovannacci et al. "Which are the main fluorophores in skin and oral mucosa? A review with emphasis on clinical applications of tissue autofluorescence". In: *Archives of Oral Biology* 105 (Sept. 2019), pp. 89–98. ISSN: 0003-9969. DOI: 10.1016/j.archoralbio.2019.07.001. URL: https://www.sciencedirect.com/science/article/pii/S0003996919302912 (visited on 12/10/2023).

[499] M. S. Viegas et al. "An improved and cost-effective methodology for the reduction of autofluorescence in direct immunofluorescence studies on formalin-fixed paraffin-embedded tissues". en. In: *European Journal of*

Histochemistry 51.1 (2007), pp. 59–66. ISSN: 2038-8306. DOI: 10.4081/1013. URL: https://www.ejh.it/index.php/ejh/article/view/1013 (visited on 12/10/2023).

[500] Nicholas Billinton and Andrew W. Knight. "Seeing the Wood through the Trees: A Review of Techniques for Distinguishing Green Fluorescent Protein from Endogenous Autofluorescence". In: *Analytical Biochemistry* 291.2 (Apr. 2001), pp. 175–197. ISSN: 0003-2697. DOI: 10.1006/abio.2000.5006. URL: https://www.sciencedirect.com/science/article/pii/S0003269700950061 (visited on 12/10/2023).

[501] Frédéric Jamme et al. "Deep UV autofluorescence microscopy for cell biology and tissue histology". In: *Biology of the Cell* 105.7 (2013), pp. 277–288. ISSN: 1768-322X. DOI: 10.1111/boc.201200075. URL: https://onlinelibrary.wiley.com/doi/abs/10.1111/boc.201200075 (visited on 12/10/2023).

[502] Yair Rivenson et al. "Virtual histological staining of unlabelled tissue-autofluorescence images via deep learning". en. In: *Nature Biomedical Engineering* 3.6 (June 2019), pp. 466–477. ISSN: 2157-846X. DOI: 10.1038/s41551-019-0362-y. URL: https://www.nature.com/articles/s41551-019-0362-y (visited on 12/10/2023).

[503] Rebekah Drezek et al. "Autofluorescence Microscopy of Fresh Cervical-Tissue Sections Reveals Alterations in Tissue Biochemistry with Dysplasia¶". en. In: *Photochemistry and Photobiology* 73.6 (2001), pp. 636–641. ISSN: 1751-1097. DOI: 10.1562/0031-8655(2001)0730636AMOFCT2.0.CO2. URL: https://onlinelibrary.wiley.com/doi/abs/10.1562/0031-8655%282001%290730636AMOFCT2.0.CO2 (visited on 12/10/2023).

[504] C. Richter et al. "Follicular fluorescence quantity to characterize acne severity: a validation study". en. In: *Skin Research and Technology* 22.4 (Nov. 2016), pp. 451–459. ISSN: 0909-752X, 1600-0846. DOI: 10.1111/srt.12286. URL: https://onlinelibrary.wiley.com/doi/10.1111/srt.12286 (visited on 01/08/2024).

[505] Shahid Nazir et al. "Evaluation of autofluorescence quenching techniques on formalin- fixed chicken tissues". en. In: *Journal of Immunological Methods* 496 (Sept. 2021), p. 113097. ISSN: 00221759. DOI: 10.1016/j.jim.2021.113097. URL: https://linkinghub.elsevier.com/retrieve/pii/S0022175921001423 (visited on 12/19/2023).

[506] Jian Yang et al. "Quenching autofluorescence in tissue immunofluorescence". en. In: *Wellcome Open Research* 2 (Sept. 2017), p. 79. ISSN: 2398-502X. DOI: 10.12688/wellcomeopenres.12251.1. URL: https://wellcomeopenresearch.org/articles/2-79/v1 (visited on 12/19/2023).

[507] R I Amann et al. "Combination of 16S rRNA-targeted oligonucleotide probes with flow cytometry for analyzing mixed microbial populations". en. In: *Applied and Environmental Microbiology* 56.6 (June 1990), pp. 1919–1925. ISSN: 0099-2240, 1098-5336. DOI: 10.1128/aem.56.6.1919-1925.1990. URL: https://journals.asm.org/doi/10.1128/aem.56.6.1919-1925.1990 (visited on 01/11/2023).

[508] D. Pinkel et al. "Fluorescent Nucleic Acid Hybridization Methods." In: *New Technologies in Cytometry*. Vol. 1063. SPIE, June 1989, pp. 123–132. DOI: 10.1117/12.951898. URL: https://www.spiedigitallibrary.org/conference-proceedings-of-spie/1063/0000/Fluorescent-Nucleic-Acid-Hybridization-Methods/10.1117/12.951898.full (visited on 12/05/2023).

[509] K Olofsson, S Hellström, and M-L Hammarström. "The surface epithelium of recurrent infected palatine tonsils is rich in T cells". In: *Clinical and Experimental Immunology* 111.1 (Jan. 1998), pp. 36–47. ISSN: 0009-9104. DOI: 10.1046/j.1365-2249.1998.00446.x. URL: https://www.ncbi.nlm.nih.gov/pmc/articles/PMC1904845/ (visited on 12/05/2023).

[510] Harvey J. Motulsky and Ronald E. Brown. "Detecting outliers when fitting data with nonlinear regression – a new method based on robust nonlinear regression and the false discovery rate". In: *BMC Bioinformatics* 7.1 (Mar. 2006), p. 123. ISSN: 1471-2105. DOI: 10.1186/1471-2105-7-123. URL: https://doi.org/10.1186/1471-2105-7-123 (visited on 12/08/2023).

[511] Ali M. Reza. "Realization of the Contrast Limited Adaptive Histogram Equalization (CLAHE) for Real-Time Image Enhancement". en. In: *The Journal of VLSI Signal Processing-Systems for Signal, Image, and Video Technology* 38.1 (Aug. 2004), pp. 35–44. ISSN: 0922-5773. DOI: 10.1023/B:VLSI.0000028532.53893.82. URL: http://link.springer.com/10.1023/B:VLSI.0000028532.53893.82 (visited on 03/24/2023).

[512] Periklis Paganos et al. "FISH for All: A Fast and Efficient Fluorescent In situ Hybridization (FISH) Protocol for Marine Embryos and Larvae". In: *Frontiers in Physiology* 13 (2022). ISSN: 1664-042X. URL: https://www.frontiersin.org/articles/10.3389/fphys.2022.878062 (visited on 12/14/2023).

[513] D. Huber, L. Voith Von Voithenberg, and G.V. Kaigala. "Fluorescence in situ hybridization (FISH): History, limitations and what to expect from micro-scale FISH?" en. In: *Micro and Nano Engineering* 1 (Nov. 2018),

pp. 15–24. ISSN: 25900072. DOI: 10.1016/j.mne.2018.10.006. URL: https://linkinghub.elsevier.com/retrieve/pii/S259000721830008X (visited on 12/14/2023).

[514] Xinyang Song et al. "IL-17RE is the functional receptor for IL-17C and mediates mucosal immunity to infection with intestinal pathogens". en. In: *Nature Immunology* 12.12 (Dec. 2011), pp. 1151–1158. ISSN: 1529-2916. DOI: 10.1038/ni.2155. URL: https://www.nature.com/articles/ni.2155 (visited on 09/27/2023).

[515] Karin Ågren. *Immune response in human tonsil tissue*. en. Inst för klinisk vetenskap, intervention och teknik / Dept of Clinical Science, Intervention and Technology, Oct. 1997. ISBN: 978-91-628-2714-4. URL: http://openarchive.ki.se/xmlui/handle/10616/43769 (visited on 09/27/2023).

[516] Qun Huang et al. "Simple hypertrophic tonsils have more active innate immune and inflammatory responses than hypertrophic tonsils with recurrent inflammation in children". In: *Journal of Otolaryngology - Head & Neck Surgery* 49.1 (June 2020), p. 35. ISSN: 1916-0216. DOI: 10.1186/s40463-020-00428-3. URL: https://doi.org/10.1186/s40463-020-00428-3 (visited on 09/27/2023).

[517] Christoph Spiekermann et al. "Increased Levels of S100A8/A9 in Patients with Peritonsillar Abscess: A New Promising Diagnostic Marker to Differentiate between Peritonsillar Abscess and Peritonsillitis". en. In: *Disease Markers* 2017 (2017), pp. 1–10. ISSN: 0278-0240, 1875-8630. DOI: 10.1155/2017/9126560. URL: https://www.hindawi.com/journals/dm/2017/9126560/ (visited on 11/20/2023).

[518] Seda Türko and Lu Babakurban. "The Role of Cytokines in the Pathophysiology of Recurrent Tonsillitis". en. In: ().

[519] N V Boiko et al. "[Proinflammatory cytokine content in the saliva of children suffering from chronic tonsillitis]". rus. In: *Vestnik otorinolaringologii* 84.3 (Jan. 2019), pp. 26–31. ISSN: 2309-1274. DOI: 10.17116/otorino20198403126. URL: https://doi.org/10.17116/otorino20198403126 (visited on 11/20/2023).

[520] Katharina Geißler et al. "Cytokine production in patients with recurrent acute tonsillitis: analysis of tonsil samples and blood". en. In: *Scientific Reports* 10.1 (Aug. 2020), p. 13006. ISSN: 2045-2322. DOI: 10.1038/s41598-020-69981-1. URL: https://www.nature.com/articles/s41598-020-69981-1 (visited on 11/20/2023).

[521] Jürgen Harder et al. "Activation of the Nlrp3 Inflammasome by *Streptococcus* pyogenes Requires Streptolysin O and NF-B Activation but Proceeds Independently of TLR Signaling and P2X7 Receptor". en. In: *The Journal of Immunology* 183.9 (Nov. 2009), pp. 5823–5829. ISSN: 0022-1767, 1550-6606. DOI: 10.4049/jimmunol.0900444. URL: https://journals.aai.org/jimmunol/article/183/9/5823/81796/Activation-of-the-Nlrp3-Inflammasome-by (visited on 07/27/2023).

[522] Regev Cohen et al. "Screening asymptomatic households for Streptococcus pyogenes pharyngeal carriage as a part of in-hospital investigation of puerperal sepsis". In: *American Journal of Infection Control* 47.12 (Dec. 2019), pp. 1493–1499. ISSN: 0196-6553. DOI: 10.1016/j.ajic.2019.05.029. URL: https://www.sciencedirect.com/science/article/pii/S0196655319306108 (visited on 12/12/2023).

[523] Rebecca Cordery et al. "Frequency of transmission, asymptomatic shedding, and airborne spread of Streptococcus pyogenes in schoolchildren

exposed to scarlet fever: a prospective, longitudinal, multicohort, molecular epidemiological, contact-tracing study in England, UK". English. In: *The Lancet Microbe* 3.5 (May 2022), e366–e375. ISSN: 2666-5247. DOI: 10.1016/S2666-5247(21)00332-3. URL: https://www.thelancet.com/journals/lanmic/article/PIIS2666-5247(21)00332-3/fulltext (visited on 12/12/2023).

[524] Asrat Anja et al. "Asymptomatic pharyngeal carriage rate of Streptococcus pyogenes, its associated factors and antibiotic susceptibility pattern among school children in Hawassa town, southern Ethiopia". en. In: *BMC Research Notes* 12.1 (Sept. 2019), p. 564. ISSN: 1756-0500. DOI: 10.1186/s13104-019-4601-9. URL: https://doi.org/10.1186/s13104-019-4601-9 (visited on 12/12/2023).

[525] Elisa Viciani et al. "Paediatric obstructive sleep apnoea syndrome (OSAS) is associated with tonsil colonisation by Streptococcus pyogenes". en. In: *Scientific Reports* 6.1 (Feb. 2016), p. 20609. ISSN: 2045-2322. DOI: 10.1038/srep20609. URL: https://www.nature.com/articles/srep20609 (visited on 03/17/2023).

[526] Wenzhao Yang and Sung-Liang Chen. "Time-gated fluorescence imaging: Advances in technology and biological applications". en. In: *Journal of Innovative Optical Health Sciences* 13.03 (May 2020), p. 2030006. ISSN: 1793-5458, 1793-7205. DOI: 10.1142/S1793545820300062. URL: https://www.worldscientific.com/doi/10.1142/S1793545820300062 (visited on 01/07/2024).

[527] Brent W. Weyers et al. "Fluorescence lifetime imaging for intraoperative cancer delineation in transoral robotic surgery". en. In: *Translational Biophotonics* 1.1-2 (Dec. 2019), e201900017. ISSN: 2627-1850, 2627-1850. DOI:

10.1002/tbio.201900017. URL: https://onlinelibrary.wiley.com/doi/10.1002/tbio.201900017 (visited on 01/07/2024).

[528] Mark Marsden et al. "Intraoperative Margin Assessment in Oral and Oropharyngeal Cancer Using Label-Free Fluorescence Lifetime Imaging and Machine Learning". In: *IEEE Transactions on Biomedical Engineering* 68.3 (Mar. 2021), pp. 857–868. ISSN: 0018-9294, 1558-2531. DOI: 10.1109/TBME.2020.3010480. URL: https://ieeexplore.ieee.org/document/9144381/ (visited on 02/06/2024).

[529] Ruoyang Yao et al. "Net-FLICS: fast quantitative wide-field fluorescence lifetime imaging with compressed sensing – a deep learning approach". en. In: *Light: Science & Applications* 8.1 (Mar. 2019), p. 26. ISSN: 2047-7538. DOI: 10.1038/s41377-019-0138-x. URL: https://www.nature.com/articles/s41377-019-0138-x (visited on 01/07/2024).

[530] Chantal Dysli et al. "Fluorescence lifetime imaging ophthalmoscopy". en. In: *Progress in Retinal and Eye Research* 60 (Sept. 2017), pp. 120–143. ISSN: 13509462. DOI: 10.1016/j.preteyeres.2017.06.005. URL: https://linkinghub.elsevier.com/retrieve/pii/S1350946217300344 (visited on 01/07/2024).

[531] M. Ochoa et al. "High compression deep learning based single-pixel hyperspectral macroscopic fluorescence lifetime imaging in vivo". en. In: *Biomedical Optics Express* 11.10 (Oct. 2020), p. 5401. ISSN: 2156-7085, 2156-7085. DOI: 10.1364/BOE.396771. URL: https://opg.optica.org/abstract.cfm?URI=boe-11-10-5401 (visited on 01/07/2024).

[532] Klaus Suhling et al. "Imaging the environment of green fluorescent protein". In: *Biophysical journal* 83.6 (2002). Publisher: Elsevier, pp. 3589–3595.

[533] Karsten König. "Clinical multiphoton tomography". en. In: *Journal of Biophotonics* 1.1 (Mar. 2008), pp. 13–23. ISSN: 1864-063X, 1864-0648. DOI: 10.1002/jbio.200710022. URL: https://onlinelibrary.wiley.com/doi/10.1002/jbio.200710022 (visited on 01/07/2024).

[534] Leng-Chun Chen et al. "Fluorescence Lifetime Imaging Microscopy for Quantitative Biological Imaging". en. In: *Methods in Cell Biology*. Vol. 114. Elsevier, 2013, pp. 457–488. ISBN: 978-0-12-407761-4. DOI: 10.1016/B978-0-12-407761-4.00020-8. URL: https://linkinghub.elsevier.com/retrieve/pii/B9780124077614000208 (visited on 01/07/2024).

[535] Wolfgang Becker. *The bh TCSPC handbook*. Becker & Hickl GmbH, 2021.

[536] Koji Sugioka. "Progress in ultrafast laser processing and future prospects". In: *Nanophotonics* 6.2 (Mar. 2017), pp. 393–413. ISSN: 2192-8614, 2192-8606. DOI: 10.1515/nanoph-2016-0004. URL: https://www.degruyter.com/document/doi/10.1515/nanoph-2016-0004/html (visited on 01/07/2024).

[537] Toshio Kurobori, Yoshio Cho, and Yukito Matsuo. "Ultrashort pulses from a cw dye laser using passive-active mode locking technique". en. In: *Optics Communications* 24.1 (Jan. 1978), pp. 41–43. ISSN: 00304018. DOI: 10.1016/0030-4018(78)90262-6. URL: https://linkinghub.elsevier.com/retrieve/pii/0030401878902626 (visited on 01/07/2024).

[538] U. Keller. "Ultrafast solid-state laser oscillators: a success story for the last 20 years with no end in sight". en. In: *Applied Physics B* 100.1 (July 2010), pp. 15–28. ISSN: 0946-2171, 1432-0649. DOI: 10.1007/s00340-010-4045-3. URL: http://link.springer.com/10.1007/s00340-010-4045-3 (visited on 01/07/2024).

[539] U. Keller et al. "Solid-state low-loss intracavity saturable absorber for Nd:YLF lasers: an antiresonant semiconductor Fabry–Perot saturable absorber". en. In: *Optics Letters* 17.7 (Apr. 1992), p. 505. ISSN: 0146-9592, 1539-4794. DOI: 10.1364/OL.17.000505. URL: https://opg.optica.org/abstract.cfm?URI=ol-17-7-505 (visited on 01/07/2024).

[540] D. E. Spence, P. N. Kean, and W. Sibbett. "60-fsec pulse generation from a self-mode-locked Ti:sapphire laser". en. In: *Optics Letters* 16.1 (Jan. 1991), p. 42. ISSN: 0146-9592, 1539-4794. DOI: 10.1364/OL.16.000042. URL: https://opg.optica.org/abstract.cfm?URI=ol-16-1-42 (visited on 01/07/2024).

[541] P. F. Curley et al. "Application of a femtosecond self-sustaining mode-locked Ti:sapphire laser to the field of laser scanning confocal microscopy". en. In: *Optical and Quantum Electronics* 24.8 (Aug. 1992), pp. 851–859. ISSN: 0306-8919, 1572-817X. DOI: 10.1007/BF00620198. URL: http://link.springer.com/10.1007/BF00620198 (visited on 01/11/2024).

[542] J Henrich, S Butcher, and M Arrigoni. "Ultrafast lasers: trends in femtosecond amplifiers—Ti: sapphire vs. ytterbium". In: *Laser Focus World* (2020), pp. 1–7.

[543] Norihiko Nishizawa. "Ultrashort pulse fiber lasers and their applications". In: *Japanese Journal of Applied Physics* 53.9 (Sept. 2014), p. 090101. ISSN: 0021-4922, 1347-4065. DOI: 10.7567/JJAP.53.090101. URL: https://iopscience.iop.org/article/10.7567/JJAP.53.090101 (visited on 01/07/2024).

[544] Wolfgang Becker and Axel Bergmann. "Lifetime imaging techniques for optical microscopy". In: *Tech-nical report, Becker & Hickl GmbH* (2003).

[545] W Gärtner et al. "Fluorescence scanning microscopy combined with subnanosecond time resolution". In: *Experimentelle Technik der Physik* 36.6 (1988), pp. 443–451.

[546] Klaus Suhling et al. "Fluorescence Lifetime Imaging". en. In: *Handbook of Photonics for Biomedical Engineering*. Ed. by Aaron H.-P. Ho, Donghyun Kim, and Michael G. Somekh. Dordrecht: Springer Netherlands, 2014, pp. 1–50. ISBN: 978-94-007-6174-2. DOI: 10.1007/978-94-007-6174-2_13-1. URL: https://link.springer.com/10.1007/978-94-007-6174-2_13-1 (visited on 01/07/2024).

[547] Michael Wahl. *Time-Correlated Single Photon Counting*. 2014. URL: https://www.picoquant.com/images/uploads/page/files/7253/technote_tcspc.pdf (visited on 01/07/2024).

[548] Xiongbo Liu et al. "Fast fluorescence lifetime imaging techniques: A review on challenge and development". In: *Journal of Innovative Optical Health Sciences* 12.05 (2019). Publisher: World Scientific, p. 1930003.

[549] René Ebrecht, Craig Don Paul, and Fred S. Wouters. "Fluorescence lifetime imaging microscopy in the medical sciences". en. In: *Protoplasma* 251.2 (Mar. 2014), pp. 293–305. ISSN: 0033-183X, 1615-6102. DOI: 10.1007/s00709-013-0598-4. URL: http://link.springer.com/10.1007/s00709-013-0598-4 (visited on 01/07/2024).

[550] Michael Wahl et al. "Photon arrival time tagging with many channels, sub-nanosecond deadtime, very high throughput, and fiber optic remote synchronization". en. In: *Review of Scientific Instruments* 91.1 (Jan. 2020), p. 013108. ISSN: 0034-6748, 1089-7623. DOI: 10.1063/1.5121412. URL: https://pubs.aip.org/rsi/article/91/1/013108/1018660/

Photon-arrival-time-tagging-with-many-channels-sub (visited on 01/07/2024).

[551] Nadia Sarfraz et al. "Visualizing orthogonal RNAs simultaneously in live mammalian cells by fluorescence lifetime imaging microscopy (FLIM)". en. In: *Nature Communications* 14.1 (Feb. 2023), p. 867. ISSN: 2041-1723. DOI: 10.1038/s41467-023-36531-y. URL: https://www.nature.com/articles/s41467-023-36531-y (visited on 01/07/2024).

[552] Farzad Fereidouni et al. "Rapid fluorescence lifetime estimation with modified phasor approach and Laguerre deconvolution: a comparative study". In: *Methods and Applications in Fluorescence* 5.3 (Sept. 2017), p. 035003. ISSN: 2050-6120. DOI: 10.1088/2050-6120/aa7b62. URL: https://iopscience.iop.org/article/10.1088/2050-6120/aa7b62 (visited on 01/07/2024).

[553] Stephanie C. Ems-McClung and Claire E. Walczak. "Using FLIM-FRET for Characterizing Spatial Interactions in the Spindle". eng. In: *Methods in Molecular Biology (Clifton, N.J.)* 2415 (2022), pp. 221–243. ISSN: 1940-6029. DOI: 10.1007/978-1-0716-1904-9_17.

[554] Darren A Smith et al. "Analysis of time-correlated single photon counting data: a comparative evaluation of deterministic and probabilistic approaches". In: *Methods and Applications in Fluorescence* 5.4 (Oct. 2017), p. 042001. ISSN: 2050-6120. DOI: 10.1088/2050-6120/aa8055. URL: https://iopscience.iop.org/article/10.1088/2050-6120/aa8055 (visited on 01/11/2024).

[555] Monika Malak et al. "Contribution of autofluorescence from intracellular proteins in multiphoton fluorescence lifetime imaging". en. In: *Scientific Reports* 12.1 (Oct. 2022), p. 16584. ISSN: 2045-2322. DOI: 10.1038/

s41598-022-20857-6. URL: https://www.nature.com/articles/s41598-022-20857-6 (visited on 01/11/2024).

[556] Mengyan Wang et al. "Rapid diagnosis and intraoperative margin assessment of human lung cancer with fluorescence lifetime imaging microscopy". en. In: *BBA Clinical* 8 (Dec. 2017), pp. 7–13. ISSN: 22146474. DOI: 10.1016/j.bbacli.2017.04.002. URL: https://linkinghub.elsevier.com/retrieve/pii/S2214647417300132 (visited on 01/11/2024).

[557] Mikhail Y. Berezin and Samuel Achilefu. "Fluorescence Lifetime Measurements and Biological Imaging". en. In: *Chemical Reviews* 110.5 (May 2010), pp. 2641–2684. ISSN: 0009-2665, 1520-6890. DOI: 10.1021/cr900343z. URL: https://pubs.acs.org/doi/10.1021/cr900343z (visited on 01/11/2024).

[558] Noël Boens et al. "Fluorescence Lifetime Standards for Time and Frequency Domain Fluorescence Spectroscopy". en. In: *Analytical Chemistry* 79.5 (Mar. 2007), pp. 2137–2149. ISSN: 0003-2700, 1520-6882. DOI: 10.1021/ac062160k. URL: https://pubs.acs.org/doi/10.1021/ac062160k (visited on 01/11/2024).

[559] Alan G. Ryder et al. "Time-domain measurement of fluorescence lifetime variation with pH". In: ed. by Gregory H. Bearman, Darryl J. Bornhop, and Richard M. Levenson. San Jose, CA, July 2001, pp. 102–109. DOI: 10.1117/12.432487. URL: http://proceedings.spiedigitallibrary.org/proceeding.aspx?articleid=900591 (visited on 01/11/2024).

[560] Alex J. Walsh et al. "Classification of T-cell activation via autofluorescence lifetime imaging". en. In: *Nature Biomedical Engineering* 5.1 (July 2020), pp. 77–88. ISSN: 2157-846X. DOI: 10.1038/s41551-020-0592-z.

URL: https://www.nature.com/articles/s41551-020-0592-z (visited on 01/11/2024).

[561] Alberto Ghezzi et al. "Multispectral compressive fluorescence lifetime imaging microscopy with a SPAD array detector". en. In: *Optics Letters* 46.6 (Mar. 2021), p. 1353. ISSN: 0146-9592, 1539-4794. DOI: 10.1364/OL.419381. URL: https://opg.optica.org/abstract.cfm?URI=ol-46-6-1353 (visited on 01/11/2024).

[562] Kamlesh Awasthi et al. "Characterization of endogenous fluorescence in nonsmall lung cancerous cells: A comparison with nonmalignant lung normal cells". en. In: *Journal of Biophotonics* 13.5 (May 2020), e201960210. ISSN: 1864-063X, 1864-0648. DOI: 10.1002/jbio.201960210. URL: https://onlinelibrary.wiley.com/doi/10.1002/jbio.201960210 (visited on 01/11/2024).

[563] Klaus Suhling et al. "Wide-field time-correlated single photon counting-based fluorescence lifetime imaging microscopy". en. In: *Nuclear Instruments and Methods in Physics Research Section A: Accelerators, Spectrometers, Detectors and Associated Equipment* 942 (Oct. 2019), p. 162365. ISSN: 01689002. DOI: 10.1016/j.nima.2019.162365. URL: https://linkinghub.elsevier.com/retrieve/pii/S0168900219309519 (visited on 01/07/2024).

[564] AV Agronskaia, L Tertoolen, and HC Gerritsen. "High frame rate fluorescence lifetime imaging". In: *Journal of Physics D-Applied Physics* 36.14 (2003). Publisher: London: The Institute of Physics and The Physical Society., pp. 1655–1662.

[565] SriniVas R. Sadda et al. "A pilot study of fluorescence lifetime imaging ophthalmoscopy in preclinical Alzheimer's disease". en. In: *Eye* 33.8

(Aug. 2019), pp. 1271–1279. ISSN: 1476-5454. DOI: 10.1038/s41433-019-0406-2. URL: https://www.nature.com/articles/s41433-019-0406-2 (visited on 10/06/2023).

[566] Susanne Jentsch et al. "Retinal fluorescence lifetime imaging ophthalmoscopy measures depend on the severity of Alzheimer's disease". en. In: *Acta Ophthalmologica* 93.4 (2015), e241–e247. ISSN: 1755-3768. DOI: 10.1111/aos.12609. URL: https://onlinelibrary.wiley.com/doi/abs/10.1111/aos.12609 (visited on 10/06/2023).

[567] Paul J Tadrous et al. "Fluorescence lifetime imaging of unstained tissues: early results in human breast cancer". en. In: *The Journal of Pathology* 199.3 (2003), pp. 309–317. ISSN: 1096-9896. DOI: 10.1002/path.1286. URL: https://onlinelibrary.wiley.com/doi/abs/10.1002/path.1286 (visited on 09/05/2023).

[568] Yasaman Ardeshirpour et al. "In Vivo Fluorescence Lifetime Imaging for Monitoring the Efficacy of the Cancer Treatment". In: *Clinical Cancer Research* 20.13 (June 2014), pp. 3531–3539. ISSN: 1078-0432. DOI: 10.1158/1078-0432.CCR-13-1826. URL: https://doi.org/10.1158/1078-0432.CCR-13-1826 (visited on 10/06/2023).

[569] Vladimir Gukassyan et al. "Application of fluorescence resonance energy transfer resolved by fluorescence lifetime imaging microscopy for the detection of enterovirus 71 infection in cells". In: *Journal of Biomedical Optics* 12.2 (Mar. 2007), p. 024016. ISSN: 1083-3668, 1560-2281. DOI: 10.1117/1.2718582. URL: https://www.spiedigitallibrary.org/journals/journal-of-biomedical-optics/volume-12/issue-2/024016/Application-of-fluorescence-resonance-energy-transfer-

resolved-by-fluorescence-lifetime/10.1117/1.2718582.full (visited on 10/06/2023).

[570] Greg A. Snyder et al. "Two-photon fluorescence lifetime imaging microscopy of NADH metabolism in HIV-1 infected cells and tissues". In: *Frontiers in Immunology* 14 (Aug. 2023), p. 1213180. ISSN: 1664-3224. DOI: 10.3389/fimmu.2023.1213180. URL: https://www.ncbi.nlm.nih.gov/pmc/articles/PMC10468605/ (visited on 10/06/2023).

[571] *Fluorescence Lifetime Imaging (FLIM) \textbackslashtextbar PicoQuant*. URL: https://www.picoquant.com/applications/category/life-science/fluorescence-lifetime-imaging-flim#description (visited on 09/06/2023).

[572] Veronika Miskolci et al. "In vivo fluorescence lifetime imaging of macrophage intracellular metabolism during wound responses in zebrafish". In: *eLife* 11 (Feb. 2022). Ed. by Serge Mostowy, Didier YR Stainier, and Robert Knight, e66080. ISSN: 2050-084X. DOI: 10.7554/eLife.66080. URL: https://doi.org/10.7554/eLife.66080 (visited on 10/06/2023).

[573] *Monitoring cellular metabolism of 3T3 upon wild type E. coli infection by mapping NADH with FLIM (Invited Paper)*. URL: https://opg.optica.org/col/abstract.cfm?uri=col-8-10-931 (visited on 10/06/2023).

[574] Wjatscheslaw Liublin et al. "NAD(P)H fluorescence lifetime imaging of live intestinal nematodes reveals metabolic crosstalk between parasite and host". en. In: *Scientific Reports* 12.1 (May 2022), p. 7264. ISSN: 2045-2322. DOI: 10.1038/s41598-022-10705-y. URL: https://www.nature.com/articles/s41598-022-10705-y (visited on 10/06/2023).

[575] Dan Elson et al. "Time-domain fluorescence lifetime imaging applied to biological tissue". en. In: *Photochemical & Photobiological Sciences* 3.8 (Aug. 2004), pp. 795–801. ISSN: 1474-905X, 1474-9092. DOI: 10.1039/

b316456j. URL: https://link.springer.com/10.1039/b316456j (visited on 01/07/2024).

[576] Colin D. McGuinness et al. "Excitation of fluorescence decay using a 265nm pulsed light-emitting diode: Evidence for aqueous phenylalanine rotamers". en. In: *Applied Physics Letters* 89.6 (Aug. 2006), p. 063901. ISSN: 0003-6951, 1077-3118. DOI: 10.1063/1.2245441. URL: https://pubs.aip.org/apl/article/89/6/063901/119765/Excitation-of-fluorescence-decay-using-a-265nm (visited on 01/07/2024).

[577] Ikuo Ashikawa et al. "Lifetime of Tyrosine Fluorescence in Nucleosome Core Particles1". en. In: *The Journal of Biochemistry* 91.6 (Apr. 1982), pp. 2047–2055. ISSN: 1756-2651, 0021-924X. DOI: 10.1093/oxfordjournals.jbchem.a133898. URL: https://academic.oup.com/jb/article-lookup/doi/10.1093/oxfordjournals.jbchem.a133898 (visited on 01/07/2024).

[578] K. Willaert et al. "Determination of the excited-state lifetimes of the tryptophan residues in barnase, via multifrequency phase fluorometry of tryptophan mutants". en. In: *Biochemistry* 31.3 (Jan. 1992), pp. 711–716. ISSN: 0006-2960, 1520-4995. DOI: 10.1021/bi00118a011. URL: https://pubs.acs.org/doi/abs/10.1021/bi00118a011 (visited on 01/07/2024).

[579] Lily H. Laiho et al. "Two-photon 3-D mapping of ex vivo human skin endogenous fluorescence species based on fluorescence emission spectra". en. In: *Journal of Biomedical Optics* 10.2 (2005), p. 024016. ISSN: 10833668. DOI: 10.1117/1.1891370. URL: http://biomedicaloptics.spiedigitallibrary.org/article.aspx?doi=10.1117/1.1891370 (visited on 01/07/2024).

[580] P. A. A. De Beule et al. "A hyperspectral fluorescence lifetime probe for skin cancer diagnosis". en. In: *Review of Scientific Instruments* 78.12 (Dec.

2007), p. 123101. ISSN: 0034-6748, 1089-7623. DOI: 10.1063/1.2818785. URL: https://pubs.aip.org/rsi/article/78/12/123101/348829/A-hyperspectral-fluorescence-lifetime-probe-for (visited on 01/07/2024).

[581] Md Abdul Kader Sagar et al. "Machine Learning Methods for Fluorescence Lifetime Imaging (FLIM) Based Label-Free Detection of Microglia". In: *Frontiers in Neuroscience* 14 (Sept. 2020), p. 931. ISSN: 1662-453X. DOI: 10.3389/fnins.2020.00931. URL: https://www.frontiersin.org/article/10.3389/fnins.2020.00931/full (visited on 01/07/2024).

[582] Beata Koziol et al. "Riboflavin as a source of autofluorescence in Eisenia fetida coelomocytes". In: *Photochemistry and photobiology* 82.2 (2006). Publisher: Wiley Online Library, pp. 570–573.

[583] D Schweitzer et al. "Towards metabolic mapping of the human retina". In: *Microscopy research and technique* 70.5 (2007). Publisher: Wiley Online Library, pp. 410–419.

[584] JR Alcala, E Gratton, and FG Prendergast. "Interpretation of fluorescence decays in proteins using continuous lifetime distributions". In: *Biophysical journal* 51.6 (1987). Publisher: Elsevier, pp. 925–936.

[585] Michael S. Roberts et al. "Non-invasive imaging of skin physiology and percutaneous penetration using fluorescence spectral and lifetime imaging with multiphoton and confocal microscopy". en. In: *European Journal of Pharmaceutics and Biopharmaceutics* 77.3 (Apr. 2011), pp. 469–488. ISSN: 09396411. DOI: 10.1016/j.ejpb.2010.12.023. URL: https://linkinghub.elsevier.com/retrieve/pii/S0939641110003644 (visited on 01/07/2024).

[586] Matthew W. Conklin et al. "Fluorescence Lifetime Imaging of Endogenous Fluorophores in Histopathology Sections Reveals Differences Between Normal and Tumor Epithelium in Carcinoma In Situ of the Breast". en. In: *Cell Biochemistry and Biophysics* 53.3 (Apr. 2009), pp. 145–157. ISSN: 1085-9195, 1559-0283. DOI: 10.1007/s12013-009-9046-7. URL: http://link.springer.com/10.1007/s12013-009-9046-7 (visited on 01/07/2024).

[587] Alex J. Walsh et al. "Optical Metabolic Imaging Identifies Glycolytic Levels, Subtypes, and Early-Treatment Response in Breast Cancer". en. In: *Cancer Research* 73.20 (Oct. 2013), pp. 6164–6174. ISSN: 0008-5472, 1538-7445. DOI: 10.1158/0008-5472.CAN-13-0527. URL: https://aacrjournals.org/cancerres/article/73/20/6164/584965/Optical-Metabolic-Imaging-Identifies-Glycolytic (visited on 01/07/2024).

[588] W. Becker. "Fluorescence lifetime imaging – techniques and applications". en. In: *Journal of Microscopy* 247.2 (Aug. 2012), pp. 119–136. ISSN: 0022-2720, 1365-2818. DOI: 10.1111/j.1365-2818.2012.03618.x. URL: https://onlinelibrary.wiley.com/doi/10.1111/j.1365-2818.2012.03618.x (visited on 01/07/2024).

[589] Jenu V Chacko and Kevin W Eliceiri. "NAD(P)H fluorescence lifetime measurements in fixed biological tissues". In: *Methods and Applications in Fluorescence* 7.4 (Oct. 2019), p. 044005. ISSN: 2050-6120. DOI: 10.1088/2050-6120/ab47e5. URL: https://iopscience.iop.org/article/10.1088/2050-6120/ab47e5 (visited on 01/07/2024).

[590] F. Poulon et al. "Comparison between fresh and fixed human biopsies using spectral and lifetime measurements: Fluorescence analysis using

one and two photon excitations". In: *2015 International Conference on Advances in Biomedical Engineering (ICABME)*. Beirut, Lebanon: IEEE, Sept. 2015, pp. 25–28. ISBN: 978-1-4673-6516-1. DOI: 10.1109/ICABME.2015.7323242. URL: http://ieeexplore.ieee.org/document/7323242/ (visited on 01/07/2024).

[591] Sourav Ganguly, Andrew H.A. Clayton, and Amitabha Chattopadhyay. "Fixation alters fluorescence lifetime and anisotropy of cells expressing EYFP-tagged serotonin1A receptor". en. In: *Biochemical and Biophysical Research Communications* 405.2 (Feb. 2011), pp. 234–237. ISSN: 0006291X. DOI: 10.1016/j.bbrc.2011.01.016. URL: https://linkinghub.elsevier.com/retrieve/pii/S0006291X11000350 (visited on 01/07/2024).

[592] Xinyi Wang et al. "Effect of Fixation and Mounting on Fluorescence Lifetime of Cellular Autofluorescence". In: *IEEE Journal of Selected Topics in Quantum Electronics* 25.1 (Jan. 2019), pp. 1–6. ISSN: 1077-260X, 1558-4542. DOI: 10.1109/JSTQE.2018.2889429. URL: https://ieeexplore.ieee.org/document/8598918/ (visited on 01/07/2024).

[593] Arne S. Kristoffersen et al. "Testing Fluorescence Lifetime Standards using Two-Photon Excitation and Time-Domain Instrumentation: Fluorescein, Quinine Sulfate and Green Fluorescent Protein". en. In: *Journal of Fluorescence* 28.5 (Sept. 2018), pp. 1065–1073. ISSN: 1053-0509, 1573-4994. DOI: 10.1007/s10895-018-2270-z. URL: http://link.springer.com/10.1007/s10895-018-2270-z (visited on 01/09/2024).

[594] Xian-Fu Zhang, Jianlong Zhang, and Limin Liu. "Fluorescence Properties of Twenty Fluorescein Derivatives: Lifetime, Quantum Yield, Absorption and Emission Spectra". en. In: *Journal of Fluorescence* 24.3 (May 2014), pp. 819–826. ISSN: 1053-0509, 1573-4994. DOI: 10.1007/s10895-

014-1356-5. URL: http://link.springer.com/10.1007/s10895-014-1356-5 (visited on 01/09/2024).

[595] Sohail Ahmed et al. *Practical manual for fluorescence microscopy techniques, Chapter 4: Fluorescence lifetime imaging microscopy by TCSPC (TD-FLIM)*.

[596] PicoQuant. *How to Work with Instrument Response Functions (IRFs) Measured with a Microscope*. Tech. rep. 2023. URL: https://www.tcspc.com/doku.php/howto:how_to_work_with_the_instrument_response_function_irf (visited on 01/12/2024).

[597] PicoQuant. *Micro Time 200 Manual*.

[598] Thomas S. Blacker et al. "Separating NADH and NADPH fluorescence in live cells and tissues using FLIM". en. In: *Nature Communications* 5.1 (May 2014), p. 3936. ISSN: 2041-1723. DOI: 10.1038/ncomms4936. URL: https://www.nature.com/articles/ncomms4936 (visited on 01/07/2024).

[599] Yousuf H. Mohammed et al. "Noninvasive in vivo human multiphoton microscopy: a key method in proving nanoparticulate zinc oxide sunscreen safety". In: *Journal of Biomedical Optics* 25.01 (Jan. 2020), p. 1. ISSN: 1083-3668. DOI: 10.1117/1.JBO.25.1.014509. URL: https://www.spiedigitallibrary.org/journals/journal-of-biomedical-optics/volume-25/issue-01/014509/Noninvasive-in-vivo-human-multiphoton-microscopy--a-key-method/10.1117/1.JBO.25.1.014509.full (visited on 01/07/2024).

[600] Alexander Boreham et al. "Time-Resolved Fluorescence Spectroscopy and Fluorescence Lifetime Imaging Microscopy for Characterization of Dendritic Polymer Nanoparticles and Applications in Nanomedicine". en. In: *Molecules* 22.1 (Dec. 2016), p. 17. ISSN: 1420-3049. DOI: 10.3390/

molecules22010017. URL: http://www.mdpi.com/1420-3049/22/1/17 (visited on 01/07/2024).

[601] Kaisa Rautaniemi et al. "Crystallization Kinetics of an Amorphous Pharmaceutical Compound Using Fluorescence-Lifetime-Imaging Microscopy". en. In: *Molecular Pharmaceutics* 15.5 (May 2018), pp. 1964–1971. ISSN: 1543-8384, 1543-8392. DOI: 10.1021/acs.molpharmaceut.8b00117. URL: https://pubs.acs.org/doi/10.1021/acs.molpharmaceut.8b00117 (visited on 01/07/2024).

[602] Márta Szaszák et al. "Fluorescence Lifetime Imaging Unravels C. trachomatis Metabolism and Its Crosstalk with the Host Cell". en. In: *PLOS Pathogens* 7.7 (July 2011), e1002108. ISSN: 1553-7374. DOI: 10.1371/journal.ppat.1002108. URL: https://journals.plos.org/plospathogens/article?id=10.1371/journal.ppat.1002108 (visited on 10/06/2023).

[603] Arunima Bhattacharjee et al. "Metabolic fingerprinting of bacteria by fluorescence lifetime imaging microscopy". en. In: *Scientific Reports* 7.1 (June 2017), p. 3743. ISSN: 2045-2322. DOI: 10.1038/s41598-017-04032-w. URL: https://www.nature.com/articles/s41598-017-04032-w (visited on 01/15/2024).

[604] Farah Qazi et al. "Real-time, label-free detection and identification of bacteria through non-invasive optical imaging". en. In: *Microbes and Infection* (Nov. 2023), p. 105263. ISSN: 12864579. DOI: 10.1016/j.micinf.2023.105263. URL: https://linkinghub.elsevier.com/retrieve/pii/S1286457923001661 (visited on 01/15/2024).

[605] Sven R. Kantelhardt et al. "In vivo multiphoton tomography and fluorescence lifetime imaging of human brain tumor tissue". en. In: *Journal*

of Neuro-Oncology 127.3 (May 2016), pp. 473–482. ISSN: 0167-594X, 1573-7373. DOI: 10.1007/s11060-016-2062-8. URL: http://link.springer.com/10.1007/s11060-016-2062-8 (visited on 01/15/2024).

[606] Volker Huck et al. "From morphology to biochemical state – intravital multiphoton fluorescence lifetime imaging of inflamed human skin". en. In: *Scientific Reports* 6.1 (Mar. 2016), p. 22789. ISSN: 2045-2322. DOI: 10.1038/srep22789. URL: https://www.nature.com/articles/srep22789 (visited on 01/15/2024).

[607] Alba Alfonso-Garcia et al. "Mesoscopic fluorescence lifetime imaging: Fundamental principles, clinical applications and future directions". en. In: *Journal of Biophotonics* 14.6 (June 2021), e202000472. ISSN: 1864-063X, 1864-0648. DOI: 10.1002/jbio.202000472. URL: https://onlinelibrary.wiley.com/doi/10.1002/jbio.202000472 (visited on 01/15/2024).